Using bio-adhesive and bio-inert surfaces to maximize biogas production and influence microbial growth in Anaerobic Digesters

Dorota Agnieszka Dobrzanska, Ir

Student number: 0962337

A thesis submitted for the degree of Doctor of Philosophy in Life Sciences with Chemistry

University of Warwick

Department of Chemistry

School of Life Sciences

June 2014

List of Figures

Table of Schemes

Table of Tables

Table of Charts

Table of Appendices

Declaration

The work described in this project was carried out in the Department Chemistry and School of Life Sciences in the University of Warwick, between April 2010 and June 2014. Unless otherwise stated, it is the work of the author and has not been submitted in whole or part of any other degree at this or any other university. Chapter 2 contains work that has been published in Langmuir [DOI: 0.1021/la4003719, *Langmuir*, 2013, 29 (9), 2961–2970] with appropriate acknowledgement of work carried out by other workers.

Acknowledgments

I would like to thank BBSRC DTG and The Perry Foundation for financial support. My supervisors: dr Andrew Marsh, dr Paul C. Taylor in the Department of Chemistry and prof. Christopher G. Dowson in the School of Life Sciences for their hospitality and support during the period of this research.

I also would like to thank dr Ben Douglas for precious advice and the Science City for great quality equipment.

Thanks to Rod Wesson in the electrical workshop for assembling the methane and CO_2 sensors and Markus Grant from mechanical workshop for making stainless steel baskets.

I very much appreciate help from dr Ivan Prokes and Edward Tunnah in regards to the NMR spectra analyses as well as dr Lijiang Song and Phil Aston for help with mass spectrometry.

Thanks to dr Benjamin Johnson and prof. Stephen Evans from the Department of Physics, University of Leeds as well as dr Marc Walker and prof. Chris McConville from the Department of Physics, University of Warwick for help with XPS measurements.

Abstract

The optimisation of biogas digesters is crucial for further development of sustainable energy sources. In this research, an integrative approach was taken to understanding how this problem can be addressed including: seeking a better understanding of protein – surface interactions on the molecular level; larger scale experiments to screen the best materials for use in laboratory scale anaerobic digesters to influence microbial growth and biofilm development as well as analysis of farm-scale data using the ADM1 multiparameter model.

The laboratory-scale experiments were undertaken to develop surfaces suitable for studying microbial immobilization. This work, currently using tertiary amines, amine oxides and comparator oligoethylene glycol studies the adsorption of two classic model proteins: lysozyme and fibrinogen using quartz crystal microbalance methods and represents important steps for selecting and exploring surface – protein interactions. The data showed that tertiary amine oxides are more resistant to non-specific protein adsorption than the corresponding tertiary amines.

Heat modified polyurethane foam was used to explore biofilm and planktonic phase microbial populations in a fixed film biogas reactor.. After four weeks the foam was analysed by 'next generation' 454-sequencing to identify the influence of the supporting materials on microbial population residing in anaerobic digesters. The results revealed that *Spirochaetes*, *Methanobacterium* and *Methanocorpusculum* associated themselves with heat modified polyurethane foams.

Finally, data from a farm-scale anaerobic digester (volatile fatty acid concentration, temperature and pH) have been gathered and entered into the ADM1 model, developed by the mathematical modelling group from Lund University, to mimic the behaviour of a laboratory scale 1.5 l reactor and identify improved conditions for methanogens stability.

The combination of approaches described above will allow the identification of which parameters will enhance the operation of anaerobic digesters and has identified surfaces that promote adhesion of particular *Bacteria* and *Archaea* in order to increase biogas production.

Abbreviations

°C	degrees centigrade
δ	shift in ppm, from NMR data
µl	microlitre
AD	anaerobic digestion
bp	base pair
BLAST	Basic Local Alignment Search Tool
BSA	bovine serum albumin
cfu	colony-forming unit(s)
COSY	correlated spectroscopy
cpm	counts per minute
DNA	deoxyribonucleic acid
DNase	deoxyribonuclease
EDTA	ethylenediaminetetraacetate
FAD, $FADH_2$	flavin-adenine dinucleotide and its fully reduced form
FFA	free fatty acid
FITC	fluorescein isothiocyanate
FTIR	Fourier transform infrared
GC, GLC	gas chromatography, gas/liquid chromatography
HPLC	high-performance liquid chromatography
IC50	concentration giving half-maximal inhibition
IR	infrared
kDa or Da	kilo Dalton, Dalton
LC/MS	liquid chromatography/mass spectrometry
m/*z*	mass-to-charge ratio, from mass spectrometric data
MCR	methyl coenzyme M-reductase
mRNA	messenger RNA

MS	mass spectrometry
Na^+/K^+-ATPase	sodium-potassium pump
NAD, NAD^+, NADH	nicotinamide-adenine dinucleotide and its oxidized and reduced forms
NADH	nicotinamideadenine dinucleotide
NCBI	United States' National Centre for Biotechnology Information
NMR	nuclear magnetic resonance
PBS	phosphate-buffered saline
PCR	polymerase chain reaction
PEG	polyethylene glycol
Pi	inorganic phosphate
R_f	thin layer chromatography
RNA	ribonucleic acid or ribonucleate
rpm	revolutions per minute
SDS	sodium dodecyl sulfate
SEM	scanning electron microscopy
THF	tetrahydrofuran
TLC	thin-layer chromatography
TMS	trimethylsilane (NMR)
Tris	tris (hydroxymethyl)aminomethane
UV	ultraviolet
VFA	volatile fatty acids
V_{max}	maximum velocity

Chapter 1: Introduction

1.1. Context

In the United Kingdom renewable energy sources contribute only 4% towards global energy production. European Union directive 2009/28/EC on Promotion of the Use of Energy from Renewable Sources regulates the target for share of energy from renewable sources to reach 15% in 2020.[1] The target uses a slightly different definition of renewable and total energy than has been used to date and includes the use of electricity and heat (and other fuels used for heating) by final consumers and energy for transport.

Development of new technologies is crucial to meeting this goal. The most popular renewable energy sources are biomass, wind and solar energy.[2] Biogas producing digesters are popular on farms but are still not widely used due to difficulties in control of the process and limited efficiency of current technologies. [3]

1.2. Benefits of biogas production

The use of agricultural waste for biogas production reduces greenhouse gas emission. Biogas installations can, as a result of their decentralized nature and the regional investment structure,[4] contribute significantly to sustainable development in rural areas and offer farmers new income opportunities. Waste is captured and used to generate energy and a by-product in the form of digestate for fertiliser is produced. Disposal costs of organic waste are reduced and the digested residue from the biogas plant has fewer odours and it is more environmentally friendly.[5]

1.3. Biogas composition

Biogas is a flammable, natural gas produced by microbes. It is odorless, colorless and contains 50-70% methane, 20-45% of carbon dioxide and small quantities of hydrogen sulphide, nitrogen, hydrogen and carbon dioxide.[6]

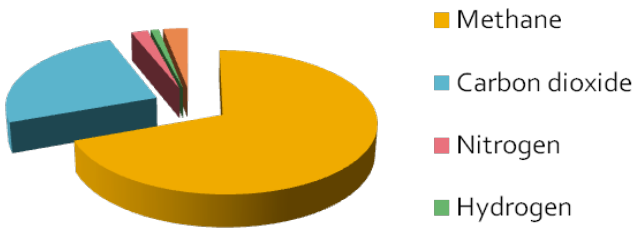

Figure 1 Biogas composition: methane 50-75%, carbon dioxide 25-45%, nitrogen 3%, hydrogen 1% and other gases 1%.

The solubility of methane in water is very low which is a significant advantage for the production process as the purification of biogas can be achieved by passing through a water scrubber (US 20100107872 A1).[7,8] Simple cleaning technology leads to an easy operation and significant reduction of costs.

The combustion of methane produces a blue flame and good amount of heat, according to the chemical formula:

$$CH_4 + 2O_2 \xrightarrow{H_c = -887\,kJ/mol} CO_2 + 2H_2O$$

Biogas can be used as a high quality fuel for cooking and lighting. One cubic meter of biogas typically contains 65% of methane and generates around 2 kWh of heat[9] (enough energy to cook a meal for a family of three).

1.4. Microbiology of anaerobic digestion (AD)

Production of biogas is based on the AD process involving a range of biochemical and physiochemical processes distinguishable broadly as five steps (*see red labels in Figure 2). During anaerobic digestion, farm, food or crop waste is transformed into biogas under anoxic conditions.

a) Decomposition is achieved by mechanical shredding;
b) Hydrolysis – it is either thermal or an enzymatic process where particulates are solubilized and larger polymers converted into simpler monomers;
c) Acidogenesis – performed by acidogenic *Bacteria*, where monomers are converted into volatile fatty acid (VFAs);[10]
d) Acetogenesis – volatile fatty acids are transformed into acetic acid, carbon dioxide and hydrogen by the acetogenic *Bacteria*,
e) Methanogenesis – acetates are converted into methane and carbon dioxide with consumption of hydrogen by methanogenic *Archaea.*[11]

The most popular classification of organisms involved in methanogenesis is determined by substrate metabolism. There are five main groups of *Bacteria* and *Archaea*:[12]

(a) Acetate-forming *Bacteria* have a symbiotic relationship with methanogens.[13] During acetogenesis, acetic acid, hydrogen and carbon dioxide are produced. Hydrogen inhibits growth of acetogens. Methane producing *Archaea* consume hydrogen and transform acetates into methane.
(b) Sulphate reducing *Bacteria* use hydrogen and acetate to produce sulfates. They compete with methanogens for available substrates. The solution to

overcome competition between two species is an increased acetate concentration. It can be achieved by regulation of temperature and pH during operation process.[14]

(c) Hydrogenotrophic methanogens reduce carbon dioxide to methane using hydrogen, according to the equation: $CO_2 + 4H_2 \rightarrow CH_4 + 2H_2O$

(d) Acetotrophic methanogens convert acetate into methane and carbon dioxide, which can be used by hydrogenotrophic *Archaea*, the main process occurs according to the following equation:

$$4HCO_2^- + H^+ + H_2O \rightarrow CH_4 + 3HCO_3^-$$

(e) Methylotrophic methanogens produce methane from available methyl groups, for example by using methanol or methylamines:

$$4CH_3OH \rightarrow 3CH_4 + HCO_3^- + H_2O + H^+$$

The overview of methane producing *Archaea* and the type of substrate consumed is presented in Table 1.

Taxonomy	Morphology	Substrates	Isolation source
Methanohalophilus			
halophilus	coccus	methanol, methylamines	marine sediment
mahii	coccus	methanol, methylamines	saline lake sediment
oregonense	coccus	methanol, methylamines dimethylsulfide	saline alkaline aquifer
portucalensis	coccus	methanol, methylamines	solar sand pond
zhilinae	coccus	methanol, methylamines	alkaline lake sediment
Methanohalobium			
evstigatus	coccus	methanol, methylamines	salt lagoon sediment
Methanosaeta			
concillii	rod	acetate	pear waste digester
barkeri	coccus	methanol, acetate methylamines	mud, sewage sludge digester
Methanothrix			
thermophila	rod	acetate	thermophilic sludge digester
Methanopyrus			
kandleri	rod	hydrogen	geothermal marine sediment

Table 1 Characterization of methanogenic consortia.

1.5. Methanogenesis

Methanogenesis is the final step of biogas production. It is a complex process that involves a series of biochemical and physiochemical steps. The methanogenesis pathway contains novel coenzymes and biochemical reactions not previously observed in other organisms.[11]

Methyl-coenzyme M reductase (MCR, EC 2.8.4.1, coenzyme B sulfoethylthiotransferase) is an especially important and unique enzyme that allows detection of methanogens from bacterial community in environmental samples.[15] This enzyme catalyses the reduction of a methyl group attached to methylcoenzyme M (2-mercaptoethanesulfonate) with formation of methane (CH_4) and the heterodisulfide.[16] MCR has been used for detection of methanogenic *Archaea* from samples collected from a full-scale anaerobic digester, revealing the following methanogenic biochemical reactions and enzymes (Figure 2).

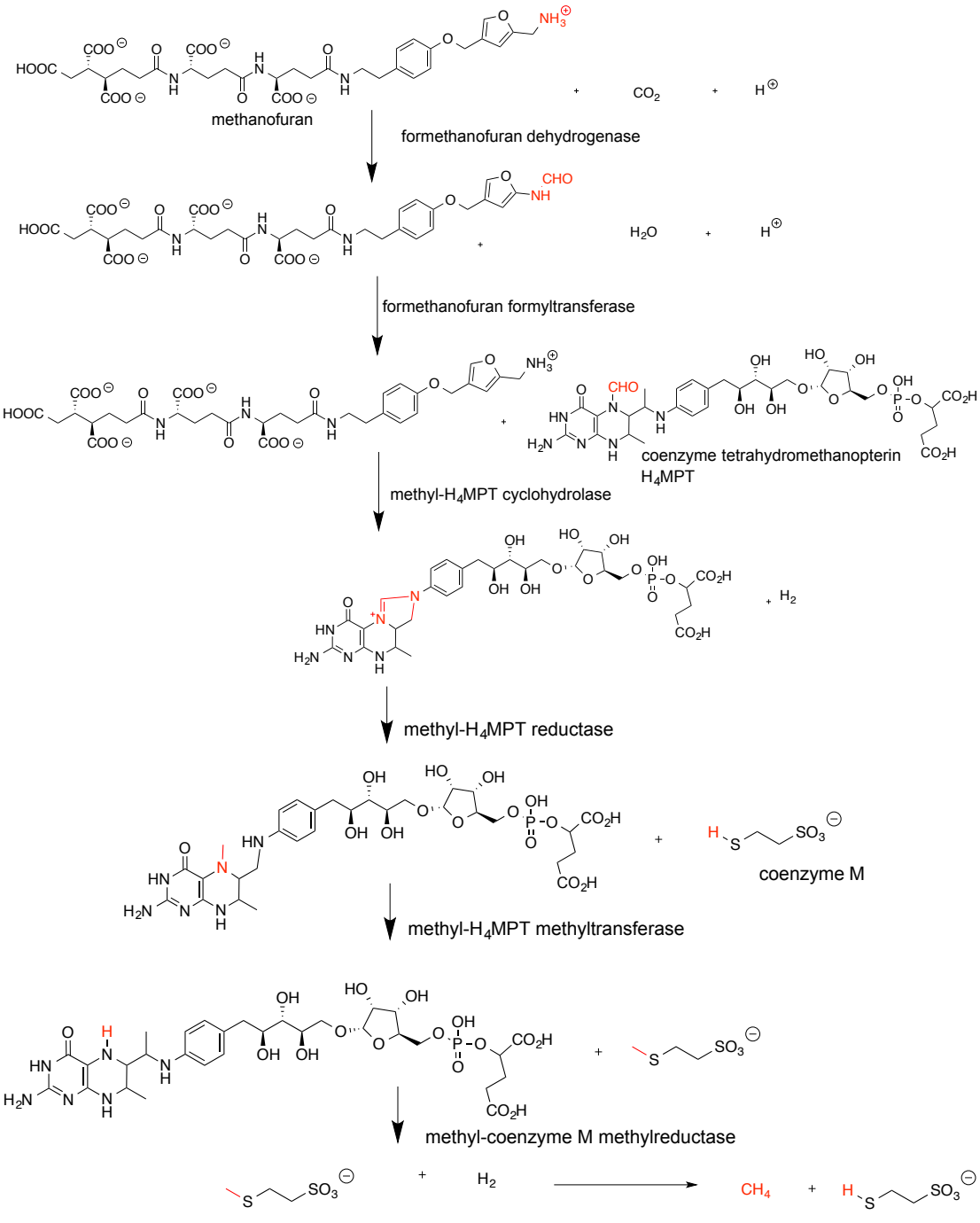

Figure 2 Key biochemical reactions during methanogenesis.[11]

1.6. Limitations to Biogas Productions

There are several factors, which determine the efficiency of the overall AD process, such as:

a) Ammonia – concentrations of ionized and nonionized forms of ammonia below 200 mg/L are optimal for anaerobic microorganisms,[17] higher levels inhibit the activity of enzymes involved in the citric acid cycle and lead to failure of the biogas production process;

b) Inhibition by substrate, product or other organisms. Energy crops, manures and waste and their mixtures are frequently used for biogas production. Knowledge of composition of feedstock is crucial to maintain stability of the process. An overview of potential substrates for biogas production is summarized in Table 2.[18]

c) pH inhibition based on disruption of homeostasis affects the growth of microbial communities.

d) High concentrations of cations (Na, K, Mg, Ca, Al) and heavy metals (Cr, Fe, Co, Cu, Zn, Cd, or Ni) can disrupt enzymatic activity and slow down the AD process.

e) Changes in temperature have a fundamental influence on the system.

f) Dissolved oxygen has lethal properties for the anaerobic community.

Feedstock	Solids %TS	Volatile Solids %VS	Retention time days	Biogas yield m^3/kg VS	CH_4 content %
Pig slurry	3-81	70-80	20-40	0.2-0.5	70-80
Cow slurry	5-12	75-85	20-30	0.2-0.3	55-75
Chicken slurry	10-30	70-80	>30	0.35-0.6	60-80
Whey	1-5	80-95	3-10	0.8-0.95	60-80
Leaves	80	90	8-20	0.1-0.3	55-60
Methanol	-	-	2-10	0.1	50-60
Maize	25-30	19-47	25-35	0.27-0.29	50-55
Straw	70	90	10-50	0.35-0.45	50-60
Garden waste	60-70	90	8-30	0.2-0.5	65
Grass silage	15-25	90	10	0.55	60-70
Fruit waste	15-20	75	8-20	0.25-0.5	50-60
Food remains	10	80	10-20	0.5-0.6	70-80

Table 2 Specification of substrates and the methane content after anaerobic digestion.[19] Table shows the relationship between the fermentable products: volatile fatty acids and methane content in biogas.

1.7. Current biogas production technologies

AD plants are based around old technology, making them large, expensive capital projects, with a track record of instability.[20] Many studies focus on the improvement of the anaerobic digestion process.[19,21-23]. The most popular solutions are characterized in Table 3.

Process	Parameters	Advantages	Drawbacks
Single, continuously stirred tank 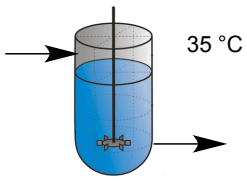	Operated at mesophilic temperature (35 °C)	Simple design	Long digestion process (over 20 days), slow removal of volatile solids, slow deactivation of pathogens, poor methane yield
Single, continuously stirred tank 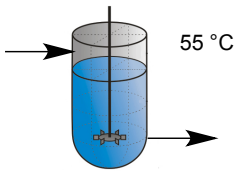	Operated at thermophilic temperature (55 °C)	Simple process design, significant reduction in the retention time, increased volatile solids removal, increased methane yield	Requires more energy to heat up the digester, less resistant to changes process parameter
Two stage system 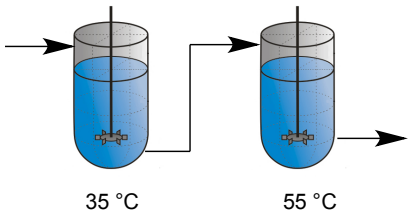	Consist of series of mesophilic and thermophilic digesters	Incorporates the benefits of both processes[24]	Complicated design, more expensive, does not reduce the digestion time[25]

Table 3 Characterization of thermophilic, mesophilic and mixed anaerobic digestion process.

In this research, the thermophilic anaerobic digestion will be further studied due to the simplicity of the process and the increased methane yield. Two substrates were chosen in order to model the process parameters:

(a) methanol as an added carbon source with trace metal solution. CH_3OH was chosen because it is an inexpensive substrate, which does not contain solids (see substrate characteristics, Table 1). Therefore it can be directly converted into methane.[26] The metal ions solution was used because the trace elements are essential co-factors of the enzymes involved in the biochemical pathway of methane generation[26].

(b) maize as an added carbon source was chosen due to the moderate amount of volatile solids in the substrate composition (Table 1), hence creating a good starting point for comparing methane yield based on the anaerobic digestion of substrates with various volatile solids levels. Full description of process parameters and modeling results are described in Chapter 5: Bioinformatics and reactors design.

1.8. Improvement of the Anaerobic Digestion Process

All modern high rate digesters are based on receiving high volumes of good quality biomass, which means predictable physical form of feedstock as well as identical biochemical composition. An improvement in physical form can be achieved by simple encapsulation of input sludge aggregates between packing materials (such as coconut coir, charcoal or nylon fibres) inside the up-flow anaerobic reactor. The supporting material has a large influence on the efficiency of the process, as the initial biomass of film may be of major importance for further biofilm growth and stability.[27-29] The effectiveness of packing material is usually measured by chemical oxygen demand (COD) and biological oxygen demand (BOD), methane yield and reduction of volatile solids.[30] Surfaces that increase adsorption of proteins[31] and

cells[32] thus have important applications in stabilization of the microbial growth in bioreactors during the biogas production process.

Lalov and Krysteva[33] implemented a covalent immobilisation process of methanogenic *Archaea* on polymeric support [poly(acrylonitrile-acrylamide)]. The process is based on addition of cells onto the activated polymer granules in formaldehyde and phosphate buffer solutions at 45 °C. The supports with immobilized biomass were packed in a plastic column inside the continuously stirred tank reactor (fixed-film type reactor – Figure 3) for biogas production. This process offers several advantages with the absence of diffusion limitations and allows possibilities for direct contact between the bound cells and the substrate solution, leading to an intense controlled reaction. However, it has not been widely used because the chemicals used for binding are often toxic and rapidly caused the death of cells even during the immobilisation.

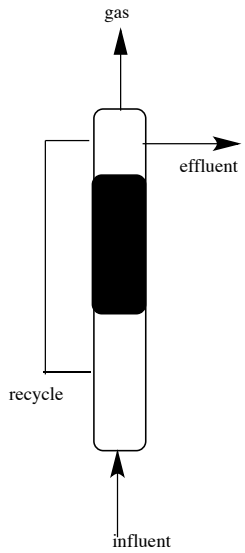

Figure 3 The design of up-flow anaerobic bed digester with recycling of influent and packed column (black box).

Other approaches have been used to investigate the roles of activated carbon and synthetic ion exchange resins in up-flow anaerobic sludge blanket. The most important features of supporting materials were the pore volume availability as well as the large size of associated surface area for the colonization of microorganisms. The immobilisation results were visualized by scanning electron microscopy (SEM). The results showed that activated carbon had higher total surface area than the anion-exchange resins, but smaller fraction of this material was accessible to *Bacteria*.[34]

A company involved in AD methodologies, Brentwood Industries, uses the "integrated fixed- film activated sludge" (IFAS) Technology (Table 4).[35] This system provides processing of additional biomass within a wastewater treatment facility in order to meet more stringent effluent parameters. There are a number of different approaches to IFAS implementation but the various configurations fall into one of two basic types: "dispersed media" entrapped in the aeration basin, and "fixed media", such as structured sheet media or knitted fabric media, fixed-in-place in the aeration basin.[36]

Types of IFAS media		
Fixed in place types	Advantages	Drawbacks
PVC Structured sheet media	• Simple to install • Low initial cost • No material losses	• May foul if rag removal is inadequate
Fabric web-type	• Simple to install • No material losses	• Prone to red worm blooms • May foul if rag removal is inadequate
Dispersed types	Advantages	Drawbacks
Polypropylene cylinders	• Excellent mixing • High surface area	• Media losses • Difficult to maintain aeration system
Sponges	• Excellent mixing • High surface area	• Media losses • Difficult to maintain aeration system

Table 4 Types of Integrated Fixed-film Activated Sludge (IFAS) media [35,37]

Dispersed media systems may use porous sponges or plastic finned-cylinder shapes that are suspended or float (depending upon material density) in the activated sludge tank. These dispersed IFAS systems provide excellent mixing and high surface area but can be expensive to implement (additional equipment is required to retain media) and operate over time. Sponges and non-compressible suspended media types will exhibit surface area loss due to abrasion and require yearly replenishment.[36,38]

Fixed media systems can be implemented with either flexible fabric media or polyvinyl chloride (PVC) structured sheet media. The flexible fabric materials are typically attached to rigid frames that are located within the activated sludge tank. Fixed media systems based on PVC structured sheet media offer an excellent combination of high performance and low cost. PVC structured sheet media are designed to maximize fluid mixing performance and oxygen transfer through the biomass on the media wall.[37]

Another method used by Ratusznei *et al.*, employed the Anaerobic Sequencing Batch Reactor (ASBR – Figure 4) with dispersed media systems. Polyurethane foam cubes contained in stainless steel baskets inside the digester were used as biofilm carriers.[39] ASBR with that kind of supporting media showed good volatile solids removal and increased biogas productivity.[40]

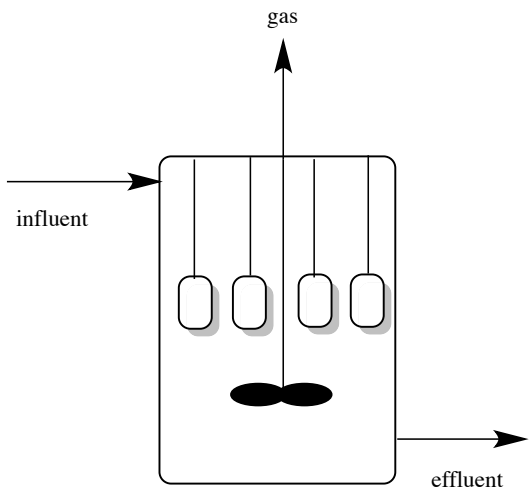

Figure 4 The design of stainless steel baskets with polyurethane foams contained in the anaerobic sequencing batch reactor.

In this research, stainless steel baskets with chemically modified polyurethane foams will be used and tested in the full-scale anaerobic digesters in order to identify the microbial population residing in Anaerobic Digester.[41]

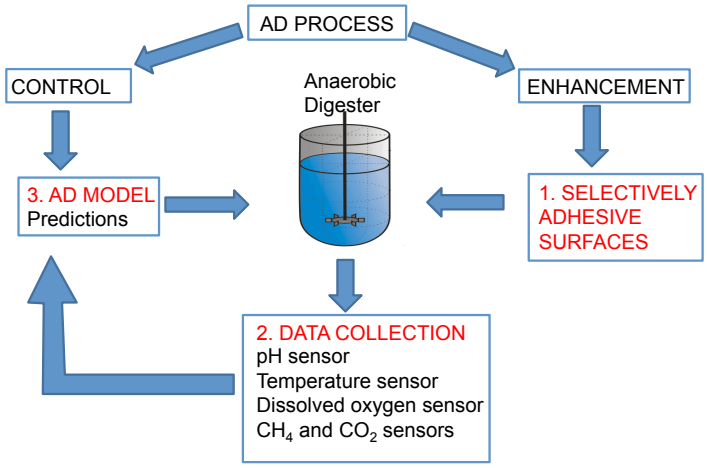

Figure 5 Integrated approach to anaerobic digester optimisation.

Figure 5 shows the ways of control and enhancement of the anaerobic digestion process. It will be achieved by implementing the library of selectively adhesive surfaces to influence microbial growth and stability (Chapter 2 and Chapter 3). Pyrosequencing analyses of 16 rRNA genes will help identifying the microbial communities residing in anaerobic digesters as well as the influence of supporting materials on methanogens (Chapter 4). The Anaerobic Digestion model No 1[42] developed by the Mathematical Simulation Group from the University of Lund will be used to predict the most important process parameters in order to maintain the stability of *Archaea* and *Bacteria* in Anaerobic Digesters (Chapter 5).

1.9. Aims

The aim of this research was development of bio-adhesive and bio-inert surfaces that would promote selective adhesion of methanogens and reduce attachment of organisms that compete with biogas producing consortia. This would be achieved by:

1. Small-scale investigations of protein – surface interactions in order to understand the mechanisms behind biofilm formation.
2. Studies on biofilm formed by a pure culture of *M.barkeri* – a versatile methanogen commonly present in anaerobic digesters.
3. Understanding what range and incidence of *Bacteria* and *Archaea* reside in a typical farm-scale digester and how the supporting materials (polyurethane foams) influence the microbial population.
4. Monitoring of methane production within a bioreactor and simulation of the experimental data by ADM1 mathematical model in order to increase the stability of process by early prediction of changes in homeostasis.

1.10. References

(1) http://eur-lex.europa.eu/LexUriServ/LexUriServ.do?uri=Oj:L:2009:140:0016:0062:en:PDF, accessed 9/08/2013.

(2) Essletzbichler, J. *Eur. Plan. Stud.,* **2012**, *20*, 791.

(3) Weiland, P. *Appl. Microbiol. Biotechnol.,* **2010**, *85*, 849.

(4) Banks, C. J.; Salter, A. M.; Chesshire, M. *Water Sci. Technol.,* **2007**, *55*, 165.

(5) Murphy, J. D.; McKeogh, E. *Renewable Energy,* **2004**, *29*, 1043.

(6) Deublein, D. S., A.; *Biogas from waste and renewable resources*; Willey: United Kingdom, 2008.

(7) Gommel, A.; Efinger, D.; Mulder, R.; Buis, H.,Purification of biogas of hydrogen sulfide., Voith Paper Patent Gmbh, **2012**.

(8) Warwick, J. B.,Biogas upgrading, U.S. Patent US 20100107872 A1, **2010**.

(9) http://www.gtmconference.ca/site/downloads/presentations/1D1 - Ross Slaughter.pdf accessed 25/07/2013.

(10) Drake L.H. *Acetogenesis*; Chapman & Hall: United Kingdom, 1994.

(11) Ferry, J. G.; Kastead, K. A. *Methanogenesis*, 2007.

(12) Ferry, J. G. *Methanogenesis. Ecology, Physiology, Biochemistry and Genetics.*; Chapman & Hall New York, 1993.

(13) Stams, A. J. M.; Elferink, S.; Westermann, P. *Biomethanation I,* **2003**, *81*, 31.

(14) Raskin, L.; Rittmann, B. E.; Stahl, D. A. *Appl. Environ. Microbiol.,* **1996**, *62*, 3847.

(15) Garcia-Maldonado, J. Q.; Bebout, B. M.; Celis, L. B.; Lopez-Cortes, A. *Int. Microbiol.,* **2012**, *15*, 33.

(16) Ellermann, J.; Hedderich, R.; Bocher, R.; Thauer, R. K. *Eur. J. Biochem.,* **1988**, *172*, 669.

(17) Liu, W. T.; Chan, O. C.; Fang, H. H. P. *Water Res.,* **2002**, *36*, 3203.

(18) Hutnan, M.; Spalkova, V.; Bodik, I.; Kolesarova, N.; Lazor, M. *Pol. J. Environ. Stud.,* **2010**, *19*, 323.

(19) Mata-Alvarez, J.; Mace, S.; Llabres, P. *Bioresour. Technol.,* **2000**, *74*, 3.

(20) Ward, A. J.; Hobbs, P. J.; Holliman, P. J.; Jones, D. L. *Bioresour. Technol.,* **2008**, *99*, 7928.

(21) Fang, H. H. P.; Chung, D. W. C. *Water Sci. Technol.,* **1999**, *40*, 77.

(22) Kim, M.; Ahn, Y. H.; Speece, R. E. *Water Res.,* **2002**, *36*, 4369.

(23) Maibaum, C.; Kuehn, V. *Water Sci. Technol.,* **1999**, *40*, 231.

(24) Song, Y. C.; Kwon, S. J.; Woo, J. H. *Water Res.,* **2004**, *38*, 1653.

(25) Zhao, Q. L.; Kugel, G. *J. Environ. Sci. Health,* **1996**, *31*, 2211.

(26) Vlissidis, A.; Zouboulis, A. I. *Bioresour. Technol.,* **1993**, *43*, 131.

(27) Araujo, J. C.; Mortara, R.; Campos, J. R.; Vazoller, R. F. *Environ. Technol.,* **2004**, *25*, 809.

(28) Chauhan, A.; Ogram, A. *Biochem. Biophys. Res. Commun.,* **2005**, *327*, 884.

(29) Perez, M.; Romero, L. I.; Rodriguez-Cano, R.; Sales, D. *Chem. Biochem. Eng. Q.,* **2006**, *20*, 203.

(30) Acharya, B. K.; Mohana, S.; Madamwar, D. *Bioresour. Technol.,* **2008**, *99*, 4621.

(31) Kane, R. S.; Deschatelets, P.; Whitesides, G. M. *Langmuir,* **2003**, *19*, 2388.

(32) Mrksich, M.; Chen, C. S.; Xia, Y. N.; Dike, L. E.; Ingber, D. E.; Whitesides, G. M. *Proc. Natl. Acad. Sci. U. S. A.,* **1996**, *93*, 10775.

(33) Lalov, I. G.; Krysteva, M. A.; Phelouzat, J.-L. *Bioresour. Technol.,* **2001**, *79*, 83.

(34) Kindzierski, W. B.; Gray, M. R.; Fedorak, P. M.; Hrudey, S. E. *Water Environ. Res,* **1992**, *64*, 766.

(35) Albizuri, J.; Grau, P.; Christensson, M.; Larrea, L. *Water Sci. Technol.,* **2014**, *69*, 1552.

(36) Kulick, F. M.; McDowell, C. S.,Anoxic bioreactor to treat wastewater, **2002**.

(37) Flamming, J. J. W., David L.; Kulick, Frank M. *Proc. Water Environ. Fed.,* **2011**, 5265.

(38) J Ye, F. K., CS McDowell *Proc. Water Environ. Fed.,* **2010**, 4200.

(39) de Oliveira, D. S.; Prinholato, A. C.; Ratusznei, S. M.; Rodrigues, J. A. D.; Zaiat, M.; Foresti, E. *J. Environ. Manage.,* **2009**, *90*, 3070.

(40) Wirtz, R. A.; Dague, R. R. *Water Environ. Res,* **1996**, *68*, 883.

(41) Sarti, A.; Pozzi, E.; Chinalia, F. A.; Zaiat, M.; Foresti, E. *Chemosphere,* **2006**, *62*, 1437.

(42) Batstone, D. J., Keller, J., Angelidaki, R.I., *Anaerobic Digestion Model No. 1*; IWA Publishing Group, 2002.

Chapter 2: Small Scale Investigations of Protein – Surface Interactions

2.1. Introduction

A basic understanding of protein – surface interactions is crucial for further development of fixed film bioreactors. It is important to identify both protein resistant and protein adhesive surfaces to discover the best supports for methanogenic *Archaea* and *Bacteria*. Selectively adhesive surfaces will influence microbial growth within anaerobic digesters and limit the biofilm formation of sulfate reducing *Bacteria*, which compete with methanogens[1] for available feedstock.[2]

Surfaces that offer control over the adsorption of proteins[3] and cells[4,5] find numerous *in vivo*[6] and *in vitro* applications, including selective cell adhesion.[7,8] For instance, grafting by atom transfer radical polymerisation from a polymer surface was used in order to produce bifunctional polymer coatings acting as absorbents for proteins and cells.[9]

Conversely, bioadhesive surfaces are also prized in nanotechnology, for example in stabilizing enzymes,[10] desirable microbial populations,[11] and hence chemistries amenable to the discovery[12-14] of both classes of surface are of great interest.[15-19]

2.1.1. Self-assembled monolayers

Self-assembled monolayers are formed by spontaneous adsorption (physi- or chemisorption) of surfactant onto solid surfaces.[20] Surfactants used for self-assembly purposes consist of head group, long chain hydrocarbons acting as backbone and functional groups responsible for physiochemical properties of SAMs. The head group structure (thiol, organosilane) guides the adsorption of SAM to the surface. Intermolecular interactions between hydrocarbons lead to good packing of surfactant

in the monolayer. SAMs are commonly used as model surfaces for investigation of interactions between biological species (proteins, cells, antibodies) and specific surface chemistries.[21-23] The modification of the head and ω-functional groups offers an excellent opportunity for use of SAMs in protein and bacterial adhesion studies, for example functionalization with the CH_3 terminal groups leads to formation of hydrophobic, anti-adherent surfaces while derivatization with COOH groups gives hydrophilic surface with good protein binding properties.[24]

2.1.2. SAM functionalization

Effect of wettability, surface charge and functionalization on protein and bacterial adhesion is studied in this chapter, using two substrates.

a) Thiol-gold self-assembled monolayers formed in solution. Alkanethiols chemisorb onto surfaces of gold forming covalent, slightly polar S-Au bonds. Van der Waals interactions between backbones lead to formation of stable and well-defined self-assembled monolayers[25-27,28] SAM formation in solution will be explored by immobilisation of thiol-acid on gold surfaces and addition of appropriate amine coupled by the peptide-coupling agent, followed by oxidation in hydrogen peroxide in ethanol (Scheme 1).

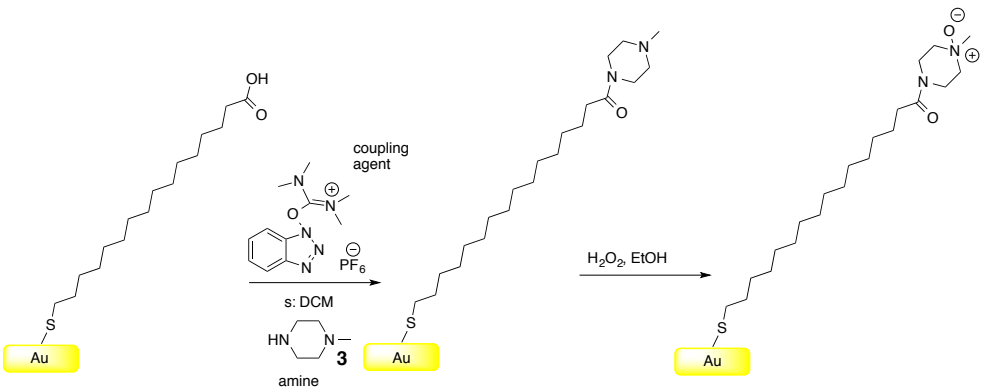

Scheme 1 Functionalization of gold-alkanethiols based SAMs.

This route was chosen because there is no chemoselective method for oxidising an amine in the presence of a thiol[29], thioester[30] or benzylsulfide[31] which have typically been used en route to SAMs in the past.

b) Silicon functionalization with pre-synthesised – alkenes immobilized by photo-activation. Photoinitiated chemistry[32-34] will be used as a method for creating self-assembled monolayers on etched, hydrogen terminated silicon (Sheme 2).[35]

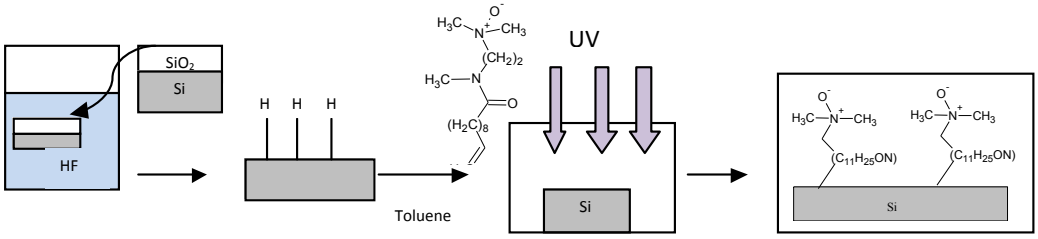

Scheme 2 Functionalization of silicon based SAMs.

Silicon is commonly used inorganic substrate for engineering purposes.[33] The packing density of silane-SiO_2 is lower than thiols on Au, however silicon based SAMs exibit higher thermal and chemical stability.[32]

The topography of surfaces can also be altered, for example porous materials have greater surface area compared with smooth surfaces offering more contact points for possible surface – protein interactions.[36]

Researchers also focus on combining topographical and chemical modifications to create multi-functional surfaces. For this reason, patterning of self assembled monolayers have been achieved by:

(a) **microcontact printing** (μCP) based on the fabrication of polydimethoxysiloxane (PDMS) stamp over silicon master, the stamp is then

peeled from the master and "inked" with alkanethiol in EtOH solution, dried and brought in contact with substrate (i.e. gold, glass, silicon oxide) giving a patterned surface.[7] It is a low cost and versatile method used by Mrksich on gold and silver substrates with patterned SAMs functionalized with hydrophobic, methyl-terminated groups separated by inert regions of substrate. The result showed that bovine capillary endometrial cells were attached only to CH_3 groups allowing easy control over activity and position of attached cells.[37]

(b) **photolithography** based on exposure of a silicon resist to UV light through a mask. The exposed regions are then removed, yielding surface patterned with silicon dioxide which can be further functionalized using alkylsiloxane SAMs. Denis *et al.* have employed a combination of SAMs and colloidal lithography to study the effect of both surface roughness and chemistry on the adhesion of collagen.

2.1.3. Forces involved in protein adsorption to surfaces

Protein adsorption to the surface is driven by intermolecular forces typically characterised as: electrostatic forces, van der Waals forces, hydrogen bond formation (between water and immobilized protein or protein and the surface itself),[38] $\pi - \pi$ interactions and the hydrophobic effect. The adsorption process also depends on intramolecular forces within the protein that could lead to change of protein conformation.[39] Larger proteins have more active sites that come into contact with surfaces. Both the sequence and charge of amino acids located on the outside of the proteins influence protein adsorption. The stability of the protein dictated by primary sequence within the protein is equally important since proteins with less

intramolecular crosslinking or secondary structural elements can easily unfold and form more contact points with surfaces.[40]

2.1.4. Adsorption of proteins to SAMs

Surface ability to bind water dramatically influences protein adsorption.[41] The current standard for protein resistance is oligo-/poly(ethylene glycol) (OEG/PEG), whose inertness is based on both an ability to interact favourably with water molecules (enthalpic stabilisation) at the same time as maintaining a relatively disordered environment (entropically favoured).[42] For short OEG chains with limited conformational change, the water barrier model has been proposed[43-45] wherein water molecules form a tightly bound interfacial layer around OEG or PEG. This provides a physical barrier and prevents direct contact between protein and surface (Figure 5a).

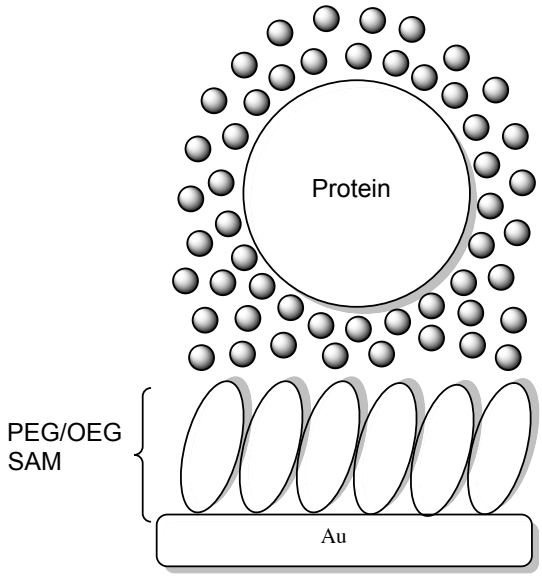

Figure 5a Water barrier formed by PEG/OEG SAM in contact with hydrated protein, figure adapted from Whitesides *et al*.[46]

The Whitesides group for the first time used well-defined alkanethiols SAMs with various headgroups to study the effect of protein adsorption.[47] Sigal *et al.* extended this work using gold SAMs functionalized with $-CH_3$, -OPh, $-CF_3$, -CN, $-COCH_3$, -

$CONHCH_3$, -OH, -EG_6OH and $CONH_2$ to study how wettability influences model protein adsorption using surface plasmon resonance. The results showed two different protein responses: small proteins were extremely sensitive to surface wettability and adsorbed well to surfaces decorated with -CH_3, -OPh and -CF_3, slightly to –CN and not at all to all other surfaces. Larger proteins were not sensitive to wettability of surfaces and absorbed to all functionalities with the exception of the EG_6OH functionalized surface.[41] Although surfaces bearing single terminal chemistry are widely reported, mixed SAMs with two or more chemical moieties are often used to create greater spatial distribution between surfactant molecules and reduce steric hindrance for binding proteins.[48]

Seeking alternatives to OEG surfaces, Holmlin *et al.*[49] reported a procedure for preparing zwitterionic self-assembled monolayers on gold. The resistance of the resulting surfaces to adsorption of a library of model proteins (for example ribonuclease A, lysozyme and fibrinogen) was examined using surface plasmon resonance (SPR). The results showed that SAMs with single charges (all positive or all negative) adsorbed a full monolayer of fibrinogen or lysozyme. Zwitterionic SAMs resisted the nonspecific adsorption of proteins approximately as effectively as oligo(ethylene glycol)-terminated alkanethiols on gold.

Recently, lotus leaf inspired,[50,51] superhydrophobic surfaces have been developed using reverse imprint lithography.[51] The excellent repellence of water droplets and resulting self-cleaning capability facilitate antifouling applications of surfaces. Wei *et al.* reported the self-assembly of low-molecular-weight gelators (LMWGs) with perfluorinated side for construction of superhydrophobic surfaces within minutes. The resulting surfaces were repellent to biological liquids, such as human serum and blood.[52]

2.1.5. Bacterial adhesion

Bacterial adhesion to self-assembled monolayers has been widely studied in the past.[53-55] Many studies using alkanethiols[56,57] and silicon[58,59] SAMs have been carried out to determine the effects of surface properties on cell attachment, spreading and proliferation. Most of these studies examine cell adhesion by the number of adherent cells, morphology, and immunofluorescent staining after several hours of incubation. Further understanding of the biophysical mechanism of cell adhesion requires real-time tracking of protein adsorption achieved by application of methods such as QCM[60]. Usually a layer of adsorbed protein facilitates the adhesion of *Bacteria* to surfaces.[61] Chapman *et al*. reported that *Bacteria* adhere to surfaces through various interactions, for example attachment of type I pili of *E. coli* to mannose groups leads to stabilization of biofilm development.[62] Surfaces containing grooves and ridges fabricated with the use of photo- or electron-beam lithography were used to study their effects on the behaviour and growth of attached cells.[63-66]

2.1.6. Archaeal cell envelope

Knowledge of specific cell structures and functions is also very important for understanding the biofilm formation process, hence literature surveys of archaeal cell envelopes have been carried out, revealing that knowledge of cell wall structure, and in particular integral membrane protein composition is significantly less developed for this class of microbes compared to prokaryotes.[67,68]. The main differences between archaeal and bacterial cell wall structures are summarized in Table 5.

Cell envelope	**Gram positive *Bacteria***	**Archaea**
Cell envelope structure	Presence of sugars: galactose, rhamnose, glucose and mannose in addition to pseudomurein.	Cell envelope similar to Gram positive *Bacteria*
Proteins	Adhesins Adhesin proteins containing Big_1 domain responsible for attachment to the cell wall	Large surfaces proteins *C* – terminal adhesin
	Adhesin proteins containing cysteine protease domain	*C* – terminal trans membrane adhesin
	Sortases - proteins covalently attached to the cell wall by membrane associated transpeptidases	LPxTG containing proteins

Table 5 Cell wall structure in Gram-positive *Bacteria* and *Archaea*.

Surface layers (S-layers) are often found in a broad range of *Bacteria* and *Archaea.* S-layers have self-assembling properties and recrystallize on solid substrates. They have been used for nanotechnology applications, for example to build supramolecular structures.[69,70] Martin-Molina *et al.* studied interactions between S-layers from *Bacillus sphaericus* at various electrolyte concentrations through scanning force microscopy, showing that electrostatic and steric interactions are dominant at long distances in S-layers.[71] Albers *et al.* reported the different cell wall structures othat exist within the broad class of *Archaea* (Figure 5b). *Methanosphaera*, *Methanothermus* and *Methanosarcina* have a thick, amorphous, multilayered coat of peptidoglycan. Surface-layer glycoproteins are located above the peptidoglycan

(*Methanothermus spp.*) or under murein layer (*Methanosarcina spp.*)

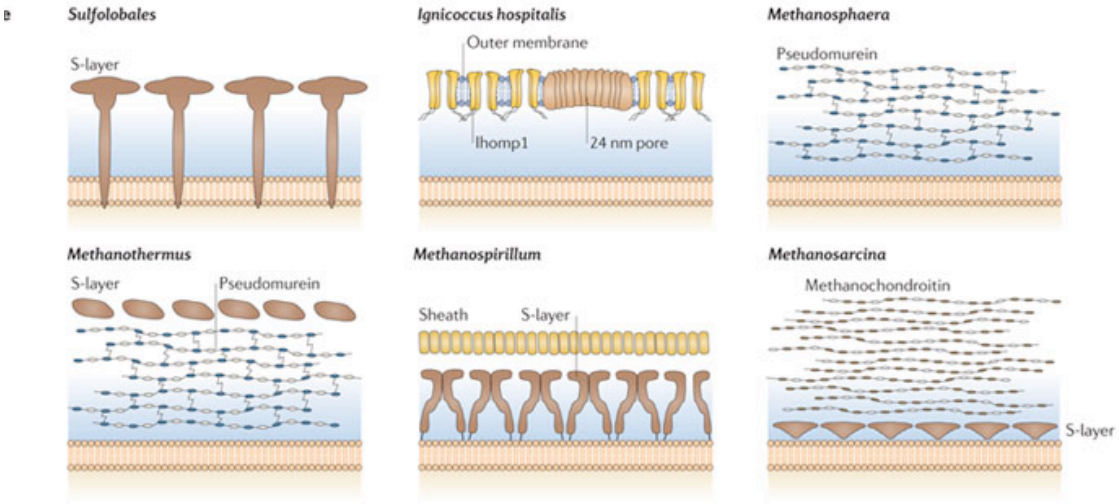

Figure 5b Side view of cell wall profiles for various *Archaea*.[67]

The location of the protein layer in a cell wall plays a crucial role in biofilm formation. A more detailed analysis of the effects of cell wall ultrastructure on biofilm formation is described in Chapter 3, but it has to be acknowledged that the complexity of bacterial and archaeal communities in an efficient anaerobic digester makes the design or discovery of surfaces for successful stabilisation a significant challenge.

2.2. Proteins chosen for adsorption and adhesion studies

Because there was less known about archaeal systems, and a more generic investigation into protein adhesion was desired initially, two archetypal model proteins were chosen: a small protein present in the secretion fluids, lysozyme, and a larger fibrous protein, fibrinogen.

Lysozyme functions by attacking the peptidoglycan cell wall of Gram-positive *Bacteria* via hydrolysis of the linking glycosidic bond.[72] Lysozyme is regarded as a 'hard' protein due to its ability to resist denaturation and exhibits concentration dependant layer formation.[73] It is positively charged in experimental conditions of pH = 7.4 PBS buffer solution.

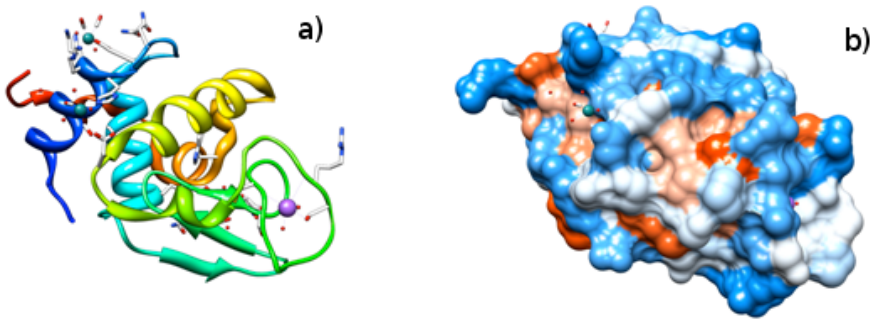

Figure 6 a) The ribbon structure of lysozyme, b) Positively charged lysozyme with hydrophobicity marked, red =hydrophobic region, blue = hydrophilic region (3IJU.pdb).

Fibrinogen is a large and abundant protein found in blood and is a major protein involved in blood coagulation. Fibrinogen is a glycoprotein consisting of two pairs of *N*-linked oligosaccharides. Glycoproteins are not commonly present in bacterial cell surfaces[74,75]. However, S-layer proteins in *Archaea* appear to be glycoproteins, mainly containing *N*-linked glycans with small proportion of *O*-linked glycans attached to threonine residues[76]. Fibrinogen, contrary to lysozyme, has evolved to possess a high surface affinity and adsorbs in a complex multistage process.[77] It is negatively charged in PBS buffer, pH 7.4.

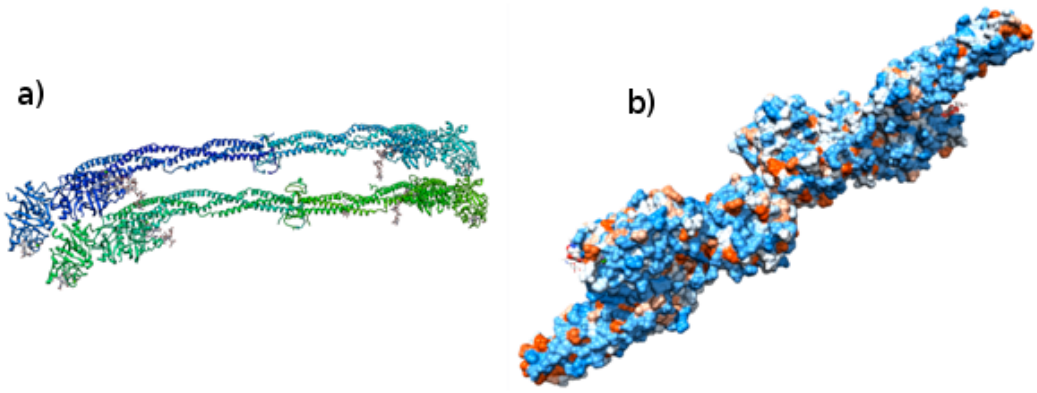

Figure 7 a) The ribbon structure of fibrinogen, b) Positively charged fibrinogen with hydrophobicity marked, red =hydrophobic region, blue = hydrophilic region. (3GHG.pdb).

These two proteins were thus anticipated to provide a good contrast in results. Surfaces which have the ability to resist the above two proteins should be able to resist a wide range of other proteins, for example those responsible for cell attachment to the surface and biofilm formation.

2.3. Hypothesis

In worked carried out by Dilly *et al*. 3,5-diaminopropylmorpholine triazine *N*-oxide found to be similar to triethylene glycol units in resistance to non-specific protein binding.[78]

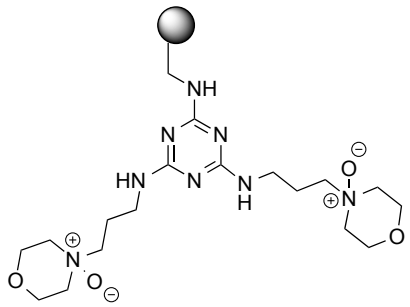

Figure 8 The structure of 3,5-diaminopropylmorpholine triazine *N*-oxide immobilised on Wang polystyrene resin.

In this chapter, the hypothesis[46] that reduction in the number of interfacial hydrogen bond donors might further reduce protein adhesion will be explored, and the extensively studied lysozyme and fibrinogen systems used to enable benchmarking of the new surfaces. For this reason a library of tertiary amines and their corresponding *N*-oxides together with control surface with triethylene glycol was synthesized (Figure 9) and tested against model proteins. Tertiary amine *N*-oxide amphiphiles[79] are known to be useful in manipulating[80,81] and crystallizing membrane proteins,[82] for DNA transfection[83,84] and are widely used in the household and personal care industry,[85] exhibiting reasonably low toxicity and biodegradability. Whilst often

considered to be neutral dipoles,[86] the acid-base behaviour of amphiphilic *N*-oxides is complex[87-89] and it has been suggested that hydrogen-bonded amphoteric pairs exist at micellar interfaces,[87,90] particularly when solution p*H* ≈ pK_a of the *N*-oxide. Furthermore, this class of amphiphiles exhibit both concentration and p*H* dependent pK_a behaviour of the *N*-oxide dipole,[91] [88,90] hence manipulating interfacial pK_a is challenging, but offers routes to the selective control of the binding of proteins and cells.

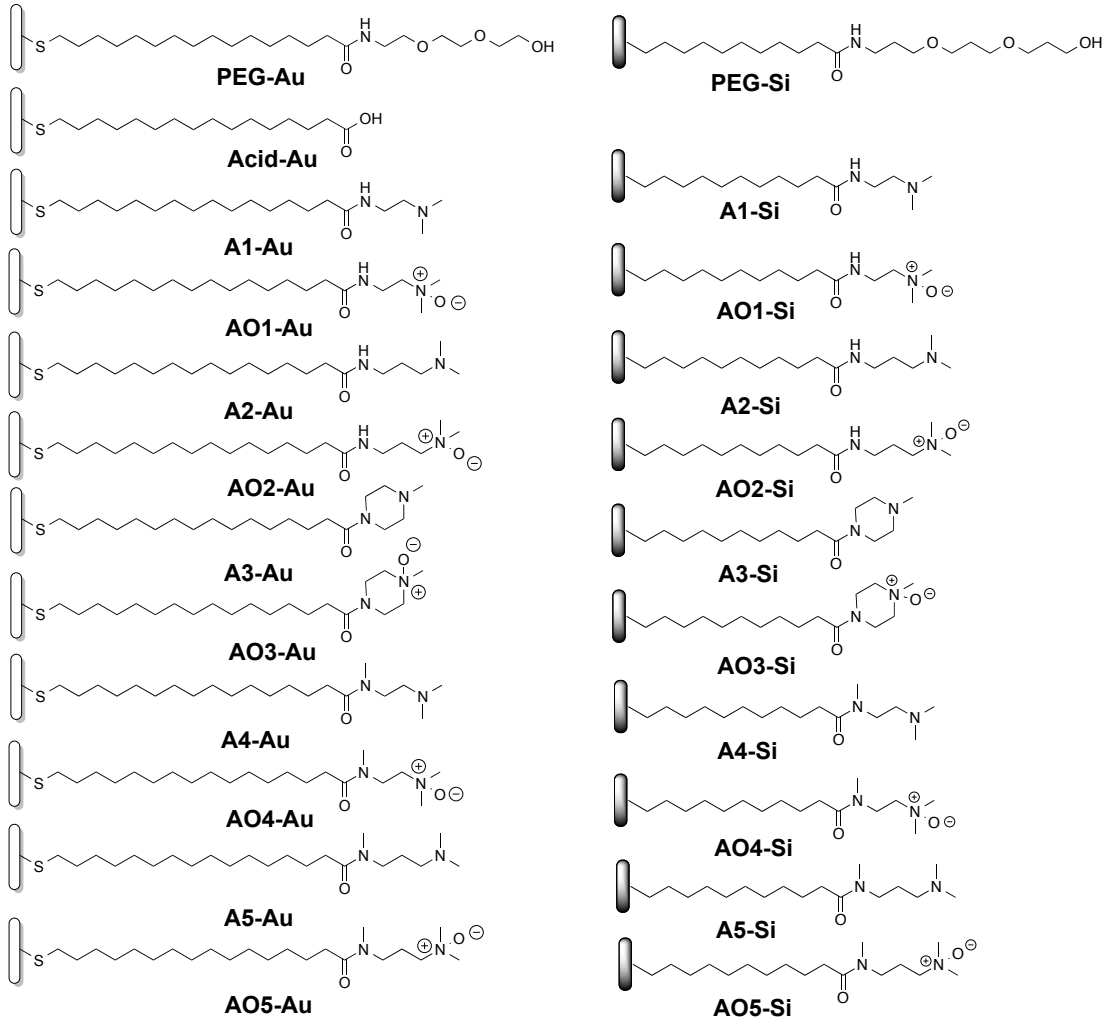

Figure 9 Left column: self assembled monolayers (SAMs) on gold, right column: SAMs on silicon.

The secondary amides are expected to form intermolecular hydrogen bonds to neighbouring molecules or intramolecular hydrogen bond between the NH and *N*-oxide moieties.[92,93] This structural element is absent for the tertiary amides and so together with the larger size of the N-Me(C=O) vs. NH(C=O) group, a more disordered interfacial region should result (Figure 10).

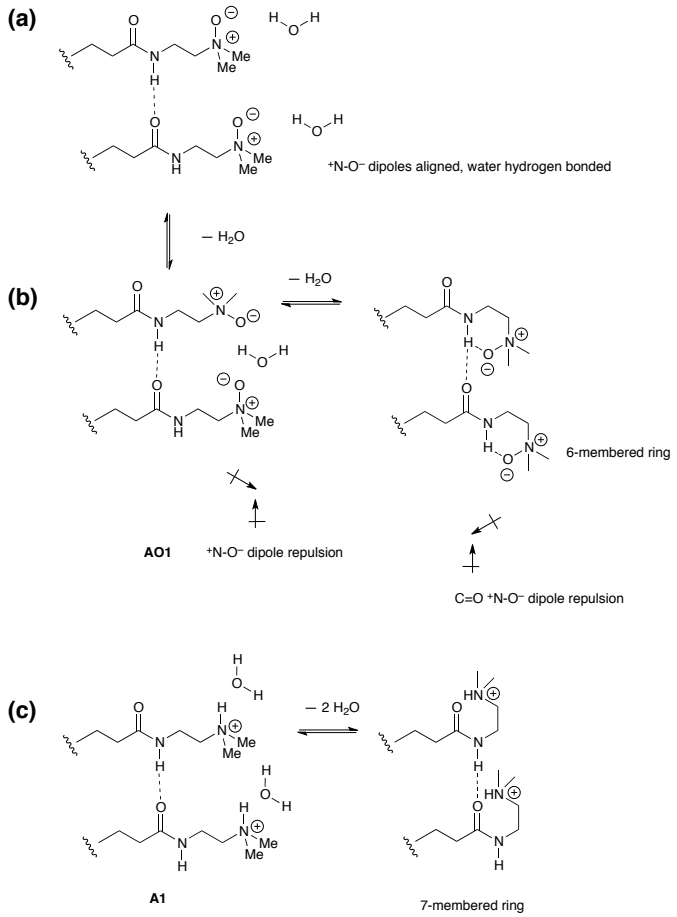

Figure 10 Possible conformations (a) and (b) for tertiary amine oxide **AO1-Au** (6-membered hydrogen bonded ring)[92] and (c) precursor amine **A1-Au** (less favourable 7-membered ring).

2.4. Techniques used for screening of kinetics of protein adsorption and the efficiency of surfaces functionalization

There are a range of techniques typically used to screen surface functionalization and monitor the protein adsorption on the surface.[94] In this research quartz crystal microbalance with dissipation monitoring (QCM-D) is used to measure protein adsorption as a function of time. Water contact angle measurements, ellipsometric thickness and atomic force microscopy will be used to further characterise surfaces and protein adsorption. X-ray photoelectron spectroscopy (XPS) analysis of surface composition will be carried out in order t confirm successful derivatization of SAMs.

2.4.1. Quartz Crystal Microbalance with dissipation monitoring

Quartz crystal microbalance with dissipation monitoring (QCM-D) is capable of measuring the changes in adsorbed mass as well as viscoelastic properties (D-factor) on the surface in nanogram range.[95] The principle of this technique is based on measuring changes in frequency of piezoelectric quartz crystal as material is adsorbed at a metallic interface. The crystal oscillating at its resonant frequency after application of an electric field.[96] Adsorption of protein causes an increase in total oscillating mass that is inversely proportional to frequency. The Sauerbrey equation describes the relationship between mass change of a piezoelectric crystal and frequency.[97]

$$\Delta f = \frac{-2\Delta m f^2}{A(\mu\rho_q)^{0.5}} = -C_f \Delta m$$

Δf = *measured resonance frequency*

A = area between electrodes (cm^2)

f = crystal frequency

Δm = *mass change*

ρ_q = *density of quartz (2.65gcm^{-3})*

μ = *Shear modulus of the crystal (2.95 10^{11} gcm^{-1}s^{-2})*

C_f = *integrated QCM sensitivity factor (17.7 ngcm^{-2})*

2.4.2. Contact Angle Measurements

Contact angle is defined as an angle formed on the solid surface and the tangent of the droplet of chosen liquid.[98] This technique allows investigating the changes in hydrophilicity of the surface.

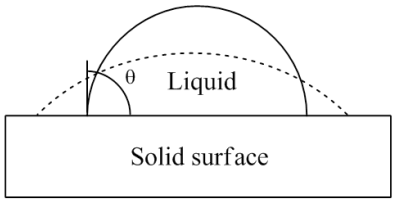

Figure 11 Contact angle between surface and liquid.

There are two possibilities for interaction between a liquid, in this case water and a surface:[99]

- $\Theta > 90$ – water wets the solid (hydrophilic surface)
- $\Theta < 90$ – water does not wet the solid (hydrophobic surface)

The Young equation describes the solid/liquid (*sl)* interface to the solid/vapour *(sv)* and the vapour/liquid *(v/l)* interface.[100]

$$\gamma_{lv} \cos\Theta = \gamma_{sv} - \gamma_{sl}$$

For the appropriate interpretation of the results the phenomenon of contact angle hysteresis has to be taken into consideration[101] A large value of hysteresis between the advancing and receding contact angles occurs when the interface between SAM and water is most disordered suggesting the presence of impurities or uneven structure of surface.[47] It is also very important to apply the appropriate statistical methods to ensure the validity of results. For each set of data contact angles were measured in triplicates and the Wilcoxon signed rank test was applied.[102] This is a nonparametric statistical hypothesis test for the case of many related measurements on a single sample and found to be the most appropriate statistical treatment for contact angle dataset.

2.4.3. Ellipsometry

Ellipsometry is an optical method, which utilizes the change of state of polarized light caused by an adsorbed film on a reflecting surface. The measured parameters can be used to evaluate the refractive index of the film, its thickness and the amount of adsorbed material. The Nanofilm ellipsometer used in this research employed a light source with a linear polarizer (P) and compensator (C) to yield an elliptically polarised beam. After reflection from the sample beam is collected by analyser (A) and imaged by CCD camera.[103]

There are four null conditions corresponding to four different sets of polarizer, compensator and analyser. Depending on the number of positions, ellipsometry can be operated under “one-zone” to “four-zone” nulling procedures. In this research a four-zone nulling measurement was performed and all P, C and A positions as well as corresponding Δ and Ψ angles were recorded.[104]

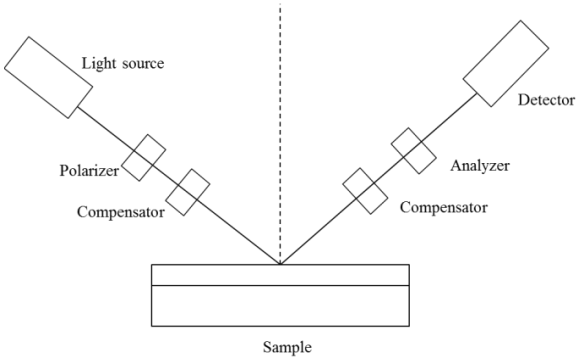

Figure 12 Schematic presentation of ellipsometer.

The basic measurement parameters in ellipsometry are the amplitude tan Ψ and phase shift Δ. The complex reflectance ratio ρ to measure Ψ and Δ is defined as [105]

$$Q = \frac{R_p}{R_s} = \tan\psi i\Delta$$

R_p = reflection coefficient for light polarized and parallel to the plane of incidence

R_s = reflection coefficient for light polarized and perpendicular to the plane of incidence

After acquisition of data, computational modelling is applied. For a sample consisting of a thin film on a substrate the simplest model is "three-layer model". It is built from the ambient, sample film, and the substrate. The following equation describes the relationship between layer thickness and measured angles.[106]

$\rho = \tan\Psi e^{i\Delta} = \rho(N_0, N_1, d, \phi_0, \lambda)$

N_0 = refractive indices of the ambient (1.00)

N_1 = refractive indices of the film (1.45),

d = the layer thickness,

ϕ_0 = *the angle of incidence,*

λ = *the wavelength,*

ρ = *function refers to a three-layer reflection model.*

2.4.4. X-Ray Photoelectron Spectroscopy

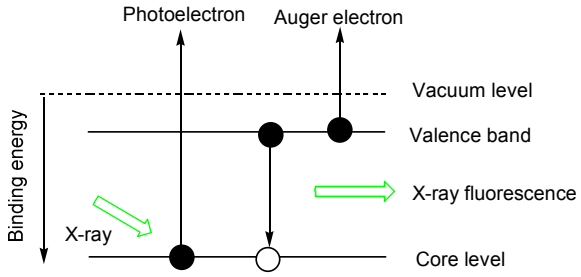

Figure 13 Schematic of XPS principles.

X-ray Photoelectron Spectroscopy (XPS) is a quantitative spectroscopic technique. It measures the average surface composition up to a depth of approximately 5 nm.[107] This technique analyses atomic concentrations and chemical states of elements present at a samples surface. The area of analysis is typically 10 mm^2. XPS uses a soft X-ray source (AlKα or MgKα) to ionise electrons from the surface of a solid sample.[108] The binding energies of these electrons are measured and are characteristic of the elements and associated chemical bonds (chemical state) in the top few atomic layers of the material (Figure 13).

2.4.5. Atomic Force Microscopy

Atomic force microscopy (AFM) is a powerful technique in surface science. It produces a high-resolution three-dimensional topographic image of the surface using a flexible microcantilever arm with a very sharp probe at the end that touches the investigated surface. The deflection of this probe due to surface roughness is detected

by the path change of a laser beam emitted from the upper side of the cantilever to a photodetector. AFM allows investigating the local properties of surfaces as well as the structure of protein deposited on the surface.[109]

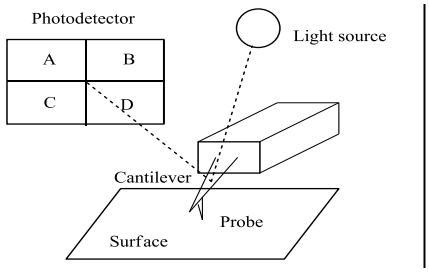

Figure 14 Schematic of AFM measurements.

2.5. Results and Discussion on Gold

2.5.1. Functionalization of gold surfaces

The classic 1-ethyl-3-(3-dimethylaminopropyl)carbodiimide (EDC) peptide coupling method[110] was explored previously both on gold self-assembled monolayers and in solution. Previous work in the Marsh group had shown the water droplet contact angles and ellipsometric thickness of the amide monolayers was sub-optimal.[111] In the preparation of analogues in solution a significant impurity co-eluted with the desired product, identified as the *O*-acyl isourea, or rearranged urea of the coupling reagent and it was not efficient to further use EDC for amide bond formation.[112] Instead of EDC three coupling agents were explored:

(a) HATU, which is a coupling reagent derived from uronium species and has been developed for the coupling reaction due to its efficiency for amide bond formation.

(b) Py-BOP, another effective coupling agent; it is used as substitute to BOP because it does not form a toxic by-product – hexamethylu rea.

(c) isobutyl chloroformate, allows formation of an activated anhydride intermediate. The reaction between this intermediate and the amine generates the desired product. Isobutyl chloroformate is an inexpensive and efficient coupling agent (Scheme 3).

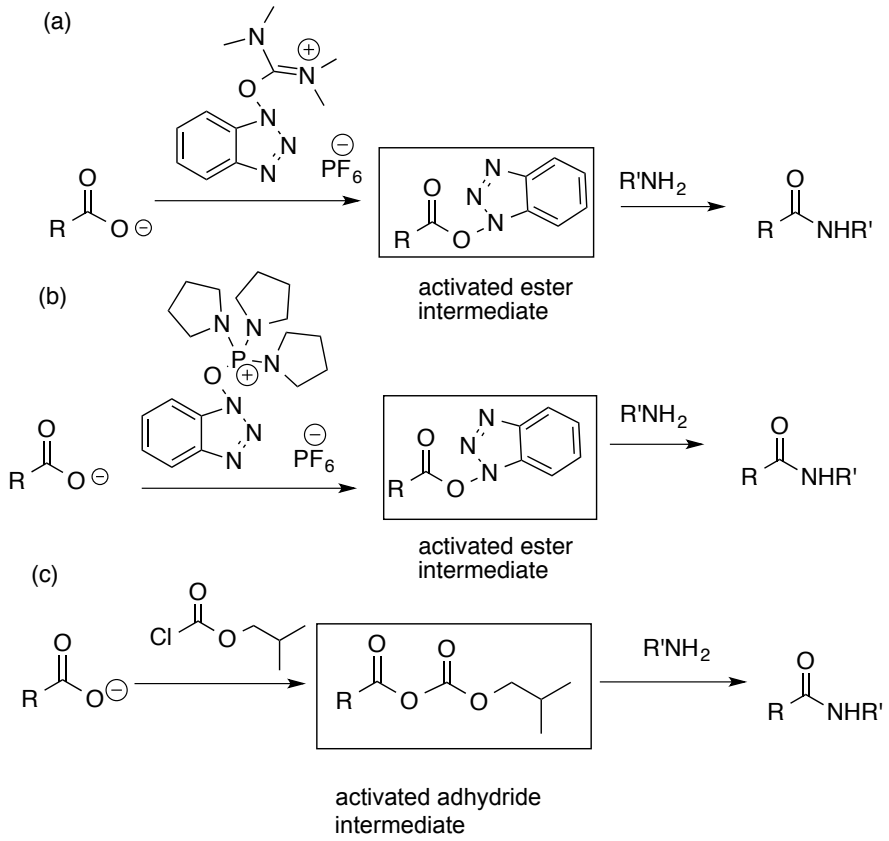

Scheme 3 Schematics of amide bond formation with (a) HATU, (b) PyBOP, (c) isobutyl chloroformate as the coupling agents.

2.5.2. Surface composition

The efficiency of coupling was estimated from survey and high-resolution XPS scans. All XPS measurements were performed in School of Physics, University of Leeds by dr Benjamin Johnson.

(a) **Coupling with HATU**. XPS analyses revealed presence of four elemental species C, N, O and S.

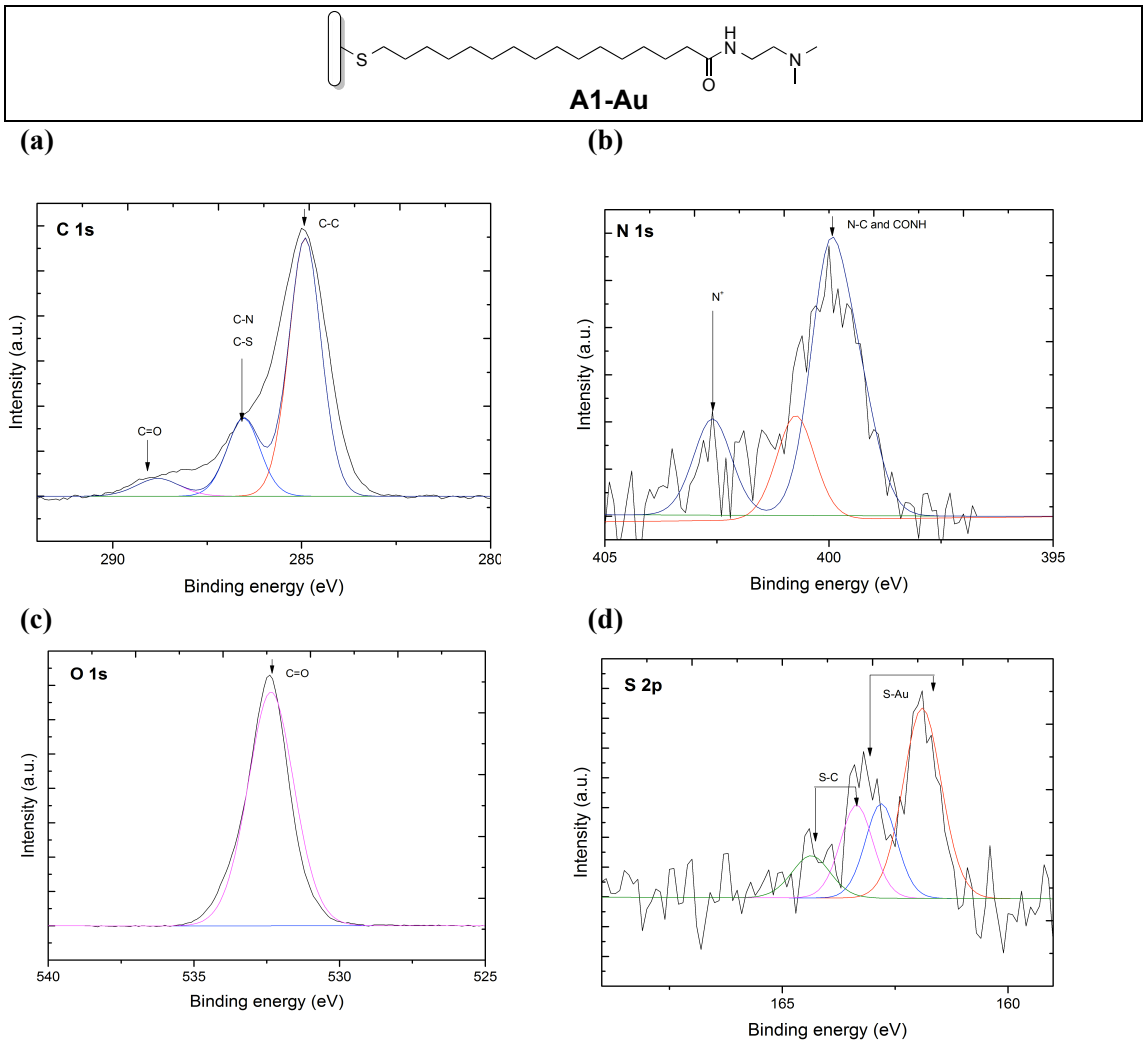

Figure 15 XPS high-resolution spectra of (a) C 1s, (b) N 1s, (c) O 1s, (d) S 2p of **A1-Au** SAM formed by use of HATU coupling agent**.**

High-resolution spectrum (Figure 15a) of C 1s shows three carbon species: a peak at 285.0 eV attributed to C-C bonds,[113] a peak at 286.5 eV corresponding to two binding environments of C-S and C-N.[113] The third smaller peak at 288.8 eV assigned to the carboxylic group.[113] The N 1s spectrum (Figure 15b) shows 399.7 eV signal assigned to C-N bond and 400.1 eV signal attributed to amide (CONH) moiety,[114] indicative of new bond formation. Third peak at 402.6 eV is assigned to protonated tertiary amine (amine coupling performed in solution causes protonation of amine).[114] The O 1s

spectrum (Figure 15c) supports presence of one peak at 532.7 eV assigned to the C=O bond.[113] The S 2p spectrum (Figure 15d) can be deconvoluted into two doublets, one at 162.0 eV (S $2p_{3/4}$) and 163.4 eV (S $2p_{1/2}$), indicating that sulphur is chemisorbed on the gold surface.[115] The second doublet at 163.9 eV and 165.0 eV is assigned to S-C bond from **A1-Au** moiety.[116]

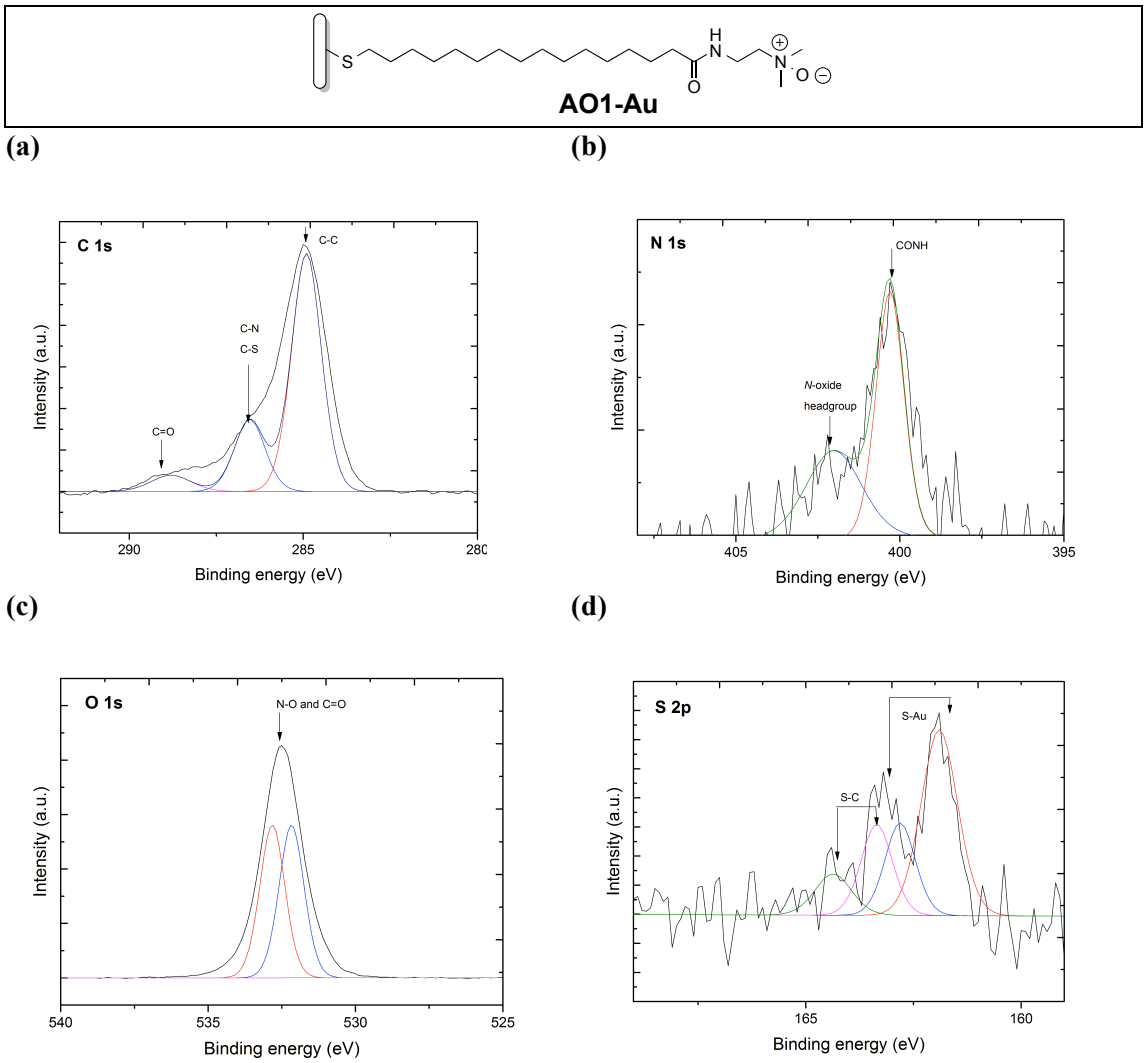

Figure 16 XPS high-resolution spectra of (a) C 1s, (b) N 1s, (c) O 1s, (d) S 2p of **AO1-Au** SAM formed by use of HATU coupling agent**.**

High-resolution spectrum (Figure 16a) of C 1s shows three carbon species: a peak at 285.0 eV attributed to C-C bonds,[113] a peak at 286.7 eV corresponding to two binding environments of C-S and C-N.[113] The third smaller peak at 288.9 eV is assigned to the

carboxylic group.[113] The N 1s spectrum (Figure 16b) shows two nitrogen species significantly different to the N 1s spectrum of **A1-Au,** a peak at 400.1 eV attributed to amide (CONH) moiety[114], indicative of new bond formation. The second broad peak at 402.6 eV is assigned to *N*-oxide headgroup[117] and confirms successful oxidation of tertiary amine. The O 1s spectrum (Figure 16c) shows a peak at 532.1 eV assigned to the C=O[114] and a peak at 533.1 eV attributed to N-O.[118] The S 2p spectrum (Figure 16d) can be deconvoluted into two doublets, one at 162.0 eV (S $2p_{3/4}$) and 163.4 eV (S $2p_{1/2}$), indicating that sulphur is chemisorbed on the gold surface.[115] The second doublet at 163.9 eV and 165.0 eV is assigned to S-C bond from **A1-Au** moiety.[116] The rest of the library of SAMs exhibits similar composition of elemental species (full data presented in Appendix 1).

b) **Coupling with Py-BOP.** Analyses of spectra for surface **A1-Au** and **AO1-Au** revealed our elemental species C, N, S and O.

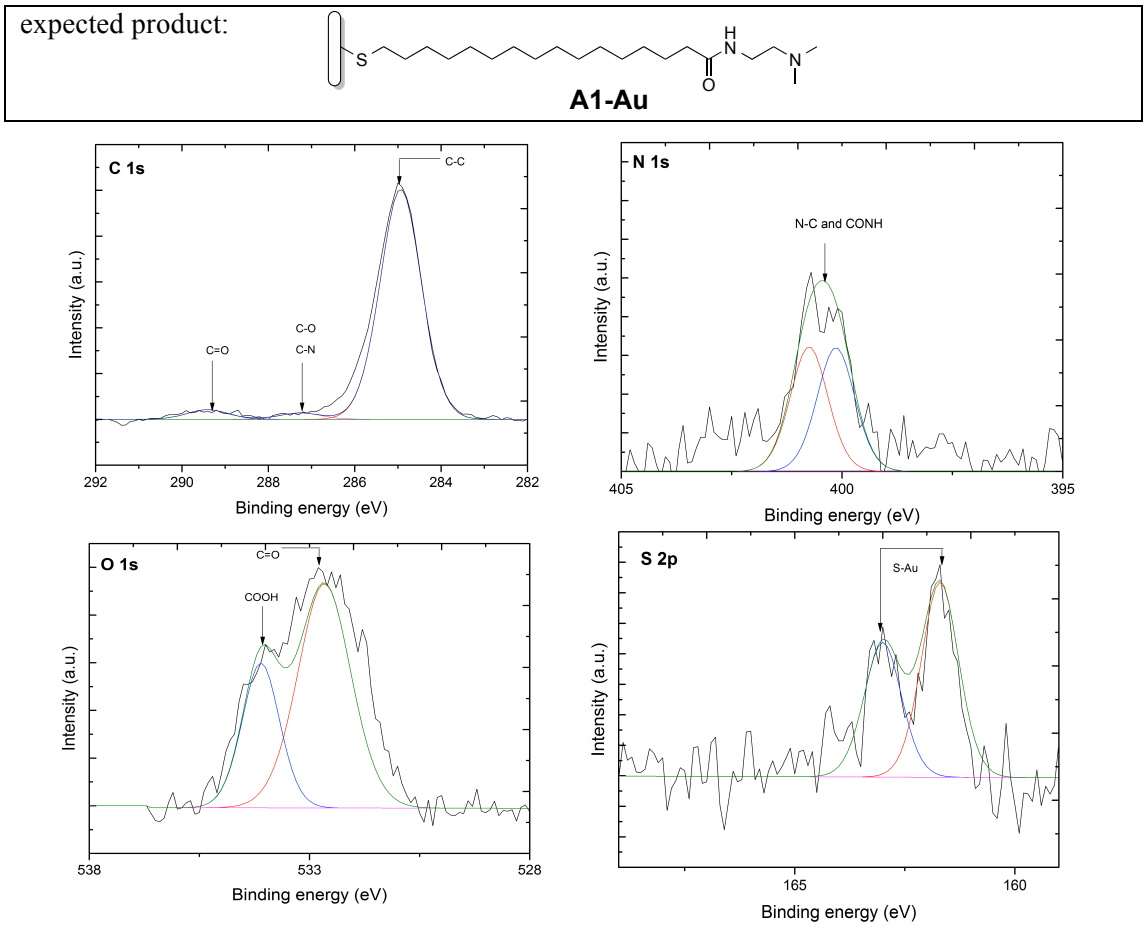

Figure 17 XPS high-resolution spectra of (a) C 1s, (b) N 1s, (c) O 1s, (d) S 2p of **A1-Au** SAM formed by use of Py-BOP coupling agent**.**

High-resolution spectrum (Figure 17a) of C 1s shows three carbon species: a peak at 285.0 eV attributed to C-C bonds,[113] a small peak at 286.7 eV corresponding to two binding environments of C-N and C-O.[113] The third small peak at 288.9 eV is assigned to the carboxylic group.[113] It is important to note that the intensity of peaks at 286.7 eV and 288.9 is very small suggesting that only a small fraction of 16-mercaptohexadecanoic acid was coupled using Py-BOP. The N 1s spectrum (Figure 17b) shows nitrogen species at 399.7 eV and 400.4 eV attributed to N-C and the amide (CONH) moiety respectively,[114] indicative of partial amide bond formation.

The intensity of the N 1s signal is very low due to the inherently small percentage of N in the monolayer confirming poor yield of amide coupling reaction. The O 1s spectrum (Figure 17c) shows two peaks: a peak at 532.7 eV assigned to the COOH group in mercaptohexadecanoic acid[113] and a lower energy species at 532.1 eV corresponding to C=O moiety.[113] The S 2p spectrum (Figure 17d) can be deconvoluted into two one doublet at 162.0 eV (S $2p_{3/4}$) and 163.4 eV (S $2p_{1/2}$), indicating that sulphur is chemisorbed on the gold surface.[115] The second doublet assigned to S-C bond is not present at 163.9 eV and 165.0 eV suggesting unsatisfactory levels of SAM functionalization.

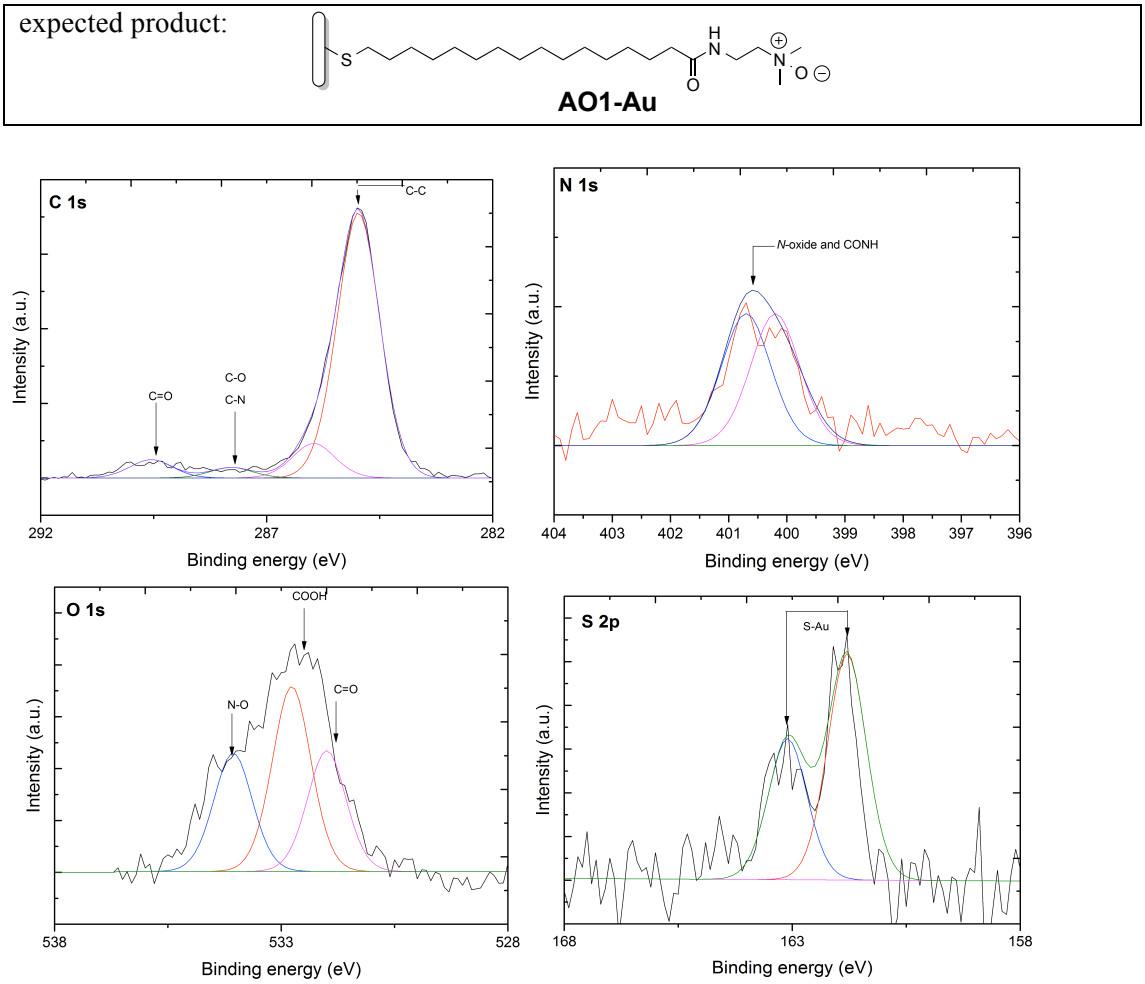

Figure 18 XPS high-resolution spectra of (a) C 1s, (b) N 1s, (c) O 1s, (d) S 2p of **AO1-Au** SAM formed by use of Py-BOP coupling agent**.**

The high-resolution spectrum (Figure 18a) of C 1s shows three carbon species: a peak at 285.0 eV attributed to C-C bonds,[113] a small peak at 286.8 eV corresponding to two binding environments of C-N and C-O.[113] The third small peak at 288.8 eV is assigned to the carboxylic group.[113] It is important to note that the intensity of peaks at 286.8 eV and 288.8 is very small suggesting that only small fraction of 16-mercaptohexadecanoic acid was coupled by Py-BOP. The N 1s spectrum (Figure 18b) shows nitrogen species at 399.5 eV and 400.4 eV attributed to N-C and the amide (CONH) moiety,[114] indicative of partial amide bond formation. The absence of peak at ~403.0 eV[117] indicates that the amine was not oxidized to form corresponding amine *N*-oxide. The O 1s spectrum (Figure 18c) shows three peaks: one at 532.1 eV corresponding to C=O moiety[113], a peak at 532.9 eV attributed to carboxylic groups

of 16-mercaptohexadecanoic acid and a higher energy signal at 533.2 eV assigned to N-O.[118] The high intensity of the peak assigned to COOH suggested high amount of unconverted acid and confirms unsuccessful coupling reaction with PyBOP. The S 2p spectrum (Figure 18d) can be deconvoluted into one doublet at 162.0 eV (S $2p_{3/4}$) and a second at 163.4 eV (S $2p_{1/2}$), indicating that sulphur is chemisorbed on the gold surface[115]. The second doublet assigned to S-C bond is not present at 163.9 eV and 165.0 eV suggesting unsatisfactory levels of SAM functionalization.

The coupling process was much less efficient and this method was eliminated for further investigations.

(c) **Coupling with isobutyl chloroformate.** Visual inspection of surfaces where coupling was attempted with isobutyl chloroformate revealed a relatively thick surface layer inconsistent with a self-assembled monolayer; hence this method was not considered further.

2.5.3. Contact angle measurements

Table 6 shows the wetting properties of the monolayers on gold surfaces, thickness estimated by calculation and measured by ellipsometry. Water wets amine oxides ($\theta(H_2O)$ = 25-30 ± 3º) better than the corresponding amines ($\theta(H_2O)$ = 33-38 ± 3º), due to the lower interfacial energy between the film and water ($\gamma_{s/l}$), attributable to the amine *N*-oxide dipole providing an attractive binding site for water molecules.

Surface	Target structure	Average static contact angle °	Δ*/°	Ellipsometric monolayer thickness (Å) measure/calc
EG-Au	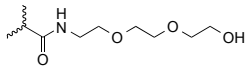	43±2	-	22/23
A1-Au	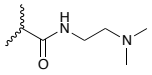	34±3	-	24/ 24
AO1-Au	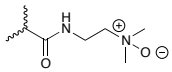	25±2	9	24/24
A2-Au	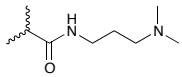	37±6	-	25/26
AO2-Au	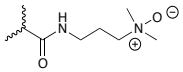	28±4	9	24/24
A3-Au	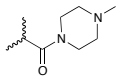	37±4	-	22/24
AO3-Au	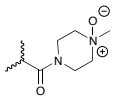	29±3	8	21/23
A4-Au	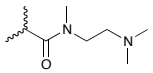	38±2	-	22/25
AO4-Au	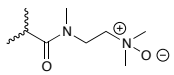	30±2	8	20/23
A5-Au	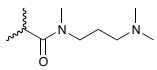	36±3	-	25/25
AO5-Au	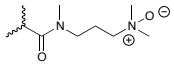	28±2	8	24/24

Table 6 Average static contact angle, ± standard deviation (SD) and the difference (Δ*) between static contact angle for tertiary amines and corresponding amine oxides as well as the thickness of monolayers estimated by calculations and measured by ellipsometry.

Calculated thickness from a molecular mechanics calculation (molecular mechanics force field, MMF gas phase optimised structure, assuming the alkane chain portion is fully extended. The orientation of aliphatic chains of the alkanethiolate was taken to

be ~30° with respect to the normal of the gold surface.[119] The calculated ellipsometric thicknesses are in agreement with measured values for samples **A1-Au**, **AO1-Au**, **AO2-Au**, **A5-Au** and **AO5-Au**, indicating the successful formation of SAMs. For ethylene glycol (**EG-Au**), **A2-Au**, **A2-Au, A3-Au, AO3-Au, A4, AO4-Au** surfaces calculated thickness is higher than measured value. This difference is caused by differences in the chain tilt and the density of SAM.[20] The average contact angle (43 ± 2°) for **EG-Au** surface is slightly higher that reported in the literature (38 ± 1°)[120], this difference could be caused by different roughness of the underlying gold used for SAM formation.

2.5.2. QCM-D measurement of protein adhesion

The degree of protein adhesion to any surface depends upon variables including most importantly, the nature of the protein(s), presence of molecules such as lipids, denaturants or other osmolytes,[121] and temperature. Four measures (i) – (iv) were taken when assessing to what extent a surface is resistant to any class of adhering protein (**Figure 19**).

(a)

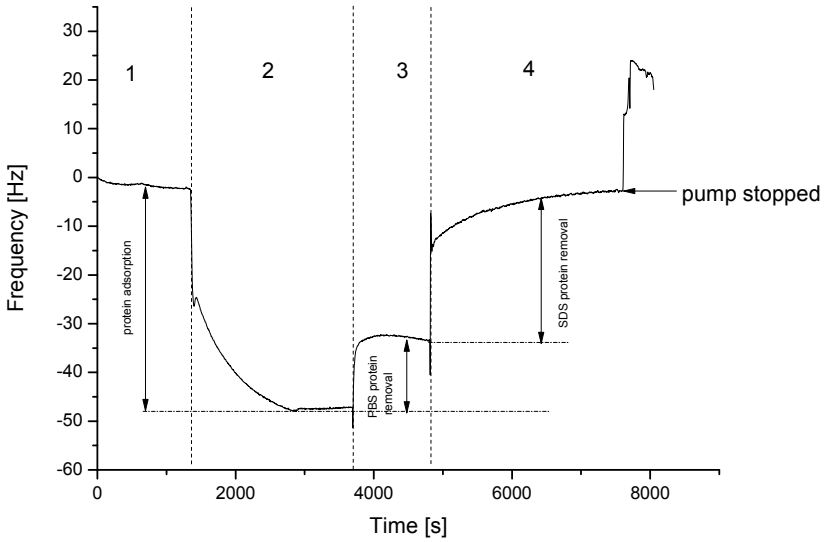

(b)

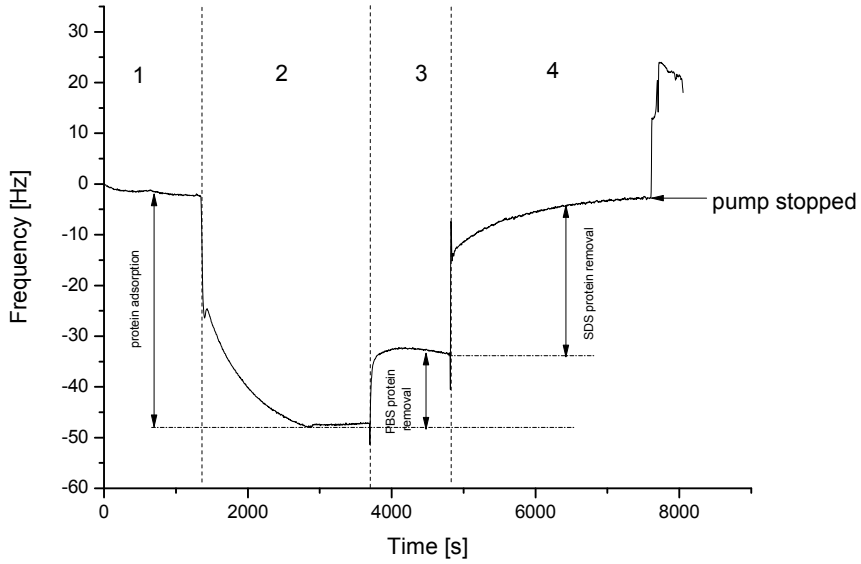

Figure 19 QCM graph shows (i) How much protein becomes adsorbed on the surface (**step 2**); (ii) how much protein is removed after rinsing with PBS buffer solution, pH = 7.4 (**step 3**) hence (iii) the total amount of protein that remains and (iv) whether

any protein remains after rinsing with a more stringent surfactant, sodium dodecylsulfate (**step 4**).

Figure 19a shows kinetic adsorption of 1 mM lysozyme in PBS buffer and Figure 19b describes kinetic adsorption of 1 μM fibrinogen in PBS buffer..

Change in frequency for adsorption of both proteins (step 2 – black column) and for the amount of proteins remaining on surfaces after wash with PBS buffer (step 3 – white column) was presented as stacked columns in order to compare QCM data for the whole library of SAMs.

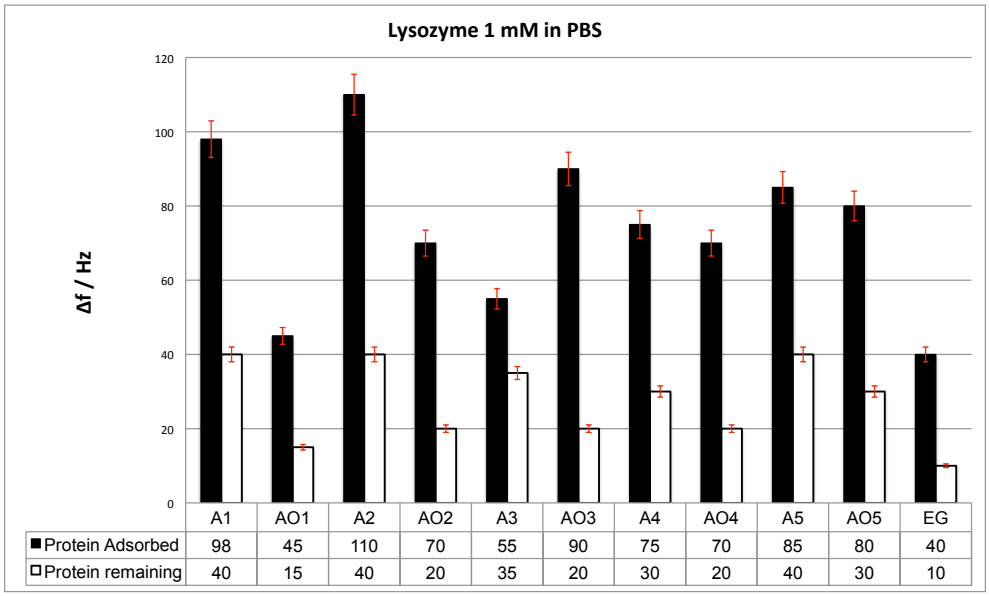

	A1	AO1	A2	AO2	A3	AO3	A4	AO4	A5	AO5	EG
■Protein Adsorbed	98	45	110	70	55	90	75	70	85	80	40
□Protein remaining	40	15	40	20	35	20	30	20	40	30	10

Chart 1 Adsorption (black) of lysozyme (1 mM) and amount of protein remaining (white) on surfaces after rinsing with PBS buffer. Error bars represent standard deviation of the mean for each surface.

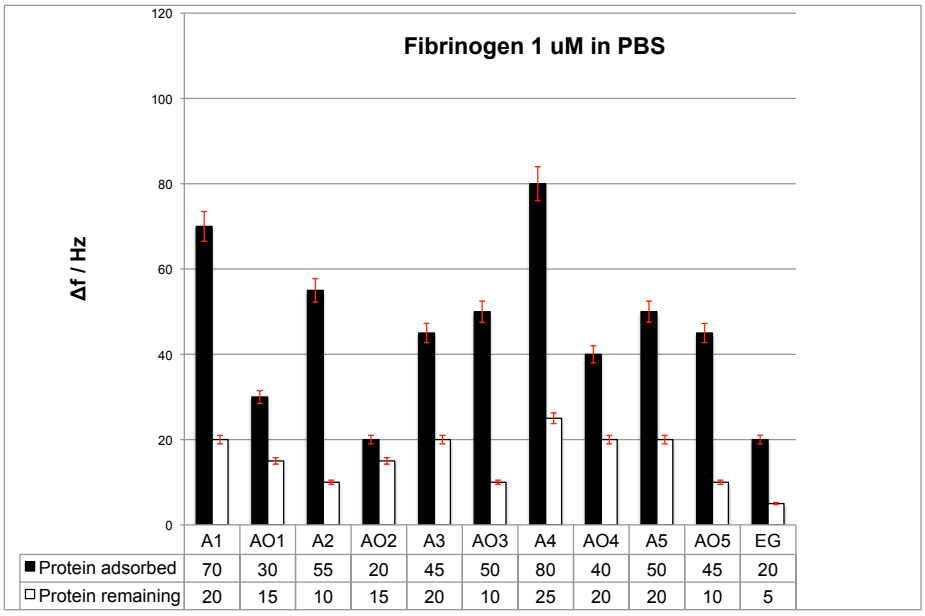

Chart 2 Adsorption (black) of fibrinogen (1 mM) and amount of protein remaining (white) on surfaces after rinsing with PBS buffer. Error bars represent standard deviation of the mean for each surface.

The first point to note in comparing data between each protein set (Chart 1 and Chart 2) is that the concentration of fibrinogen (a hydrophobic fibrous protein carrying overall anionic charge, but with key cationic residues implicated in aggregation processes)[122] is one thousand-fold less than lysozyme (a globular protein bearing surface cationic charge at pH=7.4)[123,124] indicating the nature and concentration[122,125,126] of the protein itself has by far the greatest effect on adsorption. The QCM-D data also show (Figure 19, full data in Appendix 3) that the tertiary amines adsorb both lysozyme and fibrinogen in what appears to be a two-step process leading to multilayers also consistent with significant unfolding of the protein on the more adhesive surface.[127] For better understanding of the changes in adsorption kinetics, the protein coverage per cm^2 was calculated using Saubrey equation.

Sample	Coverage [ng cm^{-2}] for surface + lysozyme (1 mM PBS)	Coverage [ng cm^{-2}] for surface + fibrinogen (1mM PBS)
A1-Au	578	413
AO1-Au	266	177
A2-Au	649	324.5
AO2-Au	413	118
A3-Au	324	265.5
AO3-Au	531	295
A4-Au	442	472
AO4-Au	413	236
A5-Au	502	295
AO5-Au	472	265.5
EG-Au	130	218

Table 7 Summary of QCM estimated protein coverage [ng cm^{-2}] for lysozyme (1 mM PBS) and fibrinogen (1μM PBS) calculated using the Sauerbrey equation: $\Delta m = -C\Delta f n^{-1}$, where:

C – 17.7 ng Hz^{-1}cm^{-2} for a 5 MHz quartz crystal, Δf – change in frequency (raw data), n – overtone number. Number of replicates or measurements = 3.

The surfaces most resistant to lysozyme adhesion are **PEG-Au** and dimethylamine *N*-oxide **AO1-Au**, displaying similar properties for fibrinogen, wherein dimethylamine *N*-oxides **AO1-Au** and **AO2-Au**, are at least as effective as the established triethylene glycol. Direct comparisons of the latter ought strictly to take account of the number of ethylene glycol units. Thus, measured per functional group, tertiary amine *N*-oxide **AO1-Au** is more effective than **PEG-Au** at resisting adhesion of the two test proteins, indicating that polymeric analogues (*cf.* Yang *et al.*[15]) are worth investigating. Whilst hydrated oligoethyleneglycol self-assembled monolayers are known to adopt gauche and helical conformations,[128-130] the detailed behaviour of amine *N*-oxides such as **AO1-AO5-Au**, is less well precedent, especially in monolayer form. Amine *N*-oxides

are recognized to stabilize cyclic structures when included in peptides, for example as proline *N*-oxide,[92,93] and TMAO has been shown to preferentially orient its methyl groups away from hydrophobic interfaces, indicating that the methyl groups are relatively polarized.[131]

2.5.3. Atomic force microscopy (full data in Appendix 2)

AFM (Figure 20) was used to image the SAMs after exposure to either a solution of lysozyme or fibrinogen for 15 min. AFM imaging was performed by dr Helena Stec in the Department of Chemistry, University of Warwick. The results show that amine *N*-oxide **AO1-Au** surface exhibits a smoother appearance with what appear to be small clusters of protein (seen in white, Figure 20(d)), very different in nature from lysozyme adsorbed on bare gold (control experiment, Figure 20(b)) or on the tertiary amine (Figure 20(c)). Lysozyme is ellipsoidal in solution with dimension 2.5 x 2.5 x 6 nm,[132] but if the protein partly unfolds,[127,133,134] especially in proximity with a surface, aggregates result.[135] These are clearly distinct from the spherical clusters on **AO1-Au** (Figure 20(d)), **AO2-Au** (Figure 21(b)) or **AO3-Au** (Figure 22(b)). The image of lysozyme on bare gold is intriguing: despite a relatively low change in QCM-D frequency for either lysozyme or fibrinogen, it has striking similarity to that for a nascent multilayer seen in Figures 18(f), 18(g) in the publication by Kim, Blanch and Radke.[136] The smoother appearance of the surface bearing isolated lysozyme clusters on *e.g.* **AO1-Au** (Figure 20(d)) is thus striking, supportive of a mechanism of clustering taking place after deposition as suggested by those authors. The protein on **AO1-Au** (Figure 20(d)) may plausibly be less denatured than that for **A1-Au** (Figure 20(c)), noting that charge-repulsion along the lysozyme polypeptide (expected to be more significant upon a charged amine, rather than neutral amine *N*-oxide surface) has been postulated as central to assembly processes.[137] The surface that adsorbed

least lysozyme **EG-Au** (Figure 23) shows much greater similarity to the amine oxides such as **AO1-Au** and **AO2-Au** under AFM imaging.

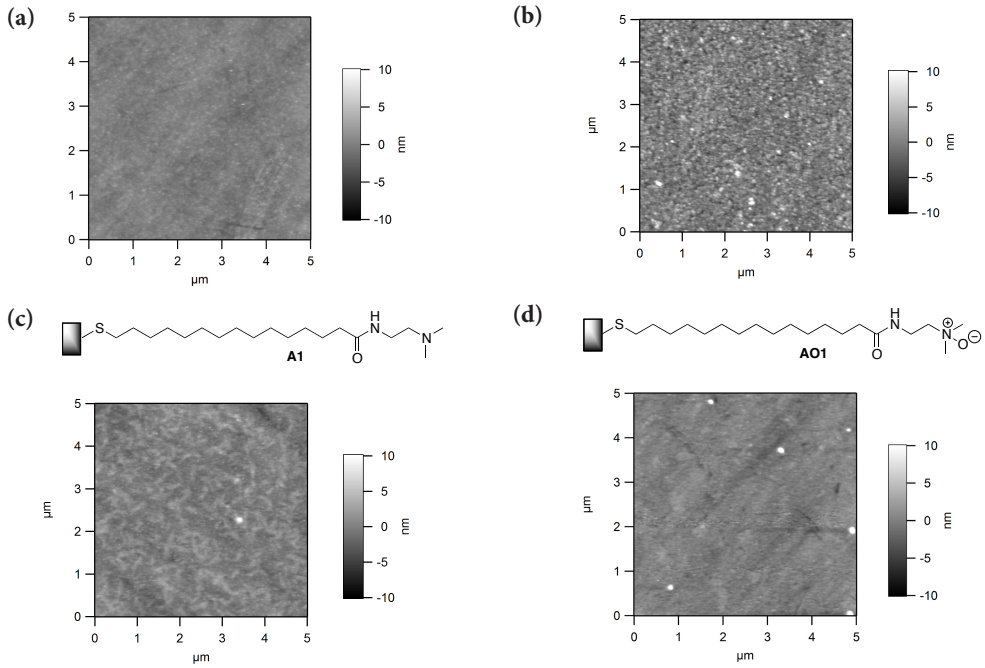

Figure 20 AFM images of: (a) bare gold QCM-D sensor; (b) plus lysozyme, 1 mM in PBS; (c) N-[2'-(dimethylamino)ethyl]mercaptohexadecanoic amide plus lysozyme, 1 mM in PBS; (d) N-[2'-(dimethylamino-N-oxide)ethyl]mercaptohexadecanoic amide self-assembled monolayer plus lysozyme 1 mM in PBS.

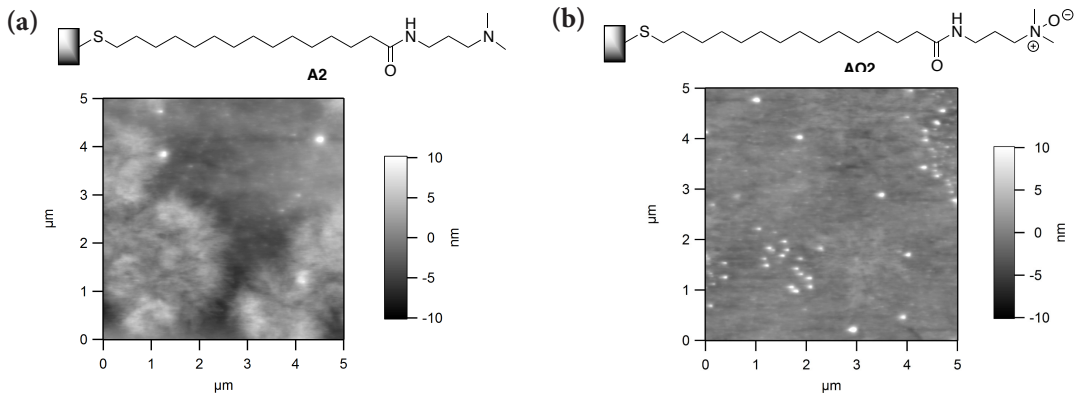

Figure 21 AFM images of: (a) N-[2'-(dimethylamino)propyl]mercaptohexadecanoic amide plus lysozyme, 1 mM in PBS; (b) N-[2'-(dimethylamino-N-oxide)propyl]mercaptohexadecanoic amide self-assembled monolayer plus lysozyme 1 mM in PBS.

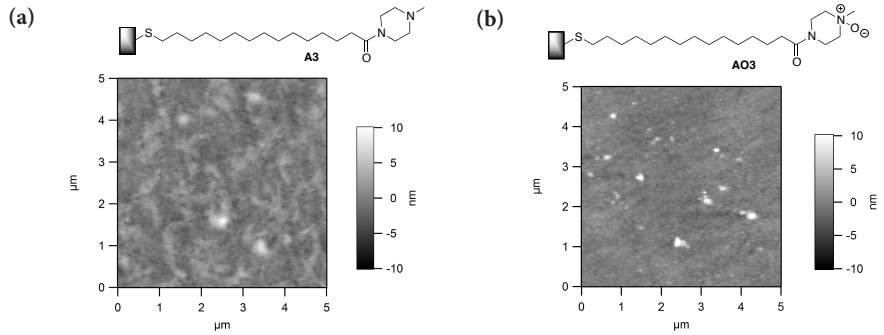

Figure 22 AFM images of: (a) 1-(4'-methylpiperazin-1'-yl-4'-amine)mercaptohexadecanoic amide self-assembled monolayer plus lysozyme, 1 mM in PBS; (b) 1-(4'-methylpiperazin-1'-yl-4'-amine-N-oxide)mercaptohexadecanoic amide plus lysozyme, 1 mM in PBS.

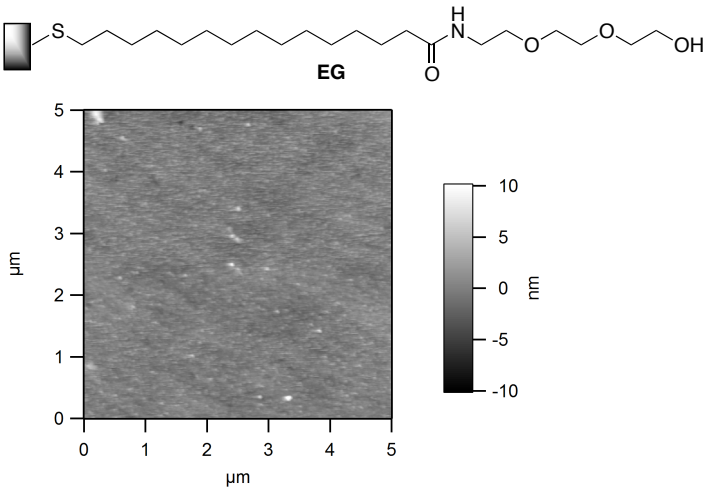

Figure 23 AFM image of N-2-2-2-hydroxyethoxy ethoxy ethyl-16- methylsulfanyl hexadecanamide self-assembled monolayer plus lysozyme, 1 mM in PBS.

In this work, the headgroup best resisting adsorption of either protein, and removal by PBS washing, **AO1-Au** ought to be able to form an unstrained 6-membered ring between NH and N-O dipole.[92] Intermolecular hydrogen bonding between amides remains possible, but repulsive dipolar interactions with the neighbouring amide might also result, adding beneficial disorder to the surface.[138] In comparison, the protonated amine **A1** probably forms a less favoured 7-membered ring, leading to a preference for a more regular, extended, rather than gauche conformation in the headgroup. Calculations based on work by Hunter[139] were performed to check the feasibility of the hypothesis.

2.5.4. Computational modeling of the head group

Calculations based on empirical equation (1) have been carried out to identify preferred hydrogen bond for amine and amine oxide headgroups.[140] Code written in Matlab® is shown in Appendix 4. Three different cases were taken into consideration:

(a) Intramolecular bond formation between amide bond hydrogen and methyl group hydrogen from the head group;

(b) Intermolecular bond formation between hydrogen in methyl group from the head group and hydrogen from water;

(c) Intermolecular bond formation between amine oxide and hydrogen atom donor in water;

(1) $\Delta\Delta G_{H\text{-}bond} = -(\alpha\beta+\alpha_s\beta_s)+(\alpha\beta_s+\alpha_s\beta)-(\alpha-\alpha_s)(\beta-\beta_s)+6$ kJ mol^{-1}

The results showed that the mostly likely hydrogen bond is estimated to form between amine oxides and water (c) with Gibbs free energy of -39.1 kJ/mol. Whilst high, this value is not out of line with medium – strong hydrogen bonds. Amine oxide binds a molecule of water to form a 6 membered ring. These hypotheses might be further explored experimentally by sum frequency generation (SFG) spectroscopy[141] and neutron diffraction.[142]

H-BOND TYPE	**$\Delta G_{H\text{-}bond}$ [kJ/mol]**
Intermolecular H-bond	
(a) amide – amine oxide	11.21
Intramolecular H-bond	
(b) amine-water	2.61
(c) amine oxide -water	-39.1

Table 8 Estimated strengths of hydrogen bonds using a free energy relationship method.

2.5.5. Summary

Preventing intra- or intermolecular H-bond formation in **AO4-Au** gives a surface that is somewhat more prone to deposition of both positively charged lysozyme and the more hydrophobic fibrinogen, although the ability of both proteins to be removed by PBS rinse remains less affected. Hence *N*-methylation, or removal of an N–H donor[46] through *N*-methylpiperazine formation, has a smaller effect on protein behaviour than *N*-oxidation itself. The excellent hydrogen bond acceptor ability of the N-O dipole[139,143] is therefore sufficient to explain the differences in contact angle, and enhanced protein resistance of amine oxides over the corresponding tertiary amines. There is nonetheless scope for optimization of the oxidation process to ensure that the monolayer integrity is unaffected, or to use preformed alkylamine *N*-oxides grafted to silicon wafers as described in the following section.

2.6. Results and Discussion on Silicon [111]

2.6.1. Functionalization of silicon wafers

A representative set of ω-alkene substituted tertiary amines **A1** - **A5-Si** (**Scheme 4**) were initially prepared by coupling undecenoic acid with primary or secondary amines using isobutyl chloroformate.[144] In the case of compounds **A3-Si, A4-Si, A5-Si**, the presence of isobutyl chloroformate-derived impurities led to use of a classic acyl chloride intermediate.[145,146]

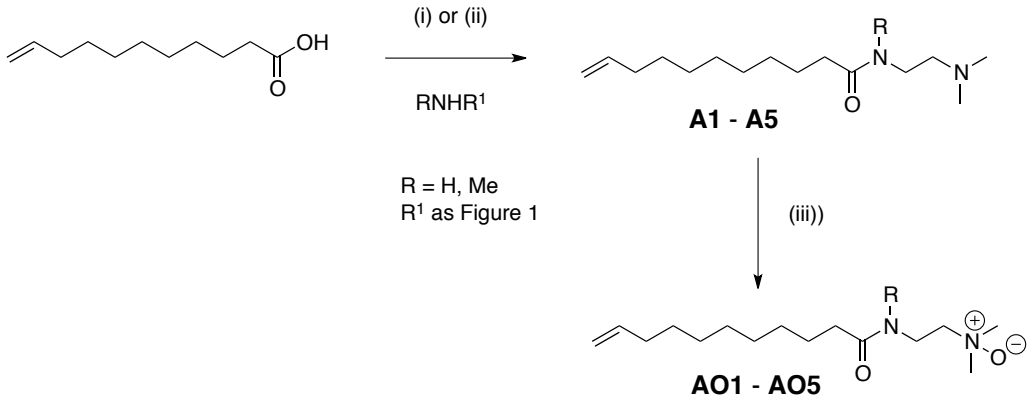

Scheme 4 Reagents and conditions: (i) isobutyl chloroformate, N-methylmorpholine, tetrahydrofuran, 0 °C; (ii) thionyl chloride, dimethylformamide, CH_2Cl_2, r.t.; (iii) m-CPBA, K_2CO_3, CH_2Cl_2, -78°C, then limonene -78 °C.

Removal of excess peroxide has been previously achieved[147] by bubbling 2-methylpropene for a few minutes at -78 °C, although the use of limonene as a sacrificial electron-rich alkene [148,149] is here found to be a more easily conducted method with improved yield.

The product amine *N*-oxides displayed significant downfield ^{1}H NMR chemical shifts for those protons adjacent to this potent dipole. In the case of *N*-methyl piperazine adduct **AO3-Si** the chemical shifts of individual axial and equatorial protons were especially dramatic, moving from amine $H^{2'}$, $H^{2''}$ $\delta = 3.61$ to exhibiting separate signals for axial protons $H^{2''}$ and $H^{2'}$ at $\delta = 4.04$ and 4.51 ppm respectively,

presumably due to desymmetrization of the 6-membered heterocycle by the preferred conformation of the amide carbonyl (Figure 24).

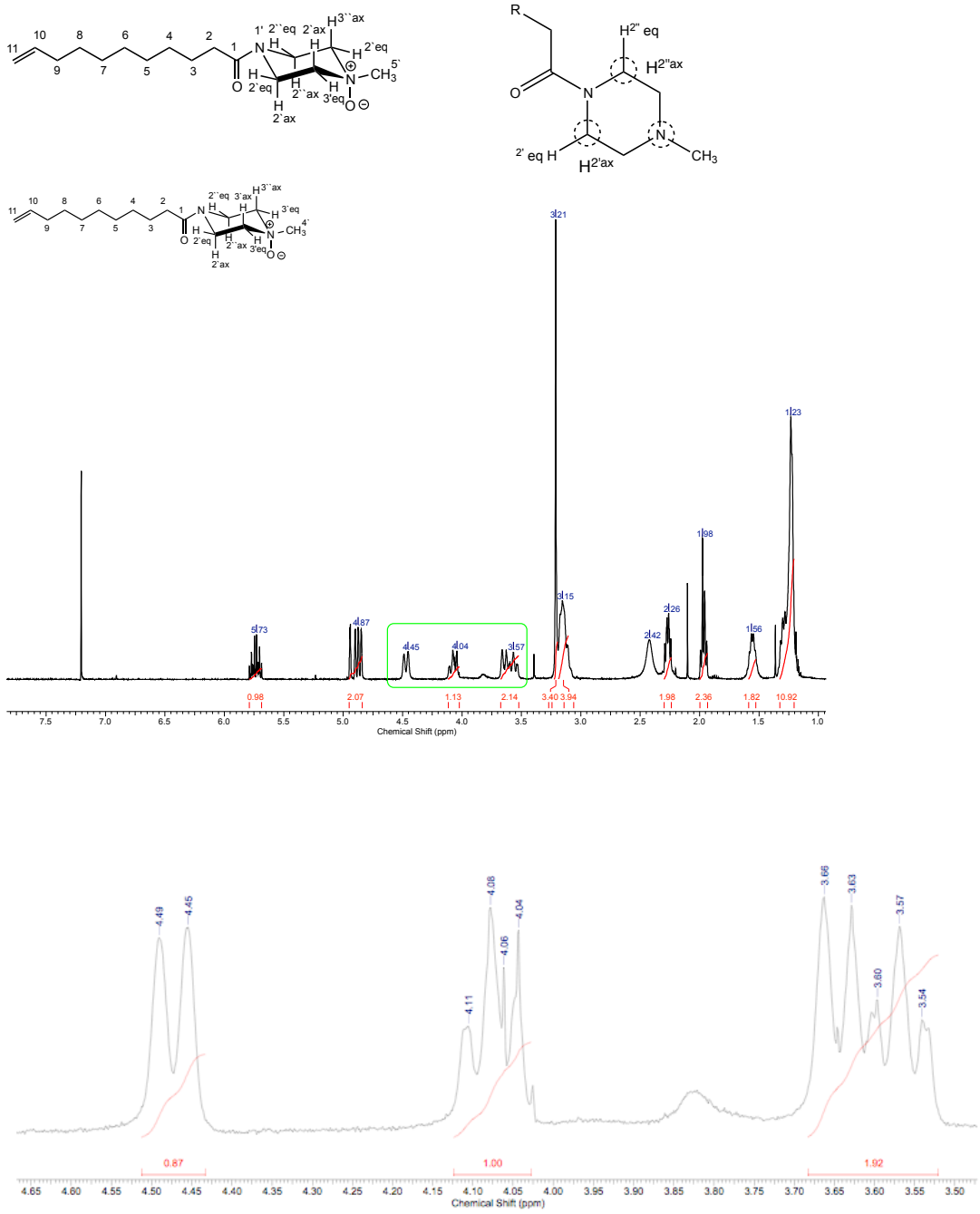

Figure 24 ^{1}H NMR spectrum recorded for 1-(4'-methylpiperazin-1'-yl-4'-amine *N*-oxide) undec-10-en-1'-one **AO3** with axial and equatorial protons.

2.6.2. Tensiometry measurements

To determine the behaviour of the amphiphilic tertiary amines in solution, all surfaces were analysed by tensiometry and a graph of surface tension versus log (concentration), (Appendix 5) enabled the critical aggregation concentration (CAC) for compounds **A1** – **A5** –Si to be determined (**Table 9**).

Amines	**A1**	**A2**	**A3**	**A4**	**A5**
CAC (mM)	4.99	4.55	5.77	4.81	3.98

Table 9 Critical aggregation concentrations for amines **A1** – **A5-Si**.

This measurement is important, because amphoteric amine oxides could be potentially used on supporting materials in anaerobic digesters. Unfortunately, it was impossible to identify the critical aggregation concentration due to high solubility of amine oxides **AO1-AO5-Si** in water.

2.6.3. Surface composition

Functionalization of SAMs via radical chain reaction using hydrogen terminated silicon and amide-coupled alkenes inhibits oxidation of the underlying silicon and enhances monolayer stability.[150] Both series of amphiphiles, the tertiary amines and their cognate *N*-oxides had been immobilized on the freshly prepared silicon hydride terminated wafers. X-ray photoelectron spectroscopy was carried out in the Department of Physics at University of Leeds by dr Benjamin Johnson in order to assess the quality of silicon SAMs.

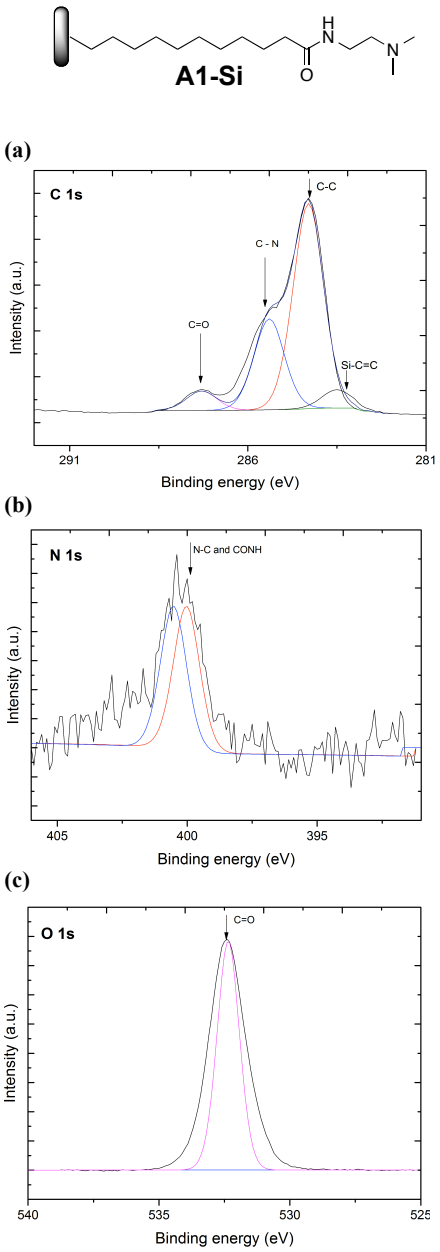

Figure 25 High-resolution C 1 s (a) and N 1s (b) and O 1s (c) XPS spectrographs for amine **A1-Si SAM**.

XPS narrow scan of C 1s spectrum (Figure 25a) shows four elemental species: predominant aliphatic chain carbon peak at 285.1 eV,[151] a signal at 286.4 eV corresponding to C-N bonded carbon,[115] a signal at 289.1 eV assigned as C=O moiety and small peak at 284.4 eV attributed to the carbon atom directly bound to the silicon surface.[152] The N 1s spectrum (Figure 25b) can be deconvoluted into one peak:

assigned to two binding environments: the sp^3 nitrogen[153] at 400.9 eV a signal at 401.8 eV assigned to amide moiety.[154] The O 1s spectrum (Figure 25c) shows one peak at 532.1 eV attributed to C=O bonds.[113]

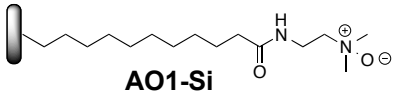

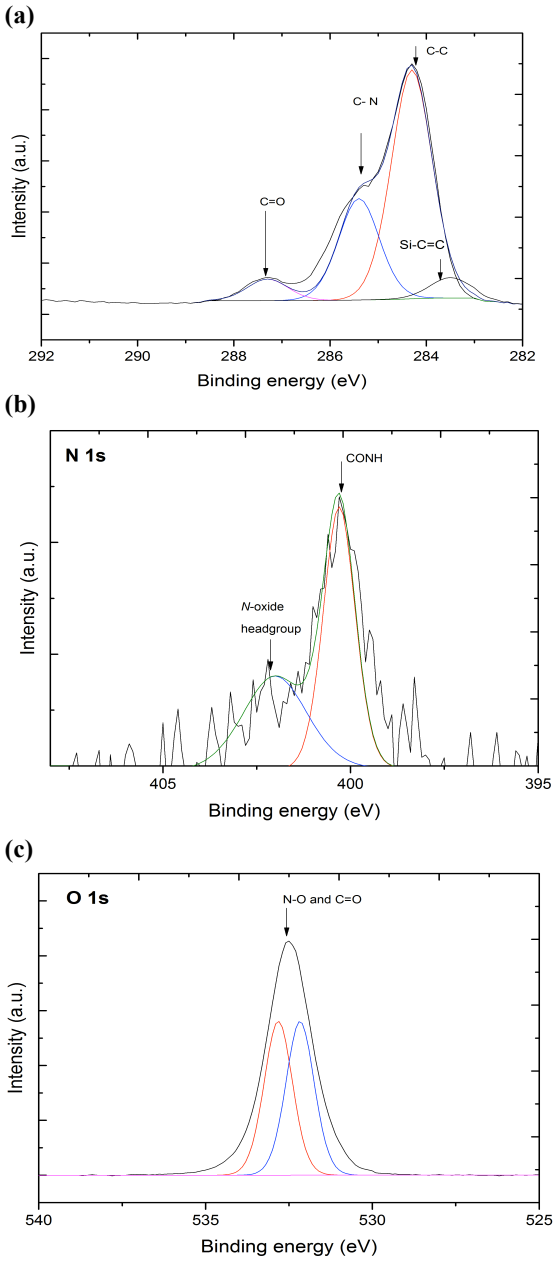

Figure 26 High-resolution C 1 s (a) and N 1s (b) and O 1s (c) XPS spectrographs for amine **AO1-Si SAM**.

XPS narrow scan of C 1s spectrum (Figure 26a) shows four elemental species: predominant aliphatic chain carbon peak at 285.0 eV,[151] a signal at 286.5 eV corresponding to C-N bonded carbon,[115] a signal at 289.0 eV assigned as C=O moiety and a signal at 284.5 eV attributed to Si-C. The N 1s spectrum (Figure 26b) can be deconvoluted into two peaks: a peak at 399.7 eV assigned to CONH and a peak at 402.6 eV attributed to *N*-oxide moiety[117] The O 1s spectrum (Figure 26c) shows a peak at 532.1 eV attributed to C=O and a peak at 533.1 eV corresponding to N-O.[118] (full data set in Appendix 6).

Elemental composition was calculated from high-resolution XPS spectra using CasaXPS software package and compared with the expected carbon to nitrogen (C:N) ratios to estimate the accuracy of surface functionalization. The measured values are in good agreement with calculated data. C:N ratios for **A1-Si**, **AO1-Si**, **A2-Si**, **A3-Si** and **AO5-Si** are slightly higher than expected due to adventitious carbon contamination that contributes strongly to the aliphatic peak C 1s (caused by the impurities present in adsorbents or the fact that an experiment has not been carried out in a clean room). The EG SAM exhibits lower than expected C/N ratio. This result is likely due to the oxidative degradation of EG chains during SAM functionalization.

Surface	XPS C 1s/ N 1s	
	expected	**measured**
EG	19:1	16:1
A1	15:2	18:2
AO1	15:2	16:2
A2	16:2	18:2
AO2	16:2	16:2
A3	16:2	16:2
AO3	16:2	16:2
A4	16:2	16:2
AO4	16:2	16:2
A5	17:2	16:2
AO5	17:2	22:2

Table 10 Calculated and XPS determined C:N ratios.

2.6.4. Properties of the silicon surfaces – contact angle data.

All the surfaces were examined by water droplet contact angle measurements performed in triplicate (Table 11). Water wets amine oxides (θH_20 = 49-43°) better than the corresponding amines (θH_20 = 53-58°). The decrease in contact angles after oxidation of tertiary amines was observed for identical functional groups immobilized on gold.[117] Water static contact angles on gold were lower than contact angles recorded on silicon. This change could be caused by the difference in the density of SAMs since it is known that monolayers on silicon do not exhibit the same level of order observed for thiol-based monolayers on gold surfaces.[20]

Surface	Target structure	Average static contact angle °	Δ/°
A1-Si	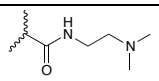	58±2	-
AO1-Si	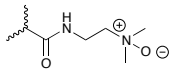	43±3	15
A2-Si	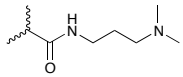	55±2	-
AO2-Si	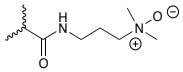	46±2	9
A3-Si	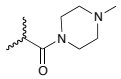	51±2	-
AO3-Si	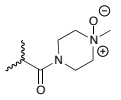	49±2	2
A4-Si	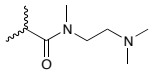	57±3	-
AO4-Si	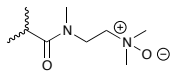	49±2	8
A5-Si	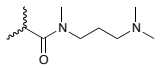	53±2	-
AO5-Si	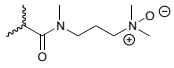	43±2	10

Table 11 Average static contact angle, ± standard deviation (SD) and the difference between contact angles measured before and after the oxidation process (Δ) for tertiary amines and corresponding amine oxides representing change in hydrophilicity measured for functionalized silicon wafers.

The library on SAMs immobilized on gold allow the real-time study of protein adsorption processes (for example by quartz crystal microbalance or similar methods),[155] etching of silicon damages the piezoelectric crystals hence this method has not been used.

The change of surface properties and the influence of protein on wettability was investigated by contact angles.

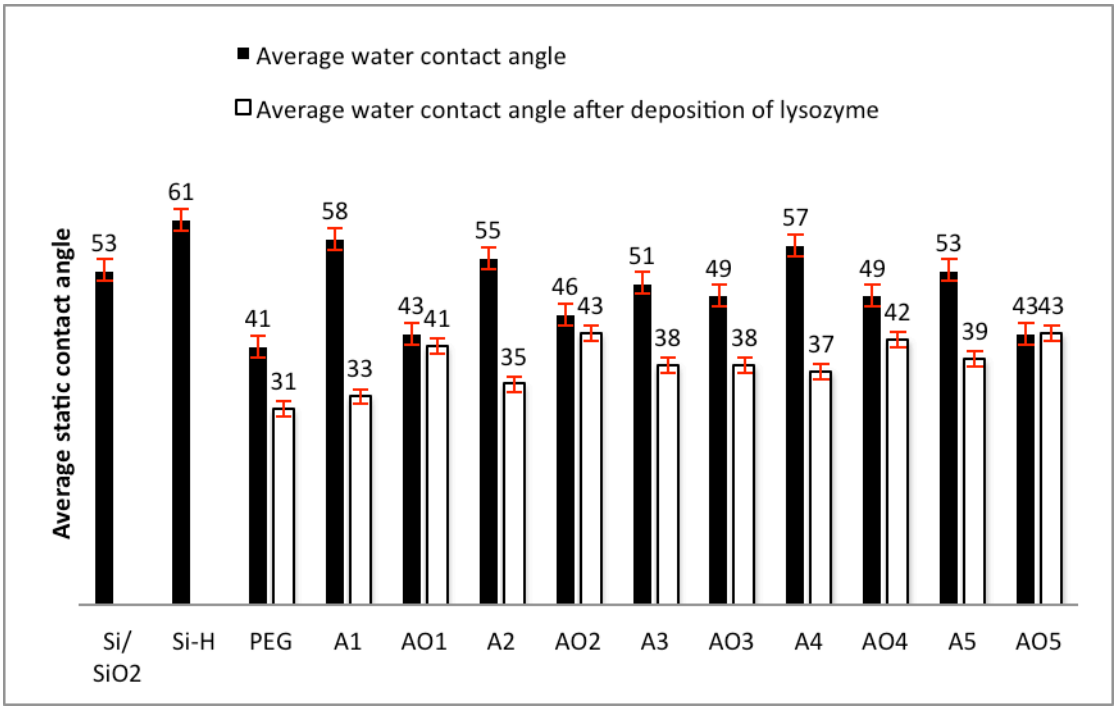

Chart 3 Average contact angle for silicon self-assembled monolayers before and after 1mM lysozyme in PBS deposition. Error bars represent 5% deviation from the average.

The results show further decrese in contact angles after incubation of functionalizaed silicon wafers in 1 mM solution of lysozyme in PBS for 15 min. The number of protein adhering to the SAMs increased as the water contact angles decreased. It is caused by the increased number of COOH- or NH_2 - terminal groups possessed by protein.[156] The lysozyme adsorption was studied by AFM, however due to many artefacts on the images the preliminary experimental data is described in Appendix 7.

2.6.5. Summary

The preparation of ω-alkenyl tertiary amine *N*-oxides in solution is shown herein to be a straightforward process that allows access to high quality monolayers on silicon surfaces.[144] We continue to investigate the adsorption of protein and cells on these new materials although we note the relative paucity of techniques for measuring adsorption of these materials on silicon substrates in real time.

In summary, a set of new ω-tertiary amine *N*-oxides was synthesized and immobilized on hydrofluoric acid-etched silicon. Further work needs to be done in order to more clearly delineate their protein-surface interactions.

2.7. Methods and Materials

2.7.1 Materials for gold functionalization

List of reagents:

1. PyBOP, 97%

2. HATU, 97%

3. isobutyl chloroformate, 98%

4. List of amines used for formation of SAMs:

SAM nomenclature	Amine
A1-Au	2-(dimethylamino)ethylamine
A2-Au	*N*,*N*-dimethyl-1,3-diaminopropane
A3-Au	*N*-methylmorpholine, 99%
A4-Au	*N,N,N′*-trimethylethylenediamine
A5-Au	*N,N,N′*-trimethyl-1,3-propanediamine

5. 30% hydrogen peroxide solution

All reagents were purchased from Aldrich and used as supplied unless otherwise stated. All solvents were purchased from Fisher and were used as supplied unless otherwise stated. Gold-coated QCM sensors were purchased from Biolin Scientific. Lysozyme from chicken white egg and fibrinogen from human plasma were purchased from Sigma-Aldrich (Molecular Biology grade). Glass microscope coverslips were assembled into an Auto306 evaporator and had 2 nm of chromium and ~200 nm of gold deposited at a rate of 0.1-0.2 nm s^{-1}. Coverslips were broken into chips as required and were placed into custom glass vials where they were cleaned in piranha solution at 80 °C for 3 min or placed into the ozone cleaner for 30 min. After

cleaning, the chips were rinsed in MilliQ water and then degassed solvent for SAM formation.

2.7.2 Preparation of gold thiol self-assembled monolayers.

Commercial gold-coated QCM sensors, and the gold-coated glass coverslips were cleaned with a piranha mixture (**CAUTION!** Prepare and dispose of small quantities (< 25 ml) only, wear heavy nitrile or butyl rubber gloves and a face mask or additional safety shield and use in an efficient fume hood). Hydrogen peroxide (30%) was added drop wise with stirring to sulfuric acid (98%) 3:1 (v/v), (note the unusual addition of aqueous solution to acid, not *vice versa*) at 80 °C. The samples were immersed in the solution for 3 min to remove organic residues, then rinsed with deionized water and dried in a gentle stream of dry nitrogen. The samples were then immediately immersed in a solution of 16-mercaptohexadecenoic acid in absolute ethanol (1 mM) for 12 hours, then rinsed with absolute ethanol, dried in a gentle stream of dry nitrogen and analyzed by X-ray photoelectron spectroscopy (XPS) without delay.

2.7.3 Secondary and tertiary amide-linked ω-tertiary amine surfaces.

Three methods were used for coupling the amines to 16-mercaptohexadecenoic acid derivatised gold surfaces as follows.

2.3.1. Benzotriazol-1-yl-oxytripyrrolidinophosphonium hexafluorophosphate (PyBOP®) (0.052 mmol, 1 eq) in CH_2Cl_2 (4 ml) was added to each gold-coated quartz sensor in a separate vial. To this vial was added the appropriate amine (0.4 mmol, 10 eq) in CH_2Cl_2 (2 ml) and gently agitated for 24h to produce surfaces **A1**-**A5**-**Au**. The derivatised sensors were washed with CH_2Cl_2 and dried in a gentle stream of dry nitrogen before use.

2.3.2. 2-(1*H*-7-Azabenzotriazol-1-yl)-1,1,3,3-tetramethyl hexafluorophosphatemethanaminiumuronium (HATU) (0.071 mmol, 1 eq) in CH_2Cl_2 (4 ml) was added to each gold-coated quartz sensor in a separate vial. To this vial was added the appropriate amine (0.4 mmol, 6 eq) in CH_2Cl_2 (2 ml) and gently agitated for 24h to produce surfaces **A1-A5-Au**. The derivatised sensors were washed with CH_2Cl_2 and dried in gentle stream of dry nitrogen before use.

2.3.3. Isobutyl chloroformate (0.2 mmol, 1 eq) in dimethylformamide (DMF, 4 ml) was added to each gold-coated quartz sensor in a separate vial in dry DMF (2 ml). To this vial was added *N*-methylmorpholine (0.09 mmol) together with the appropriate amine (0.4 mmol, 2 eq) in dry DMF (2 ml) and gently shaken for 24 h to give surfaces **A1** – **A5-Au**. The derivatised sensors were washed with CH_2Cl_2 and dried in a gentle stream of dry nitrogen before use.

2.7.4 Tertiary amine *N*-oxides.

Surfaces **A1-A5-Au** were oxidized with hydrogen peroxide (0.24 mmol of a 30% solution) in ethanol (4 ml) for 1 h (Leeds) and analysed by XPS. The sensors were washed with ethanol and dried in a gentle stream of dry nitrogen to give the corresponding amine oxides (**AO1-AO5-Au)**.

2.7.5 Control triethylene glycol surface, PEG.

The control surface bearing 1 *N*-2-2-2-hydroxyethoxyethoxyethyl-16-methylsulfanyl hexadecanamide (**PEG**) was prepared according to the procedure described by Chapman *et al.*[157]

2.7.6 Ellipsometry

The average thickness of the surfaces was determined by null ellipsometry (Nanofilm Imaging Spectroscopic Ellipsometer). Measurements yield two angles, Ψ- amplitude

ratio and Δ – phase shift. The wavelength scan from 380 nm to 900 nm was performed on three regions of interests at angle of incidence of 70 º. The Cauchy equation was used to estimate the monolayer thickness.

2.7.7 Water contact angle measurements.

Static water contact angles were measured on a KRUSS Drop Shape Analyzer 100 at room temperature. QCM sensors were washed with ethanol and dried with nitrogen immediately after each measurement. Statistical treatment with the Wilcoxon signed-rank test was used to estimate the validity of the contact angles.

2.7.8. Tensiometry

Pendant drop method was used to measure surface tension on KRUSS Drop Shape Analyzer 100 at room temperature. Each measurement was repeated 4 times and the data presented in Table 7 is an average of all measurements.

2.7.9 X-ray photoelectron spectroscopy

XPS measurements were performed using a VG Escalab 250 XPS with monochromatic aluminium K-alpha X-ray source. The spot size was 500 μm with a power of 150W. Detailed spectra of individual peaks were taken at energy of 20 eV. Binding energy was calibrated by setting the carbon 1s peak to 285 eV. Detailed spectra had a Shirley background fitted to them and peaks were assigned using mixed Gaussian-Lorentzian fits (CASA XPS software).

2.7.10 Quartz crystal microbalance with dissipation monitoring

Protein adsorption was measured using a Q-Sense E4 instrument at 20 °C in at least triplicate and the order of exposure of the surfaces to each protein was measured in both senses in all cases (*i.e.* test surface exposed to lysozyme, cleaned with sodium dodecylsulfate (SDS) then exposed to fibrinogen to acquire a first data set. A freshly

prepared surface was then exposed to fibrinogen, cleaned with SDS, and then exposed to lysozyme). No major difference was seen in the protein adsorption kinetics, or amounts of deposition observed between each order of addition. Hence the data presented in Chart 1 and Chart 2 represent the mean of triplicate data with error bars showing standard deviation.

Solutions of phosphate buffered saline (PBS), 5% SDS, fibrinogen (1 μM in PBS) and lysozyme (1 mM in PBS) were prepared and sonicated for 20 minutes prior to the experiment to mix the solutions. The sensors were placed in the chambers and PBS was pumped at a rate of 100 μl/min until the sensors' resonant frequencies equilibrated. The bathing solution was then changed to lysozyme (1 mM) in PBS solution and allowed to equilibrate, whereupon the solution was changed back to PBS to remove any protein resting on the surface. Upon equilibration the solution was finally changed to 5% SDS to more completely clean the surface, followed by a final PBS rinse. At each solution change, the pump was stopped and restarted to avoid any air intake to the system. The sensors were washed with absolute ethanol and dried with nitrogen to remove any remaining proteins. The experiment was repeated with fibrinogen (1 μM) in PBS solution.

2.7.11 Atomic Force Microscopy.

Imaging was carried out in tapping mode at room temperature in air using an Asylum Research MFP-3D atomic force microscope. Three areas of interest on the gold-coated QCM sensors bearing self-assembled ω-tertiary amines and amine *N*-oxides were selected and imaged in air. Separate sensors were exposed to solutions of lysozyme (1 mM in PBS) and fibrinogen (1 μM in PBS) and after rinsing with PBS and drying under a stream dry nitrogen gas were imaged as above.

2.7.12 Materials for silicon functionalization

Reagents were purchased from Aldrich and used as supplied unless otherwise stated. All solvents were purchased from Fisher and were used as supplied unless otherwise stated. N-type silicon [144] wafers were obtained from the NanoSilicon Group, Department of Physics, University of Warwick. Brockmann grade II/III alumina was prepared by adding 5% water by weight drop wise to neutral Brockmann grade I alumina with constant swirling. UV initiated silicon wafer derivations was carried out using 254 nm light from a UVP MRL 58 Multiple-Ray Lamp. Water used for measurements including contact angle and critical micelle concentration refers to MilliQ® water. Lysozyme from chicken white egg and fibrinogen from human plasma were purchased from Sigma-Aldrich (Molecular Biology grade).

2.7.13 General procedure A: Schotten – Baumann conditions

To a rapidly stirred biphasic solution of undecenoyl chloride (2.17 g, 18.2 mmol, 1 eq.) in CH_2Cl_2 (40 ml) and 1M NaOH (aq) at 0 °C was added *primary amine* (1 eq.) in CH_2Cl_2 (9 ml). The reaction was stirred at 0 °C for 1 h then allowed to warm to room temperature, whereupon the two phases were separated and the organic layer was washed with water (x3) and dried over $MgSO_4$. The solvent was removed under reduced pressure and the resulting oil purified by silica flash chromatography (10:1 CH_2Cl_2:MeOH) to give the *title products* **A1** – **A5-Si**.

Analytical Data (NMR spectra in Appendix 8):

General procedure **A** was used with *N*,*N*-dimethyl-1,2-ethanediamine (1.61 g, 18.3 mmol, 1 eq.) to yield *N*-[2'-(dimethylamino)ethyl]undec-10-enamide **A1-Si** as yellow oil (2.41 g, 52 %) R_f = 0.42, silica (10:1:0.5 CH_2Cl_2:MeOH:NH_3);ν_{max} (film) 3295 (N-H stretch), 2925 (C-H str.), 2854 (C-H str.), 1641 (C=O str.), 1547 (C-N str.), 1459 (C-H def.) cm^{-1}; ^1H NMR ($CDCl_3$, 400 MHz): 1.19-1.38 (m, 10H, H^4, H^5, H^6,

H^7, H^8), 1.62 (m, 2H, H^3), 2.03 (m, 2H, H^9), 2.09 (t, 2H, *J* = 7.5 Hz, H^2), 2.23 (s, 6H, 2 x $H^{4'}$), 2.40 (m, 2H, $H^{3'}$), 3.32 (q, 2H, *J* = 5.5 Hz, $H^{2'}$), 4.82-4.97 (m, 2H, H^{10}), 3.64-5.86 (ddt, 1H, *J* = 17 Hz, 10 Hz, 6.5 Hz, H^{11}), 6.09 (s, 1H, NH) ppm; ^{13}C NMR ($CDCl_3$, 75 MHz): 25.7 (C^3), 28.8-29.2 (C^4, C^5, C^6, C^7, C^8), 33.7 (C^9), 36.6 (C^2), 41.4 ($C^{2'}$), 45.6 (2x$C^{4'}$), 57.8 ($C^{3'}$), 114.1 (C^{11}), 139.2 (C^{10}), 173.2 (C^1) ppm; LSMS *m/z*: $[M+H]^+$ 255. 2 (100%); HRMS *m/z*: calculated $[M+H]^+$ $C_{15}H_{30}ON_2$ = 255.2436, found = 255.2427 $[M+H]^+$.

General procedure **A** was used with *N*,*N*-dimethyl-1,3-propyldiamine (2.10 g, 20.8 mmol) to yield *N*-[3'-(dimethylamino)propyl]undec-10-enamide **A2-Si** as a yellow oil (1.40 g, 44%) R_f = 0.37, silica (10:1:0.5 CH_2Cl_2: MeOH:NH_3); ν_{max} (film) = 3289 (N-H str.), 2925 (C-H str.), 2854 (C-H str.), 1641 (C=O str.), 1547 (C-N str.), 1460 (C-H def.) cm^{-1}; ^{1}H NMR ($CDCl_3$, 400 MHz) 1.22-1.41 (m, 10H, H^4, H^5, H^6, H^7, H^8); 1.51-1.65 (m, 2H, H^3); 2.02 (m, 2H, H^9); 2.14 (m, 2H, $H^{3'}$); 2.22 (s, 6H, 2 x $H^{4'}$); 2.37 (t, 2H, *J* = 7 Hz, $H^{2'}$), 3.23-3.32 (q, 2H, *J* = 6 Hz, $H^{1'}$), 4.84-4.97 (m, 2H, H^{11}); 5.71-5.93 (ddt, 1H, *J* = 17,Hz, 10,Hz, 6.5 Hz, H^{10}) 7.03 (s, 1H, NH) ppm;^{13}C NMR ($CDCl_3$, 75 Hz) 25.1 (C^3), 26.5 ($C^{2'}$), 28.2-28.6 (C^4, C^5, C^6, C^7, C^8), 33.1 (C^9), 36.3 ($C^{1'}$), 38.5 (C^2), 45.4 (2x$C^{4'}$), 57.9 ($C^{2'}$), 113.5 (C^{11}), 138.7 (C^{10}), 172.5 (C^1) ppm; LRMS *m/z*: $[M+H]^+$269.4 (100%) HRMS *m/z* calculated $[M+H]^+C_{16}H_{32}ON_2$= 269.2587, found = 269.2569 $[M+H]^+$.

General procedure **A** was used with 1-methylpiperazine (2.10 g, 22.0 mmol) to yield 1-(4'-methylpiperazin-1'-yl) undec-10-en-1'-one **A3-Si** as an orange oil (1.54 g, 51 %); R_f = 0.32, silica (10:1:0.5 CH_2Cl_2: MeOH:NH_3);ν_{max} (film) = 3076 (C=C-H str.), 2924 (C-H str.), 2853 (C-H str.), 2791 (C-N str.) 1640 (C=O str.), 1528 (C-N str.), 1431 (C-H def.) cm^{-1}; ^{1}H NMR ($CDCl_3$, 400 MHz) 1.22-1.41 (m, 10H, H^4, H^5, H^6, H^7, H^8); 1.49-1.60 (m, 2H, H^3); 2.02 (m, 2H, H^9); 2.16-2.39 (m, 10H, H^2, $H^{3'ax}$,

$H^{3'eq}$, H^3); 2.30 (s, 3H, NMe ($H^{5'}$)), 3.47 (dd, 2H, *J* = 8 Hz, 6.5 Hz, $H^{2',2''eq}$); 3.61 (dd, 2H, *J*= 8.5 Hz, 6.5 Hz, $H^{2',2''ax}$); 4.84-4.97 (m, 2H, H^{11}); 5.84 (ddt, 1H, *J* = 17 Hz, 10 Hz, 6.5 Hz, H^{10}) ppm; ^{13}C NMR ($CDCl_3$, 75 MHz) 24.7 (C^3), 28.2-28.8 (C^4, C^5, C^6, C^7, C^8), 32.7 (C^9), 33.2 (C^2), 41.8 ($C^{2'}$), 44.8 ($C^{2''}$), 45.2 (NMe $C^{5'}$), 54.1 ($C^{3'}$ and $C^{3''}$), 113.5 (C^{11}), 138.4 (C^{10}), 174.2 (C^1) ppm;LRMS *m/z*: $[M+H]^+$267.2 (100%); HRMS *m/z* calculated $[M+H]^+C_{16}H_{30}ON_2$= 267.2436, found = 267.2425 $[M+H]^+$.

General procedure **A** was used with *N,N,N'*-trimethyl-1,2-ethanediamine (2.10 g, 20.5 mmol) to yield *N*-[2'-(dimethylamino)ethyl]-*N*-methylundec-10-enamide **A4-Si** as a yellow oil (1.96 g, 64 %); R_f = 0.35, silica (10:1:0.5 CH_2Cl_2:MeOH:NH_3);ν_{max} (film) 3075 (C=CH str.), 2925 (C-H str.), 2854 (C-H str.), 1641 (C=O str.), 1528 (C-N str.), 1431 (C-H def.) cm^{-1}; ^{1}H NMR ($CDCl_3$, 400 MHz): 1.18-1.38 (m, 10H, H^4, H^5, H^6, H^7, H^8), 1.62 (m, 2H, H^3), 2.03 (m, 2H, H^9), 2.12-2.27 (m, 2H, $H^{1'}$, $H^{2'}$), 2.26 (s, 6H, $H^{3'}$), 2.94 (s, rotamers 3H, $H^{4'}$), 3.01 (s, rotamers 3H, $H^{4''}$), 3.24-3.38 (t, 2H, *J* = 7 Hz, $H^{1')}$, 3.45-3.61 (t, 2H, *J* = 7 Hz, $H^{2'}$), 4.82-4.98 (m, 2H, H^{11}), 5.64-5.86 (ddt, 1H, *J* = 17 Hz, 10 Hz, 6.5 Hz, H^{10}) ppm; ^{13}C NMR ($CDCl_3$, 75 MHz): 24.4 (C^3), 28.8-29.2 (C^4, C^5, C^6, C^7, C^8), 33.2 (C^9), 35.3 ($C^{4'}$), 45.0 ($C^{3'}$), 45.1 (C^2), 47.8 ($C^{1'}$), 56.1 ($C^{2'}$), 114.1 (C^1), 138.6 (C^{10}), 172.5 (C^1) ppm; LRMS *m/z*: $[M+H]^+$ 269.4 (100%); HRMS *m/z* calculated $[M+H]^+$ $C_{16}H_{32}ON_2$ = 269.2577, found = 269.2587 $[M+H]^+$.

General procedure **A** was used with *N,N,N'*-trimethyl-1,3-propanediamine (2.10 g, 20.5 mmol) to yield *N*-[3'-(dimethylamino)propyl]-*N*-methylundec-10-enamide **A5-Si** as a yellow oil (1.46 g, 56 %)R_f = 0.35, silica (10:1:0.5 CH_2Cl_2:MeOH:NH_3);ν_{max} (film) 3075 (C=CH str.), 2925 (C-H str.), 2854 (C-H str.), 1641 (C=O str.), 1528 (C-N str.), 1431 (C-H def.) cm^{-1}; ^{1}H NMR ($CDCl_3$, 400 MHz): 1.15-1.35 (m, 10H, H^4, H^5, H^6, H^7, H^8), 1.47-1.73 (m, 4H, $H^{2'}$, $H^{3'}$), 1.88-1.9 (m, 2H, H^9), 2.10-2.29 (m, 10H, H^2, $H^{3'}$, $H^{4'}$), 2.8 (s, rotamer, 3H, $H^{5'}$), 2.9 (s, rotamer, 3H, $H^{5''}$), 3.19 (m, rotamer, 2H,

$H^{1'}$), 3.45 (m rotamer, 2H, $H^{1'}$), 4.79-4.95 (m, 2H, H^{11}), 5.64-5.86 (ddt, 1H, J = 17 Hz, 10 Hz, 6.5 Hz, H^{10}) ppm; ^{13}C NMR ($CDCl_3$, 75 MHz): 24.8 (C^3), 26.0 ($C^{2'}$), 28.2-28.8 (C^4, C^5, C^6, C^7, C^8), 33.1 (C^9), 34.9 ($C^{4'}$), 44.7 ($C^{3'}$), 45.3 (C^2), 47.1 ($C^{1'}$), 56.3 ($C^{2'}$), 113.8 (C^{11}), 138.6 (C^{10}), 172.5 (C^1) ppm; LRMS *m/z*: $[M+H]^+$ 283.3 (100%) HRMS *m/z* calculated $[M+H]^+$ $C_{17}H_{34}ON_2$ = 283.2765, found = 283.2767 $[M+H]^+$.

2.7.14. General procedure B. Oxidation of ω-tertiary amines

To a dry three-necked round bottom flask under nitrogen atmosphere was added potassium carbonate (1.54 g, 11.00 mmol, 2.3 eq), and a solution of *tertiary amine* **A1-A5-Si** (1 eq.) in CH_2Cl_2 (20 ml) with stirring, and cooled to –78 ºC. A solution of 50-89% m-CPBA (1.30 g, 7.60 mmol, 1.6 eq.) in CH_2Cl_2 (20 ml) was added *via* syringe and the reaction stirred vigorously for 3 hours after which time any remaining m-CPBA was removed by addition of limonene (d = 0.84, 0.62 ml, 3.80 mmol, 0.8 eq.) *via* syringe over 10 mins. The reaction mixture was filtered through Florisil®, washed with 4:1 CH_2Cl_2:MeOH and solvent removed by reduced pressure. The residue was purified over a column of neutral alumina Brockmann grade II/III eluted with 5:1 CH_2Cl_2:MeOH, to give, after removal of solvent under reduced pressure, *title products* **AO1** – **AO5-Si**.

Analytical Data (NMR spectra in 8):

General procedure **B** was used with *N*-[2'-(dimethylamino)ethyl]undec-10-enamide **A1-Si** (1.18 g, 4.75 mmol) to yield *N*-[2'-(dimethylamine*N*-oxide)ethyl]undec-10-enamide **AO1-Si** as a white solid (0.80 g, 62%), m.p. 95-97 °C; R_f = 0.41, neutral alumina (10:1:0.5 CH_2Cl_2: MeOH: NH_3);ν_{max} (film): 3284 (N-H), 3077 (C=CH str.), 2924 (C-H str.), 2854 (C-H str.), 1642 (C=O str.), 1545 (C-H def.), 961 (N^+-O^- str.) cm^{-1}; ^{1}H NMR ($CDCl_3$, 400 MHz): 1.24-1.48 (m, 10H, H^4, H^5, H^6, H^7, H^8), 1.56-1.71 (m, 2H, H^3), 2.06 (m, 2H, H^9), 2.21 (m, 2H, H^2), 3.28 (s, 6H, 2x$H^{3'}$), 3.51 (m, 2H,

$H^{2'}$), 3.72 (m, 2H, $H^{1'}$), 4.89 (m, 2H, H^{11}), 5.72-5.91 (ddt, 1H, *J* = 17 Hz, 10 Hz, 6.5 Hz, H^{10}), 7.95 (s, 1H, NH) ppm; ^{13}C NMR ($CDCl_3$, 75 MHz): 26.8 (C^3), 30.1-30.4 (C^4, C^5, C^6, C^7, C^8), 34.9 (C^9), 35.1 (C^1), 37.0 (C^2), 58.8 ($C^{2'}$), 69.4 ($C^{1'}$), 114.8 (C^{11}), 139.5 (C^{10}), 176.6 (C^1) ppm; LSMS *m/z*: $[M+H]^+$ 271.7(100%); HRMS *m/z* calculated $[M+H]^+$ $C_{15}H_{30}O_2N_2$ = 271.2361, found = 271.2381 $[M+H]^+$.

General procedure **B** was used with *N*-[3'-(dimethylamino)propyl]undec-10-enamide **A2-Si** (3.0 g, 11.30 mmol) to yield *N*-[3'-(dimethylamine*N*-oxide)propyl]undec-10-enamide **AO2-Si** as a white/yellow solid (2.05 g, 64%), m.p. 97-99 °C; R_f = 0.43, neutral alumina (10:1:0.5 CH_2Cl_2: MeOH: NH_3);ν_{max} (film): 3278 (N-H), 3077 (C=CH str.), 2925 (C-H str.), 2854 (C-H str.), 1643 (C=O str.), 1543 (C-H def.), 903 (N^+-O^- str.) cm^{-1}; ^{1}H NMR ($CDCl_3$, 400 MHz): 1.27-1.45 (m, 10H, H^4, H^5, H^6, H^7, H^8), 1.62 (m, 2H, H^3), 2.03 (m, 2H, H^9), 2.22 (m, 2H, H^2), 3.17 (s, 6H, 2x$H^{4'}$), 3.34 (m, 4H, $H^{1'}$, $H^{3'}$), 4.88 -5.02 (m, 2H, H^{11}), 5.72-5.91 (ddt, 1H, *J* = 17 Hz, 10 Hz, 6.5 Hz, H^{10}), 7.95 (s, 1H, NH) ppm; ^{13}C NMR ($CDCl_3$, 75 MHz): 24.8 (C^3), 26.9 ($C^{2'}$), 30.1-30.4 (C^4, C^5, C^6, C^7, C^8), 34.9 (C^9), 37.1 ($C^{1'}$), 37.5 (C^2), 58.7 ($C^{4'}$), 69.4 ($C^{3'}$), 114.7 (C^{11}), 139.2 (C^{10}), 173.3 (C^1) ppm; LSMS *m/z*: $[M+H]^+$ 285.4 (100%); HRMS *m/z* calculated $[M+H]^+$ $C_{16}H_{32}O_2N_2$ = 285.2542, found = 285.2537 $[M+H]^+$.

General procedure **B** was used with 1-(4'-methylpiperazin-1'-yl-4'-amine) undec-10-en-1'-one **A3-Si** (2.45 g, 19.60 mmol) to yield 1-(4'-methylpiperazin-1'-yl-4'-amine *N*-oxide) undec-10-en-1'-one **AO3-Si** as a white solid (1.98 g, 61%), m.p. 95-97 °C; R_f = 0.41, neutral alumina (10:1:0.5 CH_2Cl_2: MeOH: NH_3),ν_{max} (film) 3079 (C=C-H str.), 2922 (C-H str.), 2852 (C-H str.), 2793 (C-N str.) 1639 (C=O str.), 1530

(C-N str.), 1434 (C-H def.), 974 (N^+-O^- str.) cm^{-1}; ^1H NMR ($CDCl_3$, 400 MHz) 1.29-1.46 (m, 10H, H^4, H^5, H^6, H^7, H^8); 1.56-1.67 (m, 2H, H^3); 1.98 (m, 2H, H^9); 2.26 (m, 2H, H^2); 3.18-3.24 (m, 4H, $H^{2'eq}$, $H^{3'eq}$ and $H^{2''eq}$, $H^{3''eq}$); 3.21 (s, 3H, N-Me ($H^{5'}$)); 3.38-4.49 (m, 2H, $H^{3''ax}$ and $H^{3'ax}$), 4.04 (m, 1H, $H^{2''ax}$), 4.51 (m, 1H, $H^{2'ax}$) 4.99 (m, 2H, H^{11}); 5.72- 5.90 (ddt, 1H, J = 17 Hz, 10 Hz, 6.5 Hz, H^{10}) ppm; ^{13}C NMR ($CDCl_3$, 75 Hz) 26.3 (C^3), 30.1-30.5 (C^4, C^5, C^6, C^7, C^8), 33.8 (C^9), 34.9 (C^2), 41.9, 37.4 ($C^{1'}$ and $C^{1''}$) , 60.7 ($C^{3'}$), 66.1, 65.9 ($C^{2'}$ and $C^{2''}$), 113.5 (C^{11}), 139.2 (C^{10}) 174.2 (C^1) ppm; LRMS *m/z:* $[M+H]^+$283.2; HRMS *m/z* calculated $[M+H]^+C_{16}H_{30}O_2N_2$= 283.2386, found = 283.2371 $[M+H]^+$.

General procedure **B** was used with *N*-[2'-(dimethylamine)ethyl]-*N*-methylundec-10-enamide **A4-Si** (2.35 g, 8.82 mmol) to yield *N*-[2'-(dimethylamine*N*-oxide)ethyl]-*N*-methylundec-10-enamide **AO4-Si** as a white solid (1.43 g, 61%), m.p. 96-98 °C;R_f = 0.35, neutral alumina (10:1:0.5 CH_2Cl_2: MeOH: NH_3);ν_{max} (film) 3075 (C=CH str.), 2925 (C-H str.), 2850 (C-H str.), 1637 (C=O str.), 1534 (C-N str.), 1458 (C-H def.) 974 (N^+-O^- str.) cm^{-1}; ^1H NMR ($CDCl_3$, 400 MHz): 1.29-1.46 (m, 10H, H^4, H^5, H^6, H^7, H^8), 1.62 (m, 2H, H^9), 2.06 (m, 2H, H^3), 2.38 (q, 2H, J = 7 Hz, H^2), 3.13 (s, rotamers, 3H, $H^{4'}$), 3.19 (s, rotamers, 3H, $H^{4''}$), 3.23 (s, 6H, $H^{3'}$), 3.45 (m, 2H, $H^{2'}$), 4.85-4.94 (2 x m, 2H, 2x$H^{1'}$), 4.96-5.05 (m, 2H, H^{11}), 5.64-5.82 (ddt, 1H, J = 17 Hz, 10 Hz, 6.5 Hz, H^{10}) ppm; ^{13}C NMR ($CDCl_3$, 75 MHz): 24.7 (C^3), 30.8-31.4 (C^4, C^5, C^6, C^7, C^8), 33.8 (C^9), 34.3 ($C^{4'}$), 36.4 (C^2) 42.9 ($C^{1'}$), 58.6 ($C^{3'}$), 67.6 ($C^{2'}$), 114.1 (C^{11}), 140.1 (C^{10}), 172.5 (C^1) ppm; LRMS *m/z*: $[M+H]^+$ 285.2 (100%); HRMS *m/z* calculated $[M+H]^+$ $C_{16}H_{32}O_2N_2$ = 285.2542, found = 285.2544 $[M+H]^+$.

General procedure **B** was used with *N*-[3'-(dimethylamine)propyl]-*N*-methylundec-10-enamide **A5-Si** to yield *N*-[3'-(dimethylamine*N*-oxide)propyl]-*N*-methylundec-10-enamide **AO5-Si** as a white solid (1.73 g, 68 %); m.p. 98-100 °C; R_f = 0.52, neutral alumina (10:1:0.5 CH_2Cl_2: MeOH: NH_3); v_{max} (film) 3077 (C=CH str.), 2924 (C-H str.), 2854 (C-H str.), 1642 (C=O str.), 1545 (C-N str.), 967 (N^+-O^- str.) cm^{-1}; ^{1}H NMR (MeOD, 400 MHz): 1.24-1.44 (m, 10H, H^4, H^5, H^6, H^7, H^8), 1.55-1.67 (m, 4H, $H^{2'}$, H^3), 2.05-2.20 (m, 5H, $H^{2''}$, H^9), 2.39 (m, 10H, H^2), 2.55 (s, rotamer, 3H, $H^{5'}$), 3.09 (s, (rotamer), 3H, $H^{5''}$), 3.29-3.34 (m, 2H, $H^{3'}$), 3.48 (m, 2H, $H^{1'}$), 3.8 (s, 6H, $H^{4'}$), 4.90-4.95 (m, 2H, H^{11}), 5.64-5.86 (ddt, 1H, *J* = 17 Hz, 10 Hz, 6.5 Hz, H^{10}) ppm; ^{13}C NMR (MeOD, 75 MHz): 22.6 ($C^{2'}$), 26.2 (C^3), 30.2-30.8 (C^4, C^5, C^6, C^7, C^8), 34.4 (C^2), 34.9 (C^{10}), 35.9 ($C^{5'}$), 45.3 ($C^{1'}$), 58.1 ($C^{4'}$), 113.8 (C^{11}), 140.6 (C^{10}), 171.3 (C^1) ppm; LRMS *m/z*: $[M+H]^+$ 299.3 (100%); HRMS *m/z* calculated $[M+H]^+$ $C_{17}H_{34}O_2N_2$ = 299.2622, found = 299.2645 $[M+H]^+$.

2.7.15. Etching (hydrogen termination) of silicon wafers.

This procedure was carried out in a laboratory designed for work with hydrofluoric acid. Safety measures such as full-face masks, full-length aprons and heavy-duty nitrile gloves were used during this procedure. A 5% HF solution was made by diluting 50% HF (10 ml) into distilled water (90 ml) in a Teflon beaker. The silicon wafers were immersed in this solution for 5 min, and then washed with distilled water, degassed ethanol (5 ml) and degassed toluene (5 ml) and dried with a gentle flow of nitrogen after each wash.

2.7.16. Functionalization of hydrogen terminated silicon surfaces.

The hydrogen terminated silicon wafers prepared above were placed in vials containing 2 mM solutions of the following amines (**A1**-**A5-Si**) and amine oxides

(**AO1**-**AO5-Si**) in degassed toluene (10 ml). Each of these vials were irradiated at 254 nm for 20 minutes with a UV lamp then each silicon wafer removed from the solution, washed with toluene (5 ml) and dried under a gentle flow of nitrogen.

2.8. References

(1) Kaur, I.; Zhao, X.; Bryce, M. R.; Schauer, P. A.; Low, P. J.; Kataky, R. *Chemphyschem,* **2013**, *14*, 431.

(2) Raskin, L.; Rittmann, B. E.; Stahl, D. A. *Appl. Environ. Microbiol.,* **1996**, *62*, 3847.

(3) Prime, K. L.; Whitesides, G. M. *J. Am. Chem. Soc.,* **1993**, *115*, 10714.

(4) Robertus, J.; Browne, W. R.; Feringa, B. L. *Chem. Soc. Rev.,* **2010**, *39*, 354.

(5) Banerjee, I.; Pangule, R. C.; Kane, R. S. *Adv. Mater.,* **2011**, *23*, 690.

(6) Meyers, S. R.; Grinstaff, M. W. *Chem. Rev.,* **2011**, *112*, 1615.

(7) Mrksich, M.; Chen, C. S.; Xia, Y. N.; Dike, L. E.; Ingber, D. E.; Whitesides, G. M. *Proc. Natl. Acad. Sci. U. S. A.,* **1996**, *93*, 10775.

(8) Hay, D. C.; Pernagallo, S.; Diaz-Mochon, J. J.; Medine, C. N.; Greenhough, S.; Hannoun, Z.; Schrader, J.; Black, J. R.; Fletcher, J.; Dalgetty, D.; Thompson, A. I.; Newsome, P. N.; Forbes, S. J.; Ross, J. A.; Bradley, M.; Iredale, J. P. *Stem Cell Res.,* **2011**, *6*, 92.

(9) Fristrup, C. J.; Jankova, K.; Hvilsted, S. *Soft Matter,* **2009**, *5*, 4623.

(10) Gibson, T. D.; Hulbert, J. N.; Parker, S. M.; Woodward, J. R.; Higgins, I. J. *Biosens. Bioelectron.,* **1992**, *7*, 701.

(11) Verrier, D.; Mortier, B.; Albagnac, G. *Biotechnol. Lett.,* **1987**, *9*, 735.

(12) Zhou, M. Y.; Liu, H. W.; Venkiteshwaran, A.; Kilduff, J.; Anderson, D. G.; Langer, R.; Belfort, G. *J. Mater. Chem.,* **2011**, *21*, 693.

(13) Gu, M. H.; Kilduff, J. E.; Belfort, G. *Biomaterials,* **2012**, *33*, 1261.

(14) Choong, C.; Foord, J. S.; Griffiths, J.-P.; Parker, E. M.; Baiwen, L.; Bora, M.; Moloney, M. G. *New J. Chem.,* **2012**, *36*, 1187.

(15) Yang, W.; Xue, H.; Li, W.; Zhang, J. L.; Jiang, S. Y. *Langmuir,* **2009**, *25*, 11911.

(16) Wu, L.; Jasinski, J.; Krishnan, S. *J. Appl. Polym. Sci.,* **2012**, *124*, 2154.

(17) Pernagallo, S.; Wu, M.; Gallagher, M. P.; Bradley, M. *J. Mater. Chem.,* **2011**, *21*, 96.

(18) Ederth, T.; Ekblad, T.; Pettitt, M. E.; Conlan, S. L.; Du, C. X.; Callow, M. E.; Callow, J. A.; Mutton, R.; Clare, A. S.; D'Souza, F.; Donnelly, G.; Bruin, A.; Willemsen, P. R.; Su, X. J. J.; Wang, S.; Zhao, Q.; Hederos, M.; Konradsson, P.; Liedberg, B. *ACS Appl. Mater. Interfaces,* **2011**, *3*, 3890.

(19) Martins, M. C. L.; Ochoa-Mendes, V.; Ferreira, G.; Barbosa, J. N.; Curtin, S. A.; Ratner, B. D.; Barbosa, M. A. *Acta Biomater.,* **2011**, *7*, 1949.

(20) Ulman, A. *Chem. Rev.,* **1996**, *96*, 1533.

(21) Netzer, L.; Sagiv, J. *J. Am. Chem. Soc.,* **1983**, *105*, 674.

(22) Hatzor, A.; Moav, T.; Cohen, H.; Matlis, S.; Libman, J.; Vaskevich, A.; Shanzer, A.; Rubinstein, I. *J. Am. Chem. Soc.,* **1998**, *120*, 13469.

(23) Nuzzo, R. G.; Allara, D. L. *J. Am. Chem. Soc.,* **1983**, *105*, 4481.

(24) Iqbal, P.; Critchley, K.; Bowen, J.; Attwood, D.; Tunnicliffe, D.; Evans, S. D.; Preece, J. A. *J. Mater. Chem.,* **2007**, *17*, 5097.

(25) Gun, J.; Iscovici, R.; Sagiv, J. *J. Colloid Interface Sci.,* **1984**, *101*, 201.

(26) Gun, J.; Sagiv, J. *J. Colloid Interface Sci.,* **1986**, *112*, 457.

(27) Maoz, R.; Sagiv, J. *J. Colloid Interface Sci.,* **1984**, *100*, 465.

(28) Lebec, V.; Landoulsi, J.; Boujday, S.; Poleunis, C.; Pradier, C. M.; Delcorte, A. *J. Phys. Chem. C,* **2013**, *117*, 11569.

(29) Schreiber, F. *Journal of Physics-Condensed Matter,* **2004**, *16*, R881.

(30) Bain, C. D. Thesis PhD Thesis, Harvard University, 1990.

(31) Boden, N.; Bushby, R. J.; Clarkson, S.; Evans, S. D.; Knowles, P. F.; Marsh, A. *Tetrahedron,* **1997**, *53*, 10939.

(32) Buriak, J. M. *Chem. Commun.,* **1999**, 1051.

(33) Buriak, J. M. *Chem. Rev.,* **2002**, *102*, 1271.

(34) Lasseter, T. L.; Clare, B. H.; Abbott, N. L.; Hamers, R. J. *J. Am. Chem. Soc.,* **2004**, *126*, 10220.

(35) Li, Y.; Calder, S.; Yaffe, O.; Cahen, D.; Haick, H.; Kronik, L.; Zuilhof, H. *Langmuir,* **2012**, *28*, 9920.

(36) Merrett, K.; Cornelius, R. M.; McClung, W. G.; Unsworth, L. D.; Sheardown, H. *J. Biomater, Sci., Polym. Ed.,* **2002**, *13*, 593.

(37) Mrksich, M.; Dike, L. E.; Tien, J.; Ingber, D. E.; Whitesides, G. M. *Exp. Cell Res.,* **1997**, *235*, 305.

(38) Leckband, D. *Annu. Rev. Biophys. Biomol. Struct.,* **2000**, *29*, 1.

(39) Hlady, V.; Buijs, J. *Curr. Opin. Biotechnol.,* **1996**, *7*, 72.

(40) Dee, K. C. P., D.A., Bizios, R.; *An Introduction To Tissue-Biomaterial Interactions*; Wiley: USA, 2002.

(41) Sigal, G. B.; Mrksich, M.; Whitesides, G. M. *J. Am. Chem. Soc.,* **1998**, *120*, 3464.

(42) McPherson, T.; Kidane, A.; Szleifer, I.; Park, K. *Langmuir,* **1998**, *14*, 176.

(43) Pertsin, A. J.; Grunze, M. *Langmuir,* **2000**, *16*, 8829.

(44) Zheng, J.; Li, L. Y.; Chen, S. F.; Jiang, S. Y. *Langmuir,* **2004**, *20*, 8931.

(45) Archambault, J. G.; Brash, J. L. *Colloids and Surfaces B-Biointerfaces,* **2004**, *33*, 111.

(46) Kane, R. S.; Deschatelets, P.; Whitesides, G. M. *Langmuir,* **2003**, *19*, 2388.

(47) Folkers, J. P.; Laibinis, P. E.; Whitesides, G. M. *Langmuir,* **1992**, *8*, 1330.

(48) Ogaki, R.; Alexander, M.; Kingshott, P. *Mater. Today,* **2010**, *13*, 22.

(49) Holmlin, R. E.; Chen, X. X.; Chapman, R. G.; Takayama, S.; Whitesides, G. M. *Langmuir,* **2001**, *17*, 2841.

(50) Neinhuis, C.; Barthlott, W. *Annals of Botany,* **1997**, *79*, 667.

(51) Bhushan, B.; Jung, Y. C. *Prog. Mater Sci.,* **2011**, *56*, 1.

(52) Wei, Q., *et.al. Adv. Mater.,* **2014**, *26*, 2029.

(53) Weincek, K. M.; Fletcher, M. *J. Bacteriol.,* **1995**, *177*, 1959.

(54) Ostuni, E.; Chapman, R. G.; Liang, M. N.; Meluleni, G.; Pier, G.; Ingber, D. E.; Whitesides, G. M. *Langmuir,* **2001**, *17*, 6336.

(55) Callow, M. E.; Callow, J. A.; Ista, L. K.; Coleman, S. E.; Nolasco, A. C.; Lopez, G. P. *Appl. Environ. Microbiol.,* **2000**, *66*, 3249.

(56) Tegoulia, V. A.; Cooper, S. L. *J. Biomed. Mater. Res.,* **2000**, *50*, 291.

(57) Scotchford, C. A.; Gilmore, C. P.; Cooper, E.; Leggett, G. J.; Downes, S. *J. Biomed. Mater. Res.,* **2002**, *59*, 84.

(58) Faucheux, N.; Schweiss, R.; Lutzow, K.; Werner, C.; Groth, T. *Biomaterials,* **2004**, *25*, 2721.

(59) Zaugg, F. G.; Spencer, N. D.; Wagner, P.; Kernen, P.; Vinckier, A.; Groscurth, P.; Semenza, G. *Journal of Materials Science-Materials in Medicine,* **1999**, *10*, 255.

(60) Lee, B. S.; Chi, Y. S.; Lee, K.-B.; Kim, Y.-G.; Choi, I. S. *Biomacromolecules,* **2007**, *8*, 3922.

(61) Habash, M.; Reid, G. *J. Clin. Pharmacol.,* **1999**, *39*, 887.

(62) Chapman, R. G.; Ostuni, E.; Liang, M. N.; Meluleni, G.; Kim, E.; Yan, L.; Pier, G.; Warren, H. S.; Whitesides, G. M. *Langmuir,* **2001**, *17*, 1225.

(63) Chou, L. S.; Firth, J. D.; Uitto, V. J.; Brunette, D. M. *J. Cell Sci.,* **1995**, *108*, 1563.

(64) Rickert, D.; Franke, R. P.; Lendlein, A.; Kelch, S.; Moses, M. A. *Journal of Biomedical Materials Research Part A,* **2007**, *83A*, 558.

(65) Mwenifumbo, S.; Li, M.; Chen, J.; Beye, A.; Soboyejo, W. *Journal of Materials Science-Materials in Medicine,* **2007**, *18*, 9.

(66) Grew, J. C.; Ricci, J. L.; Alexander, H. *Journal of Biomedical Materials Research Part A,* **2008**, *85A*, 326.

(67) Albers, S.-V.; Meyer, B. H. *Nat. Rev. Microbiol.,* **2011**, *9*, 414.

(68) Ng, S. Y. M.; Zolghadr, B.; Driessen, A. J. M.; Albers, S.-V.; Jarrell, K. F. *J. Bacteriol.,* **2008**, *190*, 6039.

(69) Sleytr, U. B.; Messner, P.; Pum, D.; Sara, M. *Angewandte Chemie (International ed. in English),* **1999**, *38*, 1034.

(70) Moll, D.; Huber, C.; Schlegel, B.; Pum, D.; Sleytr, U. B.; Sara, M. *Proc. Natl. Acad. Sci. U. S. A.,* **2002**, *99*, 14646.

(71) Martin-Molina, A.; Moreno-Flores, S.; Perez, E.; Pum, D.; Sleytr, U. B.; Toca-Herrera, J. L. *Biophys. J.,* **2006**, *90*, 1821.

(72) Nash, J. A.; Ballard, T. N. S.; Weaver, T. E.; Akinbi, H. T. *J. Immunol.,* **2006**, *177*, 519.

(73) Kim, J.; Somorjai, G. A. *J. Am. Chem. Soc.,* **2003**, *125*, 3150.

(74) Mescher, M. F. *Trends Biochem. Sci,* **1981**, *6*, 97.

(75) Mescher, M. F.; Strominger, J. L. *Abstracts of Papers of the American Chemical Society,* **1976**, *172*, 141.

(76) Yurist-Doutsch, S.; Abu-Qarn, M.; Battaglia, F.; Morris, H. R.; Hitchen, P. G.; Dell, A.; Eichler, J. *Mol. Microbiol.,* **2008**, *69*, 1234.

(77) Roach, P.; Farrar, D.; Perry, C. C. *J. Am. Chem. Soc.,* **2005**, *127*, 8168.

(78) Dilly, S. J.; Beecham, M. P.; Brown, S. P.; Griffin, J. M.; Clark, A. J.; Griffin, C. D.; Marshall, J.; Napier, R. M.; Taylor, P. C.; Marsh, A. *Langmuir,* **2006**, *22*, 8144.

(79) Chae, P. S.; Guzei, I. A.; Gellman, S. H. *J Am Chem Soc,* **2010**, *132*, 1953.

(80) Rozema, D.; Gellman, S. H. *J Am Chem Soc,* **1995**, *117*, 2373.

(81) Chae, P. S.; Laible, P. D.; Gellman, S. H. *Mol Biosyst,* **2010**, *6*, 89.

(82) Theisen, M. J.; Potocky, T. B.; McQuade, D. T.; Gellman, S. H.; Chiu, M. L. *Bba-Proteins Proteom,* **2005**, *1751*, 213.

(83) Goracci, L.; Germani, R.; Savelli, G.; Bassani, D. M. *Chembiochem,* **2005**, *6*, 197.

(84) Bordi, F.; Cerichelli, G.; de Berardinis, N.; Diociaiuti, M.; Giansanti, L.; Mancini, G.; Sennato, S. *Langmuir,* **2010**, *26*, 6177.

(85) Singh, S. K.; Bajpai, M.; Tyagi, V. K. *J Oleo Sci,* **2006**, *55*, 99.

(86) Bernier, D.; Wefelscheid, U. K.; Woodward, S. *Org. Prep. Proced. Int.,* **2009**, *41*, 173.

(87) Kawasaki, H.; Souda, M.; Tanaka, S.; Nemoto, N.; Karlsson, G.; Almgren, M.; Maeda, H. *J Phys Chem B,* **2002**, *106*, 1524.

(88) Maeda, H.; Tanaka, S.; Ono, Y.; Miyahara, M.; Kawasaki, H.; Nemoto, N.; Almgren, M. *J Phys Chem B,* **2006**, *110*, 12451.

(89) Rathman, J. F.; Christian, S. D. *Langmuir,* **1990**, *6*, 391.

(90) Kawasaki, H.; Sasaki, A.; Kawashima, T.; Sasaki, S.; Kakehashi, R.; Yamashita, I.; Fukada, K.; Kato, T.; Maeda, H. *Langmuir,* **2005**, *21*, 5731.

(91) Goracci, L.; Germani, R.; Rathman, J. F.; Savelli, G. *Langmuir,* **2007**, *23*, 10525.

(92) O'Neil, I. A.; Miller, N. D.; Peake, J.; Barkley, J. V.; Low, C. M. R.; Kalindjian, S. B. *Synlett,* **1993**, *1993*, 515.

(93) O'Neil, I. A.; Potter, A. J.; Southern, M. J.; Steiner, A.; Barkley, J. V. *Chem. Commun.,* **1998**, 2511.

(94) Hook, F.; Kasemo, B.; Nylander, T.; Fant, C.; Sott, K.; Elwing, H. *Anal. Chem.,* **2001**, *73*, 5796.

(95) Andersson, M.; Andersson, J.; Sellborn, A.; Berglin, M.; Nilsson, B.; Elwing, H. *Biosens. Bioelectron.,* **2005**, *21*, 79.

(96) Smith, A. L.; Shirazi, H. M. *Thermochim. Acta,* **2005**, *432*, 202.

(97) Sauerbrey, G. *Zeitschrift für Physikn,* **1959**, *155*, 206.

(98) Mittal, K. L. *Contact angle, wettability and adhesion*, 2002; Vol. Volume 3.

(99) Tavana, H.; Petong, N.; Hennig, A.; Grundke, K.; Neumann, A. W. *J. Adhes.,* **2005**, *81*, 29.

(100) Dobbs, H. *Int. J. Mod Phys B,* **1999**, *13*, 3255.

(101) Eral, H. B.; t Mannetje, D. J. C. M.; Oh, J. M. *Colloid. Polym. Sci.,* **2013**, *291*, 247.

(102) Wilcoxon, F. *J. Econ. Entomol.,* **1946**, *39*, 269.

(103) Goncalves, D.; Irene, E. A. *Quim. Nova,* **2002**, *25*, 794.

(104) Jin, G.; Jansson, R.; Arwin, H. *Rev. Sci. Instrum.,* **1996**, *67*, 2930.

(105) Agocs, E.; Petrik, P.; Milita, S.; Vanzetti, L.; Gardelis, S.; Nassiopoulou, A. G.; Pucker, G.; Balboni, R.; Fried, M. *Thin Solid Films,* **2011**, *519*, 3002.

(106) Petrik, P.; Fried, M.; Vazsonyi, E.; Lohner, T.; Horvath, E.; Polgar, O.; Basa, P.; Barsony, I.; Gyulai, J. *Appl. Surf. Sci.,* **2006**, *253*, 200.

(107) Crighton, J. S.; Carroll, J.; Fairman, B.; Haines, J.; Hinds, M. *J. Anal. At. Spectrom.,* **1996**, *11*, R461.

(108) Critchlow, G. W. *Trans. Inst. Met. Finish.,* **1996**, *74*, 108.

(109) Giessibl, F. J. *Rev. Mod. Phys.,* **2003**, *75*, 949.

(110) Sureshbabu, V. V.; Lalithamba, H. S.; Narendra, N.; Hemantha, H. P. *Org. Biomol. Chem.,* **2010**, *8*, 835.

(111) Cooper, A. L. *Protein surface-nteractions studied on gold and silicon*, 2011,

(112) Nakajima, N.; Ikada, Y. *Bioconjugate Chem.,* **1995**, *6*, 123.

(113) Wagner, C. D. *Handbook of X-Ray Photoelectron Spectroscopy*; Perkin-Elmer Corporation, 1979.

(114) Hooper, A. E.; Werho, D.; Hopson, T.; Palmer, O. *Surf. Interface Anal.,* **2001**, *31*, 809.

(115) Baio, J. E.; Weidner, T.; Brison, J.; Graham, D. J.; Gamble, L. J.; Castner, D. G. *J. Electron. Spectrosc. Relat. Phenom.,* **2009**, *172*, 2.

(116) Yam, C. M.; Pradier, C. M.; Salmain, M.; Marcus, P.; Jaouen, G. *J. Colloid Interface Sci.,* **2001**, *235*, 183.

(117) Dobrzanska, D. A.; Cooper, A. L.; Dowson, C. G.; Evans, S. D.; Fox, D. J.; Johnson, B. R.; Biggs, C. I.; Randev, R. K.; Stec, H. M.; Taylor, P. C.; Marsh, A. *Langmuir,* **2013**, *29*, 2961.

(118) K. Stańczyk, R. D., Z. Piwowarska, S. Witkowski *Carbon,* **1995**, *33*, 1383.

(119) Nuzzo, R. G.; Dubois, L. H.; Allara, D. L. *J. Am. Chem. Soc.,* **1990**, *112*, 558.

(120) Anand, G.; Sharma, S.; Dutta, A. K.; Kumar, S. K.; Belfort, G. *Langmuir,* **2010**, *26*, 10803.

(121) Evers, F.; Steitz, R.; Tolan, M.; Czeslik, C. *Langmuir,* **2011**, *27*, 6995.

(122) Adamczyk, Z.; Bratek-Skicki, A.; Dabrowska, P.; Nattich-Rak, M. *Langmuir,* **2011**, *28*, 474.

(123) Zhang, Y. J.; Cremer, P. S. *Proc. Natl. Acad. Sci. U. S. A.,* **2009**, *106*, 15249.

(124) Boström, M.; Tavares, F. W.; Finet, S.; Skouri-Panet, F.; Tardieu, A.; Ninham, B. W. *Biophys. Chem.,* **2005**, *117*, 217.

(125) Dyr, J. E.; Tichy, I.; Jirosuková, M.; Tobiska, P.; Slavík, R.; Homola, J.; Brynda, E.; Houska, M.; Suttnar, J. *Sensors and Actuators B: Chemical,* **1998**, *51*, 268.

(126) Adamczyk, Z.; Barbasz, J.; Ciesla, M. *Langmuir,* **2011**, *27*, 6868.

(127) Sethuraman, A.; Vedantham, G.; Imoto, T.; Przybycien, T.; Belfort, G. *Proteins: Structure, Function, and Bioinformatics,* **2004**, *56*, 669.

(128) Harder, P.; Grunze, M.; Dahint, R.; Whitesides, G. M.; Laibinis, P. E. *J. Phys. Chem. B,* **1998**, *102*, 426.

(129) Schilp, S.; Rosenhahn, A.; Pettitt, M. E.; Bowen, J.; Callow, M. E.; Callow, J. A.; Grunze, M. *Langmuir,* **2009**, *25*, 10077.

(130) Rosenhahn, A.; Schilp, S.; Kreuzer, H. J.; Grunze, M. *PCCP,* **2010**, *12*, 4275.

(131) Sagle, L. B.; Cimatu, K.; Litosh, V. A.; Liu, Y.; Flores, S. C.; Chen, X.; Yu, B.; Cremer, P. S. *J. Am. Chem. Soc.,* **2011**, *133*, 18707.

(132) Krigbaum, W. R.; Kuegler, F. R. *Biochemistry,* **1970**, *9*, 1216.

(133) Booth, D. R.; Sunde, M.; Bellotti, V.; Robinson, C. V.; Hutchinson, W. L.; Fraser, P. E.; Hawkins, P. N.; Dobson, C. M.; Radford, S. E.; Blake, C. C. F.; Pepys, M. B. *Nature,* **1997**, *385*, 787.

(134) Lu, J. R.; Su, T. J.; Thirtle, P. N.; Thomas, R. K.; Rennie, A. R.; Cubitt, R. *J. Colloid Interface Sci.,* **1998**, *206*, 212.

(135) Krebs, M. R. H.; Wilkins, D. K.; Chung, E. W.; Pitkeathly, M. C.; Chamberlain, A. K.; Zurdo, J.; Robinson, C. V.; Dobson, C. M. *J. Mol. Biol.,* **2000**, *300*, 541.

(136) Kim, D. T.; Blanch, H. W.; Radke, C. J. *Langmuir,* **2002**, *18*, 5841.

(137) Hill, S. E.; Miti, T.; Richmond, T.; Muschol, M. *Plos One,* **2011**, *6*, e18171.

(138) Herrwerth, S.; Eck, W.; Reinhardt, S.; Grunze, M. *J. Am. Chem. Soc.,* **2003**, *125*, 9359.

(139) Hunter, C. A. *Angew. Chem. Int. Ed.,* **2004**, *43*, 5310.

(140) Klindworth, A.; Pruesse, E.; Schweer, T.; Peplies, J.; Quast, C.; Horn, M.; Gloeckner, F. O. *Nucleic Acids Res.,* **2013**, *41*

(141) Howell, C.; Diesner, M.-O.; Grunze, M.; Koelsch, P. *Langmuir,* **2008**, *24*, 13819.

(142) Schwendel, D.; Hayashi, T.; Dahint, R.; Pertsin, A.; Grunze, M.; Steitz, R.; Schreiber, F. *Langmuir,* **2003**, *19*, 2284.

(143) Abraham, M. H.; Honcharova, L.; Rocco, S. A.; Acree, W. E., Jr.; De Fina, K. M. *New J. Chem.,* **2011**, *35*, 930.

(144) El-Faham, A.; Albericio, F. *Chem. Rev.,* **2011**, *111*, 6557.

(145) Montalbetti, C. A. G. N.; Falque, V. *Tetrahedron,* **2005**, *61*, 10827.

(146) Balamurugan, S.; Kannan, P. *J. Mol. Struct.,* **2009**, *934*, 44.

(147) Beecham, M. P. Thesis Supramolecular Chaperones to Assist Protein Folding, University of Warwick, 2005.

(148) Cane, D. E.; Yang, G.; Coates, R. M.; Pyun, H. J.; Hohn, T. M. *J. Org. Chem.,* **1992**, *57*, 3454.

(149) Grigoropoulou, G.; Clark, J. H. *Tetrahedron Lett.,* **2006**, *47*, 4461.

(150) Puniredd, S. R.; Assad, O.; Haick, H. *J. Am. Chem. Soc.,* **2008**, *130*, 13727.

(151) Lehner, A.; Steinhoff, G.; Brandt, M. S.; Eickhoff, M.; Stutzmann, M. *J. Appl. Phys.,* **2003**, *94*, 2289.

(152) Rueck-Braun, K.; Petersen, M. A.; Michalik, F.; Hebert, A.; Przyrembel, D.; Weber, C.; Ahmed, S. A.; Kowarik, S.; Weinelt, M. *Langmuir,* **2013**, *29*, 11758.

(153) Jansen, R. J. J.; van Bekkum, H. *Carbon,* **1995**, *33*, 1021.

(154) Metwalli, E.; Haines, D.; Becker, O.; Conzone, S.; Pantano, C. G. *J. Colloid Interface Sci.,* **2006**, *298*, 825.

(155) Dobrzanska, D. A.; Cooper, A. L.; Dowson, C. G.; Evans, S. D.; Fox, D. J.; Johnson, B. R.; Moore, C. I.; Randev, R. K.; Stec, H. M.; Taylor, P. C.; Marsh, A. *Langmuir,* **2012**,

(156) Arima, Y.; Iwata, H. *Biomaterials,* **2007**, *28*, 3074.

(157) Chapman, R. G.; Ostuni, E.; Yan, L.; Whitesides, G. M. *Langmuir,* **2000**, *16*, 6927.

Chapter 3: Characterization of methanogen culture and screening adhesion against different surface functionalities

3.1. Introduction

Biofilms are defined as populations of microorganisms attached to a surface or interface.[1] Complex communities of surface-associated cells are enclosed in extracellular polymeric substances (EPS) containing open water channels. Biofilm formation is often mediated by presence of flagella or type IV pili.[2] These surface appendages play an important role in cell – cell and cell – surface connections. Biofilm formation is initiated by the transition from a reversible to an irreversible attachment mediated by the archaeal flagella (called archaellum[3]) or type IV pili, followed by the cellular aggregation and proliferation.[4]

3.1.1. Biofilm Formation

The most important steps in biofilm formation are initiation, maturation, development and dispersion.[5] The free-floating organisms in the planktonic state start to attach to each other and then to the solid surface, often signalled by secondary metabolites called quorum sensing molecules.[6] At the beginning this process is reversible[7], but after formation of an extracellular matrix, *Bacteria* become permanently associated with surfaces and the biofilm grows further due to cell divisions.[8] *Bacteria* and *Archaea* form complex biofilms due to syntropic interaction between acetogens and methanogens. Fermentation products such as fatty acids and alcohols cannot directly be used in methanogenesis. During acetogenesis, these products are oxidized to acetate and H_2 by obligate proton reducing *Bacteria* and are further used by methanogenic *Archaea*.[9] Regulatory networks involved in

transition from free floating to biofilm-organized structures are however still unknown.[10]

3.1.2. Benefits from Biofilm Formation for Anaerobic Digestion

Biofilm based bioreactors reduce process retention time enabling treatment of more waste in a shorter time.[11] The addition of support materials, such as sepiolite ($Mg_4Si_6O_{15}(OH)_2 \cdot 6H_2O$)[12], plastic membranes[13], glass beads[14], gravel[15], sand,[11] activated carbon[16] or cigarette filter rods[17] has been shown to enhance CH_4 production by increased colonization by syntrophic microbes hence increased process stability.[4,18] There are in fact many studies focused on screening of one or a couple of supporting materials in existing ADs.[19] Less is known concerning archaeal biofilms and so this part of the research focuses on exploring functional groups that might promote biofilm formation. Syntrophic *Bacteria* and methanogens possess hydrophobic cell surfaces and are expected to adhere well to hydrophobic matrices.[20],[21] Hydrophobicity of surfaces promotes adhesion of *Bacteria*, enhancing the formation of aggregates[22] and previous research has demonstrated that hydrophobic *Bacteria* tend to attach better to hydrophobic than hydrophilic surfaces.[23,24] Thermodynamics plays a central role in regulating the binding of *Bacteria* to surfaces. The surface energy of *Bacteria* is typically smaller than the surface energy of liquids in which cells are suspended, and this mismatch causes cells to attach preferentially to hydrophobic materials (materials with lower surface energies).[25] These findings can be used to design possible targets to promote adhesion of methanogens.

3.1.3 Aims

A range of supports and functional groups (tertiary and primary amines, amine oxides and hydroxyl groups presented in Figure 27) was tested with a pure

methanogenic culture to reveal the interactions between cells and surfaces.

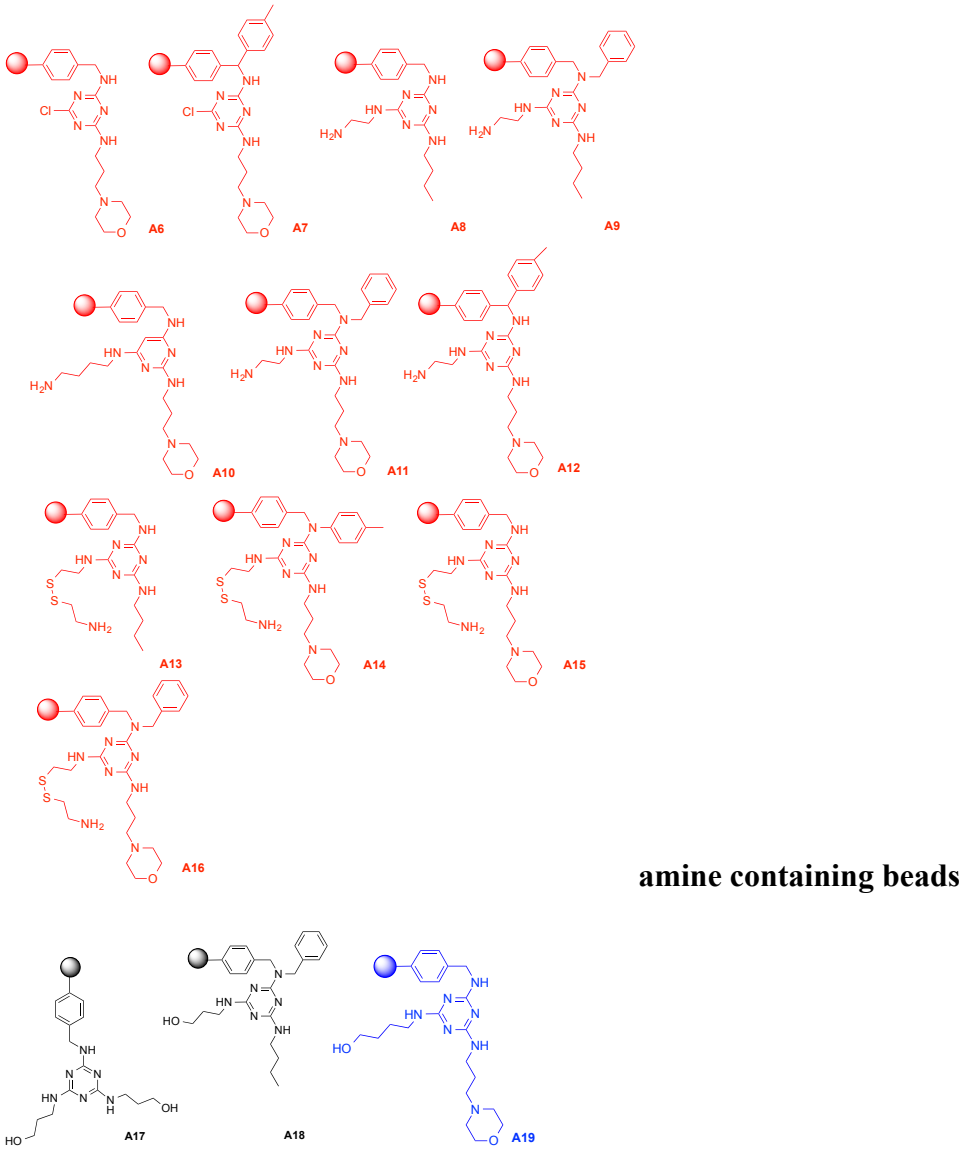

Figure 27 Selection of beads chosen for biofilm formation studies, red = amine containing beads (**A6-A16**), **black**= hydroxyl group containing beads (**A17**, **A18**) and blue = amine and hydroxyl functionalized beads (**A19**).

Methanosarcina barkeri was chosen for these studies, because it is a versatile methanogen, commonly present in anaerobic digesters.[26]

Two approaches were used:

(a) Adhesion of pure methanogenic culture - *M. barkeri* - to one-micron beads examined by flow cytometry.

(b) Adhesion of *M. barkeri* to large functionalized beads studied by a high-throughput 96-well plate fluorescent assay.

3.2. Results and discussion

3.2.1. Characterization of methanogen culture(s) used in screening experiments

3.2.1.1. Isolation of DNA from pure culture of *M. barkeri*

A pure culture of *M. barkeri* was cultivated in standard anaerobic medium (protocol A) prepared according to methods of cultivation for strict anaerobs (protocol B).

Sample name	Strain[35]	DNA yield [ng/µl]	A260/280
MB1	*Methanosarcina barkeri Fusario-DSM804*	4.4	2.4
MB2	*Methanosarcina barkeri 227-DSM1538*	4.5	2.4
MB3	*Methanosarcina barkeri FR-1 - DSM2256*	4.3	2.3
MB4	*Methanosarcina barkeri Jülich - DSM2948*	4.3	2.3

Table 12 Parameters of DNA quality and purity estimated by Nanodrop.

All samples were adequate for further analyses and subjected to Sanger sequencing.

3.2.1.2. Sanger sequencing

To determine the nucleotide sequences in DNA a standard sequencing method with DNA polymerase and specific chain-terminating inhibitors was used.[27] Isolated

DNA was amplified by polymerase chain reaction with universal primer targeting 16SrRNA gene. Figure 28 shows PCR fragments separated by size and visualized by 3% agarose gel electrophoresis.

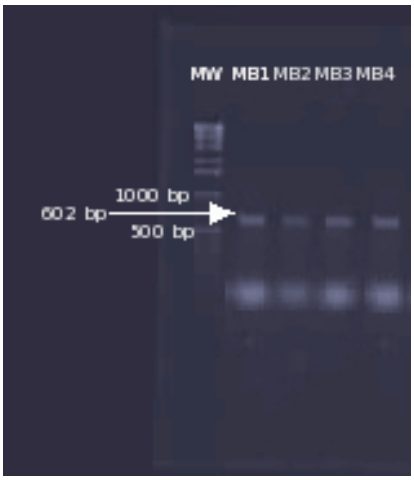

Figure 28 3% agarose gel stained with ethidium bromide for samples extracted from pure culture (MB1-MB4), PCR product present at 602 bp.[28]

Primer	**Sequence**
16S-UniF	5’ GATTAGATACCCTGGTAGTCCAC 3’
16S-UniR	5’ CCCGGGAACGTATTCACCG 3’

Primers nomenclature and sequences.

All returned sequencing results were visualised by Ape and assayed by Basic Local Alignment Search Tool (BLAST). The top hits from BLAST are shown on page 111.

Sample name	Accession number	Name	Score	E.value
MB1	CP000099	*Methanosarcina barkeri* str. Fusaro, complete genome	149	$1x10^{-34}$
MB2	CP000099	*Methanosarcina barkeri* str. 227, complete genome	127	$9x10^{-26}$
MB3	CP000099	*Methanosarcina barkeri* str. FR-1, complete genome	103	$3x10^{-22}$
MB4	CP000099	*Methanosarcina barkeri* str. *Jülich*, complete genome	107	$3x10^{-20}$

Table 13 Assignment of DNA sequences by BLAST search.

Identification of nucleotide sequences from all samples was achieved by searching in the NCBI nucleotide database using the Basic Local Alignment Sequence Test (BLAST) algorithm implemented for a standard nucleotide (blastn).[29] E (expected) value is the number of hits expected during searching of the particular database.[30] All discovered sequences (Table 13) database exhibited a low E value suggesting a good match with the submitted nucleotide sequences therefore confirm successful isolation of DNA from pure culture of *M. barkeri*.

Confocal microscopy was used in order to visualize and assess the intrinsic fluorescence of isolated and sequenced microbial strains of *M. barkeri*. Figure 29 shows *M. barkeri* isolated from (a) ditch mud (b) sewage sludge (b) and (c) broth from a farm-scale maize digester located in the UK.

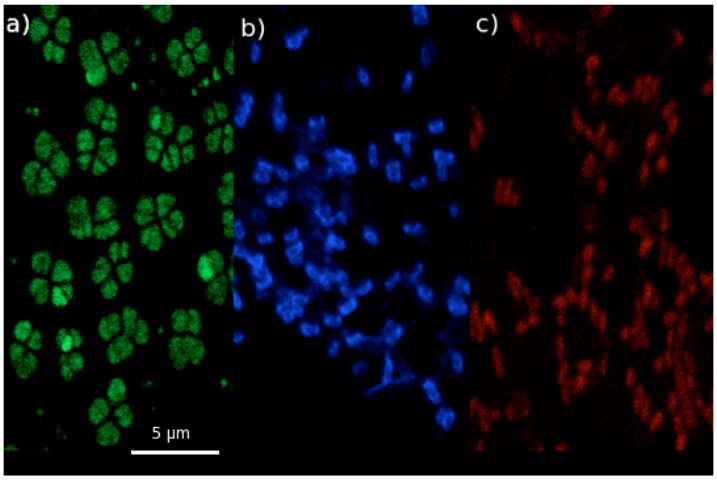

Figure 29 Detection of (a) *M. barkeri* str *Fusario,* (b) *M. barkeri* str *FR-1* (c) *M. barkeri* str *227* by confocal scanning laser microscopy. The image has been artificially coloured for better differentiation of microbial strains.

The intrinsic fluorescence was then measured by counting colony-forming units from dilution plating results against the relative fluorescence units to provide a calibration graph.

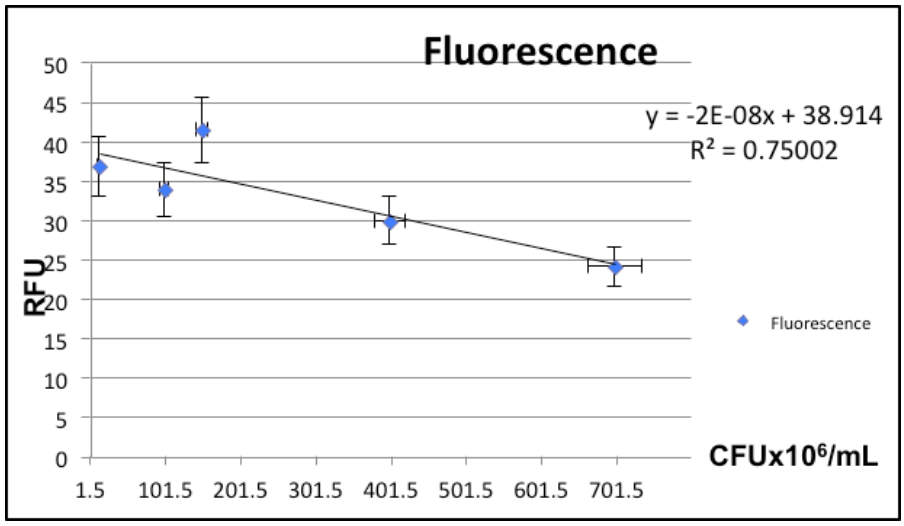

Chart 4 Colony-forming units counted from dilution plating against the relative fluorescence units measured with the Varioskan Flash.

The results show that valid assay results can be obtained for up to 4 times dilution of pure culture to obtain satisfactory fluorescence intensity that would allow easy detection of *M. barkeri* in the assay. The $1.5x10^6$ colony forming units per ml showed the highest fluorescence level of 37 RFU and this concentration would be used in the further experiments.

3.2.1.3. Imaging of agar cultured *M. barkeri* by Scanning Electron Microscopy

Pure culture of *M. barkeri* (DSMZ 804) was grown on solid medium according to the specifications for plating of *Archaea* in solidified medium (details described in protocol C) and visualised by scanning electron microscope (SEM). Examination at lower magnifications revealed uniform biofilm density over the surface and a variety of morphologies seen in the samples. Figure 30a shows microbial biofilm formed after 24 h. It is significantly different from the control image of agar (Figure 30b)

(a) (b)

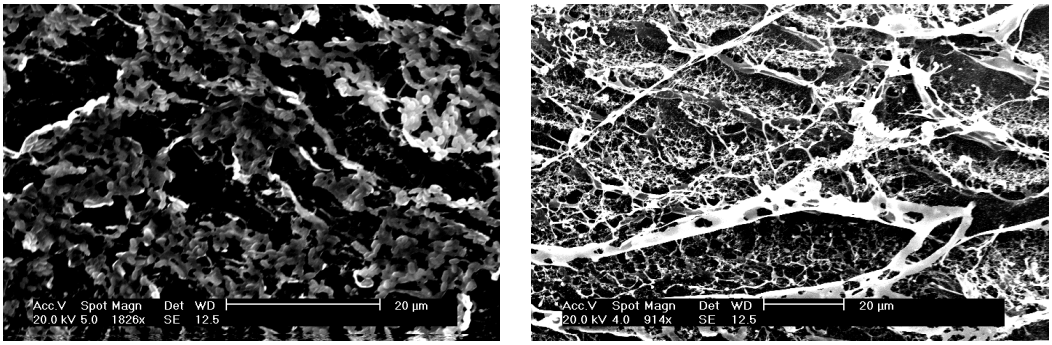

Figure 30 SEM micrographs of (a) biofilm formed after 24 hours by *M. barkeri* on solid medium, (b) control image of pure agar, scale bar = 20 µm.

The structure of biofilm was examined again after 7 days. Many rod shape cells had long filamentous appendages (Figure 31a). These structures were as long as 20 µm (filament 1) or 30 µm (filament 2).

(a)

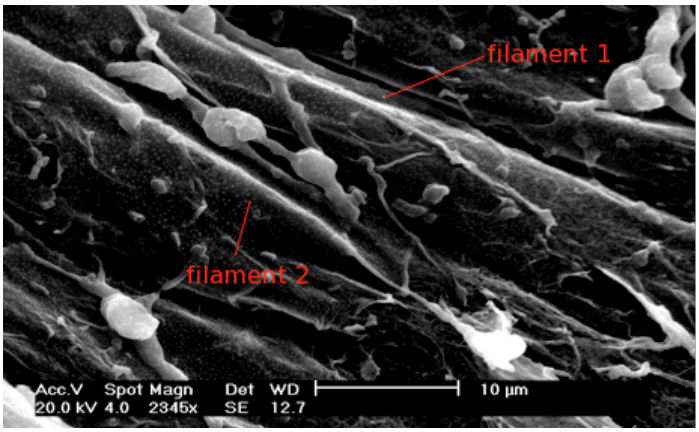

(b)

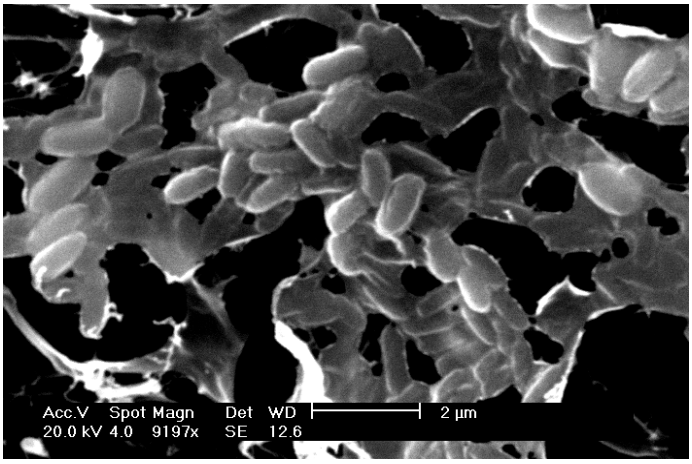

Figure 31 SEM micrograph of biofilm formed by *M. barkeri* on solid medium after 7 days viewed at (a) 2345 and (b) 9197 magnification, scale bar = 10 µm and 2 µm, respectively.

SEM micrographs revealed distinctive morphological features of biofilms formed by *Methanosarcina barkeri* such as filamentous appendages and high density of large cell aggregates, forming towering structures of coccoid cells (Figure 31a and Figure 31b). Similar biofilm structure was reported in the literature for hyperthermophilic *Archaea Sulfolobus spp* (Figure 4c and Figure 4d)[31]. This experiment gave a preliminary insight into *M.barkeri* biofilm morphology which should be studied further using diverse methanogenic *Archaea*.[32]

3.2.2. Functionalization of polystyrene beads

Commercially available 1 μm polystyrene carboxyl functionalized beads were chemically modified according to the protocol used in Chapter 2. Figure 32 shows derivatization of beads with a 2-(dimethylamino)ethylamine to give amine functionalized polystyrene beads, (**A1-PS**), resulting beads were oxidised with m-CPBA in DCM to produce the corresponding amine oxide beads **(AO1-PS**). Oxidizing agent was changed for this experiment because m-CPBA is more selective than hydrogen peroxide and it is not going to react with underlying polystyrene.[33]

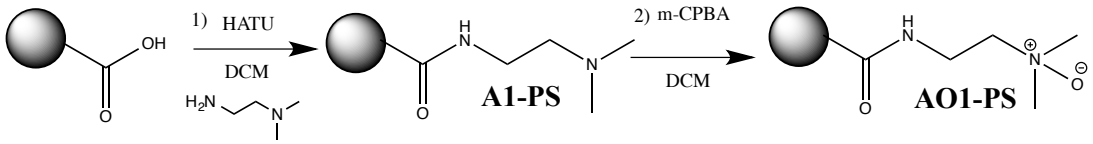

Figure 32 Amine functionalize polystyrene Wang resin (**A1-PS**) and corresponding amine oxide **(AO1-PS**).

The characteristic functional groups of the polystyrene beads before and after functionalization were characterized by infrared spectroscopy (FTIR) (Figure 33). Before oxidation the stretching of C–H bonds was recorded at 2930 cm^{-1} and 2855 cm^{-1}. The appearance of the absorption peaks at 1713 cm^{-1}, 1608 cm^{-1}, and 1460 cm^{-1} attributed to C=O stretching of carboxylic acids, C=O stretching of amides and N–H bending of the amides, respectively. After oxidation three new bands appeared (highlighted in blue boxes) at 1062 cm^{-1} (-OH bending), 1247 cm^{-1} (amine oxide) and a weak signal at 3677 cm^{-1} (free –OH) confirming successful oxidation of polystyrene beads.

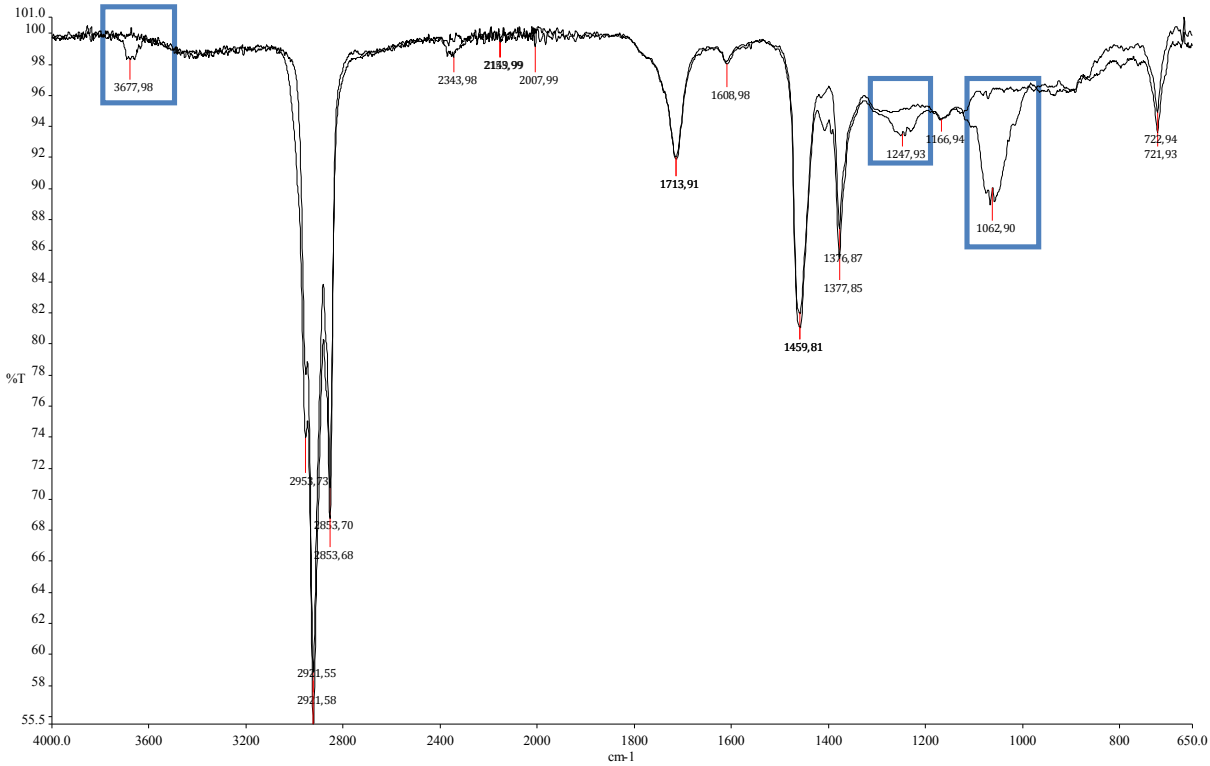

Figure 33 FTIR spectra before and after oxidation of fluorescent beads. Blue regions show appearance of new peaks after oxidation process.

3.2.3. Flow cytometry

Cytometry is widely used for the analysis of particles such as cells and beads.[34] Particle identification is usually performed with a combination of laser light scatter and electrical volume (Coulter) analysis[35]. Cells flow between two pairs of miniature electrodes with AC field applied across them. As the cell passes between the electrodes, the change in current is monitored and it gives a single cell impedance signal.[35] At low applied signal frequencies the technique provides accurate cell sizing where the impedance signal is proportional to cell volume[36].

Flow cytometry was used to screen the interactions between pure archaeal culture of *Methanosarcina barkeri* and amine (**A1-PS**) and amine oxide (**AO1-PS**) functionalized polystyrene beads. Change in size after adhesion of methanogens to microspheres was detected by change in electrical impedance. Flow cytometry

datasets presented in **Figure 34** consist of two graphs 1) 2D scatter plots of fluorescence versus impedance and 2) Histogram of the size (cube root of impedance).

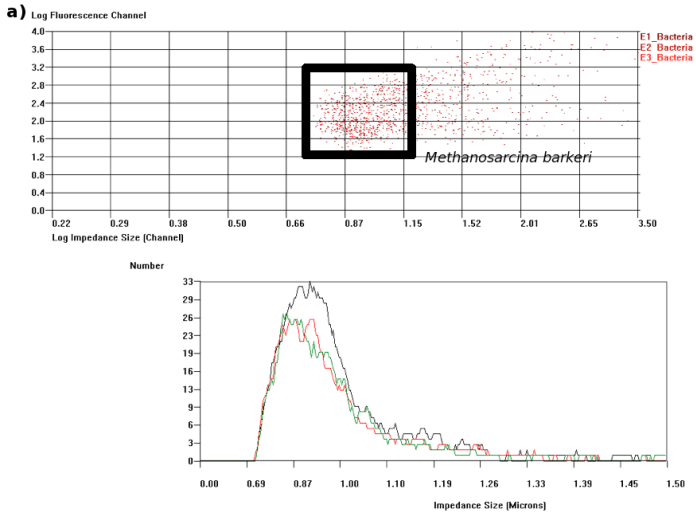

Figure 34 (a) 2D scatter plot and 1D size histogram for pure culture of *M. barkeri* ($1.5x10^6$ CFU/ml).

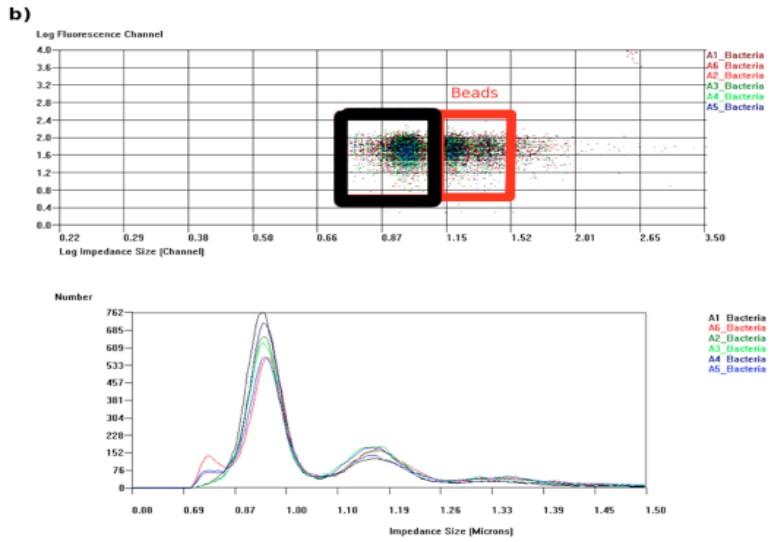

Figure 34 (b) 2D scatter plot and 1D size histogram for mixture of *M. barkeri* ($1.5x10^6$ CFU/ml) and 1.0 µm polystyrene beads functionalized with carboxyl groups.

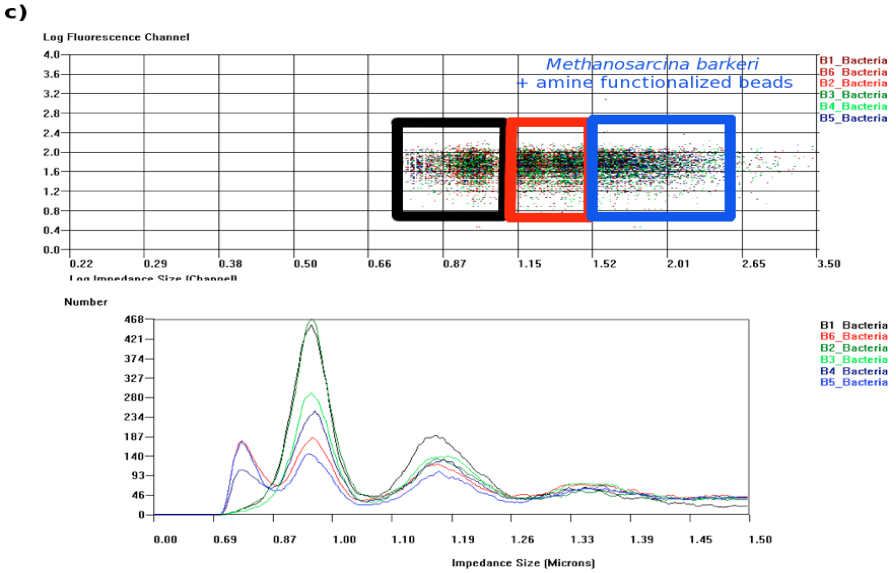

Figure 34 (c) 2D scatter plot and 1D size histogram for mixture of *M. barkeri* ($1.5x10^6$ CFU/ml) and polystyrene beads **A1-PS**.

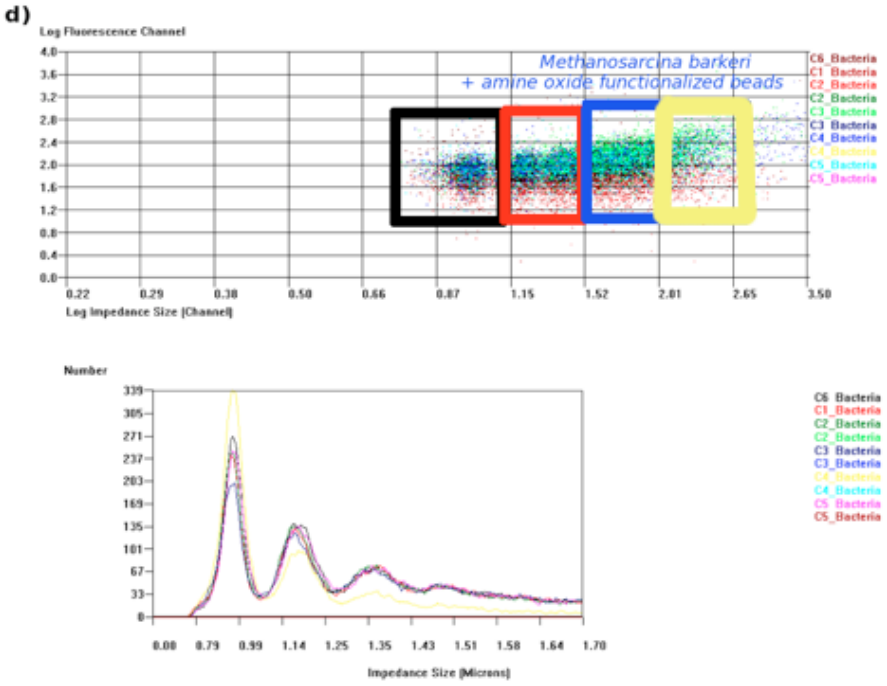

Figure 34 (d) 2D scatter plot and 1D size histogram for mixture of *M.barkeri* ($1.5x10^6$ CFU/ml) and polystyrene beads **AO1-PS.**

2D scatter plot in **Figure 34a** shows one sub-population (black frame) in a sample. This is confirmed by presence of one peak in size histogram at 0.87 μm. In **Figure 34b** two subpopulations were identified: one at 0.87 μm (black frame) corresponding to pure culture and one at 1.19 μm (red frame) belongs to methanogens bound to carboxyl beads. **Figure 34c** is depicted into three subpopulations: at 0.87 μm (black frame - methanogens), 1.19 μm (red frame - carboxyl beads and methanogens) and a new peak at 1.57 μm showing methanogens bound to the amine functionalized beads (blue frame). Four subpopulations are present in **Figure 34d:** a peak at 0.87 μm (methanogens – black frame), 1.19 μm (carboxyl beads + methanogens – red frame), 1.57 μm (amine beads and methanogens – blue frame) and a new peak at 2.02 μm (methanogens bound to oxidised beads – yellow frame). The results described above show that flow cytometry provides a method for measuring interactions between beads and *M. barkeri*. However it lacks control measurements of impedance for amine and amine oxide functionalized beads without addition of pure culture. There are nonetheless several other advantages of this approach. Firstly, the sensitivity can be easily increased to meet the specifications of the experiment by analysing more beads. This method also allows screening of interactions between beads and the population of organisms extracted from full-scale anaerobic digester.

3.2.4. High-throughput fluorescent assay for screening the influence of a variety of functional groups on microbial adhesion

Flow cytometry is a rapid method but it is limited to availability of suitable 1 μm beads as controls and the pass filters in the instrument have the fluorescence detection limits only between 620 – 720 nm. Hence this second study quantified methanogens adhesion using an automated fluorescence plate reader. The results were expressed as fluorescence intensity values. A series of three assays were

performed to test influence of custom synthesized beads on biofilm development. The assay used intrinsic fluorescence of enzyme F_{420} present in *M. barkeri*.[37] Pure culture was visualised by confocal microscopy at an excitation wavelength of 467 nm and emission range between 500-550 nm. A selection of custom made polystyrene beads synthesised in the Marsh group by Craig Wood[38] was used to compare the organisation of methanogens on primary amines (**A6- A16**), hydroxyl groups (**A17-A18**) and mixed functionalities (**A19**) as adherents (Figure 34).

The size of the triazine functionalised polystyrene beads **A6 - A19** was determined by optical microscopy at three different magnifications (Figure 35) and using a Mastersizer particle analyser (Figure 36). The latter revealed that the diameter of the beads ranged between 95-297 µm, with a median size D(0.5) of 135 µm.

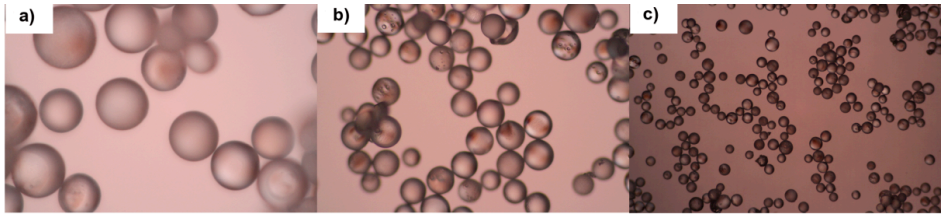

Figure 35 Images of beads magnified at (a) x 100 (b) x 60 (c) x 20

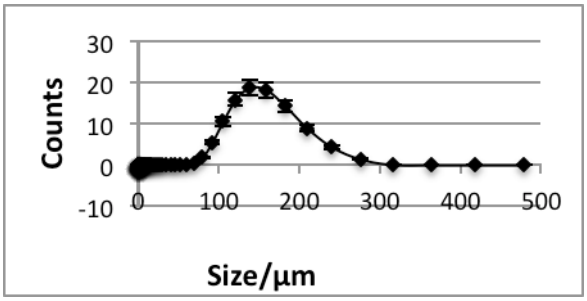

Figure 36 Size (diameter) distribution of latex beads measured by Mastersizer.

Fluorescence measured for binding of *M. barkeri* to 0.02 g of each triazine functionalized polystyrene bead type is summarized in Chart 5.

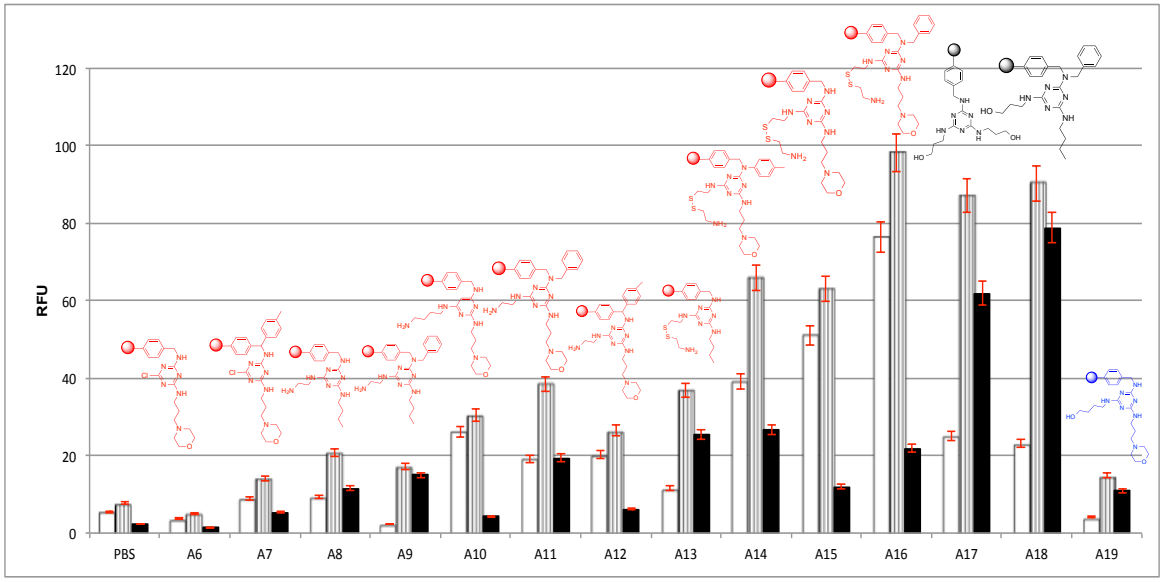

Chart 5 Fluorescence intensity for binding of *M. barkeri* to each triazine functionalized polystyrene bead suspended in (a) 100 µl PBS buffer (white bars); (b) mixture of beads and *M. barkeri* ($1.5x10^6$ CFU/ml) pure culture in 100 µl of medium after incubation for 12 h in anaerobic chamber in darkness (stippled bars) and (c) the fluorescence of pure culture calculated by subtraction (RFU for beads + pure culture) – (RFU beads) = RFU pure culture (black bars). All measurements were performed in triplicate.

These data demonstrate that the greatest intrinsic fluorescence (white bars) was observed for beads **A10**, **A11**, **A12, A14**, **A15** and **A16** that contain both morpholine and primary amine in their structure. High intrinsic fluorescence is ascribed to the protonation of amines or morpholines in PBS buffer, pH = 7.4 (forming monoprotonated or diprotonated species, see **Table 14**).

Symbol	Structure and charge at pH = 7.4	Symbol	Structure and charge at pH = 7.4
A10	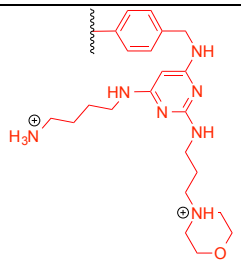	**A14**	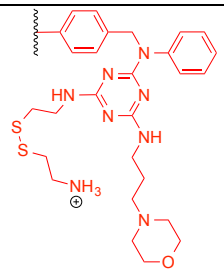
A11	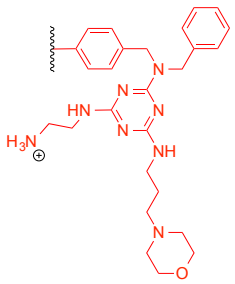	**A15**	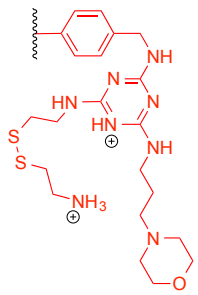
A12	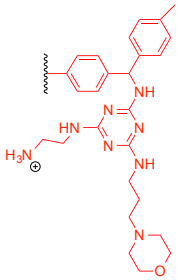	**A16**	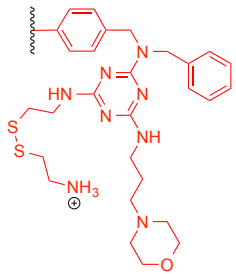
A13	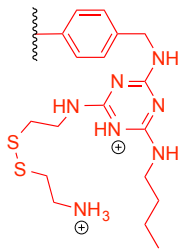	**A17**	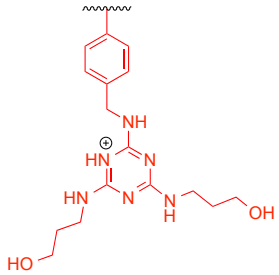

Table 14 Structures and charge distribution at pH=7.4 for beads **A10-A17**. The computed protonation characteristics (pKa) and hydrophobicities (log D, logP) of all the beads are showed in Appendix 9.

The biggest change in fluorescence after mixing with the methanogenic pure culture (black bars) was observed for beads **A17** and **A18**, possessing two hydroxyl groups or one hydroxyl group and short aliphatic chain respectively. Hydroxyl containing beads **A17** are hydrophilic[39] while beads **A18** contain a hydrophobic– CH_3 group and hydrophilic –OH moiety[39]. Surface chemistry depended studies on differences in

adhesion have been wildly investigated on proteins[39] and *Bacteria*[40,41]. Marine hydrophobic *Bacteria Cobetia marina* attached preferentially to hydrophobic surfaces.[40] *Methanosarcina barkeri* posses hydrophobic cell envelope so the attachment to beads **A18** with hydrophobic $-CH_3$ moiety is preferential and can be explained by low free surface energy. The thermodynamic theory could not explain why *Archaea* adhered onto the OH-terminated beads (**A17**), although this could be explained by the attractive electrostatic interactions between positively charged residues present in archaeal cell envelope and –OH terminated **A17** beads.

3.3 Conclusions

The results show potential applications of flow cytometry and fluorescence assay for measuring interactions between methanogens and different functional groups. There is a scope for extending the research by testing a variety of methanogens extracted from existing anaerobic digesters and fluorescent beads using FACS or fluorescent assay. However, it would be challenging due to lack of data with the specific fluorescence detection wavelengths for methanogens. The experiments would require optimisation of conditions for mixed microbial populations. Hence a different approach using high-throughput sequencing was used in the large-scale experiment described in Chapter 4. This enabled the identification of microbial communities from a large-scale anaerobic digester and the screening of their interactions with commercial supporting materials.

3.4 Methods and Materials

3.4.1. Microbial Strains

The list of microbial strains used for this research is shown in Table 15.

Strain DSMZ accession number	Name	Isolation	Geographic origin	Cultivation conditions
DSMZ 805	*Methanosarcina barkeri*	ditch mud	Germany	anaerobic, 35°C medium 120
DSMZ 1538	*Methanosarcina barkeri*	Sewage sludge digester	USA	anaerobic, 37°C medium 120
DSMZ 2256	*Methanosarcina barkeri*	sewage sludge	United Kingdom	anaerobic, 35°C medium 120
DSMZ 2948	*Methanosarcina barkeri*	sewage sludge digester	Germany	anaerobic, 35°C medium 120

Table 15 Description and origin of the microbial strains.

3.4.2. Growth and storage of *Methanosarcina barkeri*

Strict anaerobes like *M. barkeri* require working in anoxic conditions at all times. Protocol A describes how to use anaerobic chamber for growth and storage of strict anaerobes.

(Protocol A) Protocol for using anaerobic chamber

Bringing Items into the Chamber

1. Verify that the oxygen level in the camber is below 10 ppm and that the hydrogen level is above 1%. Also verify that the N_2 and the N_2 /CO_2/H_2 tanks are open and not empty.

2. Verify that the inner interchange door is sealed, and that the gas, catalyst, and vacuum systems are set to "Auto".

3. Open the outer interchange door and place items inside. Close and latch door.

4. Press the "Start" button. The following sequence should occur:

- Interchange chamber is evacuated
- Interchange chamber fills with N_2
- Interchange chamber is evacuated
- Interchange chamber fills with N_2
- Interchange chamber is evacuated
- Interchange chamber draw gas from the main chamber to equilibrate

5. Wait until the proper lights indicate that the chamber is anaerobic, and that it is safe to open the inner interchange door.

6. Open the inner interchange door by

(a) lifting the handle,

(b) rotating the handle clockwise,

(c) pushing the door towards the back of the chamber.

7. Pull interchange tray into the main chamber and unload items.

8. Reseal the inner interchange door.

Bringing Items out of the Chamber

9. Verify that the interchange chamber is anaerobic. Then, press the "Start" button. The interchange will cycle as described above. If the chamber is already anaerobic, there is no need to cycle the gases.

11. Open the inner interchange door and pull interchange tray into the main chamber.

12. Load items on the tray and return the tray to the interchange chamber.

13. Reseal the inner interchange door.

14. Open the outer interchange door and unload items.

(Protocol B) *Methanosarcina barkeri* medium and cultivation

General medium mixture

The composition of the basic medium used for all experiments was based on DSM 120 medium. The basic medium contained (per litre): 0.348 g K_2HPO_4, 0.227 g KH_2PO_4, 0.5 g NH_4Cl, 0.5 g $MgSO_4 \cdot 7H_2O$, 0.25 g $CaCl_2 \cdot 2H_2O$, 2.25 g NaCl, 0.002 g $FeSO_4 \cdot 7\ H_2O$, 1 mg sodium resazurin, 2 g yeast extract, 2 g casitone, 10 ml vitamin solution, 1 ml trace element solution. The vitamin solution was replaced with that of DSM 141 medium. The composition was as follows (per litre): 2.0 mg biotin, 2.0 mg folic acid, 10.0 mg pyridoxine hydrochloride, 5.0 mg thiamine hydrochloride, 5.0 mg riboflavin, 5.0 mg nicotinic acid, 5.0 mg calcium pantothenate, 0.1 mg vitamin B12, 5.0 mg *p*-aminobenzoate and 5.0 mg lipoic acid. The trace element solution was based on DSM SL-10 medium and contained (per litre): 1.5 g $FeCl_2 \cdot 4H_2O$, 70 mg $ZnCl_2$, 100 mg $MnCl_2$, 6 mg H_3BO_3, 190 mg $CoCl_2$ x $6H_2O$, 2 mg $CuCl_2 \cdot 2H_2O$, 24 mg $NiCl_2$ x $6H_2O$ and 36 mg $Na_2MoO_4 \cdot 2H_2O$. The trace element solution was adjusted to pH 6.5 with 7.7 M HCl.

For growth of the syntrophic acetate-oxidizing co-culture, general medium contained 80 mM sodium acetate and 10 ml methanol was used as the substrate. The medium was anaerobically dispensed into serum vials. The vials were sealed with butyl rubber stoppers fitted with caps. The medium was autoclaved for 20 min at 121 °C. The pH of the autoclaved medium was approximately 6.4. Prior to inoculation, the medium was reduced with sterile stock solutions of titanium citrate and cysteine hydrochloride. Unless otherwise noted cultures were incubated at 55 °C in the dark without shaking.

(C) Plating in solidified medium

General *Methansarcina barkeri* medium, prepared according to the protocol B, was mixed with 10g/litre of agar (Difco 0140-01-0). The mixture was boiled in a 500 ml Pyrex Florence flask under a steam of N_2/CO_2 (80:20). Prepared medium was reduced with cysteine hydrochloride (5 g/L) and the flask was secured with stopper and sterilized by autoclaving for 20 min at 121 °C. The flask was transferred to the anaerobic chamber and when it cooled to the touch (50-55°C) 10 ml of medium was dispensed to Petri dishes which were left in the chamber for 2 days to dry, then 0.2 ml of culture suspension was transferred to agar plates. Before inverting the plates suspension was allowed to soak onto the medium for a few minutes.

3.4.3. Fluorescence assay

Beads (0.02 g) were weighed and transferred to a 96-well plate in PBS buffer (100 µl), mixed with pure culture of *M. barkeri str. FR-1* and incubated overnight at 37 °C. Each fluorescence reading was replicated three times. The same mass (0.02 g) of beads was transferred to each well and suspended in 100 µl of PBS buffer. The fluorescence was measured for the first time and the same measurement was

repeated after addition of 100 µl of *M. barkeri str. FR*-in culture media and incubation for 12 h in darkness at 37 °C.

The fluorescence was measured twice at an excitation and emission wavelength of 465 and 500-550 nm, respectively, using Varioskan Flash (Thermo Fisher Scientific Inc).

3.4.4. Imaging of methanogen culture by Scanning Electron Microscopy

Agar was cut into small sections and freeze-dried. The samples were mounted onto electron microscope stubs using double-sided carbon tape and a fine layer of gold was deposited on them for 3 minutes using BioRad-E5200 sputter coater. Coated samples were observed using a JEOL T330A scanning electron microscope.

3.4.5. Molecular Biology techniques

3.4.5.1. DNA extraction

Chromosomal DNA was extracted according to the protocol described by Griffiths.[42] The resulting DNA was suspended in 50 µl of nuclease-free water and stored at -20 °C., A Nanodrop® instrument was used to assess the concentration and purity of nucleotide solutions, measuring the absorbance of nucleotides at 260 nm and proteins at 280 nm..[43]

3.4.5.2. Polymerase chain reaction (PCR)

Oligonucleotide primers were designed using PrimerSelect - part of the DNA Star sequence analysis software. Each reaction was carried in a final volume of 20 µl. Samples were run on a GeneAmp 9700 thermocycler under the following conditions: initial denaturation for 2 min at 94 °C, followed by 30 cycles of incubation at 95 °C for 5 min, denaturation at 95 °C for 30 s, annealing at 50 °C for 30 s and elongation at 68 °C for 1 min per kb.

Reagent	Volume/ µl
Buffer	4
dNTP's	0.4
Primer forward	1
Primer reverse	1
H_2O	12.4
Taq DNA polymerase	0.2
Template DNA	1
Total volume	**20 µl**

Table 16 PCR reagents mix.

3.4.5.4. DNA analyses by agarose gel electrophoresis

Agarose gels were prepared by dissolving agarose (Difco) in 1 x tris acetate - EDTA (TAE) buffer to a final concentration of 1-3 % and adding gel red stain. The size of DNA fragments was determined by comparison with a simultaneously run 1 kb ladder (0.5 µl). Gels were run at 150 V for 30 min.

3.4.5. Purification of DNA

PCR product were purified using a QIAquick PCR purification kit) Qiagen, Crawley, UK) according to the manufacturer's instructions.

3.4.6. Flow Cytometry

The size and level of fluorescence for pure culture of *M. barkeri* and 1 µm beads was measured by CellFacts II instrument (University of Warwick, Science Park, Coventry, UK). All measurements were repeated three times.

3.5. References

(1) Tenke, P.; Riedl, C. R.; Jones, G. L.; Williams, G. J.; Stickler, D.; Nagy, E. *Int. J. Antimicrob. Agents,* **2004**, *23*, S67.

(2) Siri, M. I.; Sanabria, A.; Boucher, C.; Pianzzola, M. J. *Mol. Plant-Microbe Interact.,* **2014**, *27*, 712.

(3) Jarrell, K. F.; Albers, S.-V. *Trends Microbiol.,* **2012**, *20*, 307.

(4) Leng, R. A. *Animal Production Science,* **2014**, *54*, 519.

(5) Donlan, R. M. *Clin. Infect. Dis.,* **2001**, *33*, 1387.

(6) Parsek, M. R.; Greenberg, E. P. *Trends Microbiol.,* **2005**, *13*, 27.

(7) Hinsa, S. M.; Espinosa-Urgel, M.; Ramos, J. L.; O'Toole, G. A. *Mol. Microbiol.,* **2003**, *49*, 905.

(8) Davies, D. G.; Parsek, M. R.; Pearson, J. P.; Iglewski, B. H.; Costerton, J. W.; Greenberg, E. P. *Science,* **1998**, *280*, 295.

(9) de Bok, F. A. M.; Harmsen, H. J. M.; Plugge, C. M.; de Vries, M. C.; Akkermans, A. D. L.; de Vos, W. M.; Stams, A. J. M. *Int. J. Syst. Evol. Microbiol.,* **2005**, *55*, 1697.

(10) Albers, S.-V.; Meyer, B. H. *Nat. Rev. Microbiol.,* **2011**, *9*, 414.

(11) Ueno, Y.; Tatara, M. *Enzyme Microb. Technol.,* **2008**, *43*, 302.

(12) Dong, Z.; Lu, M.; Huang, W.; Xu, X. *J. Hazard. Mater.,* **2011**, *196*, 123.

(13) Chauhan, A.; Ogram, A. *Biochem. Biophys. Res. Commun.,* **2005**, *327*, 884.

(14) Liang, Y.; Zhang, X.; Dai, D.; Li, G. *Int. Biodeterior. Biodegrad.,* **2009**, *63*, 80.

(15) Singh, S. P.; Prerna, P. *Renewable & Sustainable Energy Reviews,* **2009**, *13*, 1569.

(16) Kindzierski, W. B.; Gray, M. R.; Fedorak, P. M.; Hrudey, S. E. *Water Environ. Res,* **1992**, *64*, 766.

(17) Sabzali, A.; Nikaeen, M.; Bina, B. *Environ. Technol.,* **2012**, *33*, 1803.

(18) Gan, Y.; Qiu, Q.; Liu, P.; Rui, J.; Lu, Y. *Appl. Environ. Microbiol.,* **2012**, *78*, 4923.

(19) Chanakya, H. N.; Srivastav, G. P.; Abraham, A. A. *Current Science,* **1998**, *74*, 1054.

(20) Meierschneiders, M.; Busch, C.; Diekert, G. *Appl. Microbiol. Biotechnol.,* **1993**, *38*, 667.

(21) Boks, N. P.; Norde, W.; van der Mei, H. C.; Busscher, H. J. *Microbiology-Sgm,* **2008**, *154*, 3122.

(22) Liu, W. T.; Chan, O. C.; Fang, H. H. P. *Water Res.,* **2002**, *36*, 3203.

(23) Kang, S.; Hoek, E. M. V.; Choi, H.; Shin, H. *Sep. Sci. Technol.,* **2006**, *41*, 1475.

(24) Perez, M.; Romero, L. I.; Rodriguez-Cano, R.; Sales, D. *Chem. Biochem. Eng. Q.,* **2006**, *20*, 203.

(25) Tuson, H. H.; Weibel, D. B. *Soft Matter,* **2013**, *9*, 4368.

(26) Weiland, P. *Appl. Microbiol. Biotechnol.,* **2010**, *85*, 849.

(27) Sanger, F.; Nicklen, S.; Coulson, A. R. *Biotechnology (Reading, Mass.),* **1992**, *24*, 104.

(28) Ashimoto, A.; Chen, C.; Bakker, I.; Slots, J. *Oral Microbiol. Immunol.,* **1996**, *11*, 266.

(29) Altschul, S. F.; Gish, W.; Miller, W.; Myers, E. W.; Lipman, D. J. *J. Mol. Biol.,* **1990**, *215*, 403.

(30) Neumann, R. S.; Kumar, S.; Shalchian-Tabrizi, K. *Brief. Bioinform.,* **2014**, *15*, 484.

(31) Koerdt, A.; Goedeke, J.; Berger, J.; Thormann, K. M.; Albers, S.-V. *Plos One,* **2010**, *5*

(32) Ng, S. Y. M.; Zolghadr, B.; Driessen, A. J. M.; Albers, S.-V.; Jarrell, K. F. *J. Bacteriol.,* **2008**, *190*, 6039.

(33) Cai, X.; Sha, M.; Guo, C.; Pan, R. M. *Asian J. Chem.,* **2012**, *24*, 3781.

(34) Tkaczyk, E. R.; Tkaczyk, A. H. *Cytometry Part A,* **2011**, *79A*, 775.

(35) Shapiro, H. M. *Practical flow cytometry, Third edition*, 1995.

(36) Sun, T.; Morgan, H. *Microfluidics and Nanofluidics,* **2010**, *8*, 423.

(37) Doddema, H. J.; Vogels, G. D. *Appl. Environ. Microbiol.,* **1978**, *36*, 752.

(38) Wood, C. Thesis PhD Thesis, University of Warwick, 2010.

(39) Prime, K. L.; Whitesides, G. M. *J. Am. Chem. Soc.,* **1993**, *115*, 10714.

(40) Ista, L. K.; Callow, M. E.; Finlay, J. A.; Coleman, S. E.; Nolasco, A. C.; Simons, R. H.; Callow, J. A.; Lopez, G. P. *Appl. Environ. Microbiol.,* **2004**, *70*, 4151.

(41) Katsikogianni, M. G.; Missirlis, Y. F. *Journal of Materials Science-Materials in Medicine,* **2010**, *21*, 963.

(42) Griffiths, R. I.; Whiteley, A. S.; O'Donnell, A. G.; Bailey, M. J. *Appl. Environ. Microbiol.,* **2000**, *66*, 5488.

(43) Klindworth, A.; Pruesse, E.; Schweer, T.; Peplies, J.; Quast, C.; Horn, M.; Gloeckner, F. O. *Nucleic Acids Res.,* **2013**, *41*

Chapter 4 Comparative microbial community structures in the planktonic phase and foam supports from a full-scale anaerobic digester, fresh slurry and the sediment from a waste slurry

4.1. Introduction

The first sequencing technologies were based on sequencing by chain termination developed by Gilbert in 1973 and Sanger in 1977.[1,2] This method requires separation of DNA fragments by electrophoresis which is time consuming and labour intensive but ideal for small applications that require high accuracy.[3]

From the 1990s the method based on multiple sequencing in one reaction, called sequencing by synthesis or pyrosequencing became available.[4] It was a big step forward in terms of diversity studies that enabled sequencing of the human genome (length: 3 billion base pairs).[5] In 2000 formation of the 454 Life Sciences sequencing platform allowed a large-scale parallel, automated pyrosequencing of the metagenome of the human gut and mouth[6], soil[7], coral reefs[8], deep sea thermal vents[9], drinking water[10] and anaerobic digestion[11-13].

4.1.1. Principles of 454-sequencing

In pyrosequencing, a primer binds to the DNA template and DNA polymerase, incorporates complementary nucleotides, generating inorganic pyrophosphate as it does so (Figure 37). This pyrophosphate is converted to ATP by a sulfuylase and luciferase uses the ATP to convert luciferin to oxyluciferin, producing light in the process. This generated light is seen as a peak on a ‘pyrogram’ and the height of each peak is proportional to the number of nucleotides incorporated.[3]

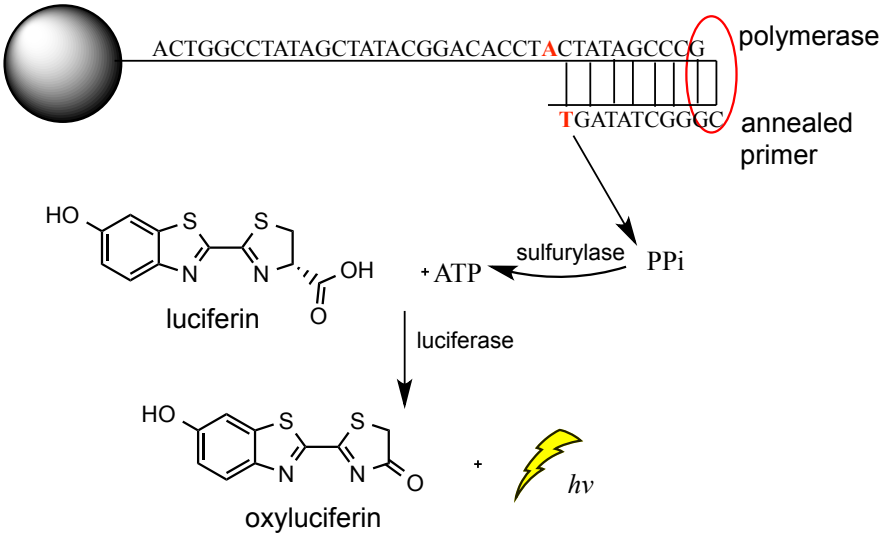

Figure 37 Schematic representation of pyrosequencing.

The samples collected from two different sites were sequenced (farm lagoon and industrial anaerobic digester broth) using specific primers with "barcode" sequences and "adaptors" (key, A, B).[14] It allowed identification of the samples and more cost-effective sequencing approach. Figure 38 shows the design of primers with barcode and adaptors

attached.

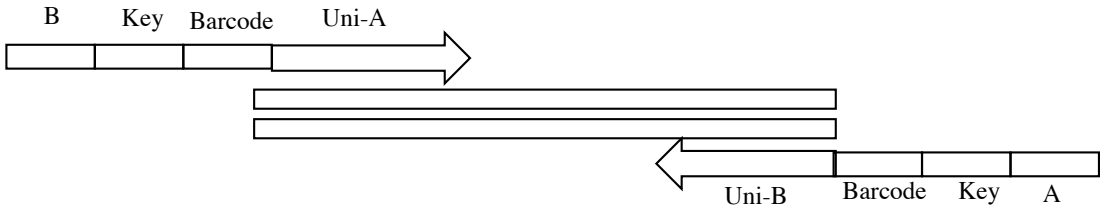

Figure 38 The design of primer sequence with barcodes and adaptors.

The microbial communities were examined using 454 – sequencing of 16S rRNA gene sequence. The primers selected for this study are shown in **Table 17**.

Primer nomenclature	Sequence	Target group
16S Uni F	AGAGTTTGATCATGGCTCAG	Domain Bacteria
16S Uni R	ACCGCGGCTGCTGGCAC	Domain Bacteria
S-D-Arch-0519-a-S-15	CAGCMGCCGCGGTAA	Domain Archaea
S-D-Arch-1041-a-A-18	GGCCATGCACCWCCTCTC	Domain Archaea

Table 17 Primer sequences and target domains used for 454 – sequencing.

The raw data from the sequencer (primers, barcodes and desired sequences) saved as .sff file was processed and analysed following the steps described in Scheme 5.

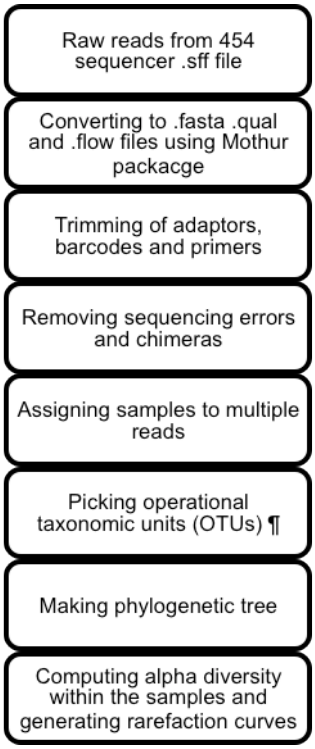

Scheme 5 Processing steps for raw 454-sequencing data.

4.2. Results and Discussion - Microbial diversity based on sequencing reads

Insight into the metagenomes of microbial communities residing in a large-scale biogas plant, on supporting materials and in the farm lagoon was thus obtained by means of the 454-pyrosequencing of 16S rRNA gene sequence followed by data

interpretation using bioinformatics strategies. Two datasets were obtained and compared:

(1) *Bacteria* and *Archaea* present in the full-scale digester (FD) compared to organisms from autoclaved polyurethane foams contained in the stainless steel baskets (Figure 43, page 153) and kept in the biogas reactor for 30 days (SM).

(2) *Bacteria* and *Archaea* present in cows rumen solids (RS) that is fed to the methane producing lagoon and the sediment from the lagoon (LS) to identify microorganism responsible for methane production in different environments.

A total of 89 084 sequences were obtained.

4.2.1. Bacterial community structure

The average length of bacterial sequences was 530 bp. After trimming primers and removal of chimeras the average sequence length reduced to 487 bp. The number of OTUs for *Bacteria* for each sample is presented in Table 18.

Sample name	OTUs
full scale digester (FD)	4254
supporting materials (SM)	5395
cow rumen solids (RS)	5813
lagoon sediment (LS)	7841

Table 18 Bacterial OTUs[15]assignment per sample.

Operational taxonomic units (OTUs[16]) were determined at a distance level of 5% (95% of base pairs match the sequence of identified organism) to compare the bacterial species among each sample. The highest OTU number was present in the lagoon sediment (LS) sample. The supporting materials (SM) contained the lowest number of OTUs. Alpha (α) diversity (within the community) was determined by

calculating the Shannon index,[15] chao1, observed species and phylogenetic distance (PD). Figure 39 was plotted based on the PD and sequences per sample.

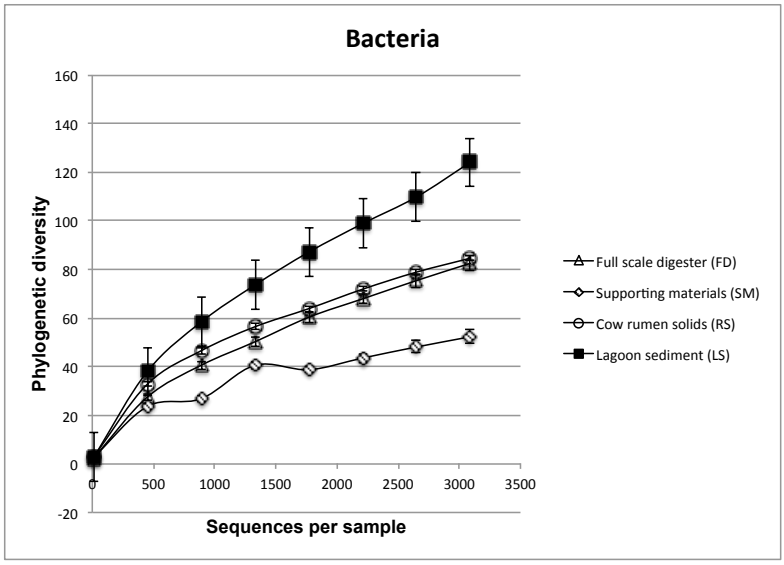

Figure 39 *Bacteria* rarefaction curves for four samples at a distance level of 5%. Bacterial sequences were assigned to the corresponding taxonomies by QIIME pipeline (http://qiime.org/index.html step-by-step guide published by Kuczynski *et.al*.[17]) and the results overview presented in Chart 6 and Chart 7.

4.2.1.1. Fruit and vegetable digester

Chart 6 shows a significant difference in bacterial diversity for the SM sample. One phylum, *Planctomycetes* (orange) which bear an anchor structure[18] was present only in SM and not in FD. Over 37 % of the sequences in SM were assigned to *Spirochaetes* (green), comparing to lower values of 4% for FD. *Chloroflexi*, a diverse class which includes aerobic thermophiles, anoxygenic phototrophs and *Bacteria* which can use polychlorinated biphenyls as an energy source[19] comprise 5% of the sequences in SM, but none in FD. Filamentous *Chloroflexi* thrive in certain habitats such as anaerobic wastewater treatment tanks[20] and sludge granules.[21] Phylum *Tenericutes*, which lack a cell wall, was only fractional (0.1%)

for SM comparing to 20% for FD. The results suggest that the presence of autoclaved foams as supporting materials select for specific organisms including *Spirochaetes* and *Plantomycetes* at the expense of those found in the planktonic phase such as *Proteobacteria*, which include *Escherichia coli* for example. *Spirochaetes* are known to play an important role in glucose metabolism in the anaerobic digesters, as described by Delbes *et al.*[22], Huang *et. al.*[23]

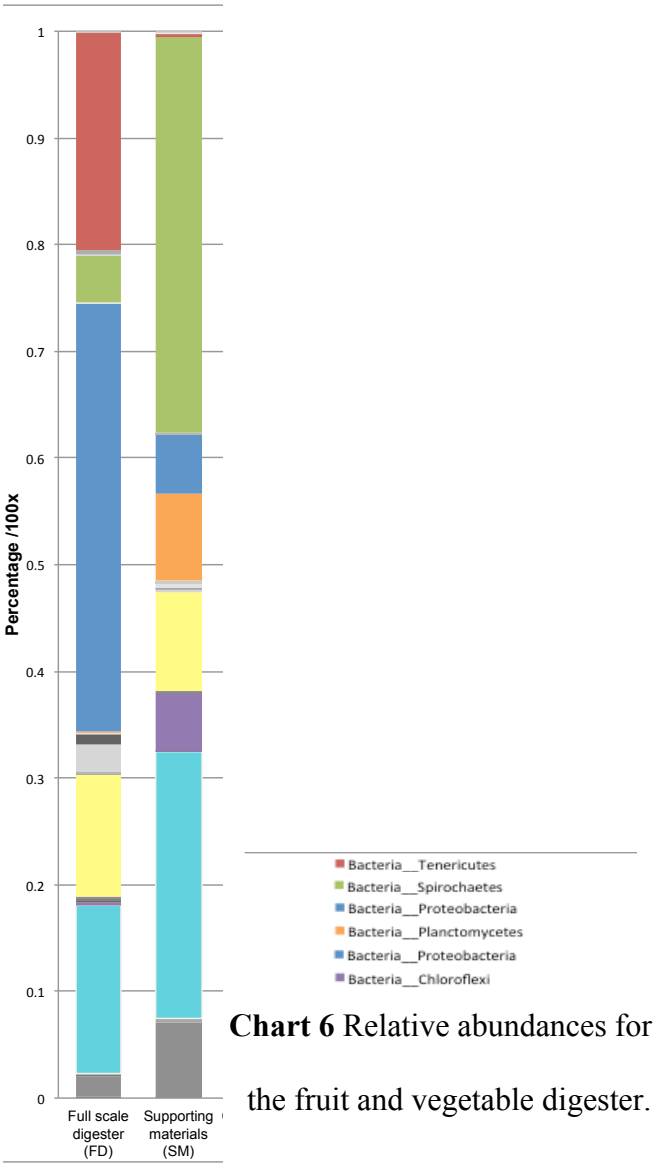

Chart 6 Relative abundances for *Bacteria* at the phylum level for the fruit and vegetable digester.

Interestingly, chart 7 shows that samples collected from different locations the slurry lagoon in Ashcott (Somerset) do not show big differences in the microbial diversity.

Four significant bacterial phyla were shared by two samples: *Bacteroidates* (light blue), *Firmicutes* (yellow), *Proteobacteria* (blue), *Spirochaetes* (green).

4.2.1.2. Analyses for samples collect at Ashcott farm

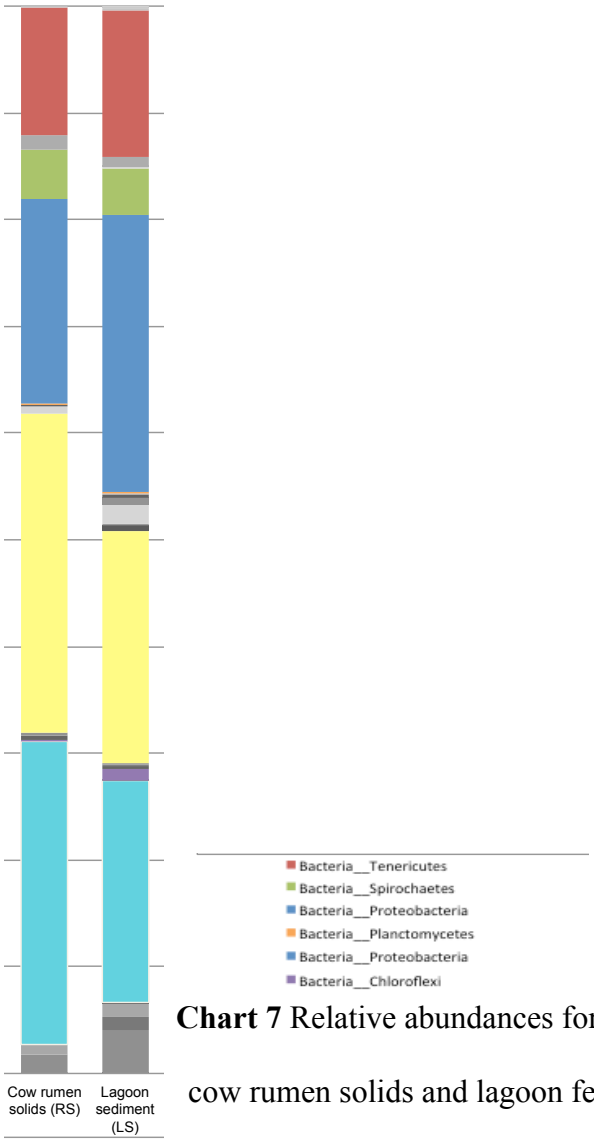

Chart 7 Relative abundances for *Bacteria* at the phylum level for the cow rumen solids and lagoon fed with cow slurry.

The same analyses were also performed to analyse the archaeal diversity.

4.2.2. Archaeal community structure

The average length of archaeal sequences was 548 bp. After trimming primers and removal of chimeras the average sequence length reduced to 505 bp. Calculations performed in order to analyse sequencing data are presented in Table 19.

Sample name	OTUs
full scale digester (FD)	2000
supporting materials (SM)	1808
cow rumen solids (RS)	2326
lagoon sediment (LS)	1641

Table 19 Archaeal OTUs assignment per sample.

Opposite to the results presented for *Bacteria*, the highest OTU number for *Archaea* was present in the cow rumen solids (RS) and sample collected from lagoon sediment (LS) contained the lowers number of OTUs as showed in Table 19 and Figure 40.

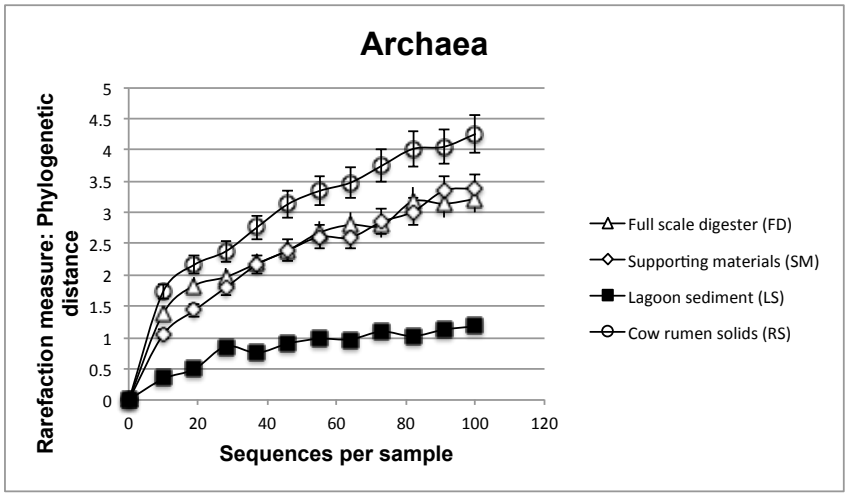

Figure 40 *Archaea* rarefaction curves for four samples at a cut off level of 5%.

The rarefaction curves (Figure 1 and Figure 3) showing the phylogenetic distance as a function of sequences per sample do not reach a plateau, showing that the diversity is still not fully discovered, despite the relatively high number of sequences obtained.

4.2.2.1. Relative abundances for *Archaea* at the phylum level for the four samples

When considering the relative proportions of *Archaea* alone (Chart 8), samples FD, RS and LS contained lower percentages of sequences related to *Crenarchaeota,* marked in red (86%, 86%, 81% respectively), compared with supporting materials (SM) where they represent 53% of archaeal OTUs. This means that the autoclaved foams used herein support a lower number of *Euryarchaeota*, which include many methanogens, marked in green than are found in the planktonic phase of the anaerobic digester (AD) or rumen solids (RS).

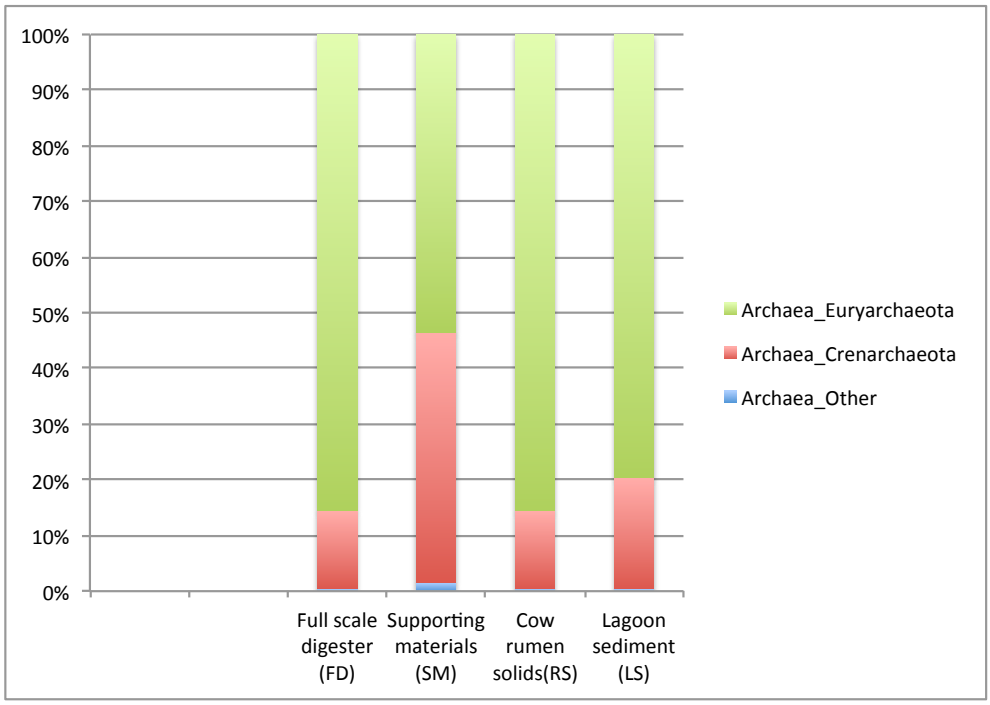

Chart 8 Relative abundances for *Archaea* at the phylum level for the four samples.

Besides the phylum, archaeal diversity and abundance was analysed in more details at class and genus level

4.2.2.2. Fruit and vegetable digester

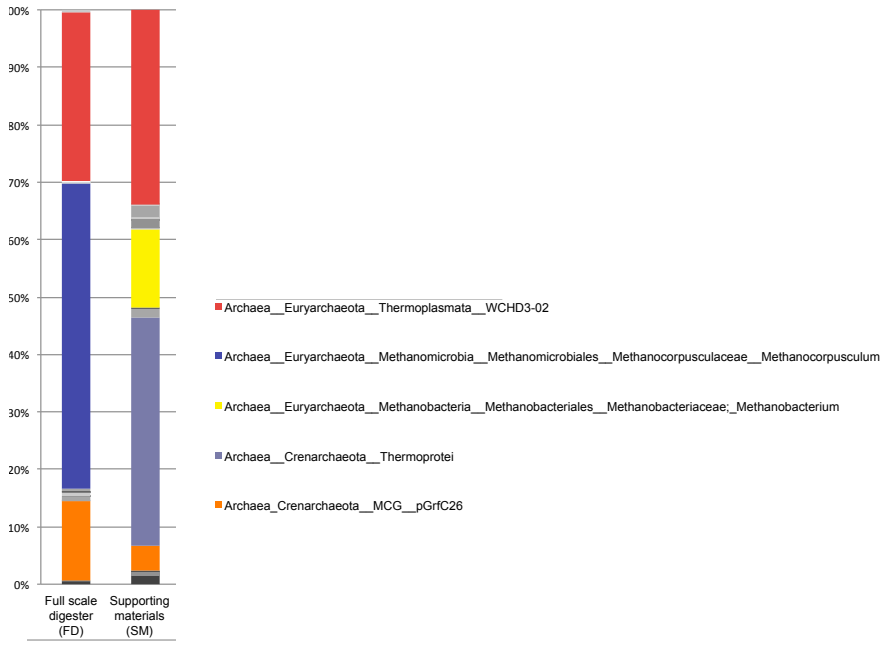

Chart 9 Relative abundances for *Archaea* at the phylum level for the fruit and vegetable digester.

Charts 9 shows sequences assignments for each sample at the genus level. Full-scale digester (FD)) shows significantly different microbial community and there are three main species present: *Thermoplasmata* class WCHD3-02 (red), *Methanocorpusculacea* genus *Methanocorpusculum* (green) and *Crenarchaeota* class *MCG__pGrfC26* (orange). *Methanocorpusculum* is observed only on supporting materials.

4.2.2.3. Analyses for samples collect at Ashcott farm

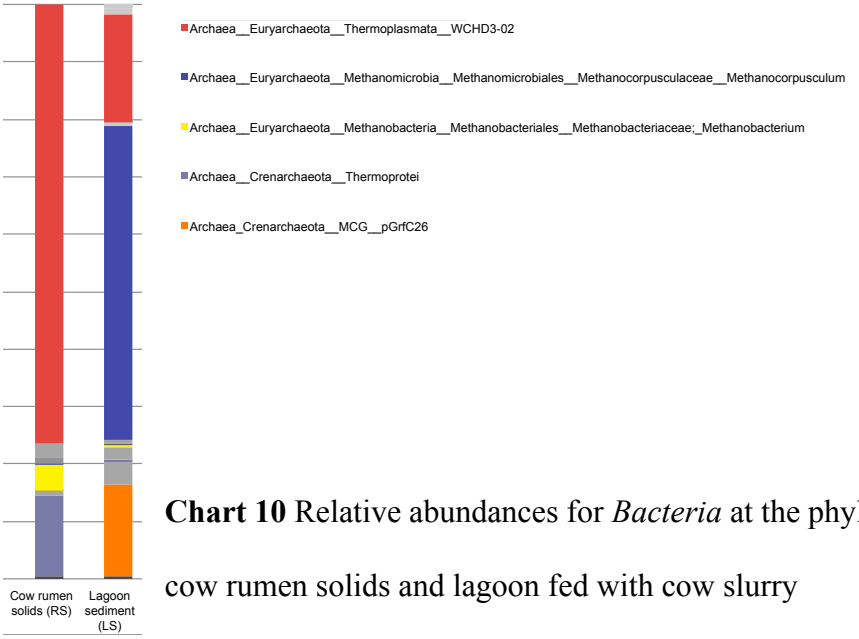

Chart 10 Relative abundances for *Bacteria* at the phylum level for the cow rumen solids and lagoon fed with cow slurry

Chart 10 shows that cow rumen solids (RS) consist of 76% of sequences assigned to *Crenarchaeota* class *MCG__pGrfC26, 14%* of *Crenarchaeota* class *Thermoprotei* (blue) *and 4% of Methanobacteriaceae* genus *Methanobacterium* (yellow).

Selective immobilisation of microorganisms can be explained by structural and chemical changes of the foam during autoclaving. The polyurethane could be partially hydrolysed and the primary amines revealed.

To quantify the density of primary amines on the polymer surface, Orange II dye method[24] was applied. This method is based on reversible electrostatic interaction between the negatively charged dye (**Figure 41)** and primary amines in acidic solution which are expected to be positively charged. After wash with pH = 12 buffer the neutral amino groups induce the release of Orange II dye into solution.

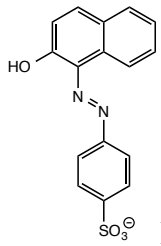

Figure 41 Structure of Orange II dye.

The measurements of absorbance of desorbed dye were performed in triplicates at λ = 484 nm (**Table 20**).

Sample	Absorbance of orange II dye
Autoclaved foam	0.48
Unautoclaved foam	0.14

Table 20 Orange II dye desorption measured at 484 nm.

Higher absorbance of orange II dye was observed for autoclaved foam confirming greater number of primary amines present on the heat modified foams. This results have to be supported by another surface analysis technique i.e. XPS.

4.3. Conclusions

Microbial communities on activated zeolites during biogas production were identified previously by single strand conformation polymorphism and described by Weiss *et.al*.[25] The new data show the diversity of both the planktonic phase and uniquely unveil those microorganisms selected on autoclaved polyurethane foam surfaces in an operational cattle slurry digester. Perhaps unsurprisingly, *Planctomycetes,* which bear a foot-like attachment, were found only on these surfaces and not in the planktonic phase. Whilst *Methanocorpusculum* were not found on the surfaces, other methanogens including *Methanobacterium* were uniquely selected on the polyurethane support. A variety of *Spirochaetes*, some of which are already known to be important for glucose metabolism, are strongly selected on autoclaved polyurethanes and this may be significant in the overall

microbial community. The 454 pyrosequencing method is powerful because it enables different supporting materials and conditions to be screened in both controlled laboratory scale and commercial biogas-producing plants in order to create community-specific genetic profiles and identify the surfaces that would attract attachment of organisms crucial for biogas production process.

Anaerobic digestion is a highly complex process. In order to maintain stable microbial populations the accurate modelling of process parameters is crucial. The internal states of anaerobic digester cannot be measured directly; therefore a detailed simulation model of full-scale anaerobic digester was used.

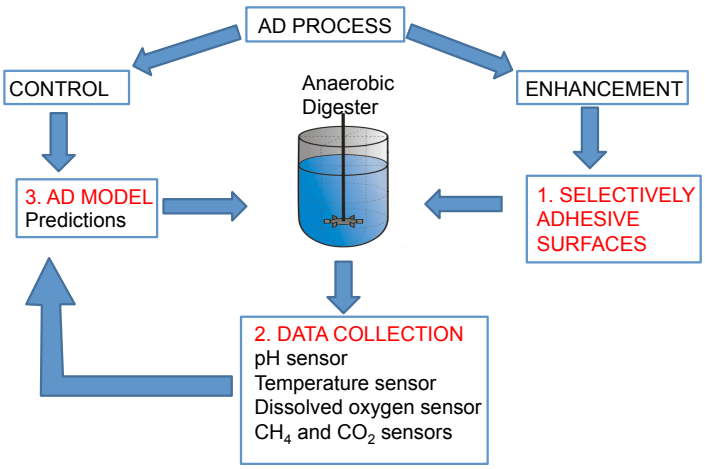

Figure 42 The integrated approach to the process anaerobic digester optimization.

Chapter 5 describes the applications of mathematical model ADM1 in order to predict process parameters collected from laboratory and farm scale biogas producing reactors.

4.4. Methods and Materials

4.4.1. Sample preparation for DNA extraction from environmental samples

Samples for total DNA extraction were collected from:

(a) An anaerobic digester with 50 l working capacity, located near London, United Kingdom, The feedstock for a digester was fruit and vegetable waste obtained from local suppliers and the anaerobic digester was operated at 35 °C. Purpose-designed stainless steel baskets (Figure 46) with polyurethane foam (Figure 47) were placed in the digester and incubated for 30 days;

(b) Rumen solids from cattle at a farm in Ashcott, Somerset and the slurry lagoon fed with them.

4.4.2. Total DNA extraction

To extract genomic DNA from samples FastDNA Spin Kit for soil (MP Biomedicals, Heidenberg, Germany) was used according to protocol described by Griffiths.[26]

The foams were placed in stomacher bags and blended at high speed for 60 s. The liquid content was transferred to a centrifuge tube and processed as described above.

The genomic DNA was stored at –20 °C until PCR amplification and metagenomic sequencing was carried out.

4.4.3. DNA quantification

The total DNA yield and purity were determined spectrometrically by NanoDrop 3300 Thermo Fisher Scientific Inc. USA, followed by electrophoresis on 0.8 % agarose gel.

4.4.4. Pyrosequencing of total DNA

The 16S rRNA gene sequences were PCR amplified using universal bacterial and archaeal target designed to achieve maximum coverage of microbial diversity[27] (Table 21).

Primer nomenclature	Sequence	Target group
16S Uni F	AGAGTTTGATCATGGCTCAG	Domain Bacteria
16S Uni R	ACCGCGGCTGCTGGCAC	Domain Bacteria
S-D-Arch-0519-a-S-15	CAGCMGCCGCGGTAA	Domain Archaea
S-D-Arch-1041-a-A-18	GGCCATGCACCWCCTCTC	Domain Archaea

Table 21 Primer pairs selected for high throughput sequencing

The following PCR conditions were used: initial denaturation at 94 °C for 20 s, 35 cycles at 94 °C, an annealing step at 55 °C for 30 s and extension at 72 °C for 30 s, before a final extension period at 72 °C, for 10 min. After initial amplification, another 3 rounds of amplification were done to add the adapters A and B adapters required for 454-pyrosequencing to specific ends of the amplified 16S rRNA fragment for library construction.

The PCR products were purified using the QIAquick PCR purification kit (QIAGEN Chin Co., Ltd, Germany) and samples were submitted for analyses to produce DNA whole-genome-shotgun library using GS Junior (Roche Applied Science, USA) performed by Micropathology Ltd, UK).

4.4.5. Statistics and sequence analyses

All data and statistical analyses were performed according to the guideline described by Kuczynski *et.al*.[17] Phylogenetic trees showing sequence abundance data were created using MEGAN 4.[28]

4.4.6. Design of stainless steel baskets for supporting materials in the reactor

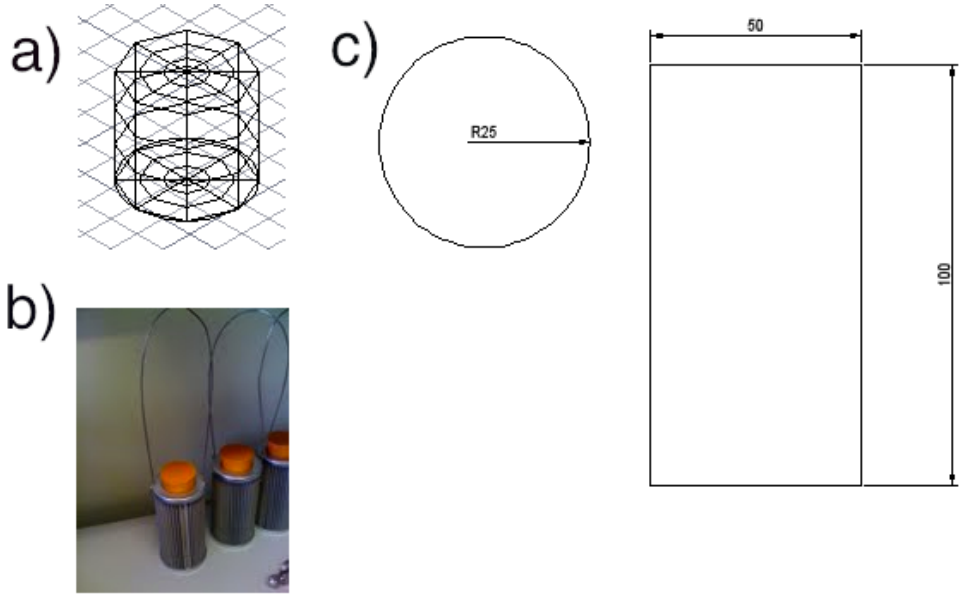

Figure 43 a) 3D.AutoCAD® drawing of baskets, b) fabricated stainless steel baskets, c) technical drawing with dimensions (in mm).

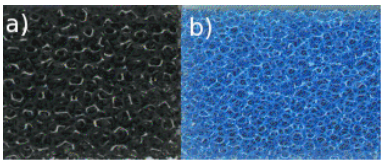

Figure 44 Optical microscopy of supporting materials – polyurethane open cell reticulated foam, a) open cell 90 ppi black polyurethane foam, b) open cell 120 ppi blue polyurethane foams shown at 20 x magnification.

4.5. References

(1) Gilbert, W.; Maxam, A. *Proc. Natl. Acad. Sci. U. S. A.,* **1973**, *70*, 3581.

(2) Sanger, F. *Biosci. Rep.,* **2004**, *24*, 237.

(3) Rothberg, J. M.; Leamon, J. H. *Nat. Biotechnol.,* **2008**, *26*, 1117.

(4) Hyman, E. D. *Anal. Biochem.,* **1988**, *174*, 423.

(5) Ronaghi, M. *Genome Res.,* **2001**, *11*, 3.

(6) Koren, O.; Spor, A.; Felin, J.; Fak, F.; Stombaugh, J.; Tremaroli, V.; Behre, C. J.; Knight, R.; Fagerberg, B.; Ley, R. E.; Backhed, F. *Proc. Natl. Acad. Sci. U. S. A.,* **2011**, *108*, 4592.

(7) Lienhard, P.; Terrat, S.; Prevost-Boure, N. C.; Nowak, V.; Regnier, T.; Sayphoummie, S.; Panyasiri, K.; Tivet, F.; Mathieu, O.; Leveque, J.; Maron, P.-A.; Ranjard, L. *Agron. Sustain. Dev.,* **2014**, *34*, 525.

(8) Coykendall, D. K.; Morrison, C. L. *Conserv. Genet. Resour.,* **2013**, *5*, 495.

(9) Star, B.; Haverkamp, T. H. A.; Jentoft, S.; Jakobsen, K. S. *BMC Microbiol.,* **2013**, *13*

(10) Liu, R.; Yu, Z.; Guo, H.; Liu, M.; Zhang, H.; Yang, M. *Sci. Total Environ.,* **2012**, *435*, 124.

(11) Lee, S.-H.; Park, J.-H.; Kang, H.-J.; Lee, Y. H.; Lee, T. J.; Park, H.-D. *Bioresour. Technol.,* **2013**, *145*, 25.

(12) Pervin, H. M.; Dennis, P. G.; Lim, H. J.; Tyson, G. W.; Batstone, D. J.; Bond, P. L. *Water Res.,* **2013**, *47*, 7098.

(13) Sundberg, C.; Al-Soud, W. A.; Larsson, M.; Alm, E.; Yekta, S. S.; Svensson, B. H.; Sorensen, S. J.; Karlsson, A. *FEMS Microbiol. Ecol.,* **2013**, *85*, 612.

(14) Parameswaran, P.; Jalili, R.; Tao, L.; Shokralla, S.; Gharizadeh, B.; Ronaghi, M.; Fire, A. Z. *Nucleic Acids Res.,* **2007**, *35*

(15) Magguran, A. E. *Measuring biological diversity*; Oxford: United Kingdom, 2004.

(16) Blaxter, M.; Mann, J.; Chapman, T.; Thomas, F.; Whitton, C.; Floyd, R.; Abebe, E. *Philos. Trans. R. Soc. Lond., B,* **2005**, *360*, 1935.

(17) Kuczynski, J.; Stombaugh, J.; Walters, W. A.; Gonzalez, A.; Caporaso, J. G.; Knight, R. *Current protocols in microbiology,* **2012**, *Chapter 1*, Unit 1E.5.

(18) Sutcliffe, I. C. *Trends Microbiol.,* **2010**, *18*, 464.

(19) Roeselers, G.; van Loosdrecht, M. C. M.; Muyzer, G. *J. Appl. Phycol.,* **2008**, *20*, 227.

(20) Bjornsson, L.; Hugenholtz, P.; Tyson, G. W.; Blackall, L. L. *Microbiology-Sgm,* **2002**, *148*, 2309.

(21) Sekiguchi, Y.; Yamada, T.; Hanada, S.; Ohashi, A.; Harada, H.; Kamagata, Y. *Int. J. Syst. Evol. Microbiol.,* **2003**, *53*, 1843.

(22) Delbes, C.; Moletta, R.; Godon, J. J. *Environ. Microbiol.,* **2000**, *2*, 506.

(23) Huang, L. N.; Zhou, H.; Zhu, S.; Qu, L. H. *FEMS Microbiol. Ecol.,* **2004**, *50*, 175.

(24) Noel, S.; Liberelle, B.; Robitaille, L.; De Crescenzo, G. *Bioconjugate Chem.,* **2011**, *22*, 1690.

(25) Weiss, S.; Zankel, A.; Lebuhn, M.; Petrak, S.; Somitsch, W.; Guebitz, G. M. *Bioresour. Technol.,* **2011**, *102*, 4353.

(26) Griffiths, R. I.; Whiteley, A. S.; O'Donnell, A. G.; Bailey, M. J. *Appl. Environ. Microbiol.,* **2000**, *66*, 5488.

(27) Klindworth, A.; Pruesse, E.; Schweer, T.; Peplies, J.; Quast, C.; Horn, M.; Gloeckner, F. O. *Nucleic Acids Res.,* **2013**, *41*

(28) Huson, D. H.; Mitra, S.; Ruscheweyh, H.-J.; Weber, N.; Schuster, S. C. *Genome Res.,* **2011**, *21*, 1552.

Chapter 5: Bioinformatics and reactors design

5.1. Introduction

To improve understanding of the biogas production process a systems model was used and implemented into Matlab®/Simulink. In this research the implementation of the model has been tested and validated against data collected from a full-scale fruit and vegetable waste fed reactor operated at 55 ° C as well as a modified commercial 1 L laboratory scale reactor fed with methanol or maize as an added carbon source. It was planned that this method would allow the future use of the digester with confidence and development of simple and reliable way for prediction of process parameters in order to maintain microbial stability.

Anaerobic Digestion Model No. 1 (ADM1), developed by the International Water Association (IWA) Task Group for Mathematical Modelling of Anaerobic Digestion Processes has been widely used both for lab- and full-scale anaerobic reactors[1,2]. ADM1 or its modified version has been implemented in anaerobic co-digestion of various substrates (corn, farm waste, food waste) to predict process stability.[3-5]

In silico prediction of process parameters (pH or long chain fatty acid concentration) minimizes the possibility of process instability or inhibition. Modelling of anaerobic digestion has been widely developed since early 1970s (simple model described by Graef and Andrews)[6-8], two reactions model used by Bernards *et al.*[9,10] and more accurate representations (IWA ADM1).[11]

The ADM1 model mimics five main processes involved in anaerobic digestion:

(a) disintegration

(b) hydrolysis

(c) acidogenesis

(d) acetogenesis

(e) methanogenesis

It consists of 26 dynamic state equations, 19 bioconversion processes, including Monod kinetics of substrate formation, 3 gas transfer processes, acid – base additions and pH computation.[1]

The type of reactor used also influences parameters used in the model. [4]

5.1.2. Fixed film bioreactors

There are several types of fixed film bioreactors.

(a) Simple anaerobic filters with support media such as synthetic plastic or ceramic tiles, cigarette filters or foams with a high void volume and specific surface area. In this type of system, hydraulic retention time (HRT) ranges from 0.5 to 4 days and loading rate from 5 to 15 kg COD/m^3/day. Mu *et al.*[12] applied the ADM1 model for prediction of process parameters, using a multivariable control system to improve system stability and performance.

(b) Fluidized bed reactors contain microbes attached to bio-carriers, such as sand, granular activated carbon, shredded tires, or synthetic plastic media. Another type of suspended growth system is an up flow anaerobic sludge blanket (UASB) reactor

that promotes formation of dense biomass aggregates known as granules. Granule diameters range from 1-3 mm, and settle with velocities around 60 m/h. Since the superficial up-flow velocity of the waste stream is maintained at <2 m/h, the granules readily settle, forming a sludge blanket at the reactor bottom.[13]

(c) In an anaerobic sequencing batch reactor (ASBR), all stages of wastewater treatment (filling, reaction, sedimentation, and decanting) happen sequentially in one tank. Due to sequential operation, a single reactor can serve as a reaction vessel and settling tank. Biomass is retained due to bioflocculation and biogranulation, similar to a UASB reactor. A larger reactor volume is required with a continuous process. The construction of reactor is simpler and are often used for industrial wastewater treatment.[14] The ASBR is suitable to treatment of animal manure and other biowastes with total solids contents between 1-4%.[15] An anaerobic contact process is a CSTR with an external tank to settle biomass. The degassifier removes carbon dioxide and methane bubbles that may attach to biomass and prevent settling. In this research the ASBR reactor was used for all the experiments.

The objectives of this study were:

(a) to test the mathematical model against data collected from large scale anaerobic digester;
(b) to validate the mathematical model against data collected from laboratory scale anaerobic digester.

5.2. Results and Discussion

5.2.1 Preliminary experiments – methane production estimated by biomethane potential (BMP) assay

Serum vials were inoculated and methane production measured using gas chromatography for period of 2 weeks. Specific methane production is shown in Chart 10. The characteristics of inoculum and substrate used in the assay are presented in Table 22. The experiment was carried out under mesophilic conditions (35 ± 2 °C).

Substrate	**Characteristics**			
	Moisture content (%)	Volatile solids VT (%)	C/N ratio	pH
Cellulose	70%	12.5	–	7.2
Inoculum	**Characteristics**			
	Total solids TS (%)	Volatile solids VT (%)	TCOD mg/L	pH
Mesophilic inoculum from fruit and vegetable digester	2.2	1.2	27	7.9

Table 22 Characterization of cellulose and the inoculum used in the BMP assay.

Figure 45 presents the serum bottles (a) freshly inoculated (b) digestion time = 5 days (c) digestion time = 10 days and (d) digestion time = 15 days.

Figure 45 Assay vessels for anaerobic biodegradability tests after (a) 1 day, (b) 5 days, (c) 10 days, (d) 15 days.

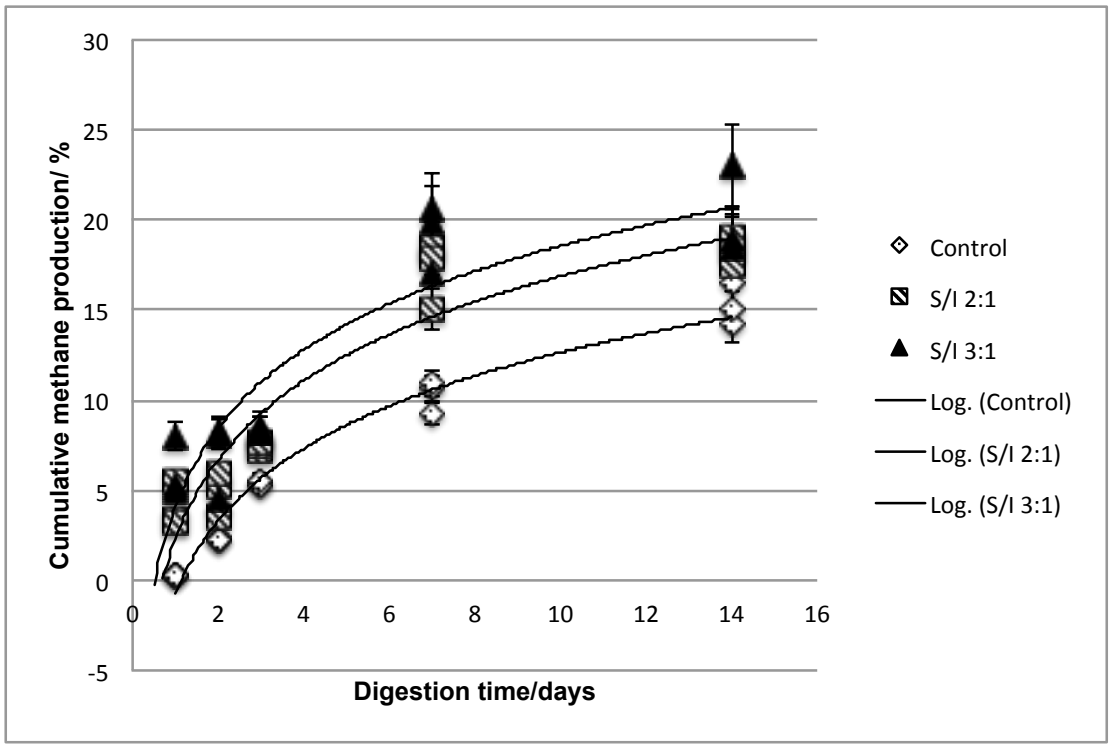

Chart 11 Specific methane production from BMP assay, diamonds – control experiment with inoculum and no substrate , squares – incoulum with added cellulose (substrate to inoculum ratio S/I = 2:1), triangles – inoculum with added cellulose (S/I = 3:1).

Preliminary biochemical methane potential tests indicated significant methane production from the control. It shows that the fruit and vegetable inoculum contains a lot of undigested organic matter and possibly the degassing process was too short. The change in substrate to inoculum ratio does not hugely influence methane production. However, methane production increases with higher concentration of substrate. Longer pre-incubation step is crucial for elimination of any entrapped biodegradable substrates present in inoculum.

5.2.2 Anaerobic digestion model No. 1

ADM1 was implemented to mimic biochemical reactions and methane production within the full scale and laboratory scale reactors. The constants for disintegration and hydrolysis for this study were equal to typical values reported in the literature[16] as presented in Table 23.

Parameter	Name	Value	Unit
K_{dis}	Disintegration constant	0.5	d^{-1}
$K_{hyd\ Ca}$	Carbohydrate hydrolysis constant	10	d^{-1}
$K_{hyd\ Pr}$	Protein hydrolysis constant	10	d^{-1}
$K_{hyd\ Li}$	Lipid hydrolysis constant	10	d^{-1}

Table 23 Initial kinetic parameters used in the model.

In first instance data collected from full-scale anaerobic digester was compared to the simulated values obtained from model.

5.2.3 Modeling of biogas composition, volatile fatty acids levels and pH during anaerobic digestion of fruit and vegetable waste in full scale bioreactor

The substrate characterization was performed to identify the moisture content, volatile solids, C/N ratio and pH (data presented in Table 24)

Substrate	Characteristics			
	Moisture content (%)	M Volatile solids VT (%)	C/N ratio	pH
Mixed fruit and vegetable waste[14]	85	89	36.4	6.2

Table 24 Characterization of fruit and vegetable waste used in the modelling process.

Simulation output

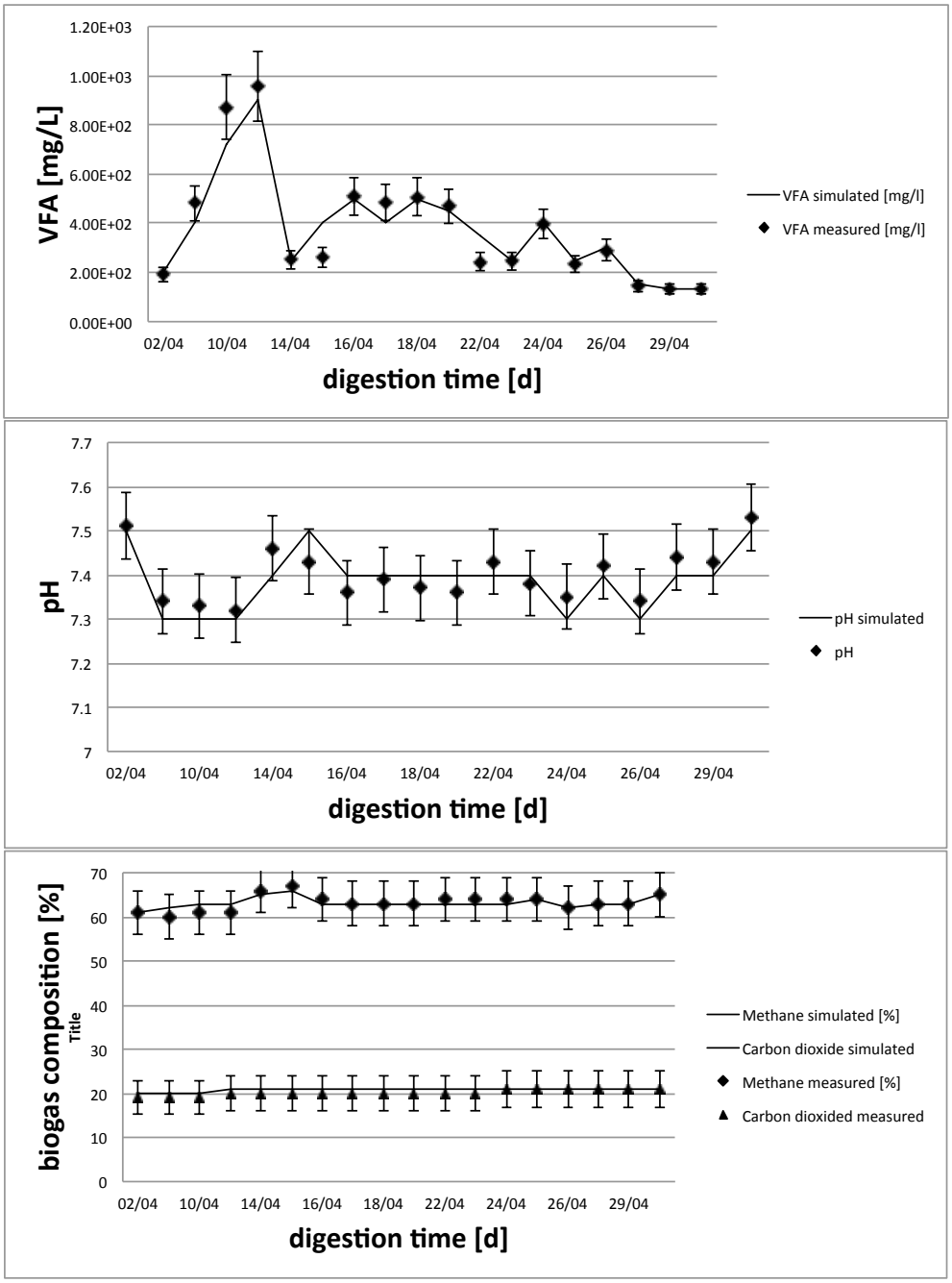

Chart 12 Data collected by operator of a large-scale anaerobic digester fed with vegetable and fruit waste (markers) *vs*. ADM1 model prediction (solid black line).

The comparison of model outputs and data from the large-scale digester show good prediction of the full-scale process (Chart 12). Changes in pH and VFA are predicted accurately. There are some fluctuations in the pH stability caused by variable amount

of fruit waste used for anaerobic digestion, hence the increase in acid concentration and ultimately change in pH that was not detected by the model. Overall biogas composition was simulated well using the ADM1 model.

4.2.4 Laboratory scale experiments

Figure 46 shows the apparatus used for measuring methane production in a laboratory scale bioreactor. The system consists of a glass reactor vessel heated by an electric blanket to maintain the thermophilic conditions (55 ± 2 °C), automatically titrated acid/base additions to adjust pH to 8.1 and gas sensors to measure CO_2 and CH_4 production.

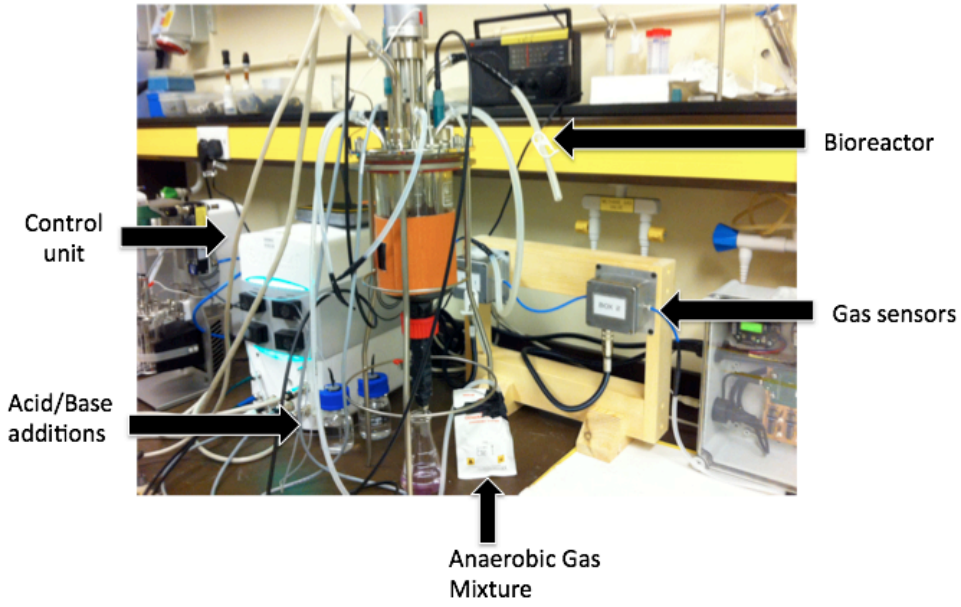

Figure 46 The laboratory scale apparatus for biogas production.

The 1 L reactor fed with methanol once a day in the experimental week produced 0.1 m^3 of biogas per day. After feeding intervals the measured parameters returned always to its original values indicating good process stability. Figures 47 and 48 show pH, temperature and biogas composition (%CH_4 and % CO_2) for the laboratory reactor fed with methanol or maize respectively.

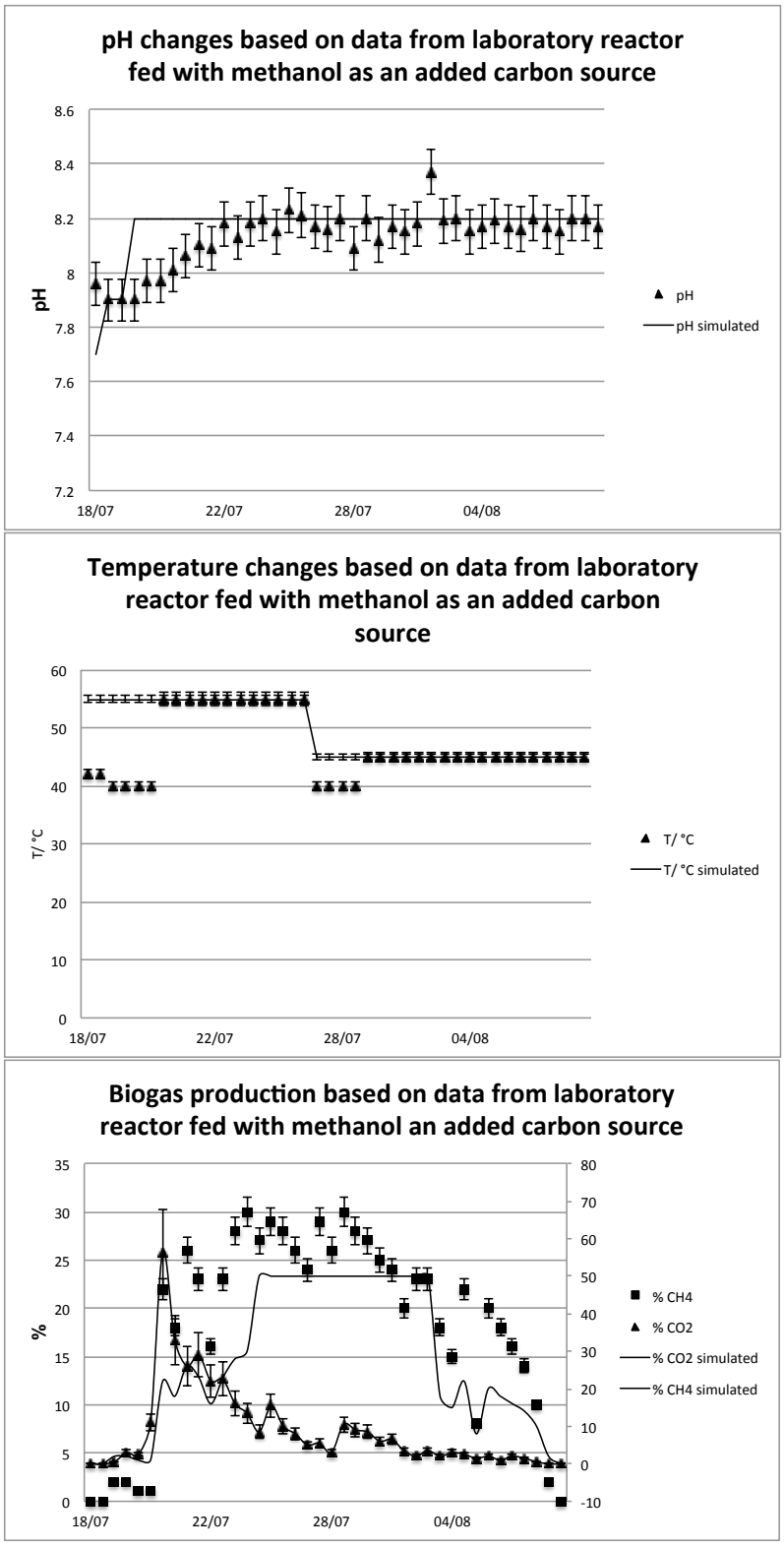

Figure 47 Kinetics of reactor fed with methanol as an added carbon source (pH = 8.1) at 55 °C.

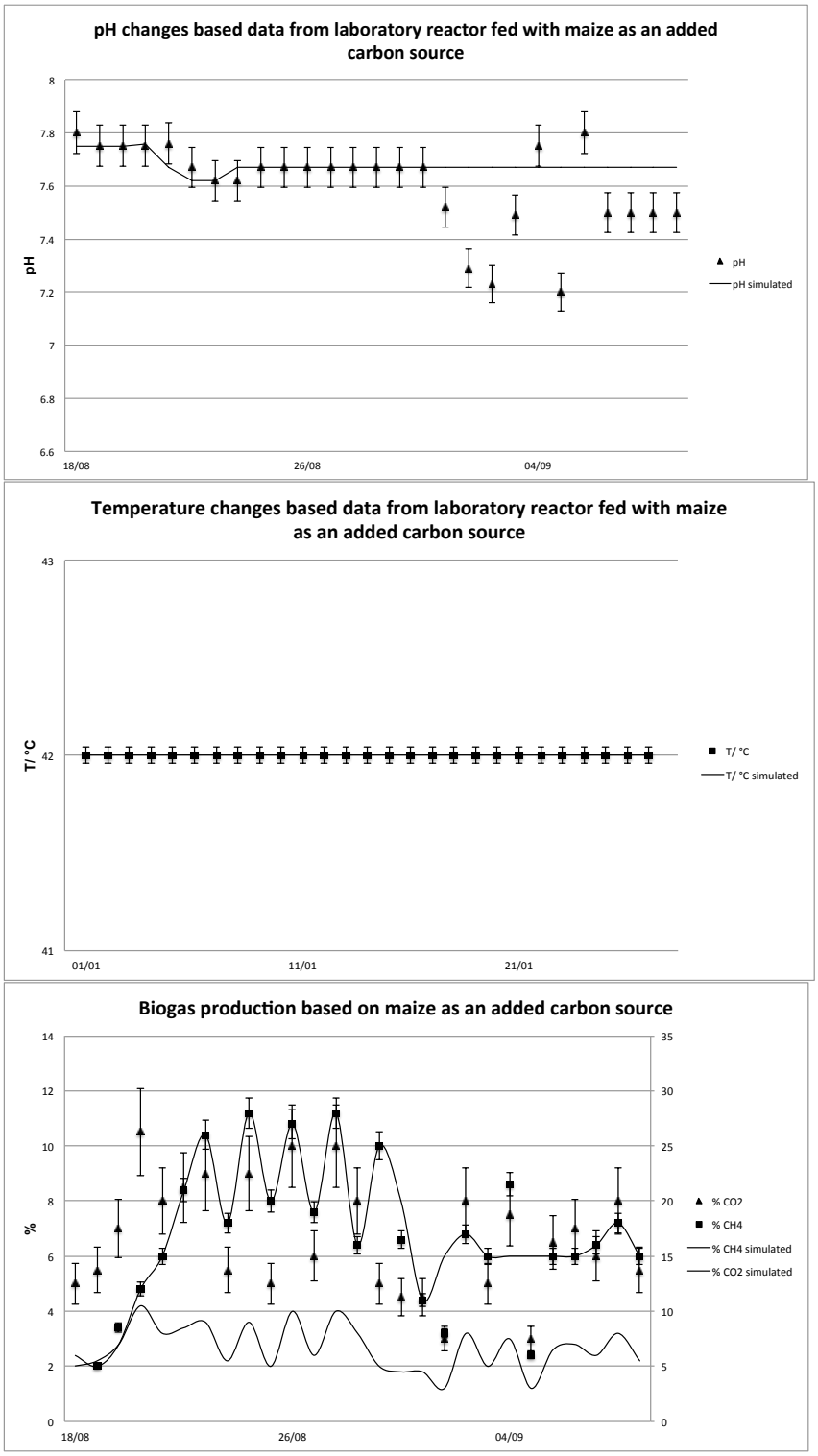

Figure 48 Kinetics of the reactor fed with maize as an added carbon source (pH = 7.9) at 42 °C.

The 1 L reactor fed with maize produced 0.5 m^3 of biogas per day. ADM1 model predictions, using previously reported literature values for hydrolysis coefficients,

were able to reflect most of the trends that were reported for a variety of digester configurations[4,5,16,17]. The model is able to mimic not only batch, but also semi-continuous production of biogas. There were however consistent deviations between the model predictions and observed values for biogas composition in the maize fed reactor. Changes in Matlab® code may need to be applied in order to improve the model estimation of biogas composition under continuous reactor operation. It may be necessary to more closely examine the relationship between pH and rate coefficients in this regard.

5.3. Conclusions

The ADM1 model was tested to simulate both full scale and laboratory scale reactors fed with different types of substrates (food and vegetable waste, maize, methanol). It showed good results for simulating of a range of processes, for instance batch mesophilic assay (Chart 12) and semi-continuous thermophilic process (Figures 45 and 46). The main limitation of the model is that not all input parameters were obtained by analyses; many values have been extracted from the literature (hydrolysis ratios, substrates compositions, total solids and nitrogen). Besides this drawback, the simulation results extend the applicability of the ADM1 to a wide range of anaerobic processes and have allowed the first prediction of process parameters in order to maintain the stability of microorganisms in our laboratory scale system.

5.4. Methods and Materials

5.4.1 Substrate characterization

Full analyses: moisture content (TS), volatile solids (VS) and C/N ratios were found in the literature for each substrate.[17]

5.4.2 Inoculum characterization

Fresh inoculum was collected from anaerobic digester with 50 l working capacity, located near London, United Kingdom (51°50'N, 0°5'E), The feedstock for a digester was fruit and vegetable waste obtained from local suppliers and the anaerobic digester was operated at 35 °C. Pre-designed stainless steel baskets with polyurethane foams were placed in the digester and incubated for 30 days. All tested parameters were given in Table 14.

5.4.3 Biochemical methane potential (BMP) assay

The experiment was designed based on protocol described by Lim *et al.*[18]

An anaerobic digestion assay was performed in triplicates to determine the biomethane potential of inoculum collected from the farm scale anaerobic digester and cellulose as an added carbon source. The Hungate technique under mesophilic conditions for cultivating anaerobes was applied.[19] Serum bottles with rubber stoppers were uses as the mini batch digesters. 2:1 and 3:1 substrate to inoculum (S:I) ratios were used to screen the influence of substrate concentration on methane production. The standard anaerobic medium was prepared and anaerobically transferred to the bottles (see next paragraphs).

5.4.4 Medium

Standard anaerobic medium was prepared according to the protocol described by Nielsen *et al.*[20] Table 17 shows the composition of stock solutions. 10 ml of A, 2 ml of B, 1 ml of (C), 1 ml of (D) and 1 ml of (E) from stock solutions were added to 975 ml of water to avoid precipitation. Medium was degassed with 80% N_2 and 20% CO_2 gas mixture to remove any oxygen present. Reducing agent (titanium citrate) was added to the vials to a final concentration of 0.025%.

Solution	Composition [g/L]
A	100 NH_4Cl,
	10 NaCl,
	10 Mg_2Cl_2 $6H_2O$,
	5 $CaCl_2$ $2H_2O$
B	200 K_2HPO4 $3H_2O$
C	0.5 resazurin
D	2 $FeCl_2$ $4H_2O$,
	0.05 H_3BO_3,
	0.05 $ZnCl_2$,
	0.038 $CuCl_2$ $2H_2O$,
	0.05 $MnCl_2$ $4H_2O$,
	0.05 $(NH_4)Mo_7O_{24}$ $4H_2O$,
	0.05 $AlCl_3$,
	0.05 $CoCl_2$ $6H_2O$,
	0.092 $NiCl_2$ $6H_2O$,
	0.05 ethylenediaminetraacetate,
	0.1 Na_2SeO_3 $5H_2O$
	1ml HCl to adjust pH of the solution
E	2 mg/l biotin, 2 mg/l folic acid, 10 mg/l pyridoxine acid, 10 mg/l riboflavin, 5 mg/l thiamine hydrochloride, 0.1 mg/l cyanocobalamine, 5 mg/l nicotinic acid, 5 mg/l aminobenzoic acid, 5 mg/l lipoic acid, 5 mg/l panthothenic acid

Table 25 The composition of anaerobic medium

Data collection

A commercial gas chromatograph (Unicam, model GCD) equipped with a highly sensitive flame ionization detector was used for this study. Helium was selected as carrier gas at flow 25 ml/min. Gas (100 µl) was collected from each assay bottle and injected into the GC under atmospheric pressure. Methane yield was measured as suggested in work carried out by Fedorak *et al.*[21]

5.4.5 Anaerobic conditions

Anaerobic workstation was used to provide an oxygen-free environment for methane production experiment. Chamber contains palladium catalyst wafers and desiccant wafers to maintain strict anaerobic conditions to less than 10 ppm O_2 (according to the specifications provided by the manufacturer). High purity N_2 is used for purging the chamber initially and the working anaerobic gas mixture was N_2:H_2:CO_2 proportioned at 85:10:5.

5.4.6 Reactor experiments

The Applikon bench scale digesters (1 L volume) fitted with mechanical mixers were used (an example of the system is showed in Figure 42). The temperature of the reactor was set at 55 ± 2 °C. The control unit allowed remotely operation and all the data collected during an experiment to be stored.

5.5. References

(1) Batstone, D. J., Keller, J., Angelidaki, R.I., *Anaerobic Digestion Model No. 1*; IWA Publishing Group, 2002.

(2) Lauwers, J.; Appels, L.; Thompson, I. P.; Degreve, J.; Van Impe, J. E.; Dewil, R. *Prog. Energy Combust. Sci.,* **2013**, *39*, 383.

(3) Bordeleau, E. L.; Droste, R. L. *Water Sci. Technol.,* **2011**, *63*, 291.

(4) Fezzani, B.; Ben Cheikh, R. *J. Hazard. Mater.,* **2009**, *172*, 1430.

(5) Boubaker, F.; Ridha, B. C. *Bioresour. Technol.,* **2008**, *99*, 6565.

(6) Andrews, J. F. *Water Res.,* **1974**, *8*, 261.

(7) Vitasovic, Z.; Andrews, J. F. *Water Pollut. Res. J. Can.,* **1989**, *24*, 479.

(8) Vitasovic, Z.; Andrews, J. F. *Water Pollut. Res. J. Can.,* **1989**, *24*, 497.

(9) Lopez, I.; Borzacconi, L. *Chem. Eng. J.,* **2009**, *146*, 1.

(10) Bernard, O.; Hadj-Sadok, Z.; Dochain, D.; Genovesi, A.; Steyer, J. P. *Biotechnol. Bioeng.,* **2001**, *75*, 424.

(11) Blumensaat, F.; Keller, J. *Water Res.,* **2005**, *39*, 171.

(12) Mu, S. J.; Zeng, Y.; Wu, P.; Lou, S. J.; Tartakovsky, B. *Bioresour. Technol.,* **2008**, *99*, 3665.

(13) Hulshoff Pol, L. W.; de Castro Lopes, S. I.; Lettinga, G.; Lens, P. N. L. *Water Res.,* **2004**, *38*, 1376.

(14) Ersahin, M. E.; Gomec, C. Y.; Dereli, R. K.; Arikan, O.; Ozturk, I. *J. Biomed. Biotechnol.,* **2011**, *2011*, 953065.

(15) Li, B.; Sun, Y.-l.; Li, Y.-y. *J. Zhejiang Univ. Sci. B.,* **2005**, *6*, 1115.

(16) Gali, A.; Benabdallah, T.; Astals, S.; Mata-Alvarez, J. *Bioresour. Technol.,* **2009**, *100*, 2783.

(17) Kleerebezem, R.; Van Loosdrecht, M. C. M. *Water Sci. Technol.,* **2006**, *54*, 167.

(18) Lim, S. J.; Fox, P. *Biotechnol. Bioprocess Eng.,* **2013**, *18*, 306.

(19) Miller, T. L.; Wolin, M. J. *Appl. Microbiol.,* **1974**, *27*, 985.

(20) Nielsen, H. B.; Angelidaki, I. *Bioresour. Technol.,* **2008**, *99*, 7995.

(21) Fedorak, P. M.; Knettig, E.; Hrudey, S. E. *Environ. Technol. Lett.,* **1985**, *6*, 181.

Chapter 6: Summary and future work

The strongly multidisciplinary and operational approach described in this thesis has allowed identification of surfaces for use in anaerobic digesters in order to promote selective adhesion of methanogens and specific *Bacteria*.

The molecular investigations in Chapter 2 gave insight into the structure-activity relationships in new self-assembled monolayers. The most protein resistant surface functionalized with a dimethylamine *N*-oxide headgroup (**AO1**) provided material with a similar level of resistance to the widely used triethylene glycol which will be of value in a range if biointerfacial systems.

The treatment of self-assembled monolayers containing tertiary amines with oxidant (hydrogen peroxide) changes their resistance to non-specific protein adhesion. This information was used during selection of commercially available beads and resins for studying biofilm formation by pure culture of *Methanosarcina barkeri* in Chapter 3.

Tertiary amine, amine *N*-oxide, morpholine and hydroxyl functionalized beads were chosen in order to screen effect of surface chemistry on archaeal adhesion. The greatest influence on *M. barkeri* adhesion was observed with hydrophobic methyl functionalized polystyrene resins (**A18**) suggesting that surface hydrophobicity is of value in selecting microbes including methanogens.

Large-scale investigations involved identification of *Bacteria* and *Archaea* attached to steam autoclaved polyurethane foams by means of 454-pyrosequencing technologies. *Methanobacterium* commonly present in biogas plants as well as *Spirochaetes* responsible for glucose metabolism during anaerobic digestion were selected on autoclaved polyurethanes. Autoclaved polyurethane foam is thus a good candidate for

the selective immobilisation of organisms and enhancement of biogas process stability.

Importantly, it has been shown that the ADM1 systems-based model can be implemented for both farm and laboratory scale, providing a convenient means of investigating what effects modulating pH, temperature and feedstock components have on microbial stability and biogas yield.

The future work on this project will include:

(a) Introduction of a variety of supporting materials including non-autoclaved polyurethane foam to the lab scale fermenter and characterization of microbial diversity by 454-high throughput sequencing.

(b) Measurements of methane production in reactors with and without the supporting materials (control experiments) to screen and understand how the selectively immobilised organisms influence biogas production.

(c) Confirmation of the important hypothesis that during autoclaving, the polyurethane surface structure is partly hydrolysed and revealing primary amines, which causes selective immobilisation of microorganisms.

This final point has significant meaning beyond anaerobic digester optimisation and emphasizes why autoclave sterilisation is strongly contra-indicated for medical usage of these polymers.[1] Whilst this is recognised, the increasing use of diverse polymer types in biomedical devices cautions that excellent chemical understanding of materials used in engineering applications remains of the highest priority.

6.1. References

(1) Shintani, H. *Biomed. Instrum. Technol.,* **1995**, *29*, 513.

Appendix 1 XPS data for tertiary amine and corresponding amine *N*-oxide functionalized on gold.

XPS analyses of coupling efficiency with Py-BOP

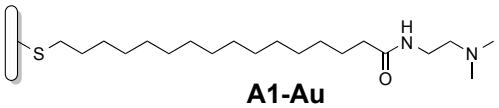

A1-Au

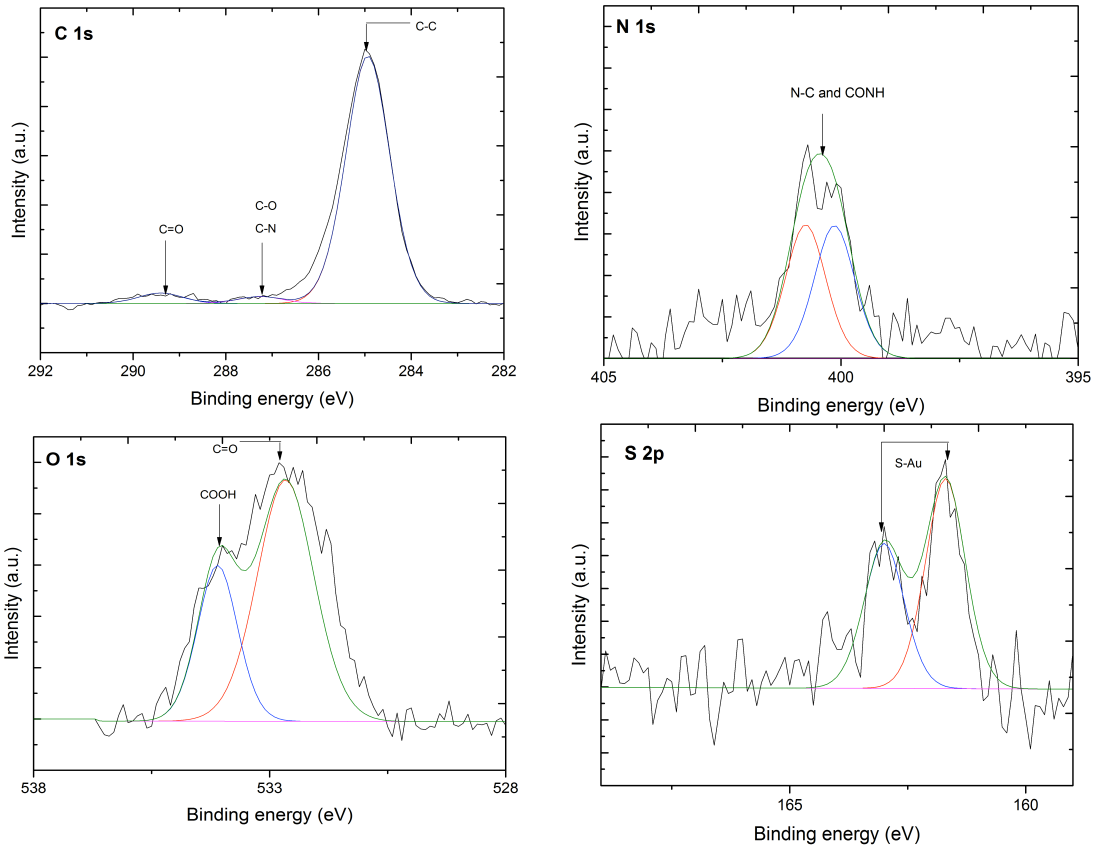

Summary of analyses performed by XPS

Binding energy/ eV	Assignment
285.0	C-C
286.8	C-O, C-N
288.8	C=O
399.7 and 400.4	N-C and CONH
532.7	COOH
532.1	O=C
162.1 and 163.4	S-Au

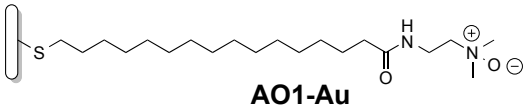

AO1-Au

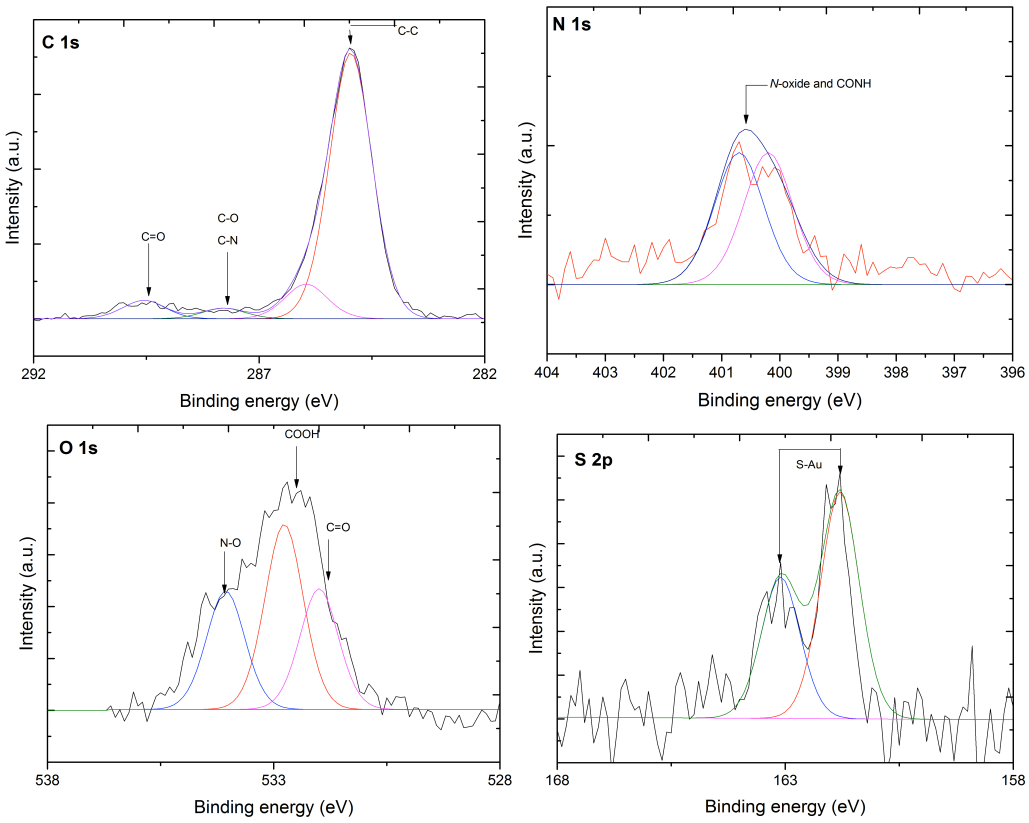

Summary of analyses performed by XPS

Binding energy/ eV	Assignment
285.0	C-C
286.7	C-O, C-N
288.9	C=O
399.5 and 401.9	CONH and *N*-oxide
532.1	O=C
532.9	COOH
534.1	O-N
162.0 and 163.4	S-Au

XPS analyses of coupling efficiency with HATU

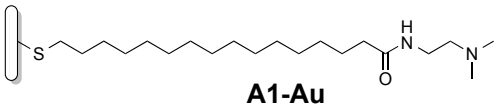

A1-Au

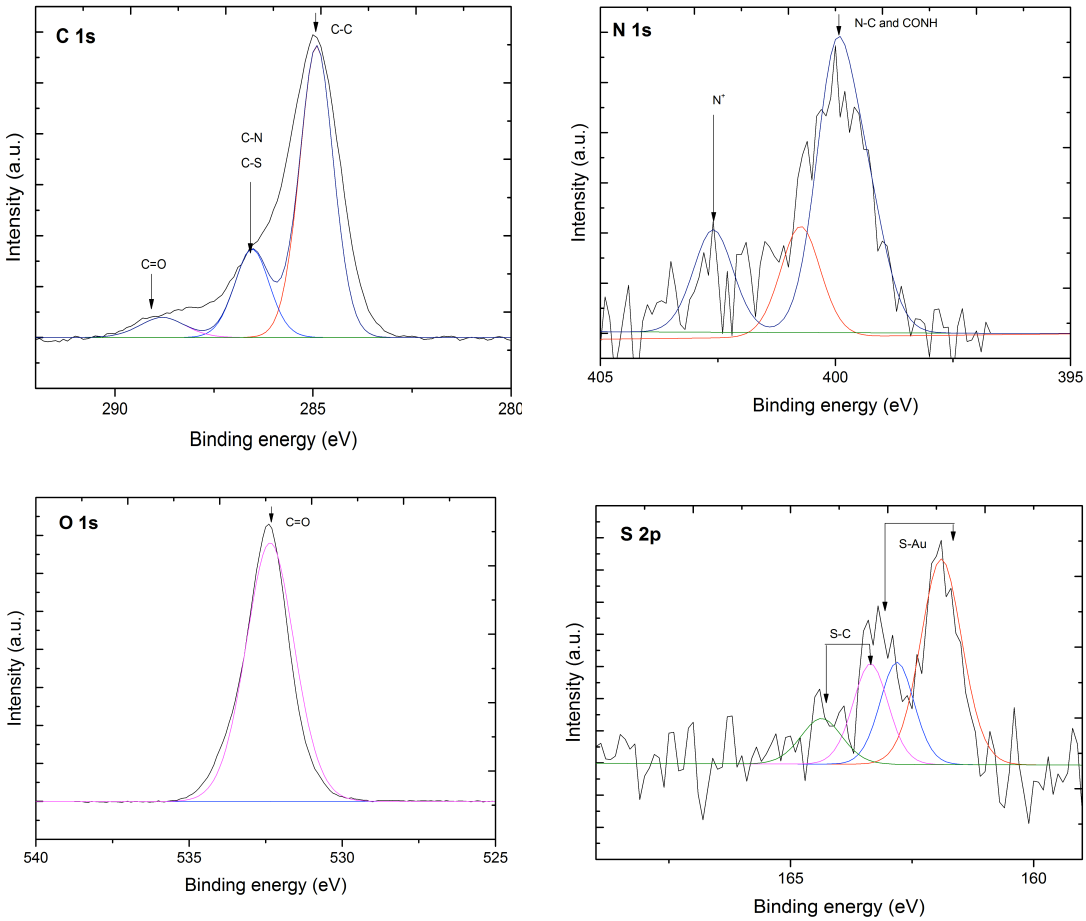

Summary of analyses performed by XPS

Binding energy/ eV	Assignment
285.0	C-C
286.5	C-N, C-S
288.8	C=O
399.7 and 401.1	N-C and CONH
402.6	N^+
532.7	O=C
163.9 and 165.0	S-C
162.0 and 163.4	S-Au

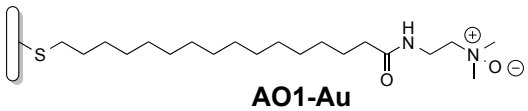

AO1-Au

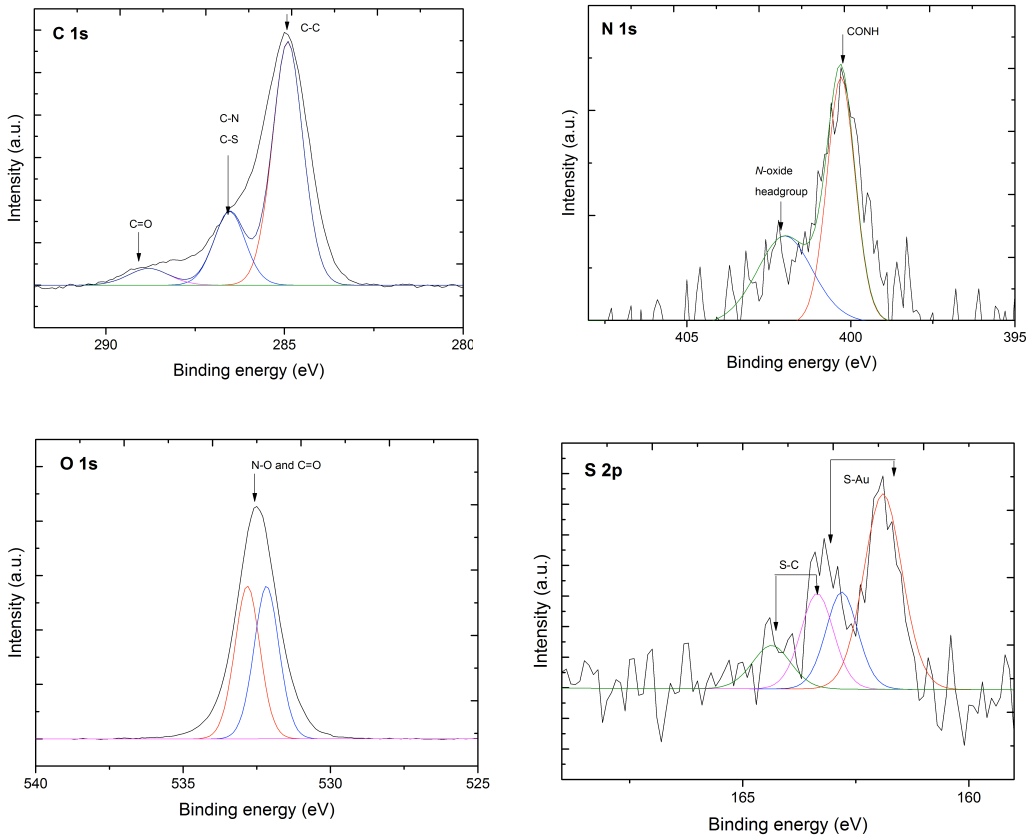

Summary of analyses performed by XPS

Binding energy/ eV	Assignment
285.0	C-C
286.8	C-N, C-S
288.8	C=O
400.1	CONH
402.6	*N*-oxide
532.7 and 533.1	O=C and O-N
163.9 and 165.0	S-C
162.0 and 163.4	S-Au

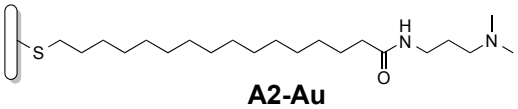

A2-Au

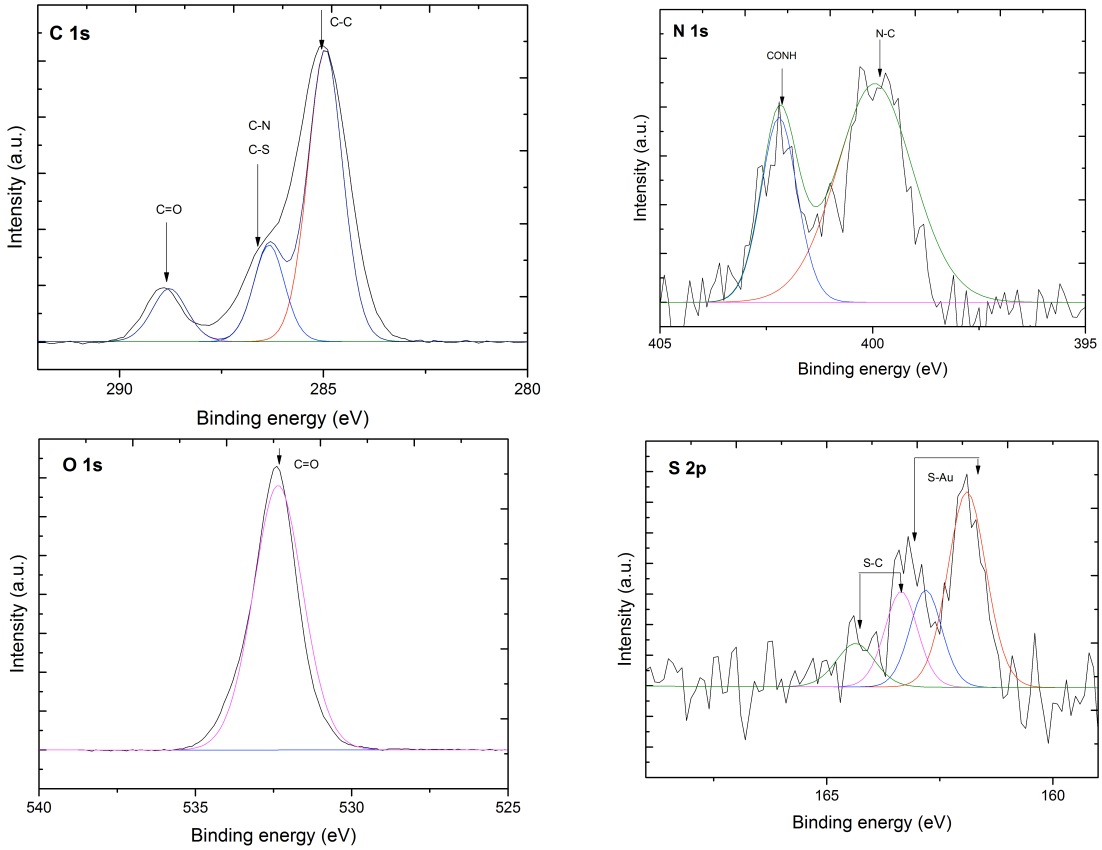

Summary of analyses performed by XPS

Binding energy/ eV	Assignment
285.0	C-C
287.3	C-N, C-S
289.4	C=O
400.2	N-C
401.9	CONH
532.6	O=C
163.9 and 165.0	S-C
162.0 and 163.4	S-Au

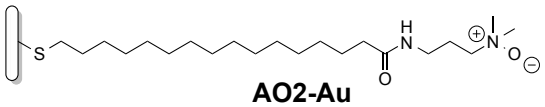

AO2-Au

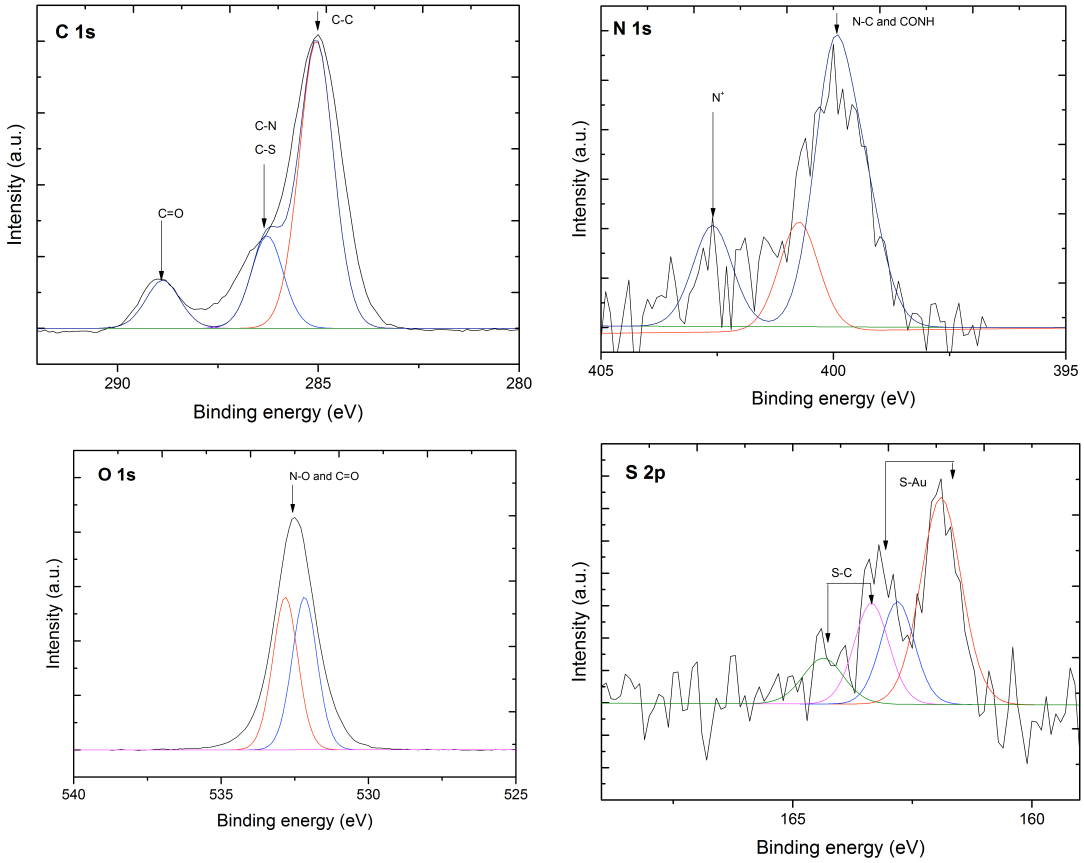

Summary of analyses performed by XPS

Binding energy/ eV	Assignment
285.0	C-C
287.4	C-N, C-S
289.3	C=O
398.3	N-C
400.3	CONH
402.6	*N*-oxide
532.4 and 533.1	O=C and N-O
163.9 and 165.1	S-C
162.1 and 163.4	S-Au

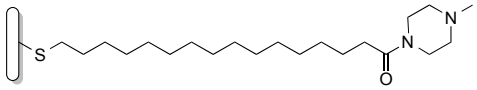

A3-Au

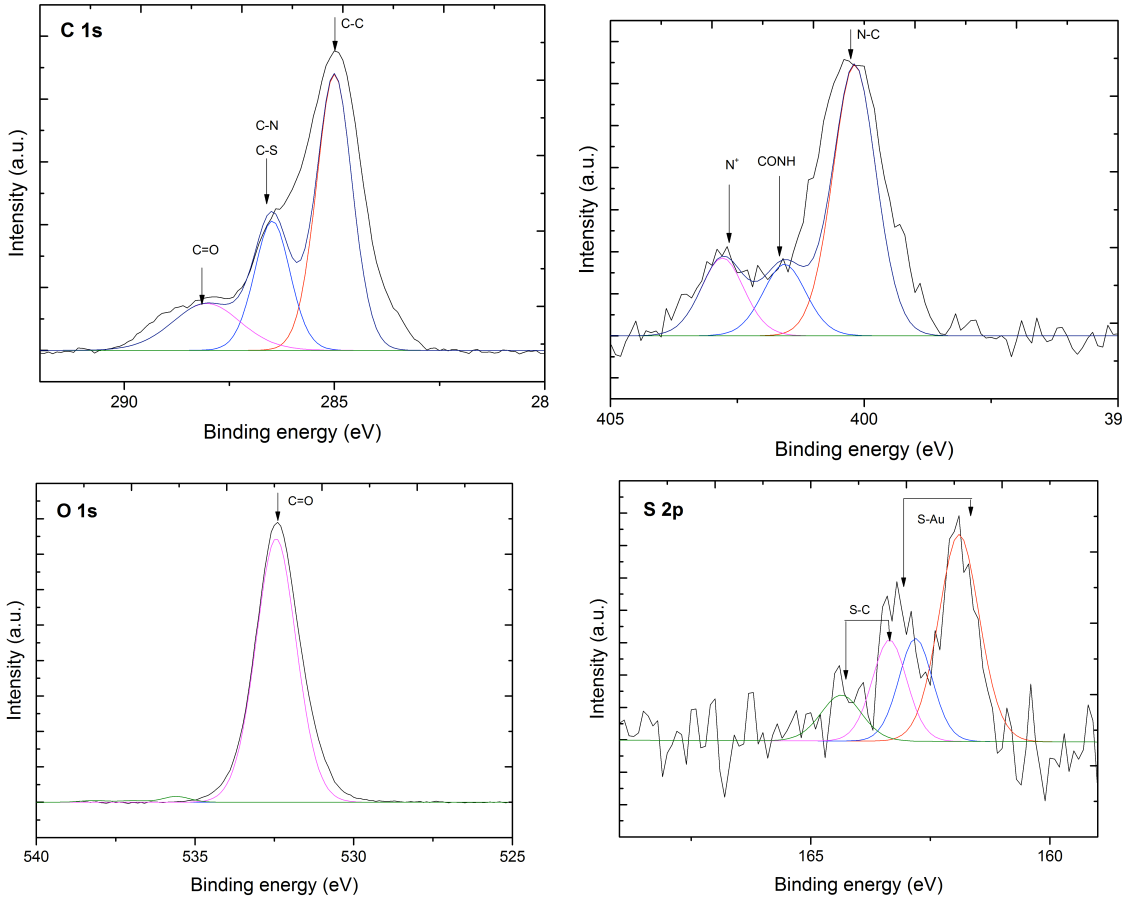

Summary of analyses performed by XPS

Binding energy/ eV	Assignment
285.0	C-C
287.3	C-N, C-S
289.4	C=O
400.4	N-C
401.8	CONH
402.8	N^+
532.9	O=C
163.9 and 165.0	S-C
161.9 and 163.2	S-Au

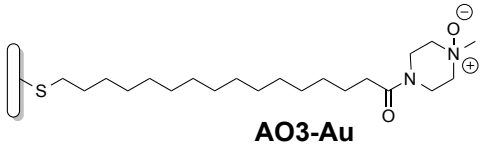

AO3-Au

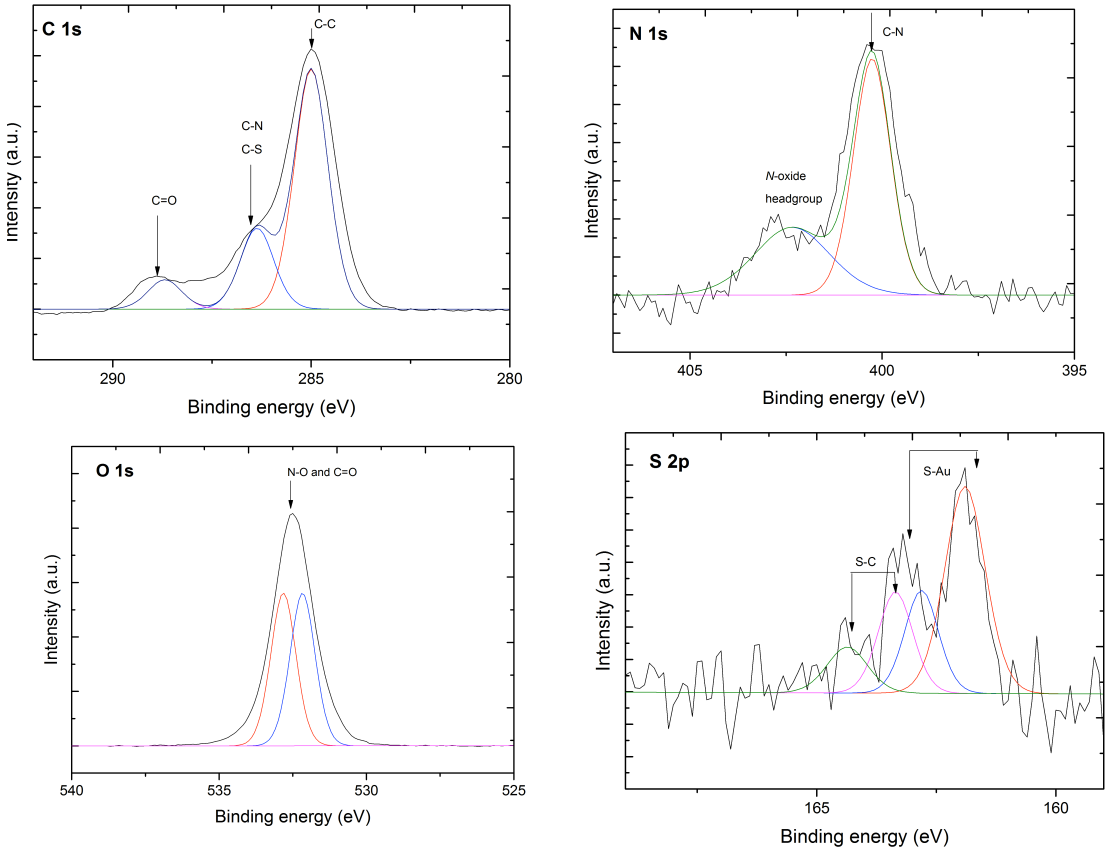

Summary of analyses performed by XPS

Binding energy/ eV	Assignment
285.0	C-C
287.3	C-N, C-S
289.4	C=O
400.1	C-N from CONH moiety
402.6	*N*-oxide
532.1	O=C
533.1	O-N
163.9 and 165.0	S-C
162.0 and 163.3	S-Au

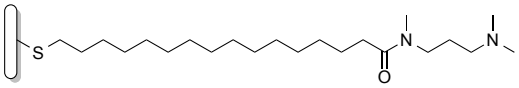

A5-Au

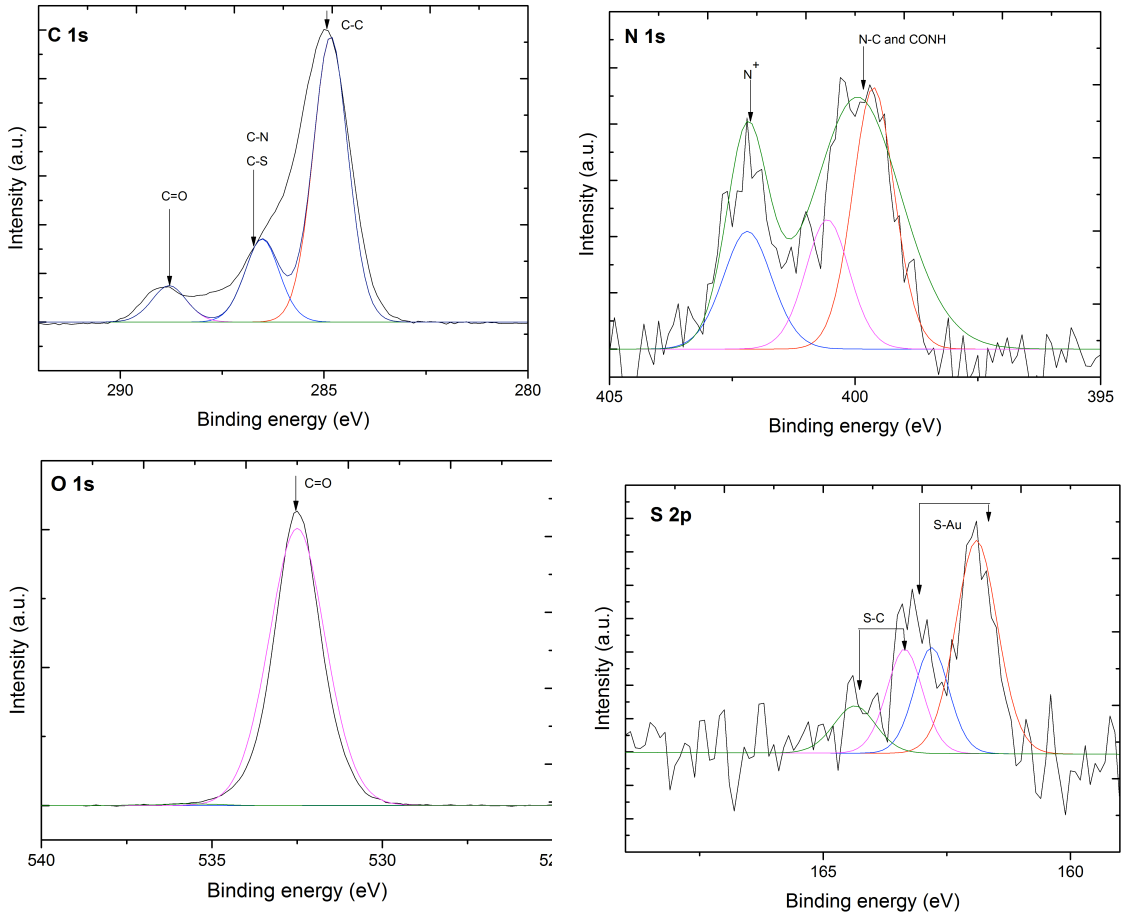

Summary of analyses performed by XPS

Binding energy/ eV	Assignment
285.0	C-C
287.3	C-N, C-S
289.4	C=O
399.7 and 400.2	N-C and CONH
402.1	N^+
532.1	O=C
163.9 and 165.0	S-C
162.0 and 163.4	S-Au

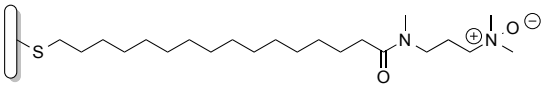

AO5-Au

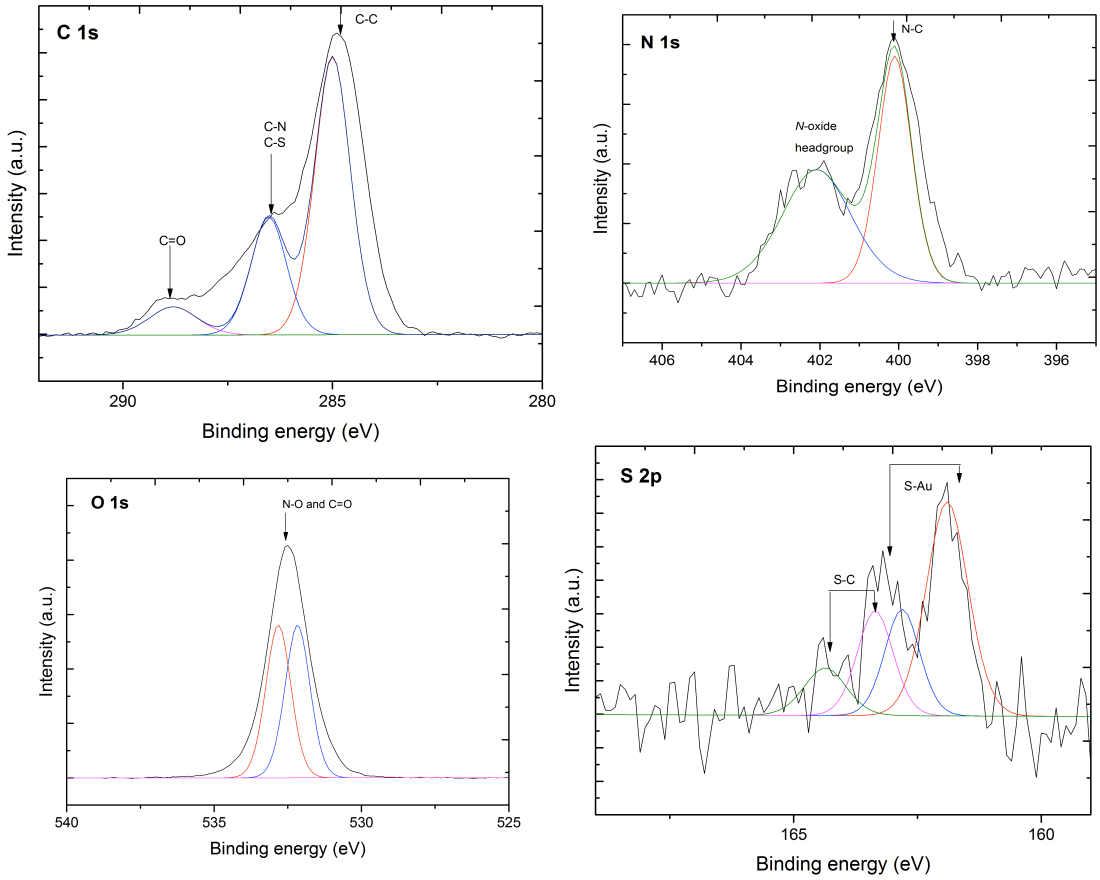

Summary of analyses performed by XPS

Binding energy/ eV	Assignment
285.0	C-C
287.3	C-N, C-S
289.4	C=O
400.2	C-N from CONH moiety
402.6	*N*-oxide
532.8	O=C
533.2	O-N
163.9 and 165.1	S-C
162.1 and 163.4	S-Au

Appendix 2 AFM images of gold surfaces

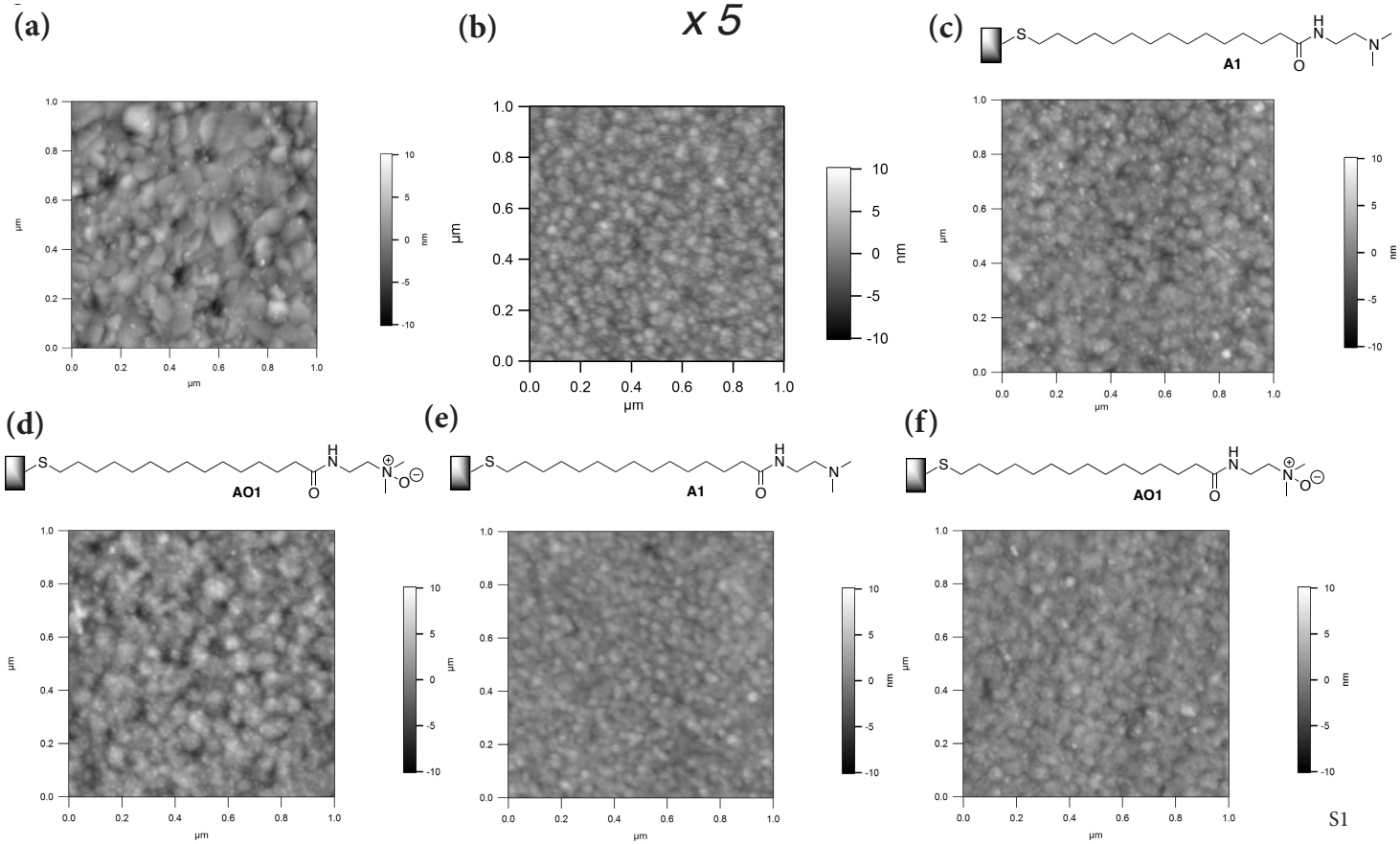

S1

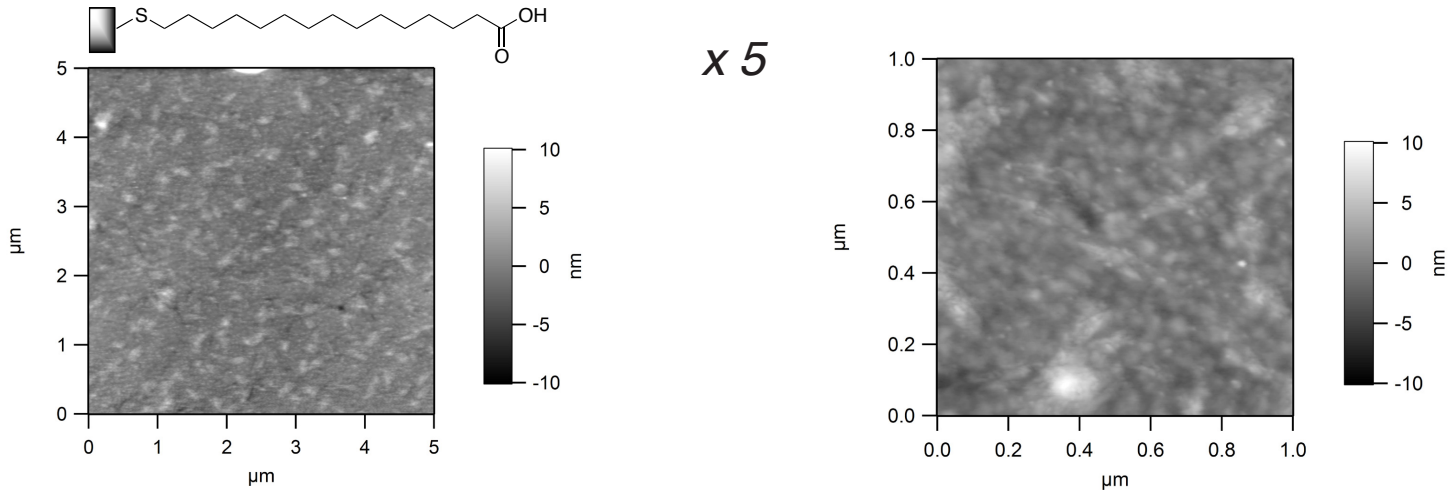

Mercaptohexadecanoic acid self-assembled monolayer and x5 magnification.

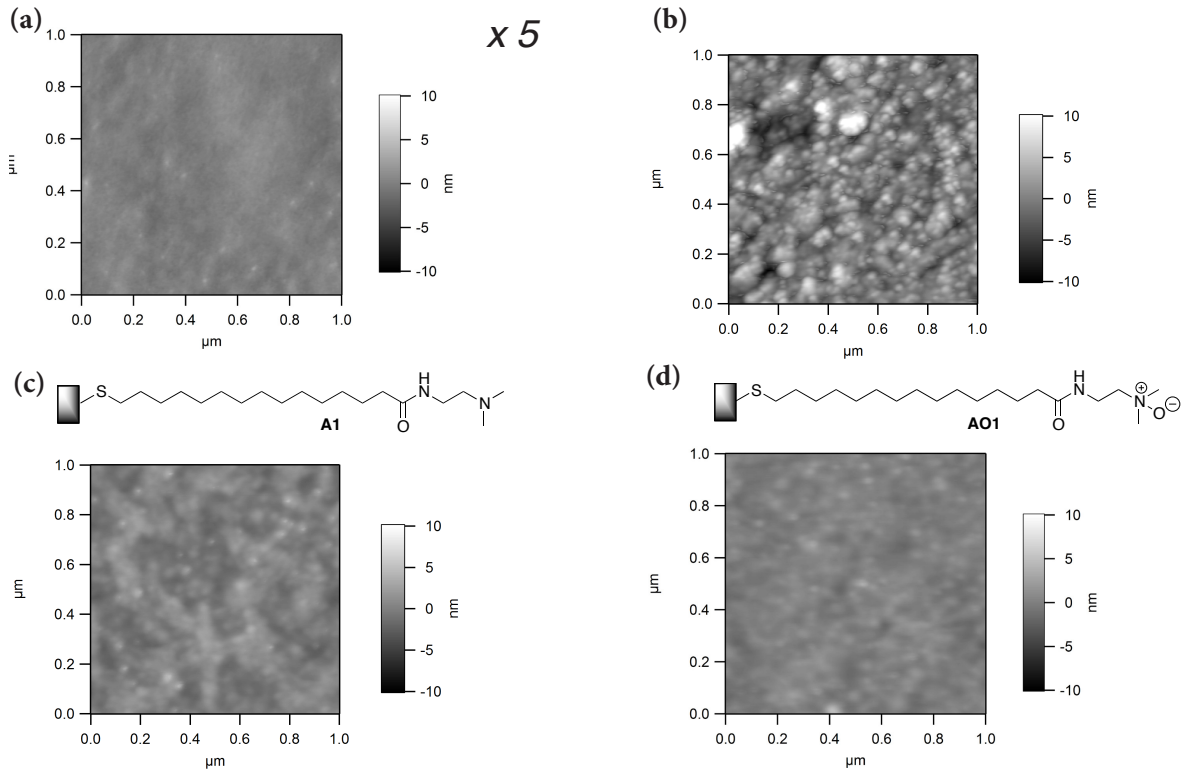

(a) Magnifications x5 of bare gold sample A; (b) plus lysozyme, 1 mM in PBS; (c) *N*-[2'-(dimethylamino)ethyl]mercaptohexadecanoic amide plus lysozyme, 1 mM in PBS; (d) *N*-[2'-(dimethylamino-*N*-oxide)ethyl]mercaptohexadecanoic amide self-assembled monolayer plus lysozyme 1 mM in PBS.

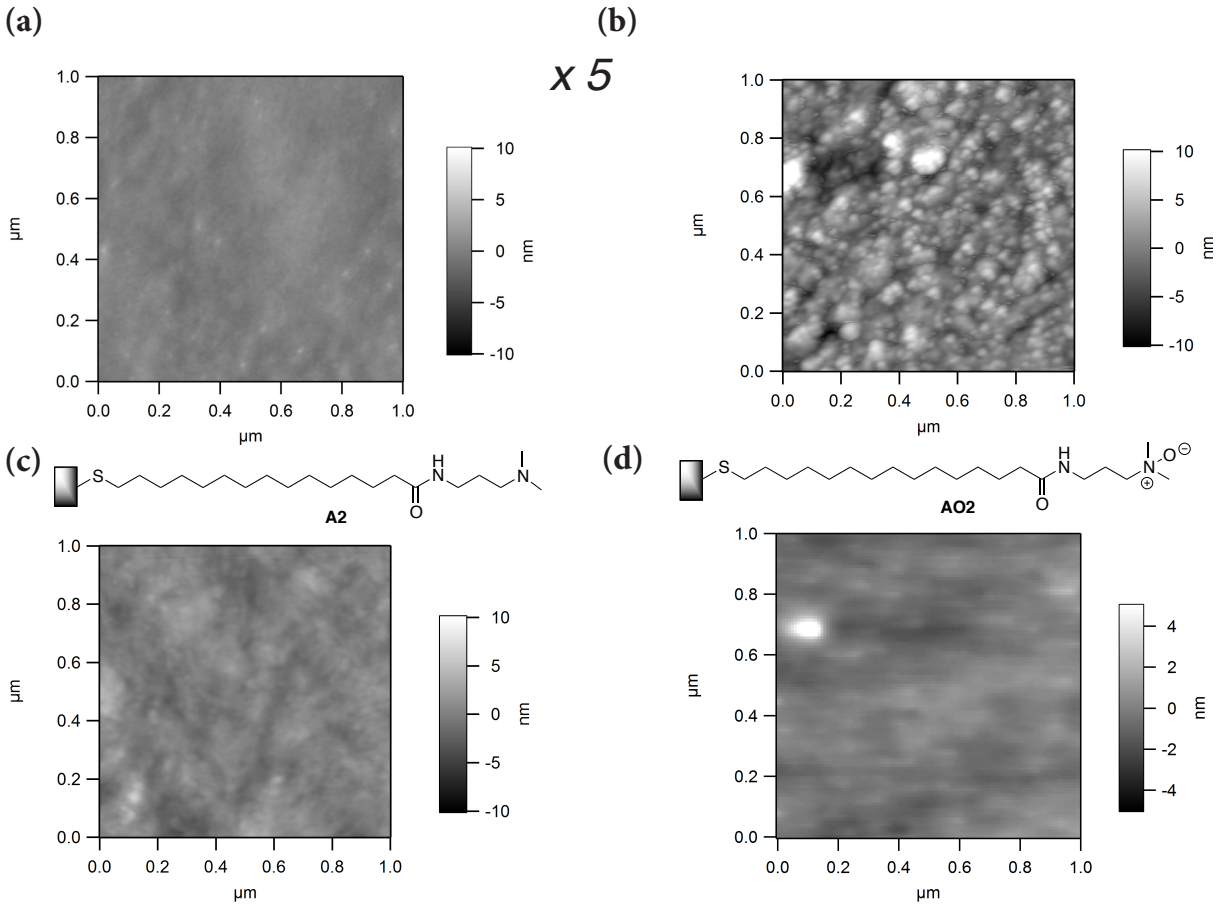

(a) Magnifications x5 of bare gold sample A; (b) plus lysozyme, 1 mM in PBS; (c) *N*-[2'-(dimethylamino)propyl]mercaptohexadecanoic amide plus lysozyme, 1 mM in PBS

(d) *N*-[2'-(dimethylamino-*N*-oxide)propyl]mercaptohexadecanoic amide self-assembled monolayer plus lysozyme 1 mM in PBS.

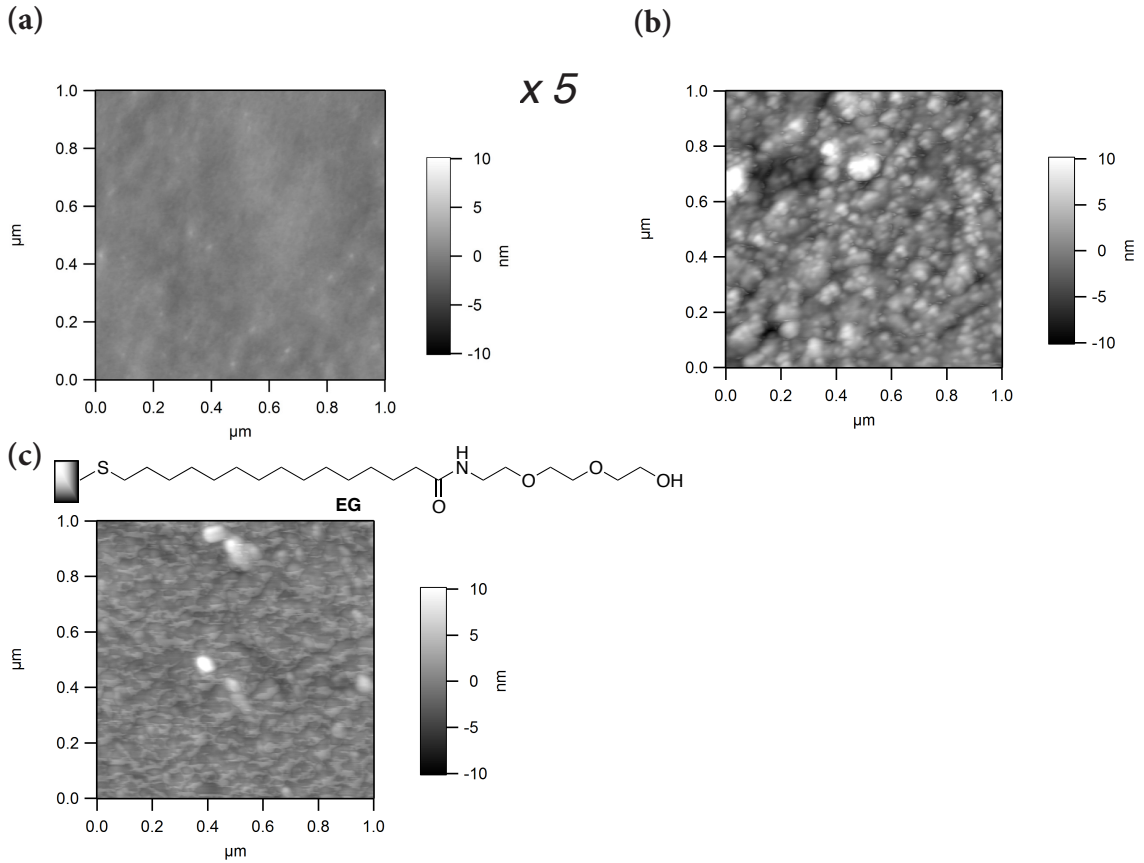

Magnifications x5 of (a) bare gold sample A; (b) plus lysozyme, 1 mM in PBS; (c) 1-aminotriethyleneglycol mercaptohexadecanoic amide self-assembled monolayer plus lysozyme, 1 mM in PBS

Appendix 3 Quartz Crystal Microbalance studies of protein adsorption on gold surfaces

QCM-D data from lysozyme deposition (1 mM in PBS) on tertiary amines **A1 - A5-Au** and corresponding tertiary amine oxides **AO1 - AO5-Au**

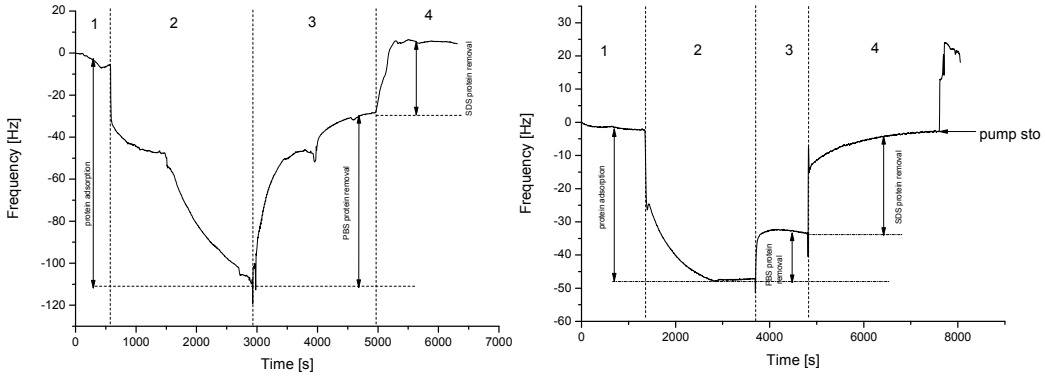

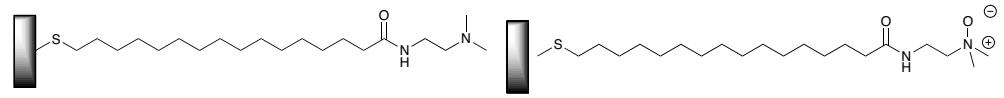

A1 **AO1**

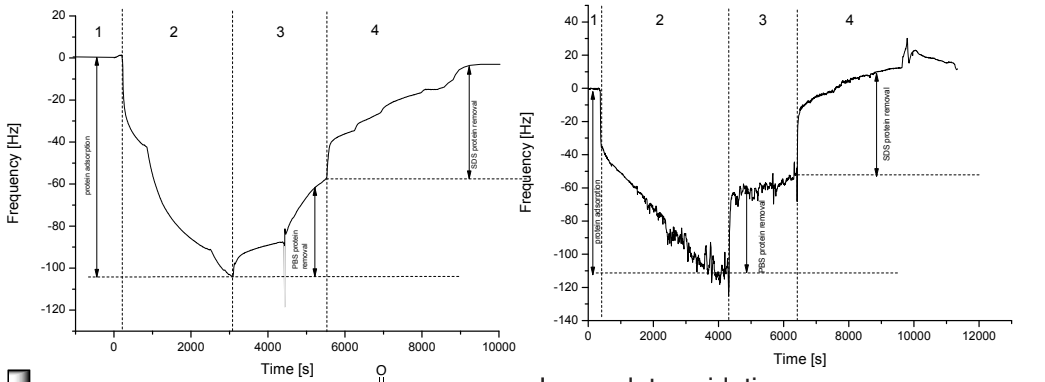

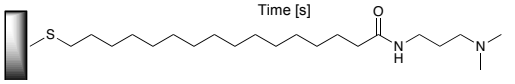

Incomplete oxidation

A2 **A02**

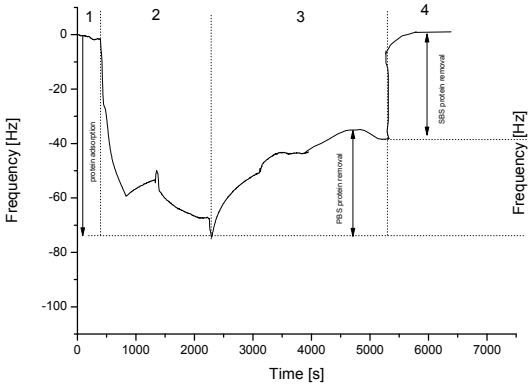

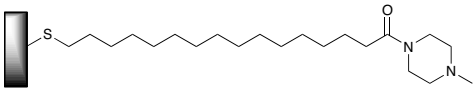

A3

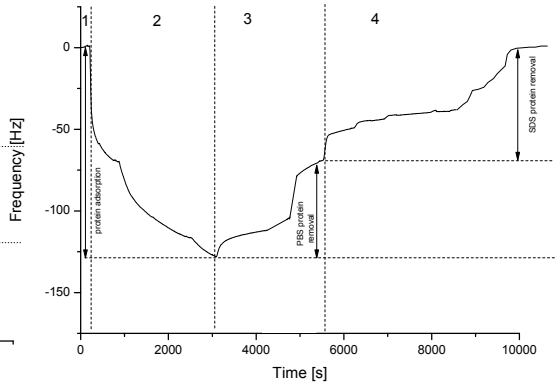

Incomplete oxidation

AO3

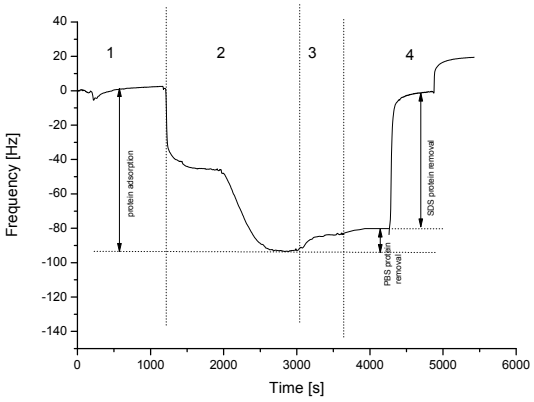

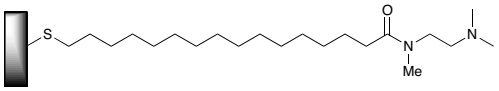

A4

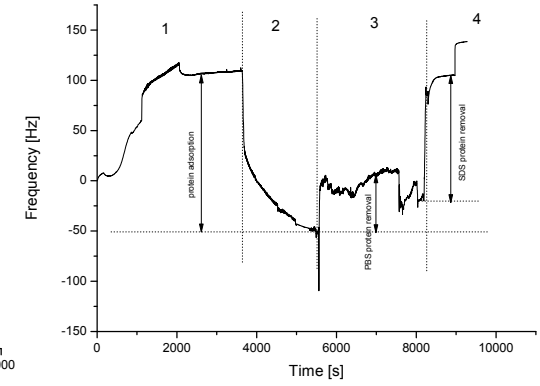

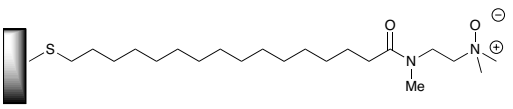

AO4

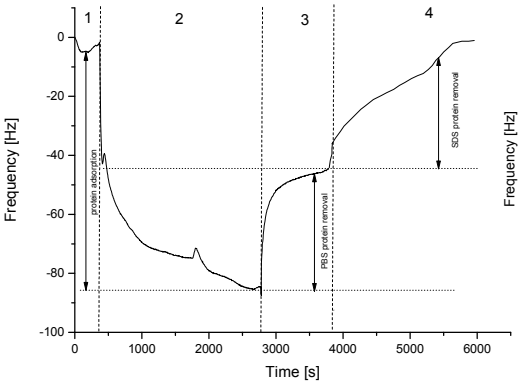

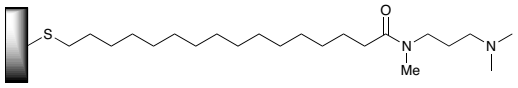

A5

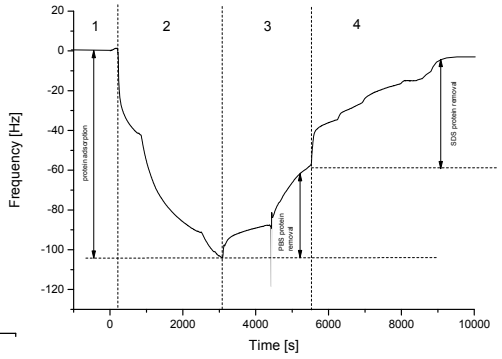

Incomplete oxidation

AO5

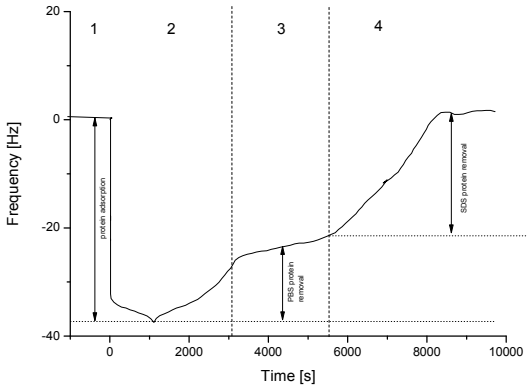

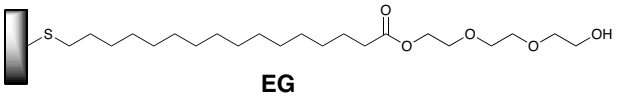

EG

QCM-D data from fibrinogen deposition (1 mM in PBS) on tertiary amines A1 - A5 and corresponding tertiary amine oxides AO1 - AO5

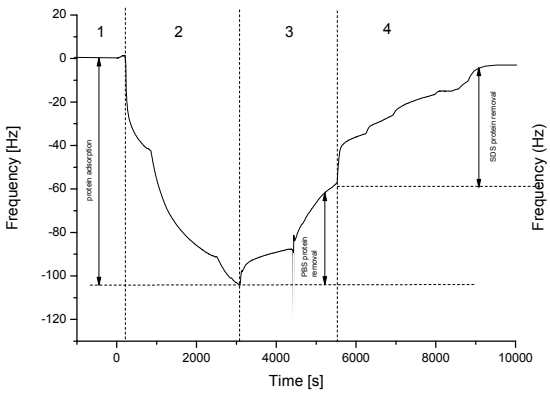

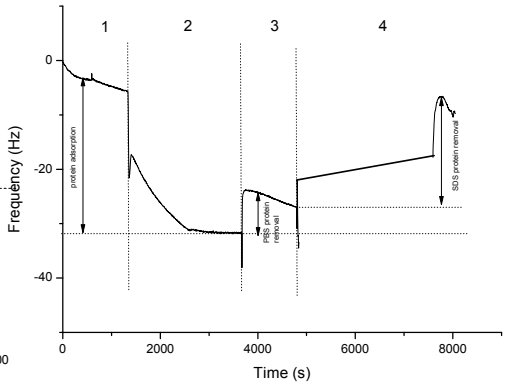

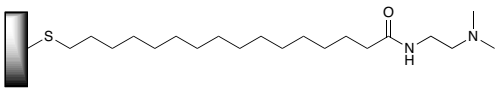

A1

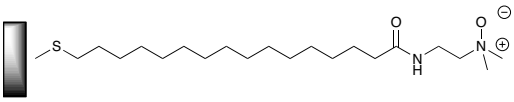

AO1

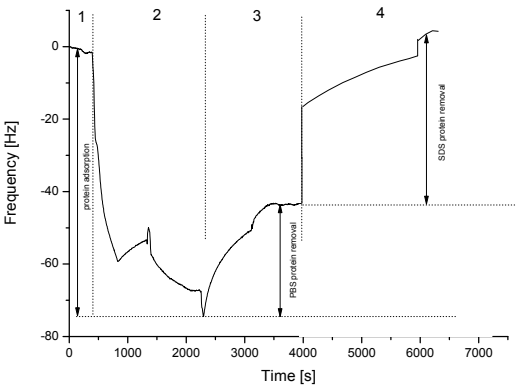

A2

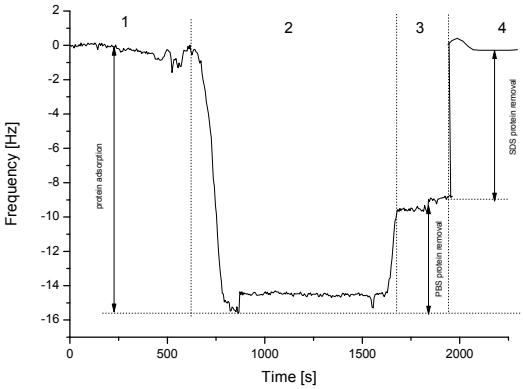

A02

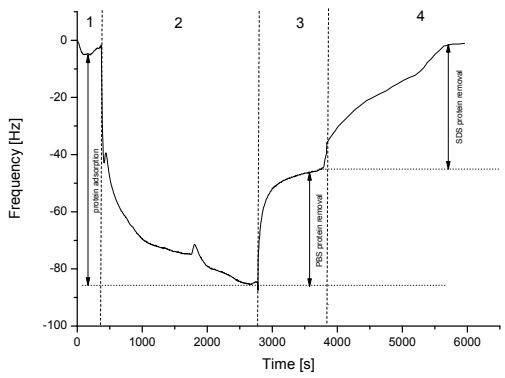

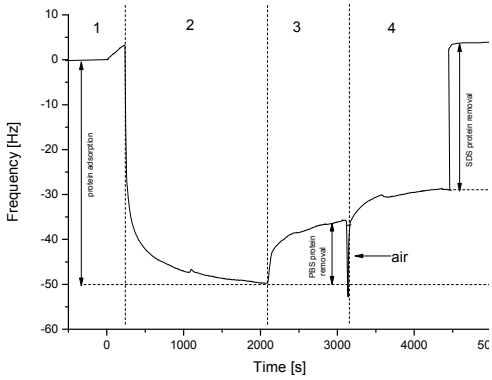

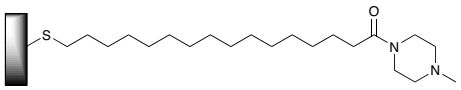

Incomplete oxidation

A3 **AO3**

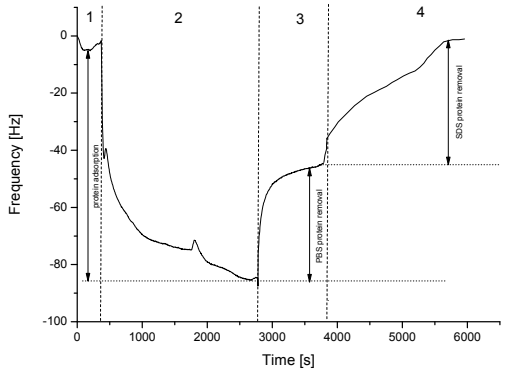

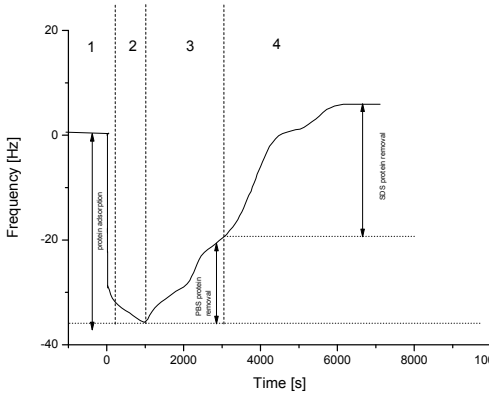

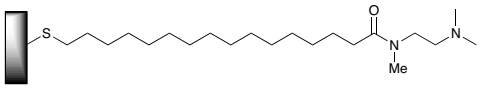

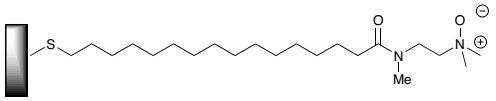

A4 **AO4**

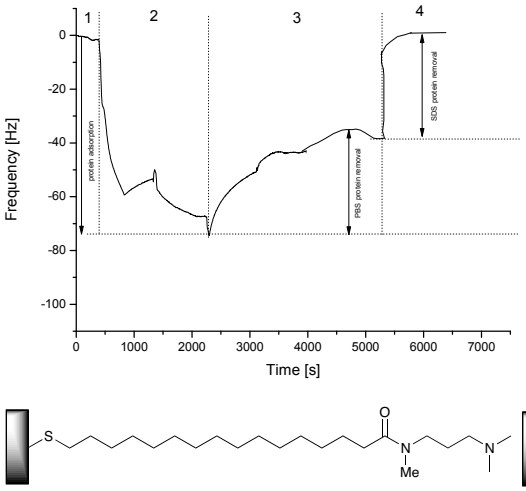
1
2
3
4
Frequency [Hz]
Time [s]
protein adsorption
PBS protein removal
SDS protein removal
S
O
N
Me
N

A5

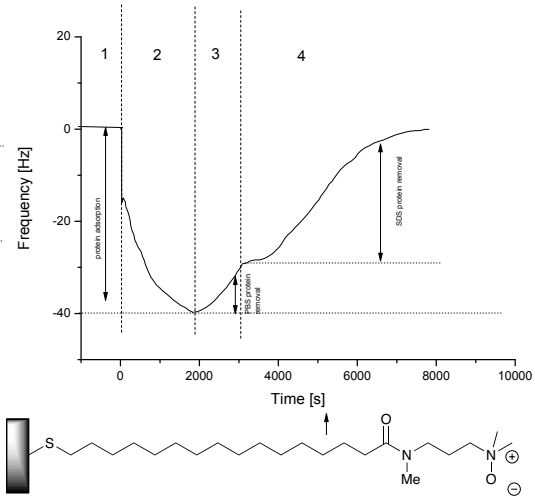
1
2
3
4
Frequency [Hz]
Time [s]
protein adsorption
PBS protein removal
SDS protein removal
S
O
N
Me
N
O

AO5

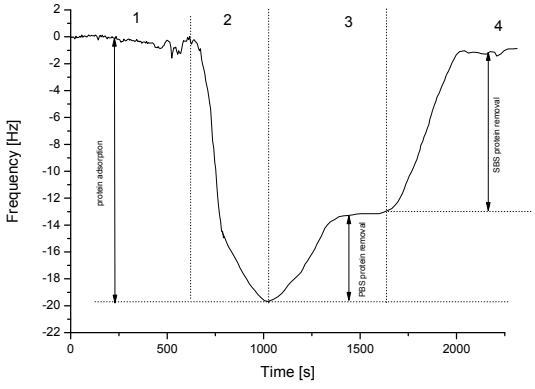
1
2
3
4
Frequency [Hz]
Time [s]
protein adsorption
PBS protein removal
SBS protein removal

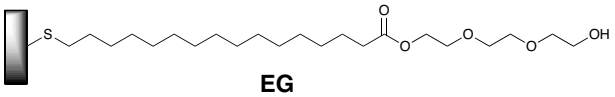
S
O
O
O
O
OH

EG

Appendix 4 Matlab code developed to calculate Gibbs free energy following methods developed by C A Hunter, University of Sheffield.[1]

```
function [] = chi_alpha(a_H20,b_H20,a_amine)

temperature = 298;
gas_constant = 8.314;

a_amine_vector = 0.1:0.1:10;

a_amine_length = length(a_amine_vector);
chi_alpha_vector = zeros(a_amine_length);

for counter = 1:a_amine_length;

a_amine = a_amine_vector(counter);

c_H20 = a_H20*b_H20;
delta1 = a_amine*b_H20;

chi_alpha = 1/(1+exp(-1*(delta1-0.5*c_H20)/(temperature*gas_constant)));

chi_alpha_vector(counter) = chi_alpha;

end

plot(a_amine_vector,chi_alpha,'b.')


end
```

```
function [] = chi_beta(a_H20,b_H20,b_amine)

temperature = 298;
gas_constant = 8.314;

a_amine_vector = 0.1:0.1:10;

a_amine_length = length(a_amine_vector);
chi_beta_vector = zeros(a_amine_length);

for counter = 1:a_amine_length;

a_amine = a_amine_vector(counter);
```

```
c_H20 = a_H20*b_H20;
delta2 = b_amine*a_H20;

chi_beta = 1/(1+exp(-1*(delta2-0.5*c_H20)/(temperature*gas_constant)));
chi_beta_vector(counter) = chi_beta;

end

plot(a_amine_vector,chi_beta,'b')


end
function [] = chi_solvent(a_H2O,b_H2O)

temperature = 298;
gas_constant = 8.314;

a_amine_vector = 0.1:0.1:10;

a_amine_length = length(a_amine_vector);
chi_solvent_vector = zeros(a_amine_length);

for counter = 1:a_amine_length;

a_amine = a_amine_vector(counter);

c_H2O = a_H2O*b_H2O;

chi_solvent = 1/(1+exp((-0.5*c_H2O)/(temperature*gas_constant)));


chi_solvent_vector(counter) = chi_solvent;

end

plot(a_amine_vector,chi_solvent,'b.')


end
```

```
function [] = free_energy(a_H20,b_H20,b_amine)

temperature = 298;
gas_constant = 8.314;

a_amine_vector = 0.1:0.1:10;

a_amine_length = length(a_amine_vector);
free_energy = zeros(a_amine_length,1);
```

```
for counter = 1:a_amine_length;

a_amine = a_amine_vector(counter);

c_H20 = a_H20*b_H20;
c_amine = a_amine*b_amine;
delta1 = a_amine*b_H20;
delta2 = b_amine*a_H20;

chi_alpha = 1/(1+exp(-1*(delta1-0.5*c_H20)/(temperature*gas_constant)));
chi_beta = 1/(1+exp(-1*(delta2-0.5*c_H20)/(temperature*gas_constant)));
chi_solvent = 1/(1+exp((-0.5*c_H20)/(temperature*gas_constant)));

free_energy_hydrogen = -1*c_amine + chi_alpha*delta1 + chi_beta*delta2-
(0.5*chi_alpha + 0.5*chi_beta + chi_solvent - 1)*c_H20;

free_energy(counter) = free_energy_hydrogen;

end

plot(a_amine_vector,free_energy)

end
```

```
function [free_energy_hydrogen] =
free_energy_oxide(a_H2O,b_H2O,a_amine,b_amine)

temperature = 298;
gas_constant = 8.314;

c_H2O = a_H2O*b_H2O;
c_amine = a_amine*b_amine;
delta1 = a_amine*b_H2O;
delta2 = b_amine*a_H2O;


chi_alpha = 1/(1+exp(-1*temperature*gas_constant*(delta1-0.5*c_H2O)));
chi_beta = 1/(1+exp(-1*temperature*gas_constant*(delta2-0.5*c_H2O)));
chi_solvent = 1/(1+exp((-0.5*c_H2O)/(temperature*gas_constant)));

free_energy_hydrogen = -1*c_amine + chi_alpha*delta1 + chi_beta*delta2-
(0.5*chi_alpha+0.5*chi_beta+chi_solvent-1)*c_H2O;

free_energy_oxide = free_energy_hydrogen

end
```

```
function [free_energy1] = free_energy1(a_H2O,b_H2O,a_amine,b_amine)
```

```
temperature = 298;
gas_constant = 8.314;

c_H2O = a_H2O*b_H2O;
c_amine = a_amine*b_amine;
delta1 = a_amine*b_H2O;
delta2 = b_amine*a_H2O;


chi_alpha = 1/(1+exp(-1*(delta1-0.5*c_H2O)/(temperature*gas_constant)));
chi_beta = 1/(1+exp(-1*(delta2-0.5*c_H2O)/(temperature*gas_constant)));
chi_solvent = 1/(1+exp((-0.5*c_H2O)/(temperature*gas_constant)));

free_energy1 = -1*c_amine + chi_alpha*delta1 + chi_beta*delta2-
((0.5*chi_alpha+0.5*chi_beta+chi_solvent-1)*c_H2O);


 end
```

(1) Hunter, C. A. *Angew. Chem. Int. Ed.,* **2004**, *43*, 5310.

Appendix 5 Surface tension measuremnts on tertiary amine amphiphiles

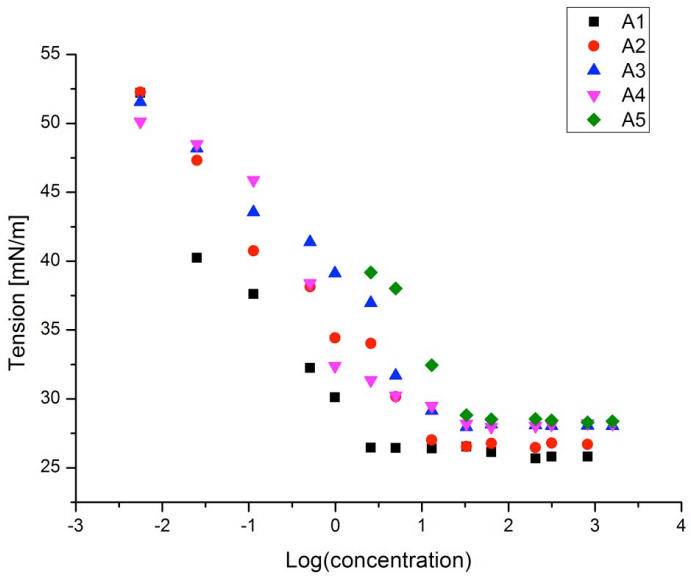

Surface tension versus log concentration (mM) of amines: (squares) **A1-Si**, (circles) **A2-Si**, (triangles) **A3-Si**, (reversed triangles) **A4-Si**, (rhombuses) **A5-Si.**

Appendix 6 XPS analyses of tertiary amine and corresponding amine N-oxide functionalized SAMs

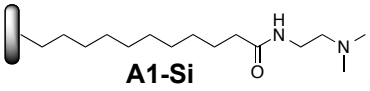

A1-Si

(a)

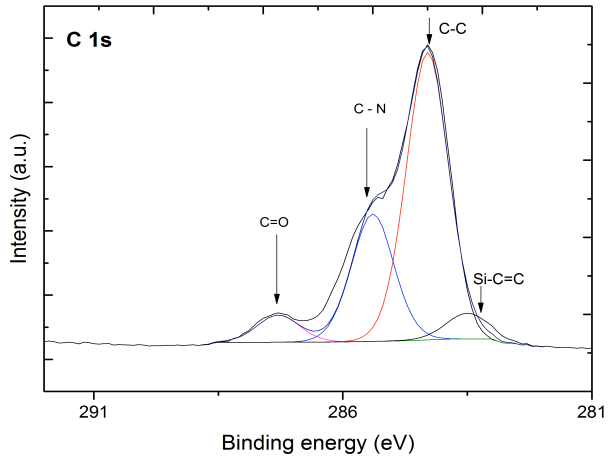

Assignment
284.4 eV Si-C=C
285.1 eV C-C
286.4 eV C-N
289.1 eV C=O

(b)

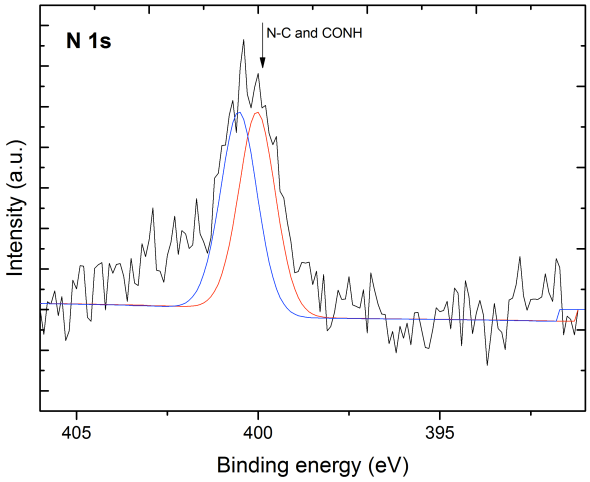

400.9 eV N-C
401.8 eV CONH

(c)

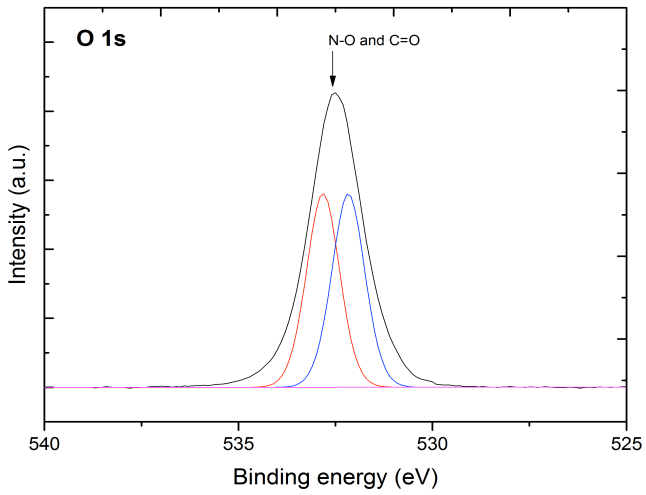

532.1 eV C=O

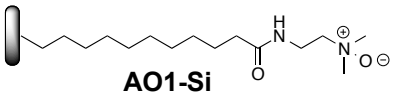

(a)

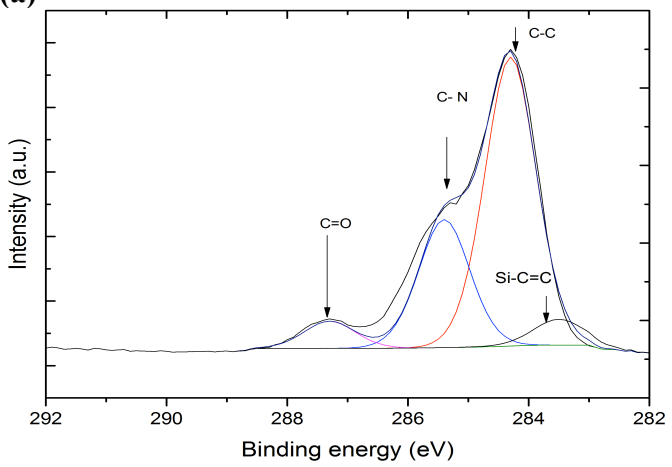

Assignment
284.5 eV Si-C=C
285.0 eV C-C
286.5 eV C-N
289.0 eV C=O

(b)

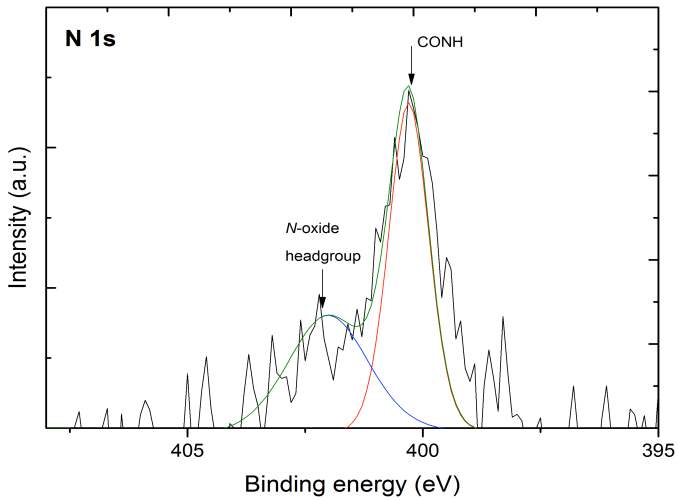

399.7 eV C-N
401.2 eV CONH
403.2 eV *N*-oxide

(c)

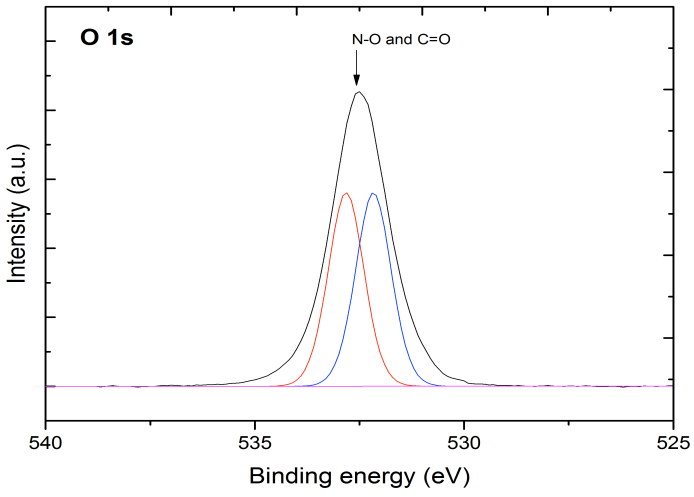

532.0 eV C=O
533.2 eV N-O

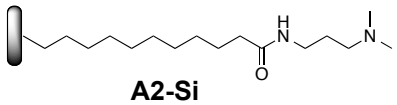

(a) **A2-Si**

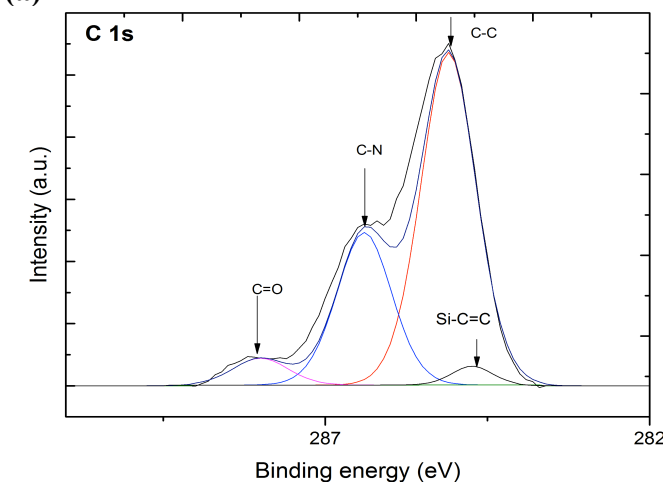

Assignment
284.5 eV Si-C=C
285.0 eV C-C
286.8 eV C-N
289.0 eV C=O

(b)

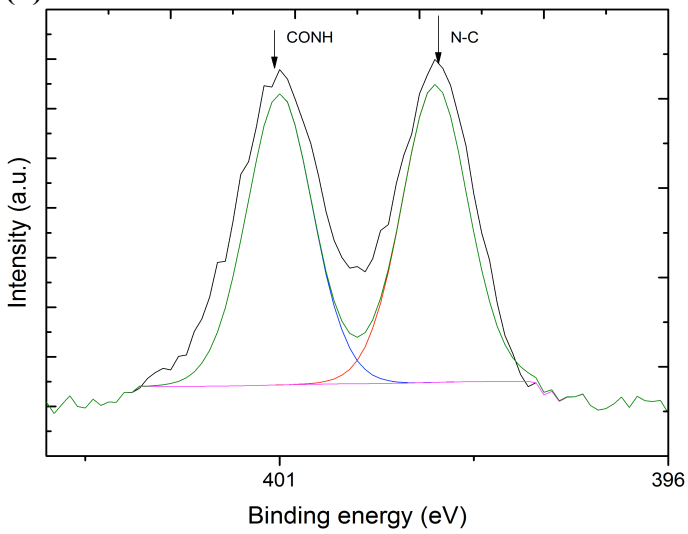

400.0 eV N-C
401.9 eV CONH

(c)

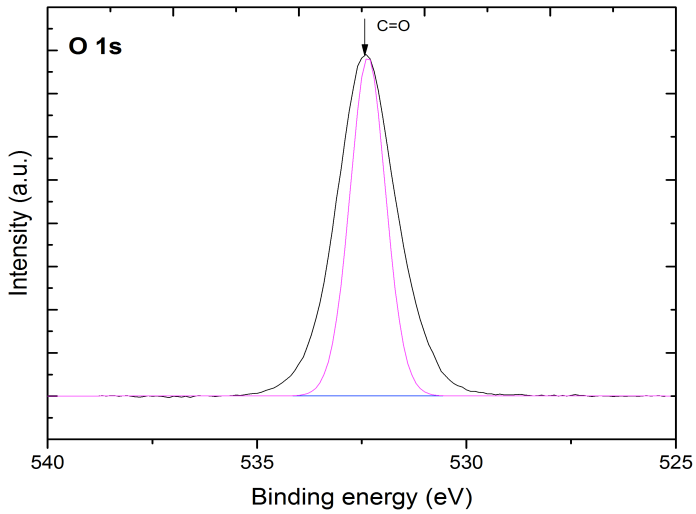

532.5 eV C=O

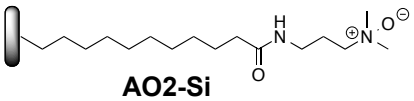

AO2-Si

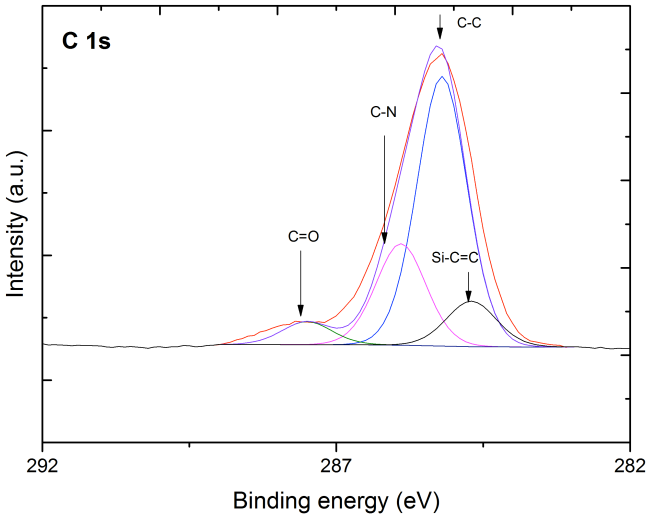

(a)

Assignment
284.5 eV Si-C=C
285.0 eV C-C
286.5 eV C-N
288.9 eV C=O

(b)

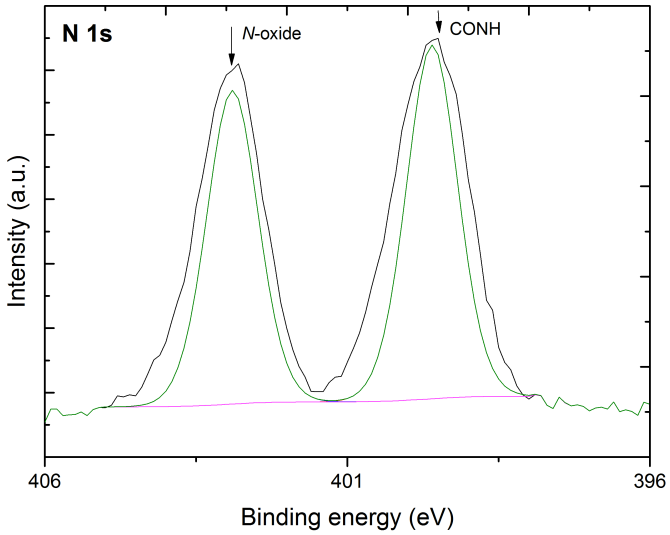

400.9 eV CONH
402.5 eV *N*-oxide

(c)

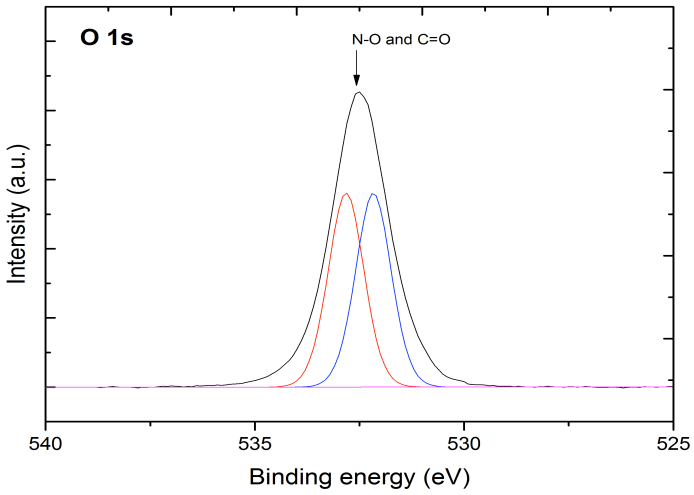

531.9 eV C=O
533.2 eV N-O

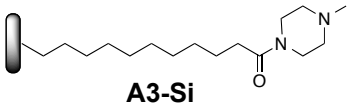

A3-Si

(a)

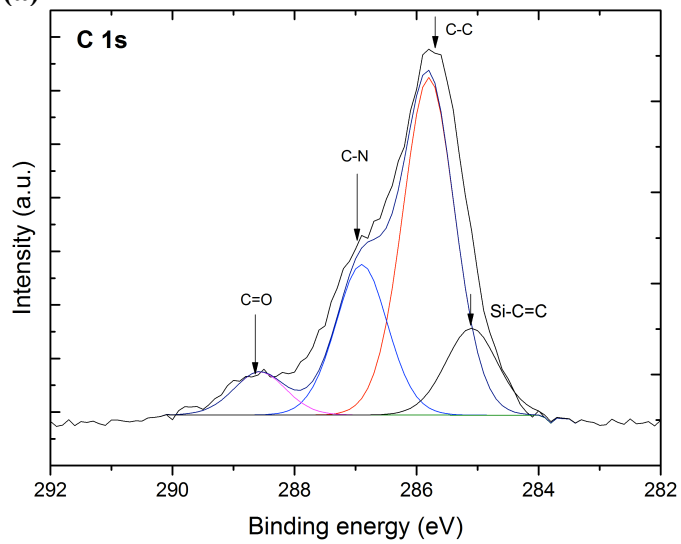

Assignment
284.9 eV Si-C=C
285.2 eV C-C
286.9 eV C-O, C-N
288.9 eV C=O

(b)

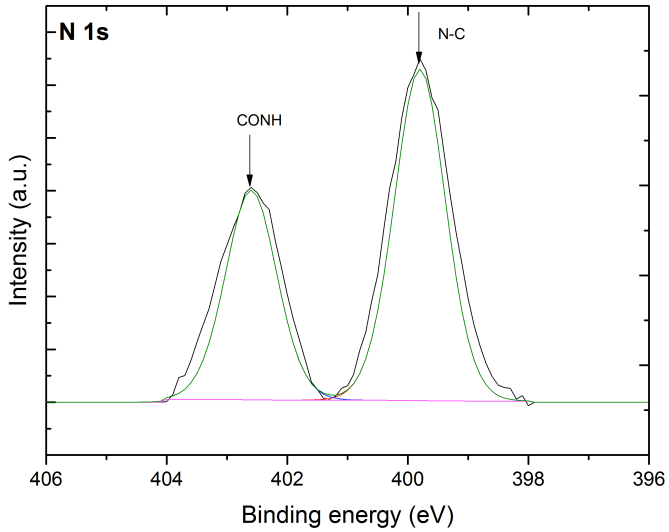

400.0 eV N-C
402.9 eV CONH

(c)

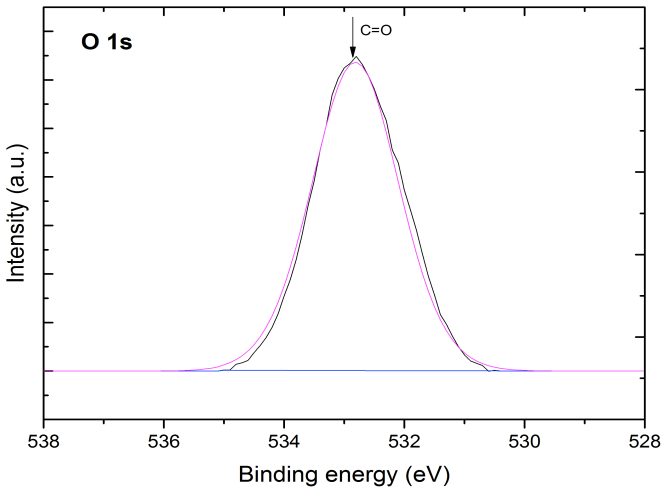

533.1 eV C=O

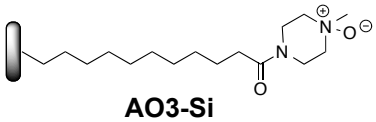

AO3-Si

(a)

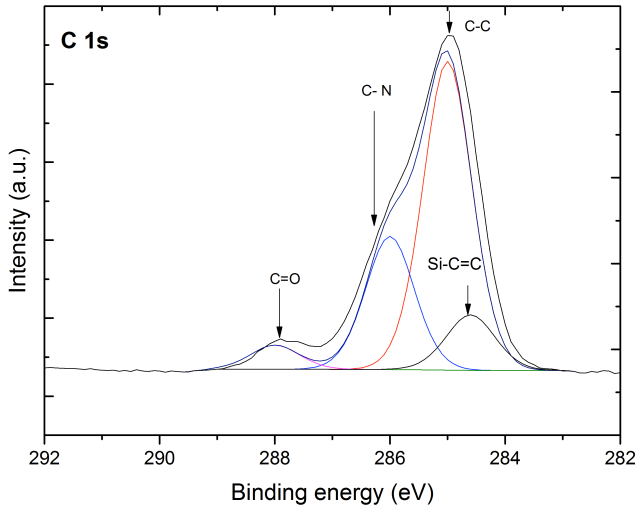

Assignment
284.5 eV Si-C=C
285.0 eV C-C
286.1 eV C-N
299.1 eV C=O

(b)

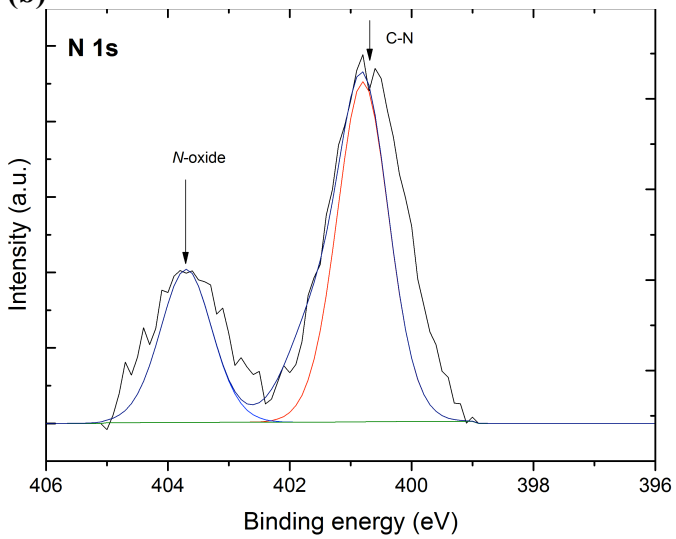

400.9 eV CONH
403.9 eV *N*-oxide

(c)

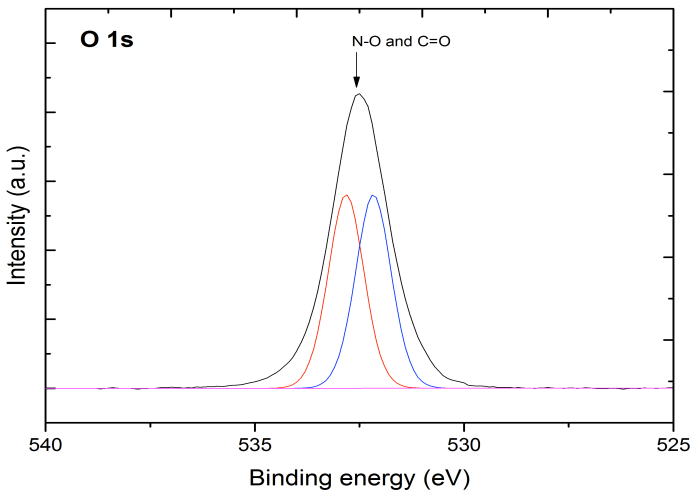

532.9 eV C=O
533.2.eV N-O

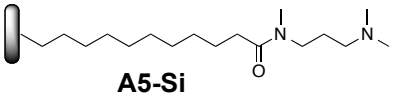

A5-Si

(a)

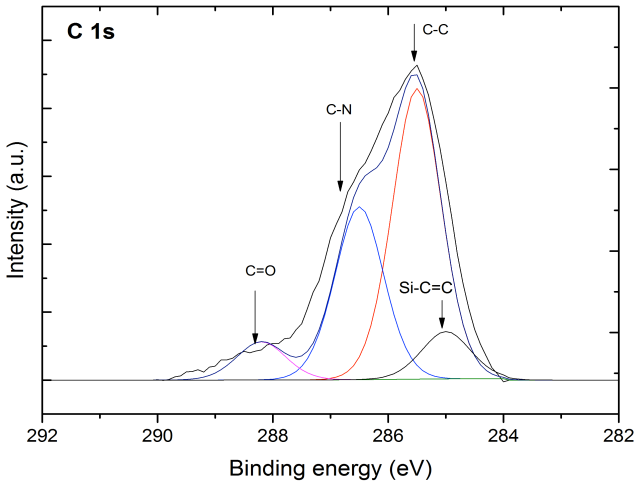

Assignment
284.9 eV Si-C=C
285.0 eV C-C
286.5 eV C-N
288.3 eV C=O

(b)

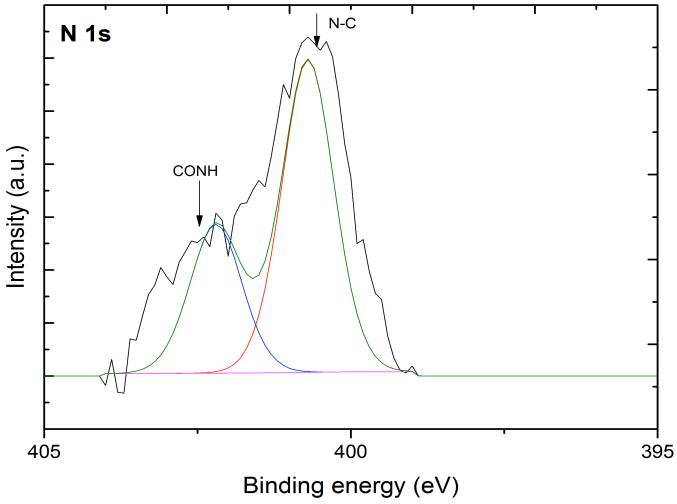

400.3 eV N-C
402.8 eV CONH

(c)

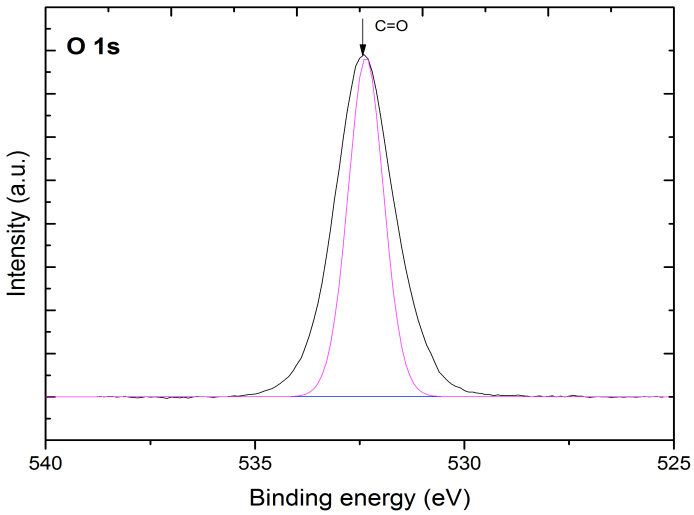

532.0 eV C=O

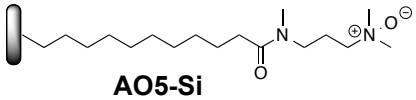

(a)

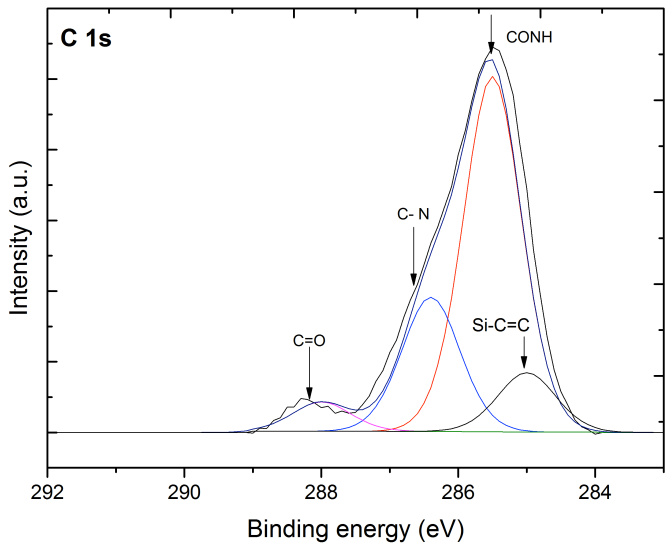

Assignment
284.9 eV Si-C=C
285.0 eV C-C
286.2 eV C-N
288.2 eV C=O

(b)

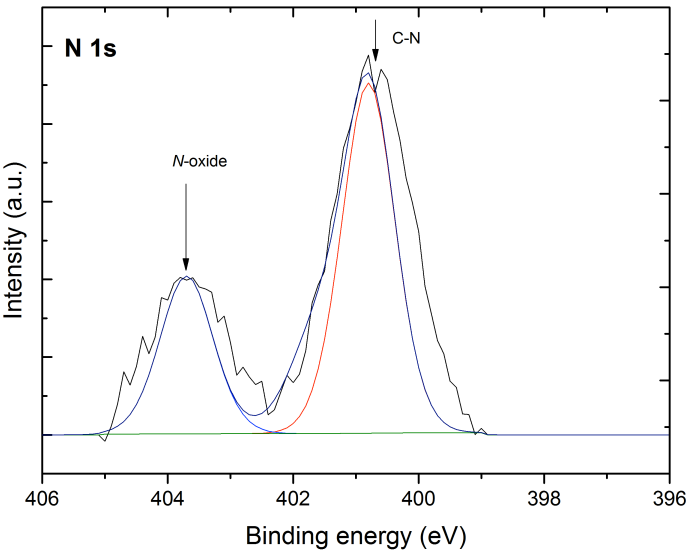

402.1 eV C-N from CONH
403.9 eV *N*-oxide

(c)

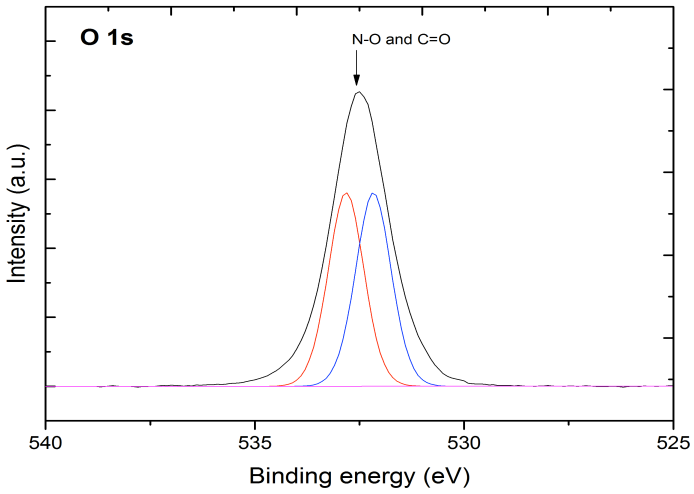

532.2. eV C=O
533.2 eV N-O

Appendix 7 AFM images of silicon surfaces

(a) Native silion wafer (111) (b) etched silicon wafer (111) (c) N-[2'-(dimethylamino)ethyl]undecanoic amide SAM (d) N-[2'-(dimethylamino)ethyl]undecanoic amine oxide SAM

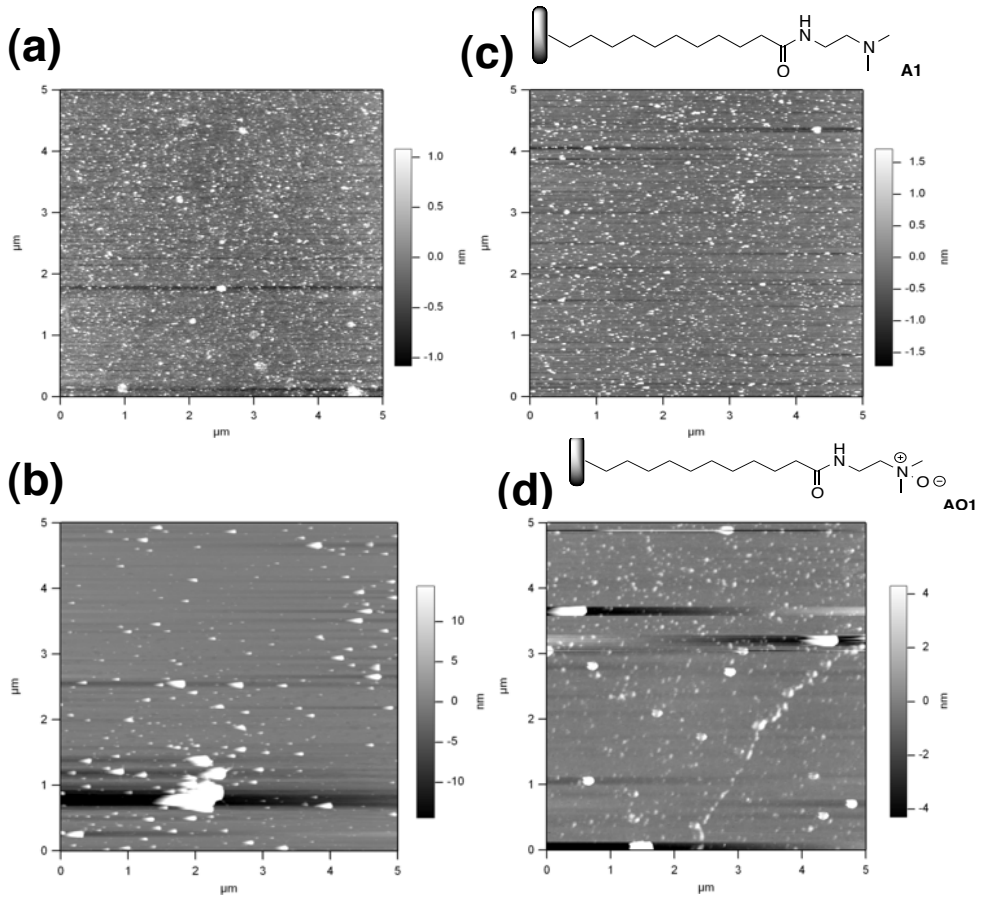

(a) N-[2’-(dimethylamino)ethyl]undecanoic amide SAM plus 1 mM lysozyme in PBS; (b) N-[2’-(dimethylamino)ethyl]undecanoic amine oxide SAM plus 1 mM lysozyme in PBS (c) N-[2’-(dimethylamino)ethyl]undecanoic amide SAM plus 1 μM fibrinogen in PBS; (d) N-[2’-(dimethylamino)ethyl]undecanoic amine oxide SAM plus 1 μM fibrinogen in PBS

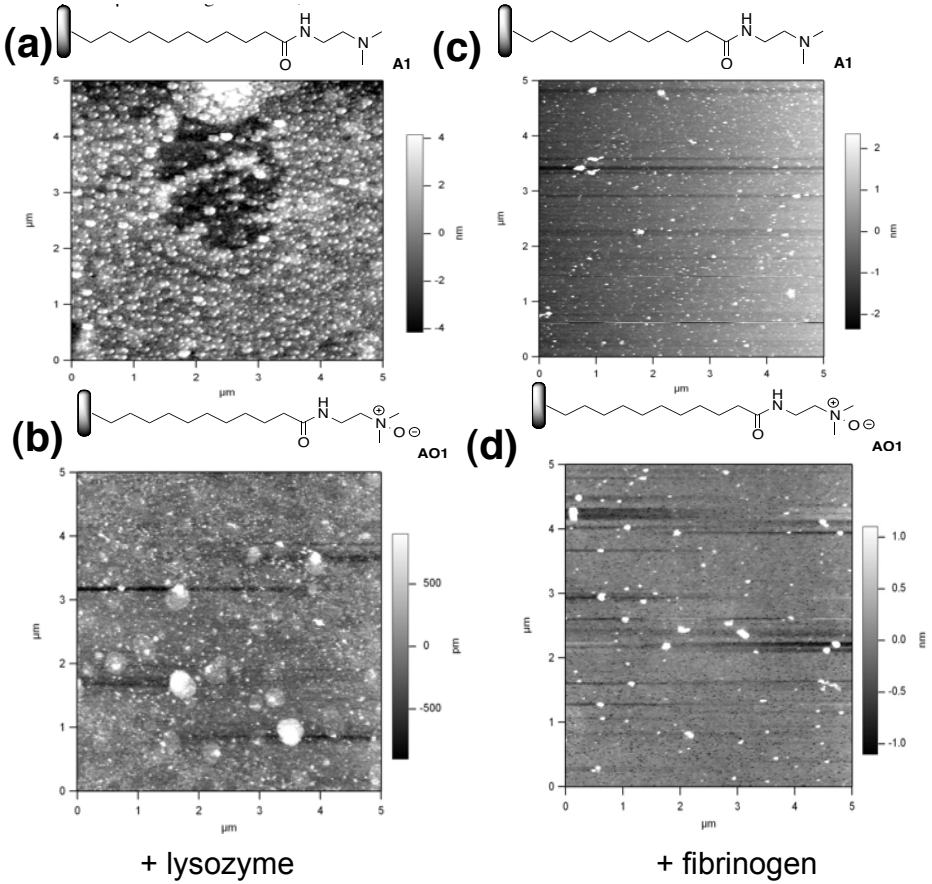

Appendix 8 H^1NMR and ^{13}C NMR spectra.

A1

A1.esp

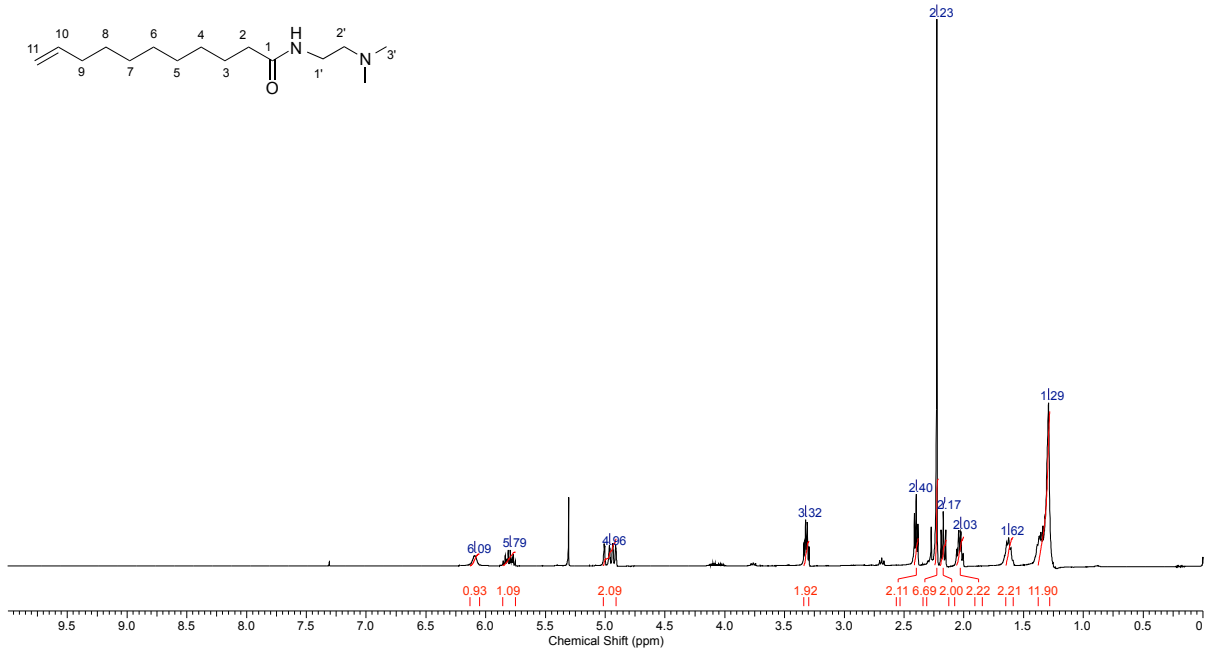

C_A1.001.1r.esp

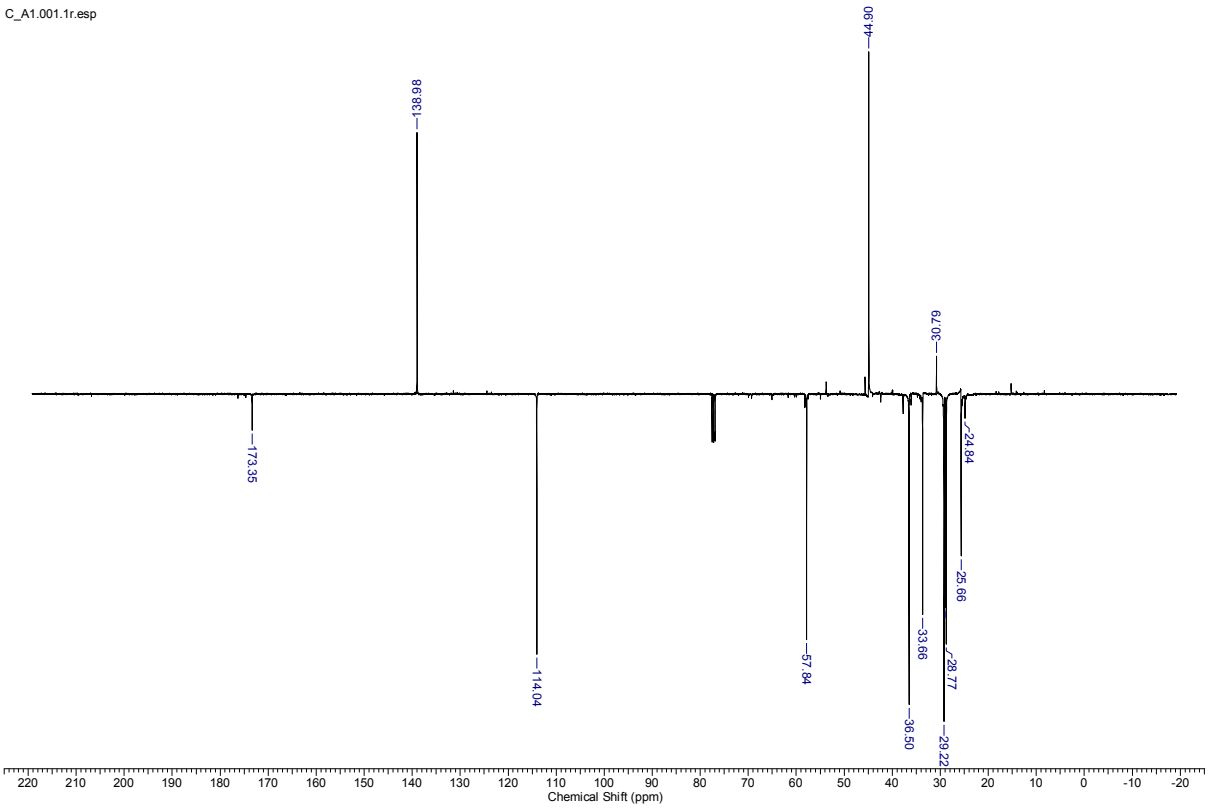

A2

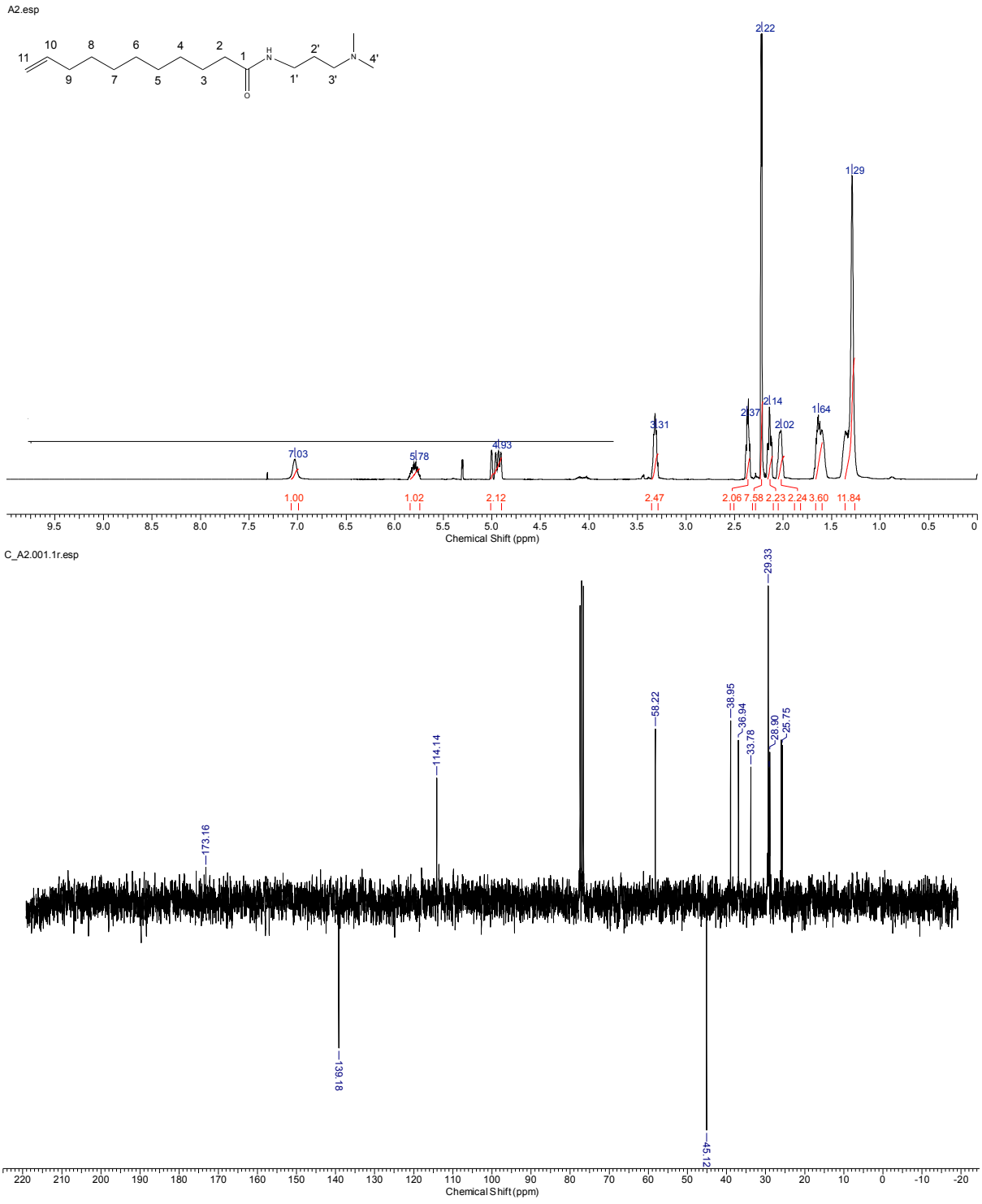
A2.esp
2.22
1.29
2.14
2.37
1.64
3.31
2.02
7.03
5.78
4.93
1.00
1.02
2.12
2.47
2.06
7.58
2.23
2.24
3.60
11.84
Chemical Shift (ppm)
C_A2.001.1r.esp
29.33
58.22
38.95
36.94
33.78
28.90
25.75
114.14
173.16
139.18
45.12
Chemical Shift (ppm)

A3

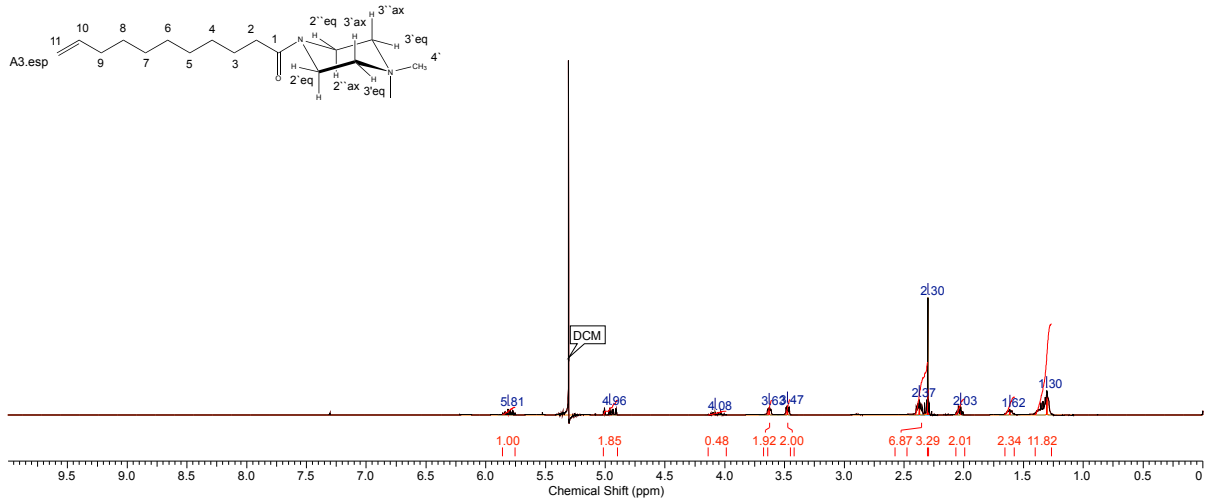
A3.esp
DCM
5.81
4.96
4.08
3.63
3.47
2.30
2.37
2.03
1.62
1.30
1.00
1.85
0.48
1.92
2.00
6.87
3.29
2.01
2.34
11.82
Chemical Shift (ppm)

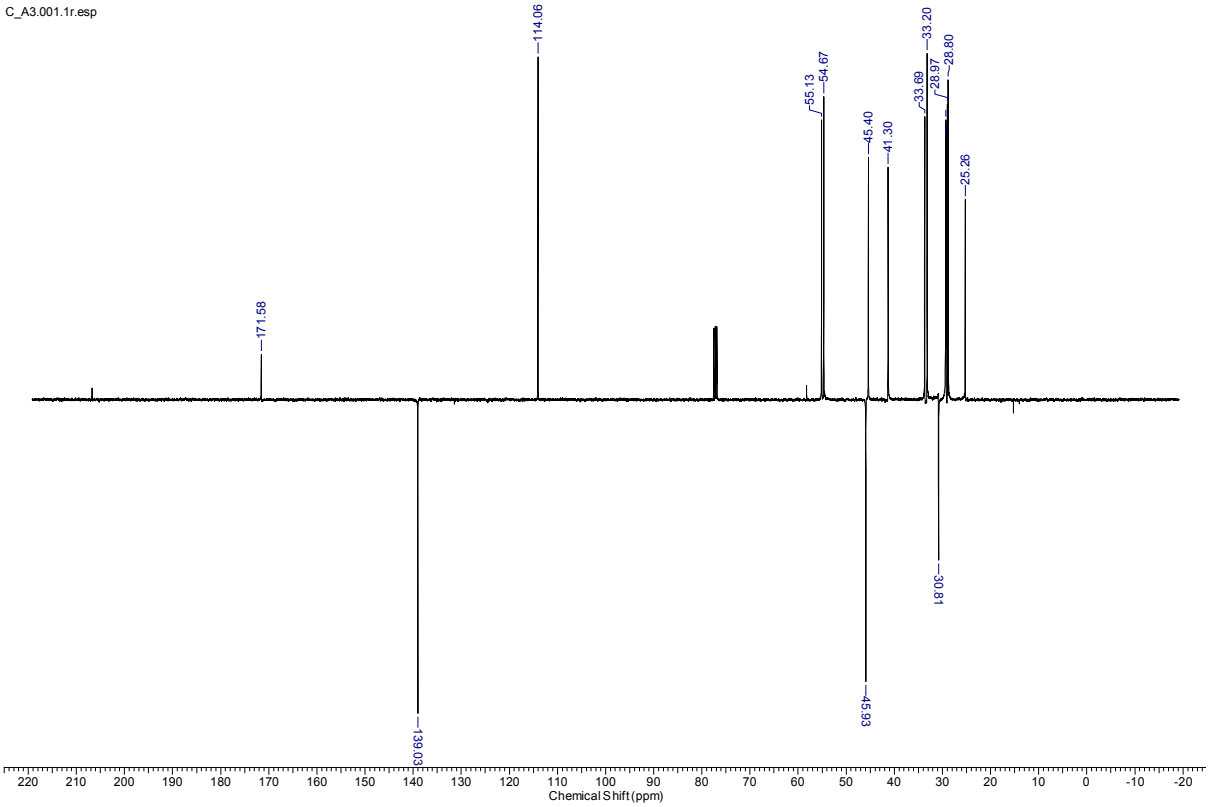
C_A3.001.1r.esp
171.58
114.06
139.03
55.13
54.67
45.40
41.30
33.69
33.20
28.97
28.80
25.26
30.81
45.93
Chemical Shift (ppm)

A4

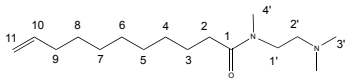
11
10
9
8
7
6
5
4
3
2
1
O
N
4'
2'
1'
N
3'

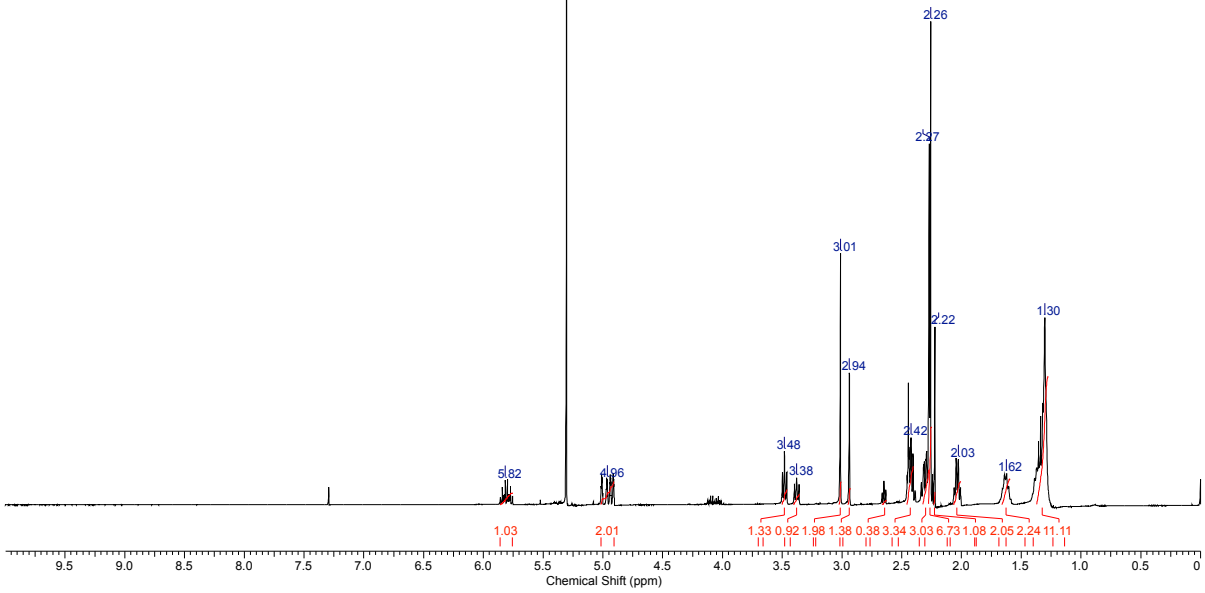
2.26
2.57
3.01
2.22
1.30
2.94
3.48
3.38
2.42
2.03
1.62
5.82
4.96
1.03
2.01
1.33 0.92 1.98 1.38 0.38 3.34 3.03 6.73 1.08 2.05 2.24 11.11
9.5 9.0 8.5 8.0 7.5 7.0 6.5 6.0 5.5 5.0 4.5 4.0 3.5 3.0 2.5 2.0 1.5 1.0 0.5 0
Chemical Shift (ppm)

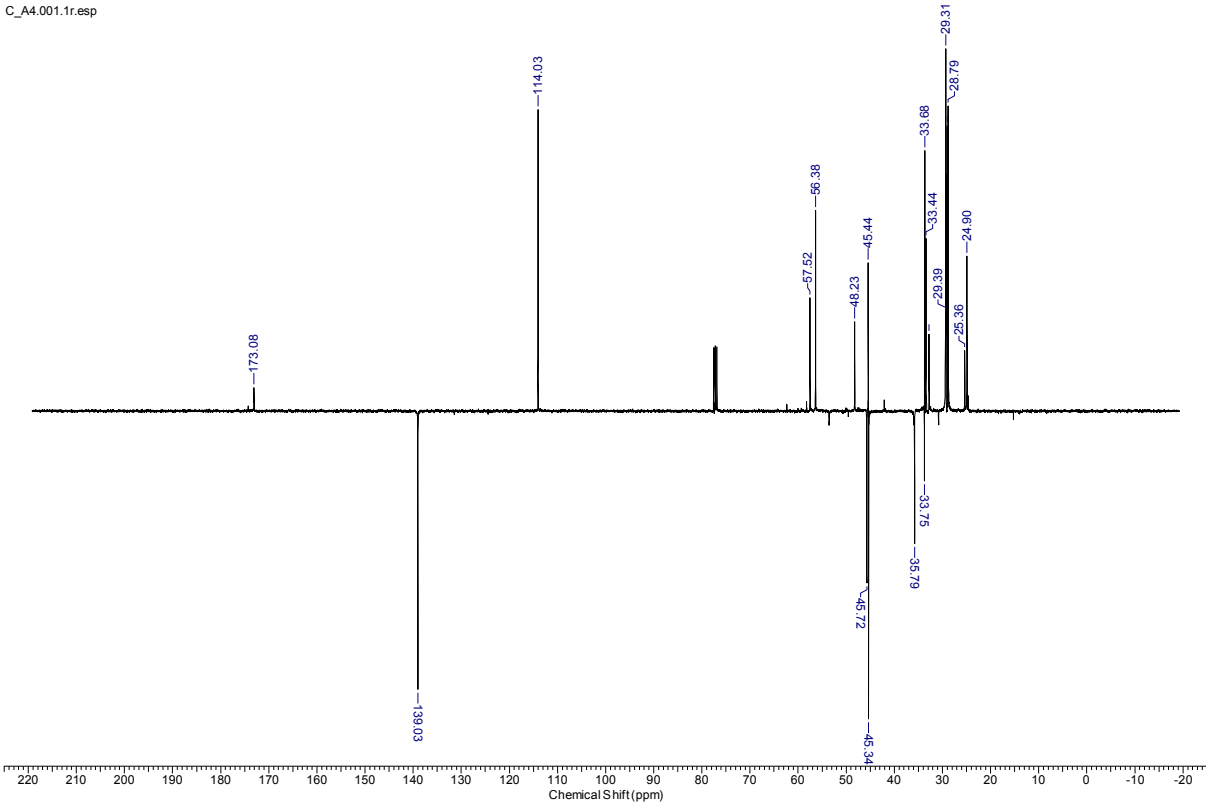
C_A4.001.1r.esp
29.31
28.79
114.03
33.68
56.38
33.44
45.44
24.90
57.52
48.23
29.39
25.36
173.08
33.75
35.79
45.72
139.03
45.34
220 210 200 190 180 170 160 150 140 130 120 110 100 90 80 70 60 50 40 30 20 10 0 -10 -20
Chemical Shift (ppm)

A5

A5.esp

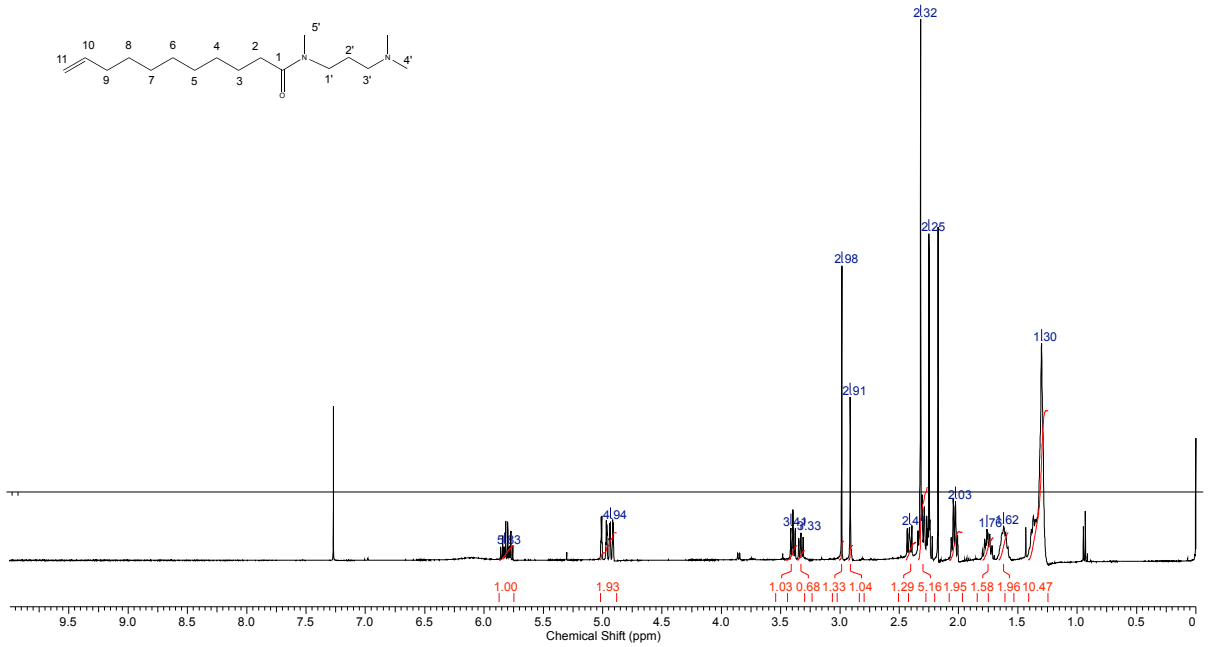

C_5.001.1r.esp

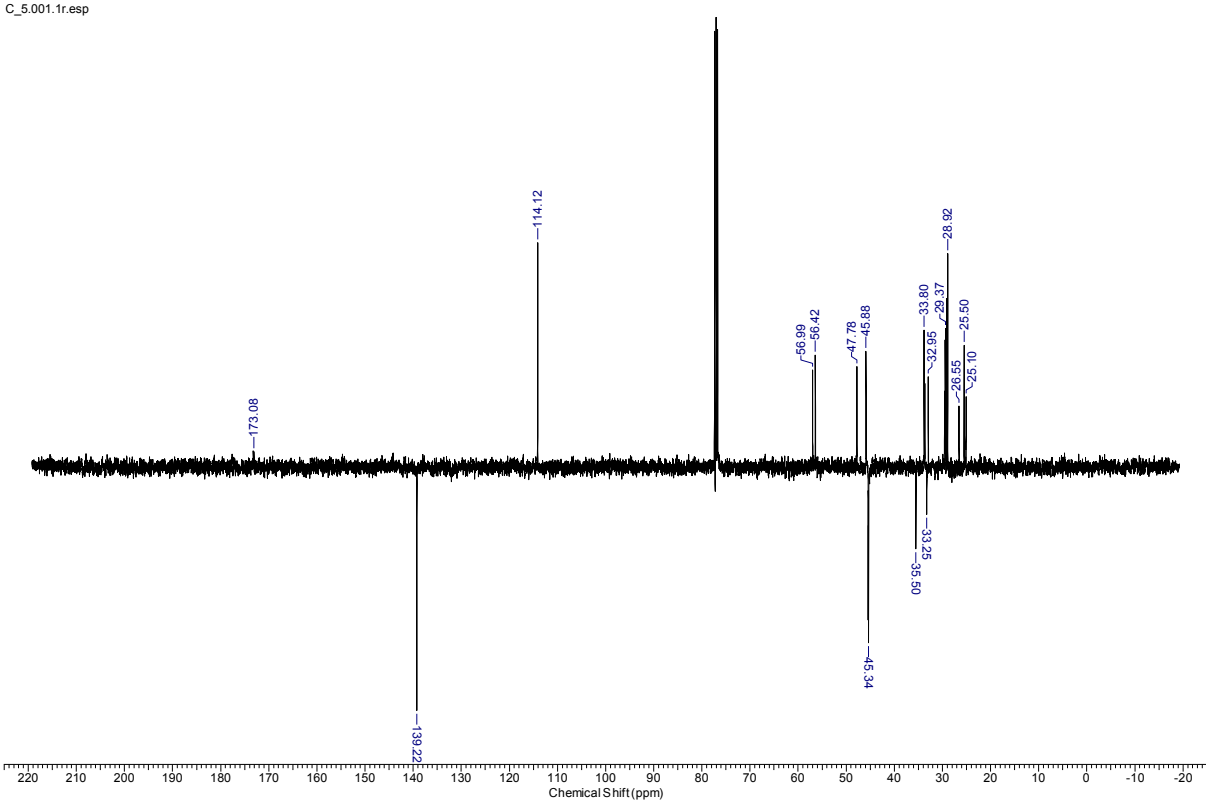

AO1

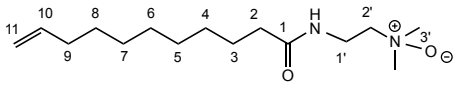
11
10
8
6
4
2
1
H
N
2'
3'
O
9
7
5
3
1'
O

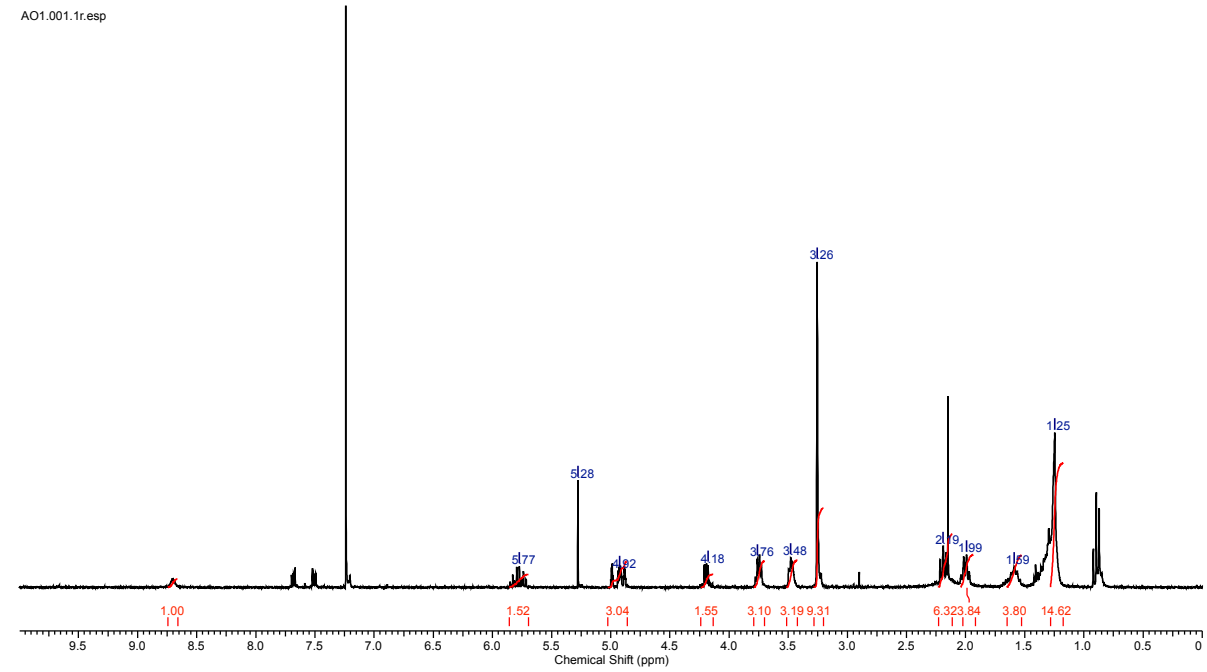
AO1.001.1r.esp
3.26
5.28
1.25
5.77
4.82
4.18
3.76
3.48
2.79
1.99
1.69
1.00
1.52
3.04
1.55
3.10
3.19
9.31
6.32
3.84
3.80
14.62
Chemical Shift (ppm)

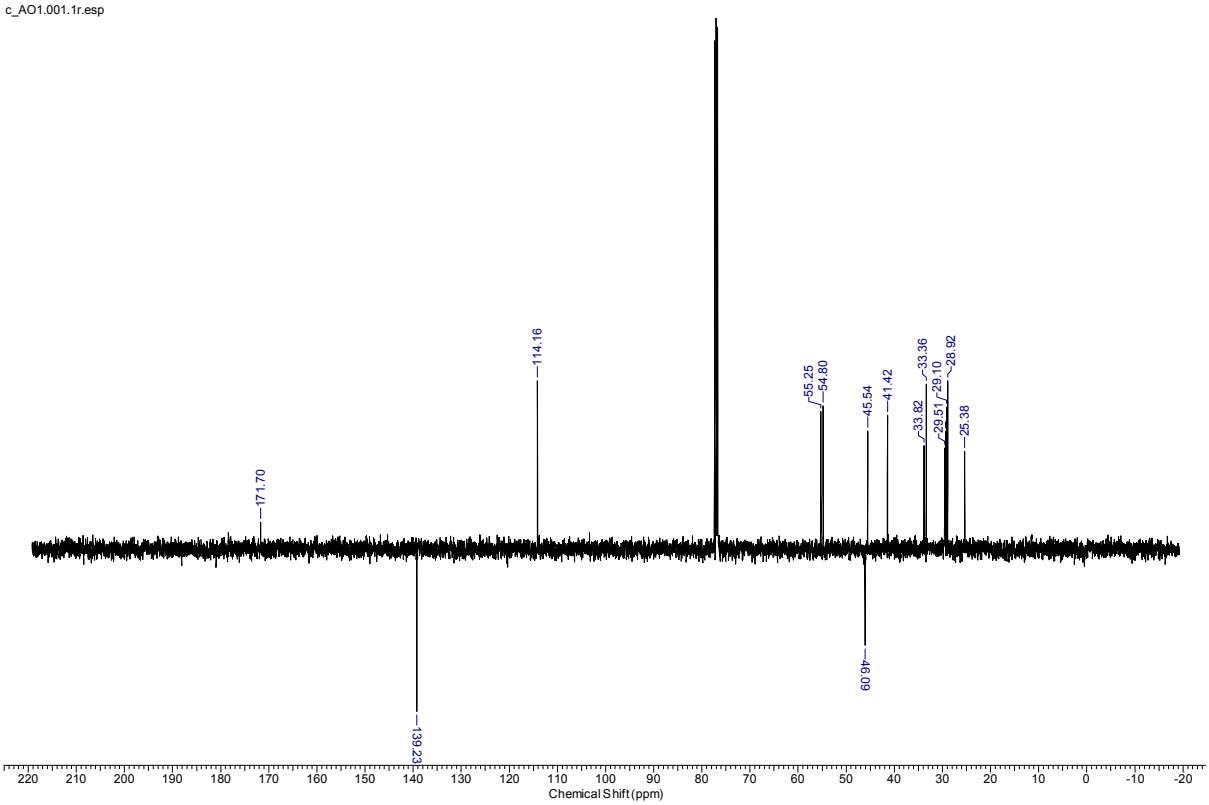
c_AO1.001.1r.esp
171.70
114.16
55.25
54.80
45.54
41.42
33.82
33.36
29.51
29.10
28.92
25.38
60.96
139.23
Chemical Shift (ppm)

AO2

AO2.esp

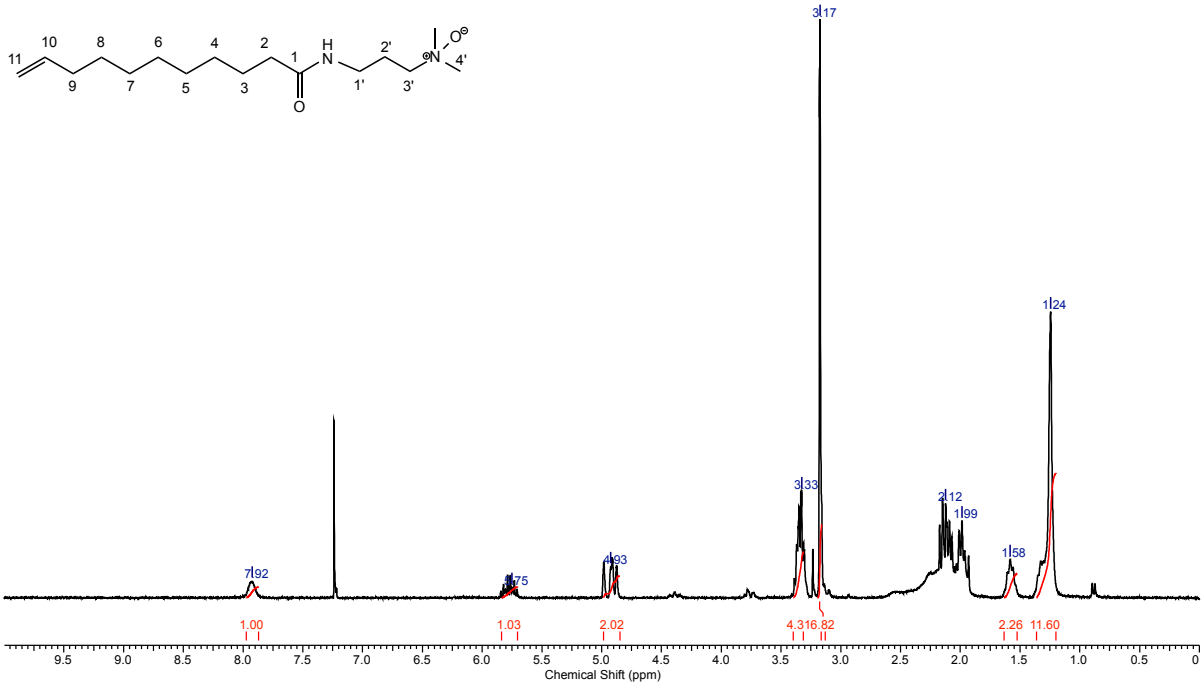

C_AO2.001.1r.esp

1.5

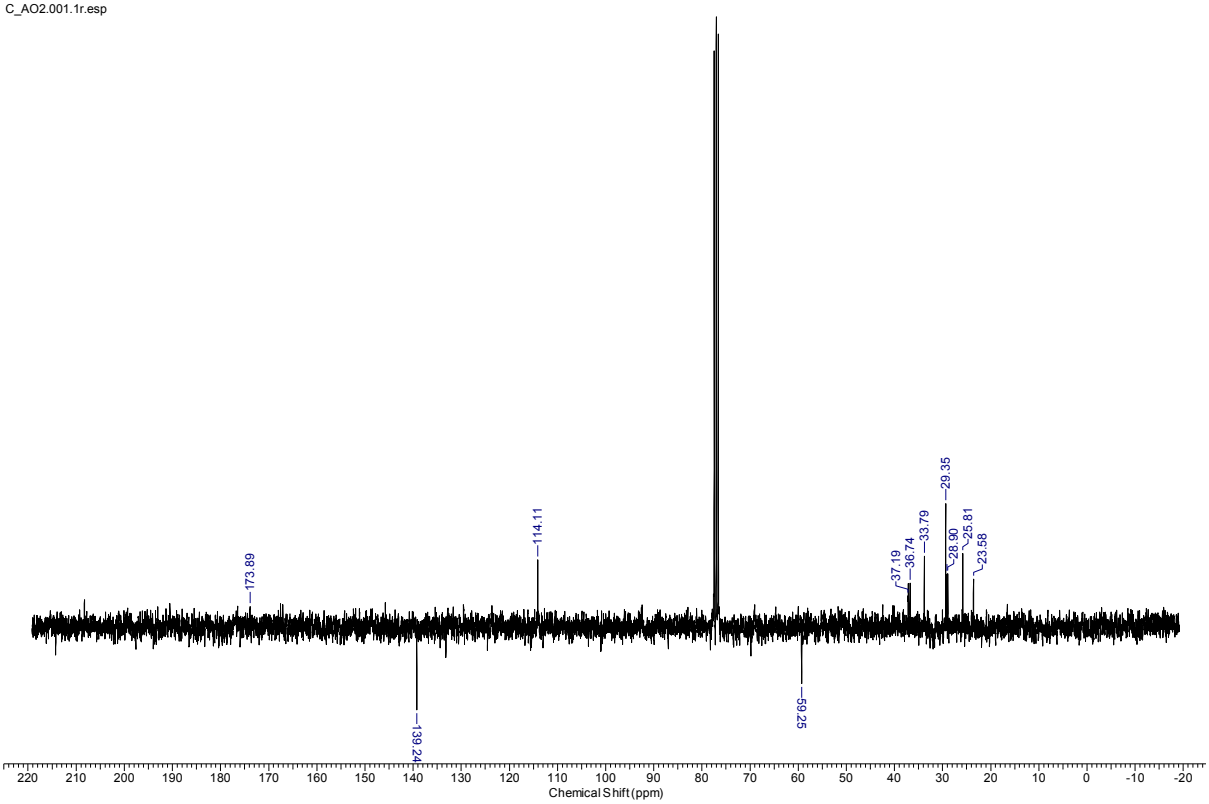

AO3

AO3.001.1r.esp

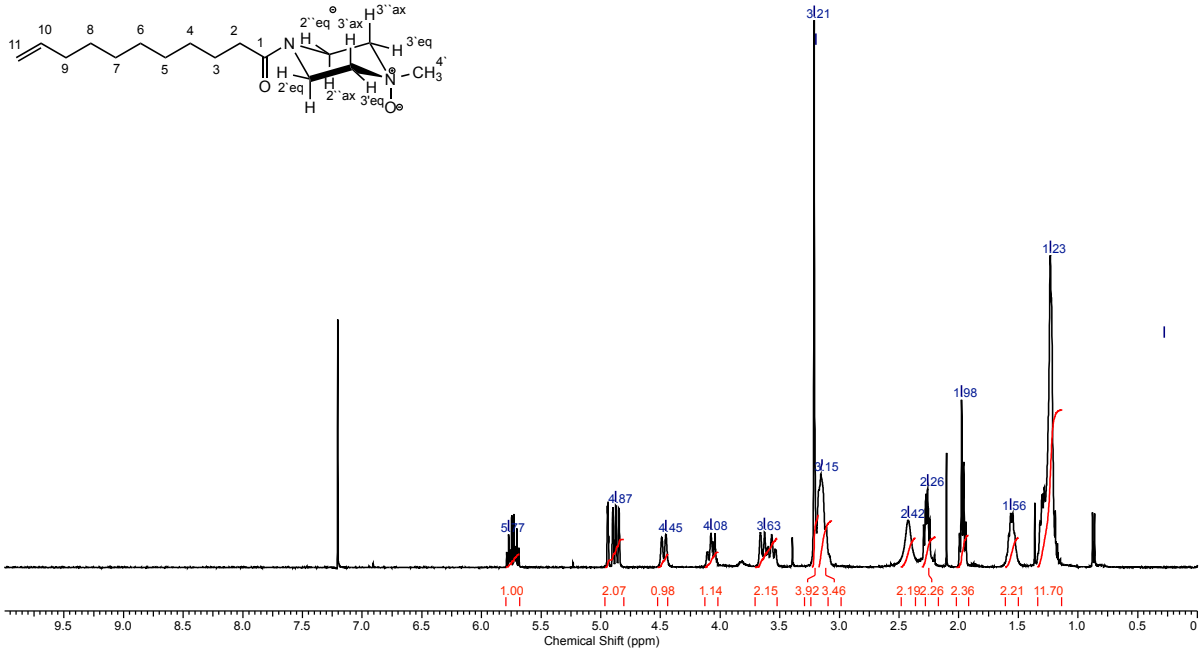

C_AO3.001.1r.esp

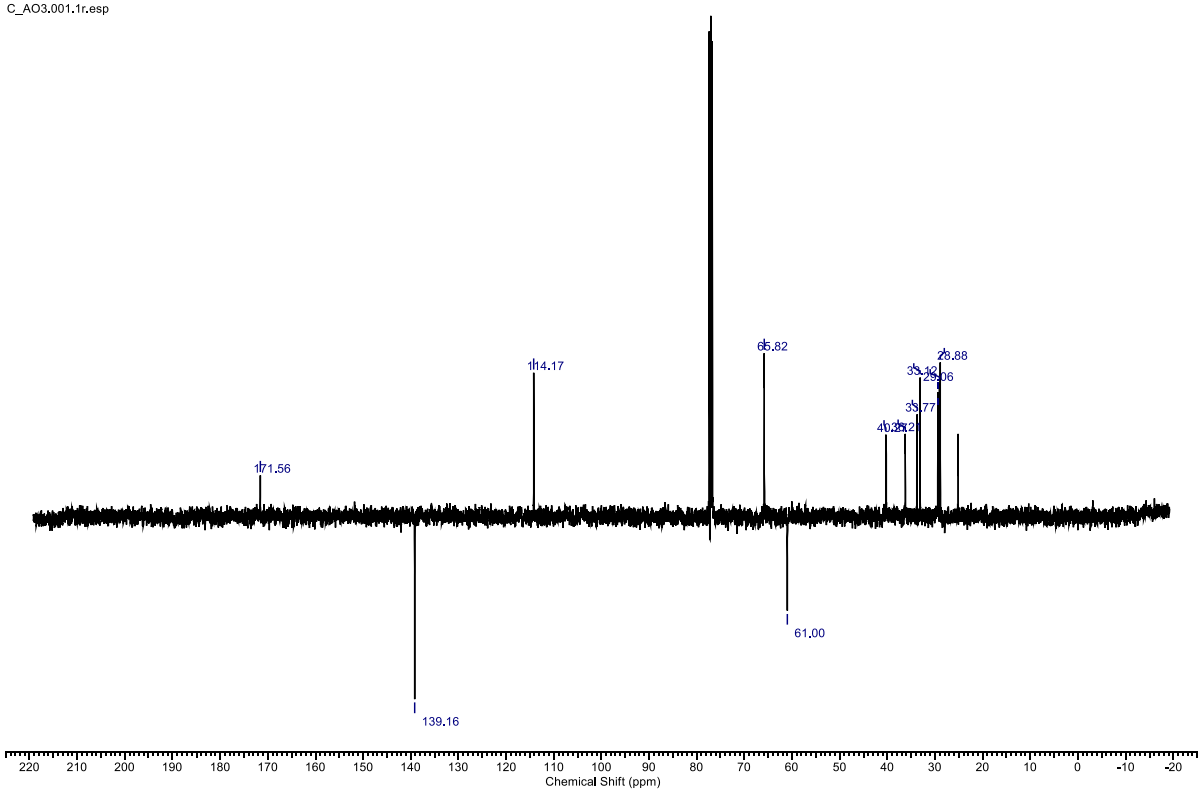

AO4

AO4.001.1r.esp

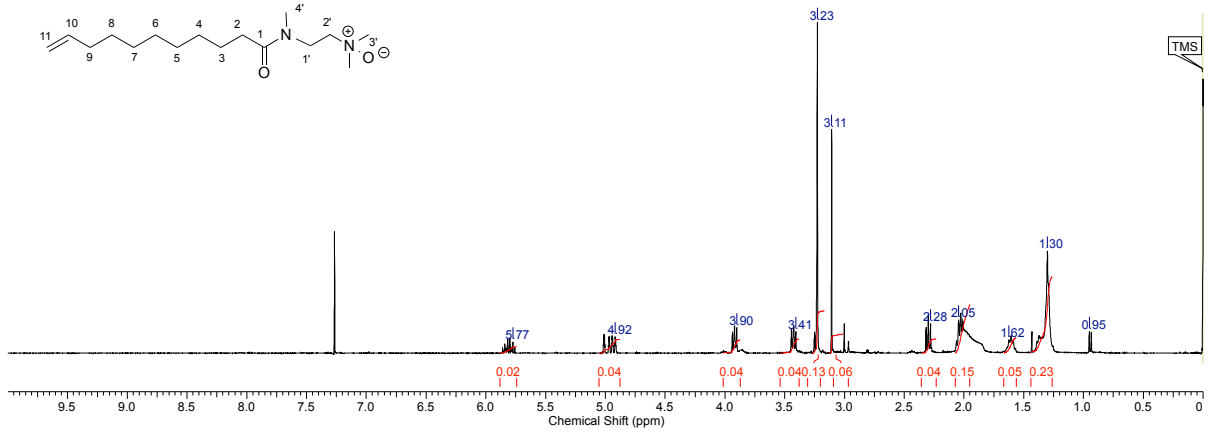

c_AO4.001.1r.esp

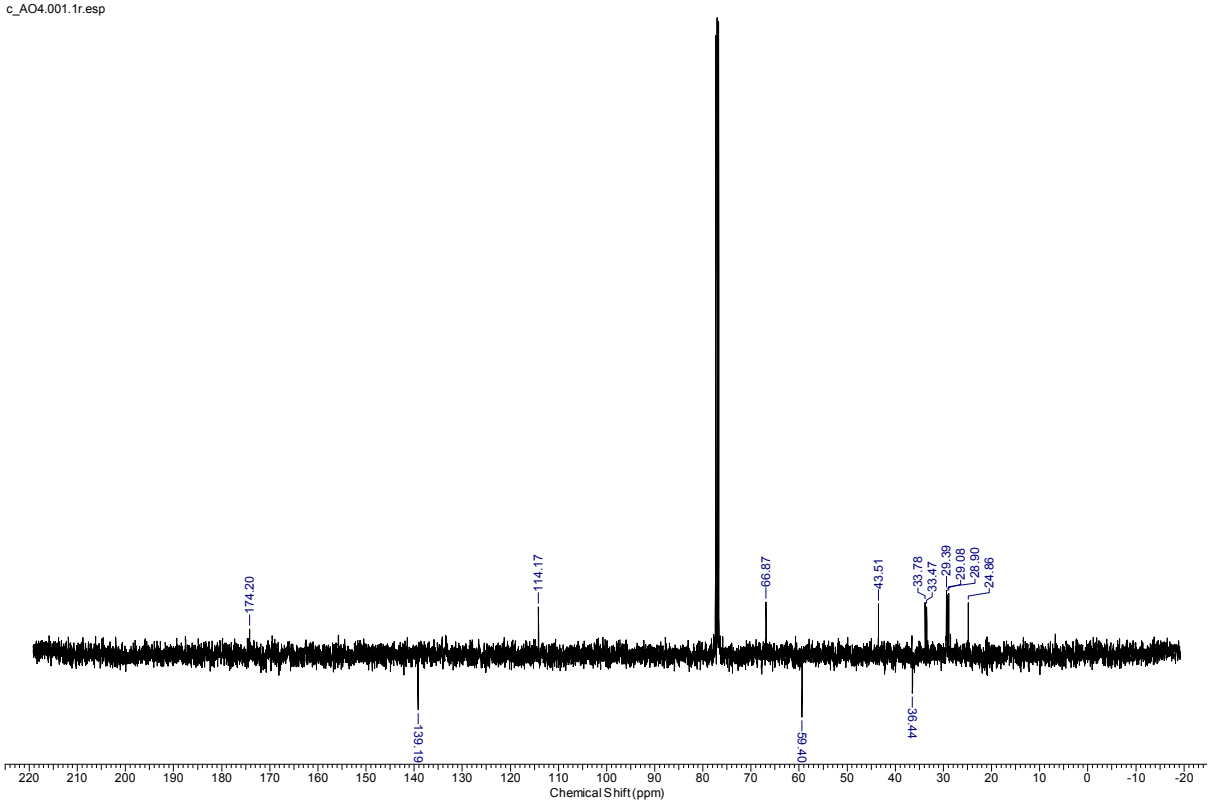

AO5 (in CD_3OD)

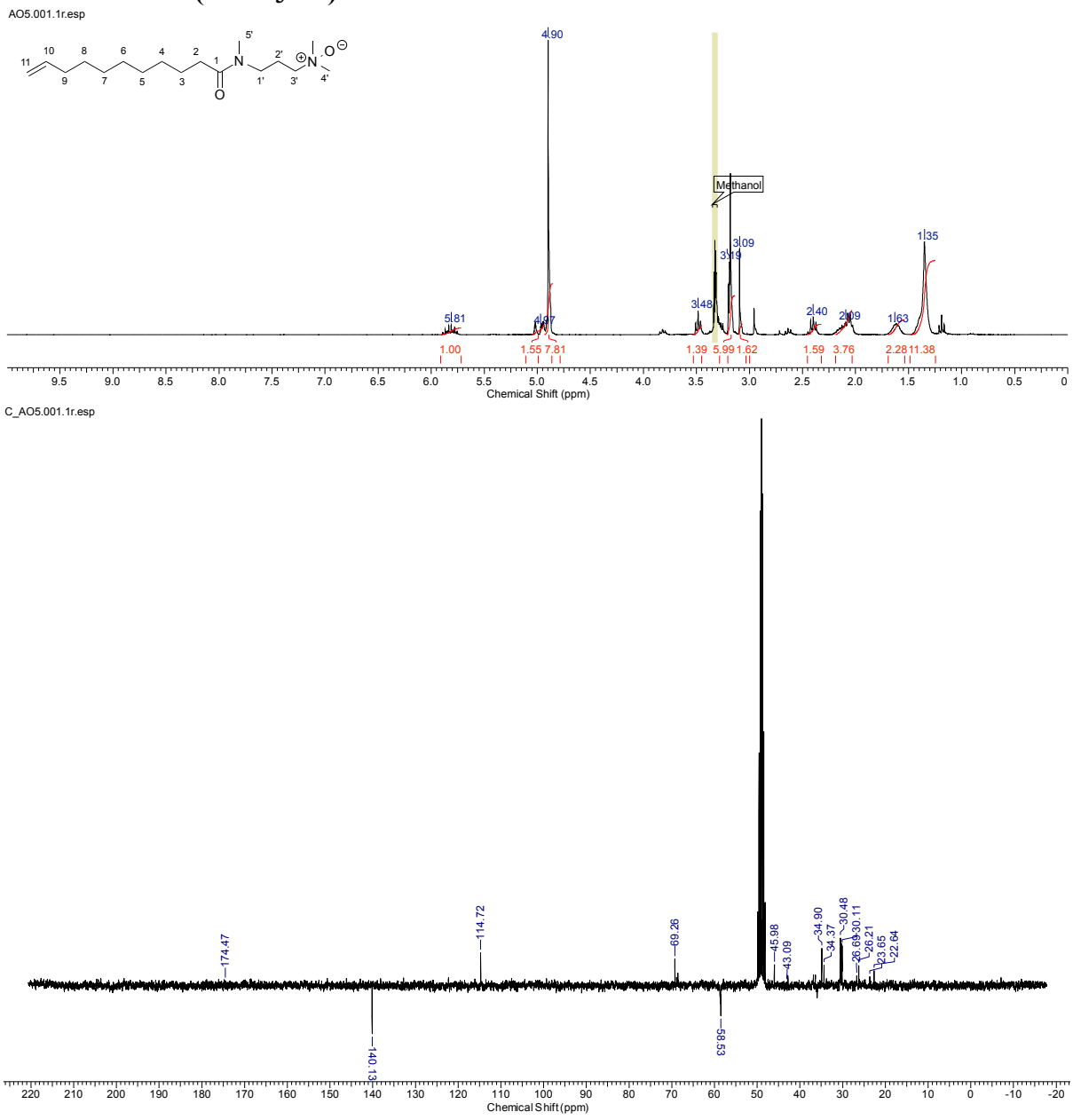
AO5.001.1r.esp
Methanol
Chemical Shift (ppm)
C_AO5.001.1r.esp
174.47
140.13
114.72
69.26
58.53
45.98
43.09
34.90
34.37
30.48
30.11
26.69
26.21
23.65
22.64
Chemical Shift (ppm)

Appendix 9 Characterization of polystyrene beads – pKa, logP and logD values calculated using chemicalize.org.

There are four major ionisation pathways found:

(a) the deprotonation of protonated triazine

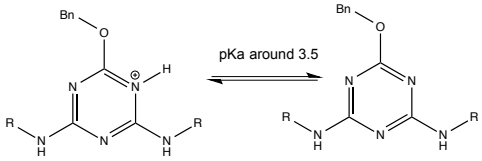

(b) the deprotonation of protonated morpholine

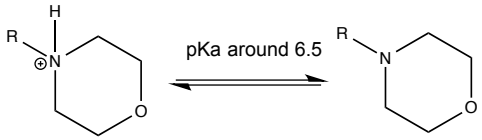

(c) the deprotonation of protonated primary amine

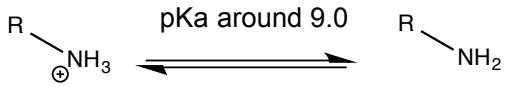

(d) the deprotonation of hydroxyl group

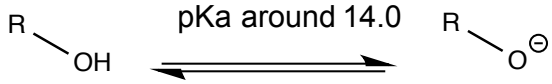

Symbol	Structure	calc. pKa pH = 7.4	logP	est. logD pH =7.4
A6	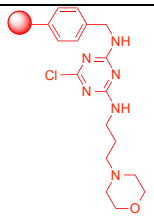	**3.0 (triazine)** **6.9 (morpholine)**	**3.2**	**3.4**

A7	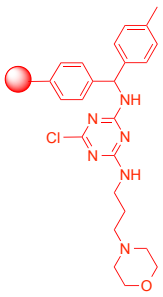	**3.1 (triazine)** **6.9 (morpholine)**	**5.5**	**5.4**
A8	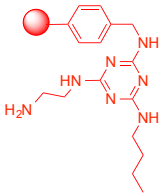	**7.5 (triazine)** **9.6 (primary amine)**	**3.1**	**0.5**
A9	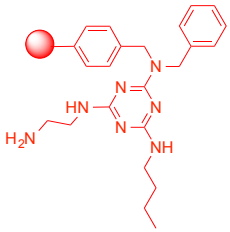	**5.6 (triazine)** **9.6 (primary amine)**	**5.3**	**3.0**
A10	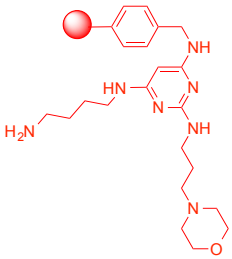	**7.2 (triazine)** **10.2 (primary amine)**	**2.2**	**-0.7**
A11	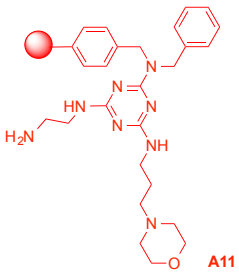	**5.3 (triazine)** **6.9 (morpholine)** **9.6 (primary amine)**	**3.8**	**1.2**
A12	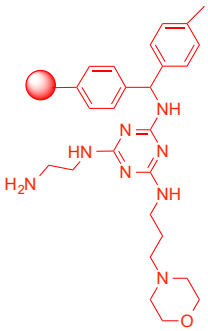	**6.6 (morpholine)** **7.57 (triazine)** **9.62 (primary amine)**	**3.9**	**0.2**
A13	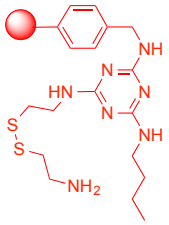	**1.3 (triazine)** **9.6 (primary amine)**	**3.7**	**0.4**

A14	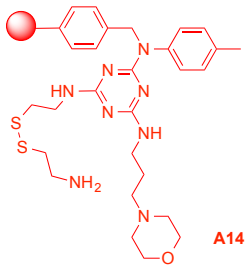	**6.0 (triazine)** **7.0 (morpholine)** **9.6 (primary amine)**	**5.0**	**2.4**
A15	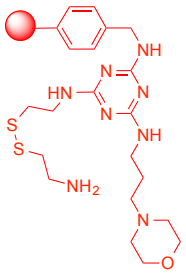	**6.7 (morpholine)** **8.0 (triazine)** **9.6 (primary amine)**	**2.3**	**-1.3**
A16	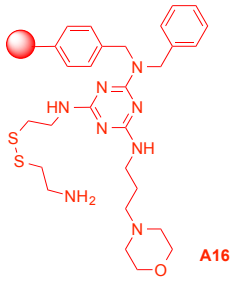	**6.0 (triazine)** **7.0 (morpholine)** **9.6 (primary amine)**	**4.5**	**1.8**
A17	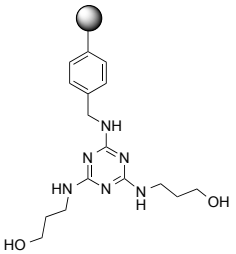	**8.0 (triazine)**	**1.29**	**0.2**
A18	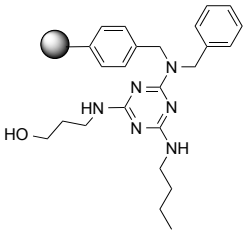	**6.2 (triazine)**	**5.4**	**5.4**
A19	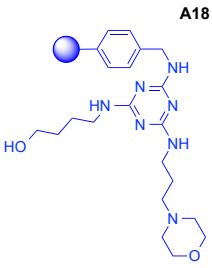	**6.7 (morpholine)** **8.0 (triazine)**	**2.3**	**1.4**

Intrinsic fluorescence of beads in PBS and fluorescence of beads in culture medium at 467 nm.

Major microspicies at pH = 7.4	Fluorescence
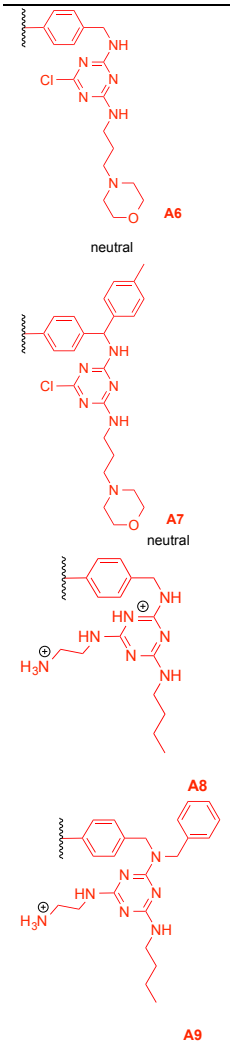	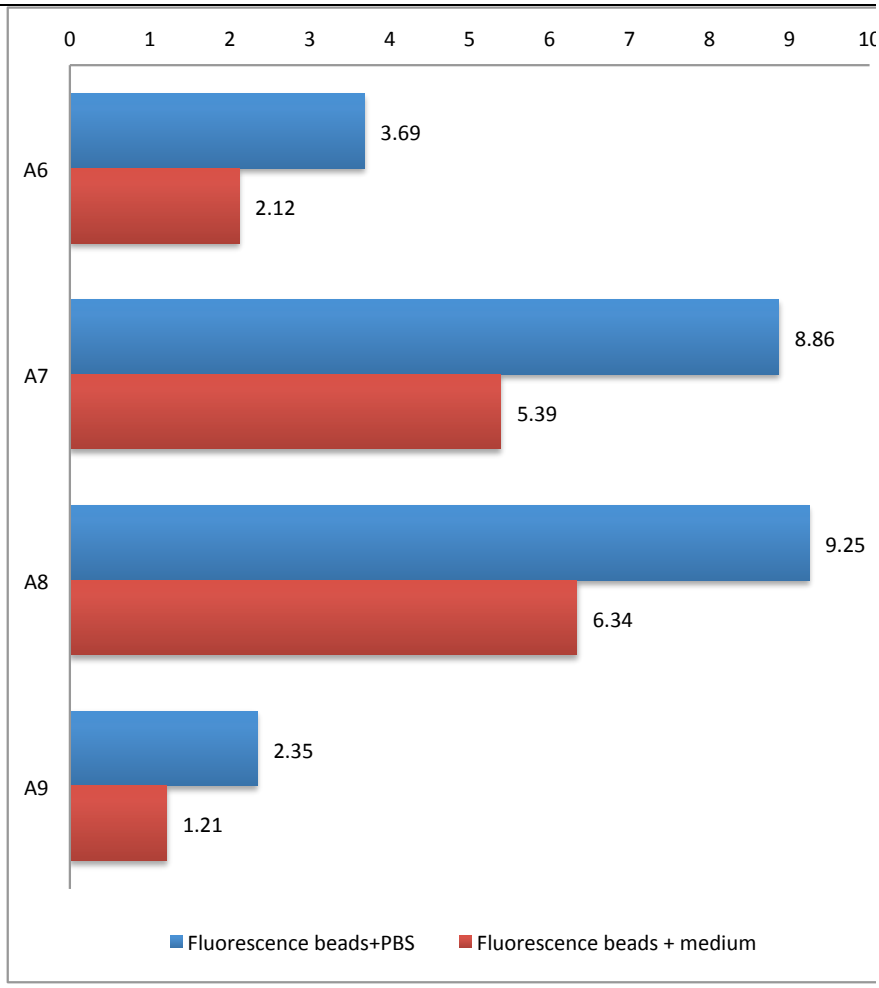

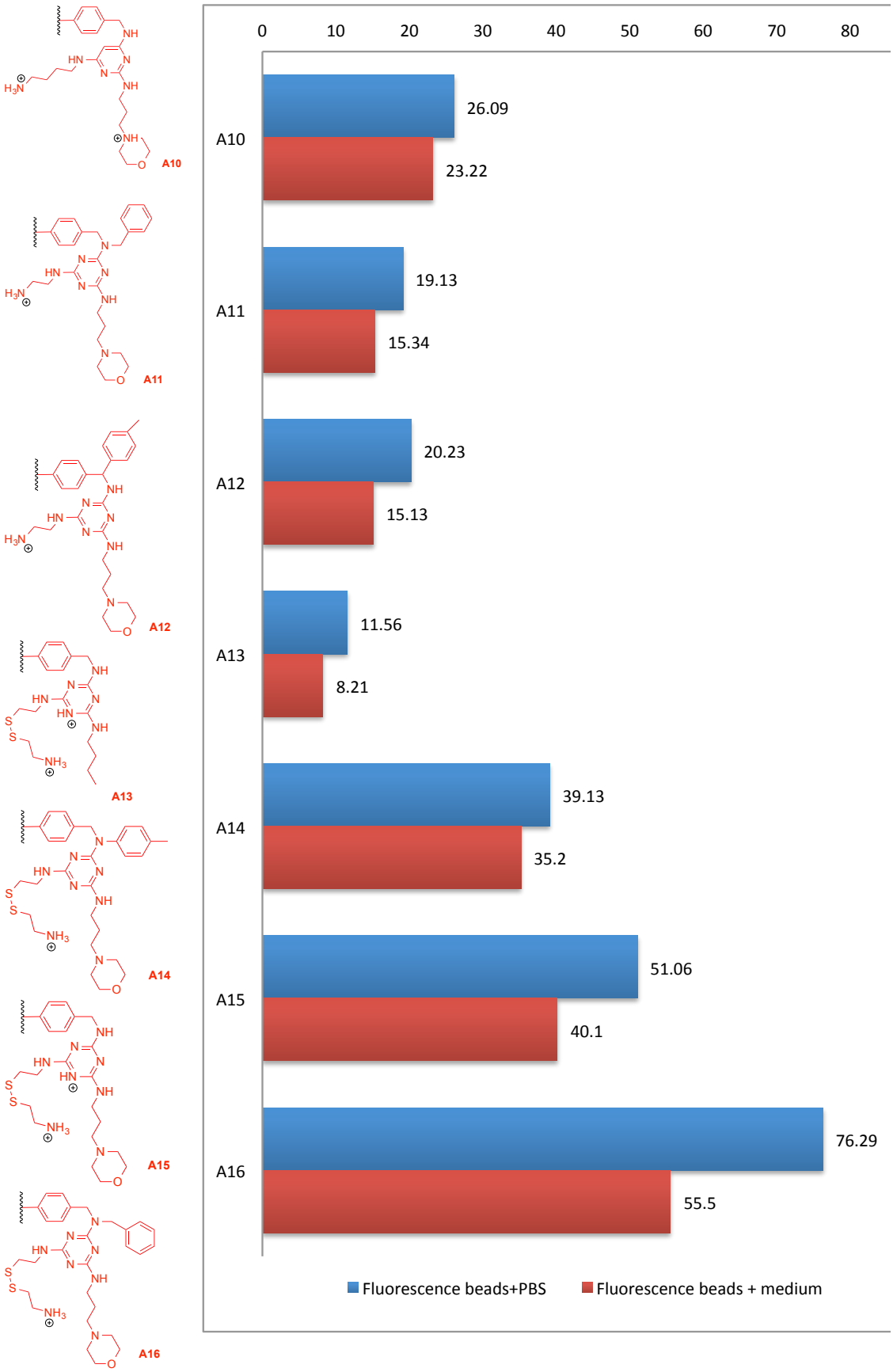
A10
A11
A12
A13
A14
A15
A16
0
10
20
30
40
50
60
70
80
A10
26.09
23.22
A11
19.13
15.34
A12
20.23
15.13
A13
11.56
8.21
A14
39.13
35.2
A15
51.06
40.1
A16
76.29
55.5
Fluorescence beads+PBS
Fluorescence beads + medium

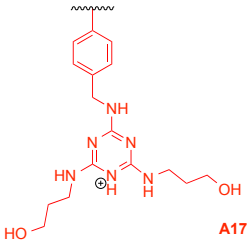
NH
N
N
HN
N
H
N
H
OH
HO
A17

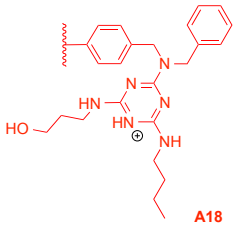
N
N
HN
N
HN
NH
HO
A18

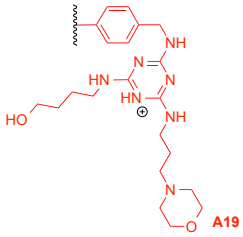
NH
N
HN
N
HN
NH
HO
N
O
A19

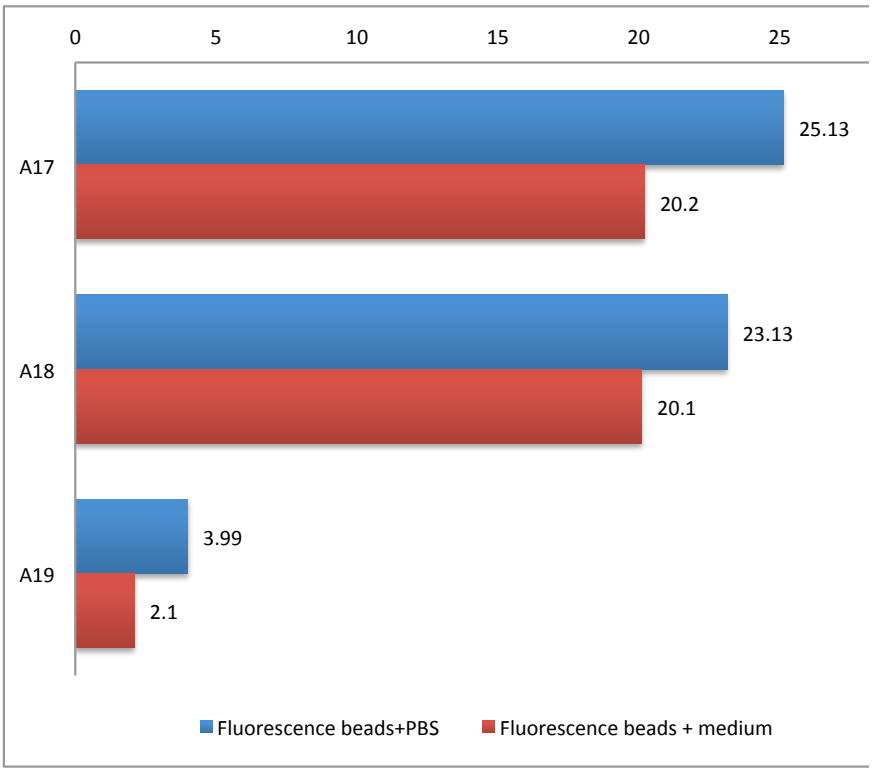
0
5
10
15
20
25
A17
25.13
20.2
A18
23.13
20.1
A19
3.99
2.1
Fluorescence beads+PBS
Fluorescence beads + medium